THE UNIVERSITY *of* EDINBURGH

Title	Expression of CX_3CL1 (Fractalkine) in renal tubular epithelial cells and the regulation of CX_3CL1 by stimulation of the thromboxane prostanoid receptor
Author	Durkan, Anne Maria.
Qualification	PhD
Year	2012

Digitisation notes:

- Page number 142 is skipped in original document

The Expression Of CX_3CL1 (Fractalkine) In Renal Tubular Epithelial Cells And The Regulation Of CX_3CL1 By Stimulation Of The Thromboxane Prostanoid Receptor.

Anne Maria Durkan

MD

The University of Edinburgh

2012

Abstract

Most renal diseases have a common end inflammatory pathway, which is associated with a leukocytic infiltrate. Chemokines are small proteins that are responsible for the chemoattraction of leukocytes into areas of injury or insult. CX_3CL1, also known as fractalkine, exists as a transmembrane protein as well as a soluble protein. It acts as a cell adhesion molecule in addition to its chemoattractant properties.

This thesis firstly examines the distribution of CX_3CL1 in renal tubular epithelial cells (RTEC) and in the second part of the thesis the regulation of CX_3CL1 by stimulation of the thromboxane prostanoid (TP) receptor is examined.

The localisation of CX_3CL1 was initially demonstrated primarily on the apical surface of tubular epithelial cells in human renal biopsy specimens with histological diagnoses of acute tubular necrosis and acute allograft rejection. A cell model was then developed in MDCK cells to examine the distribution more closely.

There are a limited number of mechanisms potentially responsible for the trafficking of CX_3CL1 to the apical membrane and it was established that N-glycosylation of CX_3CL1 is required for its presence on the apical membrane of RTEC.

The mobility of CX_3CL1 within the cell membrane was next assessed and it was shown to be relatively immobile. We hypothesized that this would promote cell adhesion and indeed further experiments confirmed that CX_3CL1 in RTEC does promote adhesion of cells bearing the cognate receptor.

Given that CX_3CL1 and thromboxane A_2 are both found in similar inflammatory conditions, are both present early in the inflammatory process and that stimulation of the TP receptor has been shown to regulate other chemokines, we next evaluated the effect of stimulation of TP on CX_3CL1. We found that both total and surface cellular levels of CX_3CL1 were reduced following stimulation of TP. A maximal nadir was present after 30-60 minutes and the levels returned to baseline by 4 hours.

The mechanism for the loss of CX_3CL1 was then assessed. CX_3CL1 is known to recycle between the cell surface and an internal compartment. No effect of TP stimulation was seen on the endocytosis or exocytosis of CX_3CL1. Stimulation of TP was however, shown to stimulate tumour necrosis factor-α converting enzyme (TACE) via ERK phosphorylation. TACE inducibly cleaves CX_3CL1, releasing the soluble chemokine. TACE siRNA was used to knock down TACE gene expression and this prevented the loss of cellular CX_3CL1, confirming that TP stimulation induces TACE cleavage of CX_3CL1. The results of further experiments are discussed in the discussion chapter.

Acknowledgements

I would like to thank first and foremost, my supervisor Dr Lisa Robinson for her invaluable guidance and mentorship. I would also like to thank my co-workers without whom this work would not be completed. In particular I am indebted to Soumitra Tole, who made a significant contribution to the completion of the work investigating the effect of TP stimulation on CX_3CL1 (see below), and to Dr Todd Alexander who offered invaluable technical assistance as well as comradeship and moral support. I am also grateful to the other members of the Robinson lab, namely: Guang-Ying Liu, Min Rui, Joe Femia, Laura Jones, Yi-Wei Huang.

I would also like to thank Professor Sergio Grinstein who allowed me to work in his laboratory and who provided me with a rich learning environment (and many reagents).

I would also like to acknowledge the following; Dr Andrew Herzenberg for providing renal biopsy specimens, Michael Ho for technical assistance, Bob Temkin for assistance with the electron microscopy, Mike Woodside and Paul Paroutis for help in the imaging facility, the staff of the flow cytometry facility in the Research Institute, Hospital for Sick Children, Toronto and Prof. Neil Turner who was my nominated local supervisor. In addition, my thanks go to Dr Stephen Alexander who offered helpful advice in the thesis preparation and allowed me

time to complete this work and to Liz Barnes, statistician at the University of Sydney, who painstakingly went over the statistical analysis for each experiment.

I was financially aided by 1) the Research Institute Scholarship, Hospital for Sick Children, Toronto and 2) the NAPRTCS/Roche Paediatric Nephrology Research Scholarship and I am immensely grateful for these awards.

Finally, but not least, I wish to thank my loving husband, Davinder, for his unfailing support throughout, and I offer my apologies to both him and my beautiful daughter, Maya, for being absent for prolonged periods of time and for missing so many weekend activities. Without the encouragement of my family and the imminent arrival of our second child, this work would never have been completed. This thesis is dedicated to you and to my parents, without whose previous support, I would never have been in a position to undertake this work.

Individual Contributions

Anne Durkan – All immunofluorescence staining and microscopy, the Western blots, examination of biopsy specimens, preparation for electron microscopy, cholesterol depletion and cholesterol assays, FRAP data generation and analysis for the membrane mobility experiments and for the endocytosis experiments, the cell adhesion assays in RTEC, the staining, microscopy and analysis for the exocytosis experiments, the staining of cells for flow cytometry under all conditions (TP stimulation, inhibition of TP stimulation, inhibition of TACE, inhibition of ERK phosphorylation, inhibition of PLC) and the analysis of this data and the TACE colocalisation experiments.

Guang-Ying Liu – created the stable cell lines of MDCK-CX_3CL1, MDCK-CX_3CL1-GFP and ECV-CX_3CL1-GFP cells.

Min Rui-Crow – created the stable cell line of MDCK-CX_3CL1-360 cells.

Todd Alexander – taught me how to do Western blots, immunofluorescence staining and FRAP and offered invaluable advice with microscopy techniques. He also contributed to the experimental design and performed the initial adhesion assays with primary tubular epithelial cells and human PBMCs.

Soumitra Tole – completed the FACS analysis and repeated some Western analysis.

Yi-Wei Huang - the CX_3CL1 shedding studies using siRNA TACE and ADAM-10.

Joe Femia – (summer student) RNA isolation in HK-2 cells.

Laura Jones – (summer student) some preliminary FACS preparation (with AD).

Jerry Pan – (summer student) repeated the adhesion assays with PTEC and PBMCs.

Lisa Robinson – Project supervisor.

Chapter 1. Introduction

Chronic renal impairment is a significant health burden and the Western world, in particular but by no means exclusively, is experiencing an exponential increase in patients requiring renal replacement therapy. While a large number of aetiologies contribute to injury, many of these converge on common immune and non-immune pathways of inflammation and scarring, which are discussed in greater depth below. We are particularly interested in the chemokine CX_3CL1 and its receptor CX_3CR1 as mediators of injury and as potential targets for therapeutic intervention. The role of chemokines, especially CX_3CL1, as recruiters of macrophages and other leukocytes in renal disease is outlined and we then discuss the regulation of this chemokine, it's mode of action and the effects of inhibition of the chemokine-receptor pair. We also review the thromboxane pathway as a potential initiator and site for intervention in inflammation and examine the cross-talk between this pathway and chemokines.

Mechanisms of Renal Disease Progression

The renal response to injury is outlined briefly below and will be expanded on in the following pages. The initial injury to the kidney may be the result of toxins, immune complexes, hypoxia, infection, protein overload, vasoactive agents such as angiotensin II, or mechanical stress, amongst others. These insults promote the secretion

of pro-inflammatory mediators such as cytokines and chemokines from the renal cells, with subsequent leukocytic infiltration. This initiation process is followed by an amplification process, whereby the leukocytes themselves secrete more proinflammatory mediators, thus exaggerating the response. Infiltrating neutrophils and macrophages generate radical oxygen species and lipid mediators adding to the local tissue damage. Macrophages also secrete various growth factors, which stimulate mesangial cell proliferation and matrix synthesis. Although the initiation response is usually compartmentalised, i.e. an insult to the glomerulus results in an inflammatory response within the glomerulus, the amplification response may extend into other areas such that glomerular growth factors, for example, may spill over into the tubules and stimulate the tubulointerstitial cells. Similarly circulating factors may have effects away from the initial insult. The amplification phase is followed either by progression to chronic inflammation and fibrosis or repair and resolution depending on the cytokine profile of the local environment and the macrophage phenotype activated. It is proposed that fibrosis is a maladaptation of a normal healthy response to injury but it is not clear what promotes fibrosis over repair.

At the cellular and molecular levels, the pathophysiology of renal fibrosis is complex with involvement of both resident and infiltrating cells. It is a dynamic process that is regulated at multiple levels, but critical to the process is the ability to accumulate extracellular matrix.

Depending on the site and nature of the initial injury, the major renal fibrogenic cells are glomerular mesangial cells, interstitial fibroblasts and tubular epithelial cells. Bone marrow derived cells may also play a role (1).

Hypotheses of Renal Fibrosis

To explain the effect of the initial insult on the final outcome, two, not necessarily mutally exclusive, hypotheses, have been put forward to explain progressive renal damage and interstitial fibrosis. The first theory suggests that the proximal tubule is the site of primary insult. This insult then exposes the tubular epithelial cells to increased amounts of protein, which results in more protein reabsorption by the tubules. This 'protein overload' then stimulates an inflammatory response with subsequent increased interstitial matrix formation. The second theory has a glomerular origin and suggests that any loss of renal functioning mass results in glomerular hyperfiltration and intraglomerular hypertension. This triggers glomerular hypertrophy and proliferation and is associated with crescent formation. This glomerular expansion encroaches on the glomerular-tubular junction causing obstruction, with eventual tubular destruction and interstitial fibrosis (2, 3). Furthermore, endothelial damage leads to podocyte loss and denudment of the basement membrane, allowing the ultrafiltrate to reach the tubulointerstitial space, where it triggers an inflammatory response.

There may be different mechanisms at play in glomerular versus interstitial fibrosis.

In the first of the models, that of increased protein reabsorption by tubular epithelial cells, the reabsorbed proteins cause damage to lysosomal pathways, increase secretion of growth factors, such as Transforming Growth Factor-β (TGF-β), Fibroblast Growth Factor (FGF), Endothelial Growth Factor (EGF), Tumour Necrosis Factor-α (TNF-α) and Platelet Derived Growth Factor (PDGF) and increase oxidative stress responses in the tubular epithelial cells (4-6). Furthermore, stressed tubular cells release various chemokines including CCL2, CCL5 and CX_3CL1 (7-9). These proteins are chemotactic for leukocytes and facilitate the infiltration of leukocytes into the damaged area. The injured tubular cells also release other factors such as connective tissue growth factor (CTGF), endothelin-1 (ET-1) and fibronectin that contribute to the fibrotic process. There is a positive feedback loop formed in which infiltrating macrophages release more chemokines and growth factors. Infiltrating T cells release gamma-interferon and other cytokines that activate chemokines and other inflammatory cells. In addition, the renal tubular epithelial cells also add to the autocrine and paracrine regulation of cytokine and chemokine production.

In the glomerular origin of fibrosis model, there is loss of nephron mass with increased single nephron function and increased intraglomerular pressure. There is also endothelial damage, which results in exposure of the endothelium to profibrotic factors such as angiotensin II (Ang II), endothelin-1 (ET-1), connective tissue growth factor (CTGF) and plasminogen activator inhibitor-1 (PAI-1).

Angiotensin II and Renal Injury

Angiotensin II has both haemodynamic effects, contributing to the increased intraglomerular pressure, and non-haemodynamic effects. It stimulates the glomerular and tubular secretion of growth factors such as TGF-β, PDGF and basic Fibroblastic Growth Factor (bFGF), cytokines such as TNF-α, cell adhesion molecules such as Vascular Cell Adhesion Molecule-1 (VCAM-1) and it also stimulates smooth muscle cell proliferation, stimulates mesangial cell hypertrophy and induces PAI-1 (10-13). The relationship between AngII and TGF-β pathways is complex. AngII stimulates TGF-β secretion via protein kinase C (PKC) and it also stimulates the production of the TGF-β receptor. Furthermore, AngII can activate Smad 2 and 3 independently of TGF-β, via an extracellular signal-regulated kinase 1/2 (ERK1/2) pathway (14).

Plasminogen activator inhibitor-1 and Renal Injury

PAI-1 is the primary inhibitor of tissue-type plasminogen activator (t-PA) and urokinase-type plasminogen activator (u-PA). These two proteins activate plasminogen, forming plasmin, which degrades fibrin. Not only do t-PA, u-PA and plasmin degrade extracellular proteins, they also activate latent matrix metalloproteinases, such as MMP-1 and MMP-3, which also promote matrix breakdown. However, the pro-fibrotic effects of PAI-1 are not all associated with its ability to decrease proteolysis. It can also modulate cell migration and may play a role in epithelial to mesenchymal transformation (EMT) (15). PAI-1 expression is induced by AngII and aldosterone, both dependently and independently of TGF-β (16).

Transforming Growth Factor-β and Renal Injury

Although factors, including cytokines, hormones and haemodynamic factors are important for the resolution of inflammation, with or without scarring, the most crucial factor seems to be Transforming Growth Factor-β (TGF-β). Furthermore, TGF-β appears to act as a common link between many of the other profibrogenic pathways, such as angiotensin II, which is upstream of TGF-β, and connective tissue growth factor, which is downstream of TGF-β.

In most cells TGF-β is a growth inhibitor however in mesenchymal cells it has biphasic properties and both stimulates and inhibits growth (17). In the fibrotic kidney increased TGF-β signalling is achieved by many mechanisms such as increased TGF-β gene expression, enhanced post-translational activation of the protein, release of TGF-β from latent complexes and increased receptor expression. In addition, there is demonstrable loss of Smad transcriptional co-repressor protein function allowing unconstrained TGF-β signalling (18).

TGF-β is produced by various renal cells, including endothelial cells, renal tubular epithelial cells and macrophages. Its release is brought about by numerous stimuli, including renin/angiotensin II, complement activation, Toll-like receptor-2 (TLR-2) activation and protein overload. Activation of TGF-β results in many downstream effects. In the kidney, it contributes to the inflammatory infiltration and the promotion of apoptosis of podocytes (19). It stimulates the transcription of extracellular matrix genes in mesangial, endothelial and renal tubular cells (20). It stimulates PAI-1 in a positive feedback loop and most of the pro-fibrogenic actions of PAI-1 are exerted via TGF-β (21). It inhibits proteinases such as Tissue Inhibititory Matrix Proteinases (TIMPs) and collagenases, which prevent matrix breakdown and degradation. It induces CTGF with the subsequent increased proliferation of renal fibroblasts and extracellular matrix production (22). Finally, TGF-β is a

major trigger for epithelial to mesenchymal transformation, which has been shown to be significant in the fibrosis pathway, particularly in the later stages. Iwano *et al* showed that up to 36% of fibroblast specific protein-1 (FSP-1) positive fibroblasts were derived from renal proximal tubules in a model of unilateral obstruction (23). More recently the transformation of endothelial cells to mesenchymal cells has also been recognised (24). TGF-β also has immunomodulatory effects and deficient mice die of overwhelming inflammation. Moreover, transgenic mice with overexpression of TGF-β are protected from renal fibrosis, establishing an anti-inflammatory role for this growth factor (25). These profibrogenic factors and pathways are not unique to kidney injury but are involved in any injury repair throughout the body.

Repair versus Fibrosis

Following a glomerular injury, macrophages may stimulate mesangial cells to secrete type IV collagen, laminin and fibronectin, which contribute to glomerulosclerosis and fibrosis. In addition, mesangial expansion causes narrowing or complete obliteration of glomerular capillaries, resulting in damage to podocytes in the glomeruli and a downstream effect on the peritubular capillaries causing ischaemia to the tubules. The infiltrating leukocytes continue to secrete proinflammatory mediators and activated renal tubular cells also produce cytokines and chemokines, propagating the inflammatory effect. The resultant fibrosis is from both the proliferation of resident

fibroblasts and from epithelial to mesenchymal transformation of tubular epithelial cells. Finally in the terminal phase of the inflammatory process, there is cessation of the leukocytic infiltrate but continued synthesis of the extracellular matrix by the fibroblasts. Myofibroblasts contribute to the contraction of the fibrous tissue leading to a shrunken kidney, as is often found in end stage renal failure.

Monocytes/Macrophages in Inflammation

The leukocytic infiltrate is paramount to the inflammatory response and monocytes and macrophages make up an important component of this infiltrate. Traditionally monocytes have been described as the circulating mononuclear leukocytes, which then mature into macrophages upon infiltration into tissues. It is now recognised that there is also a reservoir of monocytes in the spleen that has the potential to be rapidly deployed to sites of injury, prior to the increase in bone marrow derived monocytes (26). Monocytes transdifferentiate into macrophages, dendritic cells or osteoclasts, dependent on the local environment. Human monocyte subsets are distinguished by the expression patterns of CD14 and CD16, ($CD14^{++}CD16^{-}$ classical, $CD14^{+}CD16^{++}$ nonclassical and $CD14^{++}CD16^{+}$ intermediate). Mouse monocyte subsets have also been described, distinguished largely by the markers Ly6C (or Gr1), CCR2 and CX_3CR1 (27). Approximately 40% of murine monocytes are $Ly6C^{lo}CX_3CR1^{hi}CCR2^{-}$ and 60% are

$Ly6C^{hi}CX_3CR1^{lo}CCR2^+$. These distinct populations have different functions, many of which are not fully elucidated.

Monocytes are derived from macrophage/dendritic cell progenitors (MDPs) in the bone marrow and egress from the bone marrow in a CCR2 dependent manner (27, 28). They have a short half-life in the circulation of 1 day in mice and about 3 days in humans with longer half-lives being noted for $CX_3CR1^{hi}Ly6C^{lo}$ monocytes compared to the $CX_3CR1^{lo}Ly6C^{hi}$ subgroup (27, 29). Generally $CX_3CR1^{lo}Ly6C^{hi}$ monocytes are termed inflammatory whereas $CX_3CR1^{hi}Ly6C^{lo}$ monocytes are thought to be non-inflammatory but this is a gross over-simplification. In adoptive transfer studies of $CX_3CR1^{lo}Ly6C^{hi}$ monocytes into a non-inflammatory environment there was movement back into the bone marrow and these same monocytes switched to the $CX_3CR1^{hi}Ly6C^{lo}$ phenotype within 3 days and were again found in the circulation (30). It therefore seems likely that the differentiation of MDPs is not a terminal event.

Many studies have demonstrated an early increase in $CX_3CR1^{lo}Ly6C^{hi}$ monocytes in the first few days following a tissue injury, for example following myocardial infarction (31), skeletal muscle injury (32) and in liver injury (33). This is followed by an increase in $CX_3CR1^{hi}Ly6C^{lo}$ monocytes during the recovery phase. However, a further study provides evidence for very early recruitment of $CX_3CR1^{hi}Gr1^{lo}$ monocytes in the first hour post-injury (34). This pivotal study demonstrated that $CX_3CR1^{hi}Gr1^{lo}$ monocytes crawl along the

endothelium in a lymphocyte function-associated antigen-1 (LFA-1) dependent manner, in a surveillance mode. Furthermore there was a sixfold decrease in this patrolling in CX_3CR1 deficient mice suggesting that CX_3CR1, via LFA-1, has an important role in the rapid immune response to injury and infection. This study also showed that the extravasated $CX_3CR1^{hi}Gr1^{lo}$ monocytes promoted the differentiation into classical macrophages, as discussed below, whereas $CX_3CR1^{lo}Gr1^{hi}$ monocytes, which arrive in the damaged tissue later in the process, promoted dendritic cell differentiation.

Macrophage subsets

Macrophage terminology has also evolved over the past decade. Macrophages are now classified into the subgroups M1 (classically activated) and M2 (alternatively activated), with M2 being further subdivided into M2a, M2b and M2c. Differentiation into a particular macrophage phenotype is dependent on the local cytokine milieu and each different phenotype produces a distinct profile of inflammatory agents and has unique surface markers (Table 1).

Table 1
Macrophage activation states and functions

Macrophage phenotype	Activation state	Stimuli	Phenotypic function	Cytokine and inflammatory profile	Unique surface markers
M1	Classical activation	IFN-γ + LPS, TNF, GM-CSF, TLR/IL-1R ligand	Proinflammatory Th1 response	IL-1, IL-12, IL-15, IL-18, IL-23, TNF-α, IL-6, MCP-1, CCL2, CCL3, CCL4, CCL20/MIP-3a ROS, NO, iNOS, NOS2	CD86, CD80, MHC class II^{hi}, IL-1R, IL-12^{hi}, IL-23^{hi}, IL-10^{lo}
M2	Alternate activation (M2a polarization)	IL-4 or IL-13	Th2 responses, type II inflammation	Fibronectin, BIG-H3, arginase-1, TNF-α, IL-6, IGF, CCL13/MCP-4, CCL22, CCL18, β2 integrins	Mannose receptor, scavenger receptor, MHC class II^{hi}, decoy IL-1R11, FIZZI/Ym-1
	Type II activation (M2b polarization)	Immune complex + TLR/IL-1R ligands	Immunoregulation, Th2 activation	IL-10, TNF-α, IL-1, IL-6, IL-12, SPHK1, CCL1	CD86, MHC class II^{hi}, IL-10^{hi}, IL-12^{lo}
	Deactivated (M2c polarization)	IL-10, TGF-β, glucocorticoids	Immunosuppression, matrix remodeling, tissue repair	IL-10, IL-1β, IL-6, TGF-β, ECM proteins, CCL16, CCL18, arginase-1	SLAM (CD150), mannose receptor, MHC class II^{lo}

BIG-H3, fasciclin domain 4 protein; MIP, macrophage inflammatory protein; SLAM, signaling lymphocytic activation molecule; SPHK1, sphingosine kinase 1. Note that *FIZZI* and *Ym1* gene expression is characteristic of the alternative pathway of macrophage activation.

From Macrophage diversity in renal injury and repair. Ricardo SD, van Goor H, Eddy AA. Journal of Clinical Investigation, 2008 118(11) 3522-3530.

Chemokines: regulators of injury

A leukocytic infiltrate is crucial to any inflammatory process and this requires signals to direct the extravasation of leukocytes to the site of injury. This signal is achieved by chemokines, which are a subgroup of the cytokine family and currently number approximately fifty. Most chemokines are small, secreted proteins (approximately 8-13 kDa), though two chemokines are larger transmembrane proteins (35, 36). The chemokines are classified into 4 groups; C, CC, CXC and CX_3C, based on the number of conserved cysteine residues and any amino acids between them, in the N-terminus. The major known role of chemokines is that of chemoattraction for leukocytes bearing the appropriate receptor but they are also involved in other processes such as cell migration in organogenesis, cell survival during inflammation,

leukocyte degranulation and anti-tumour immunity. The two known transmembrane chemokines, CX_3CL1 and CXCL16 also act as cell adhesion molecules (37-39). Tables 2 and 3 demonstrate the major chemokines with their known receptors and predominant functions.

Abbreviations used in tables 2 and 3:

MIP – macrophage inflammatory protein, MCP- macrophage chemoattractant protein, RANTES- regulated on activation, normal T expressed and secreted, HCC- haemofiltrate chemokine, TARC- thymus and activation-regulated chemokine, MDC- macrophage derived chemokine, SLC- secondary lymphoid-tissue chemokine, TECK- thymus-expressed chemokine, PF4- Platelet factor 4, BRAK- Breast and kidney expressed chemokine, ELC- Epstein Barr ligand chemokine, MEC- mammary-enriched chemokine, GCP- granulocyte chemotactic protein, COPD – chronic obstructive pulmonary disease, GRO- growth-regulated oncogene, ENA- epithelial cell derived neutrophil activating peptide, MIG- monokine induced by interferon-ζ, IP- interferon-inducible protein, I-TAC- interferon-inducible T-cell alpha chemoattractant, BCA-1- Bcell chemoattractant 1, SR-PSOX- scavenger receptor for phosphatidylserine-containing oxidized lipids, RA- rheumatoid arthritis, MS- multiple sclerosis, AS- atherosclerosis, IBD- inflammatory bowel disease.

Ligand	*Receptor(s)*	*Associated Disease(s) or Functional Pathway*
CCL1	CCR8	Granuloma formation, dendritic cell migration to lymph nodes, type 2 cellular immunity
CCL2 (MCP-1)	CCR2	Atherosclerosis, RA, MS, type 2 diabetes mellitus
CCL3 (MIP-1α)	CCR1	Rheumatoid arthritis, multiple sclerosis
CCL4 (MIP-1β)	CCR1, CCR5	RA, MS, HIV-1 co-receptor, transplant rejection
CCL5 (RANTES)	CCR5	HIV-1 co-receptor, transplant rejection, atherosclerosis
CCL6 (MRP-2)	CCR1	Allergy
CCL7 (MCP-3)	CCR2	Midbrain development
CCL8 (MCP-2)	CCR1, CCR2B, CCR5	MS
CCL9/CCL10 (MRP-2)	CCR1	
CCL11 (eotaxin)	CCR2, CCR3, CCR5	Allergic asthma, rhinitis
CCL12 (MCP-5)		
CCL13 (MCP-4)	CCR2, CCR3, CCR5	
CCL14 (HCC-1)	CCR1	SLE
CCL15 (MIP-5, HCC-2)	CCR1, CCR3	
CCL16 (HCC4)	CCR1, CCR2, CCR5, CCR8	
CCL17 (TARC)	CCR4	Parasitic infections, graft rejection, T-cell homing to skin
CCL18 (MIP-4)		
CCL19 (ELC)	CCR7	Transport of T cells and dendritic cells to lymph

		nodes, antigen presentation, cellular immunity
CCL20	CCR6	Allergic asthma, mucosal humoral immunity, intestinal T-cell homing
CCL21 (SLC)	CCR7	
CCL22 (MDC)	CCR4	Graft rejection, parasitic infection
CCL23 (MIP-3)	CCR1	
CCL24 (eotaxin-2)	CCR3	
CCL25 (TECK)	CCR9	Inflammatory bowel disease, homing of T cell and IgA^+ plasma cells to gut
CCL26 (eotaxin-$_3$)	CCR_3	
CCL27 (PESKY)	CCR10	T cell homing to intestine and skin
CCL28 (MEC)	CCR3, CCR10	T cell homing to intestine and skin

Table 2. The CC Family of Chemokines and Chemokine Receptors

Ligand	*Receptor(s)*	*Associated disease or Pathway*
CXCL1 (GRO-1)	CXCR2	Inflammatory lung disease, COPD, angiogenic for tumour growth
CXCL2 (GRO-2, MIP2α)	CXCR2	
CXCL3 (GRO-3, MIP2β)	CXCR2	
CXCL4 (PF4)	CXCR4B	
CXCL5 (ENA-78)	CXCR2	
CXCL6 (GCP-2)	CXCR1, CXCR2	Inflammatory lung disease, COPD
CXCL7		
CXCL8 (IL-8)	CXCR1, CXCR2	
CXCL9 (MIG)	CXCR3(A&B)	Inflammatory skin disease, transplant rejection, MS
CXCL10 (IP-10)	CXCR3(A&B)	Transplant rejection
CXCL11 (I-TAC)	CXCR3(A&B)	
CXCL12	CXCR4	HIV-1 co-receptor, tumour metastasis, haematopoiesis
CXCL13 (BCA-1)	CXCR5	Formation of B cell follicles, breast cancer
CXCL14 (BRAK)		
CXCL15 (lungkine)		
CXCL16 (SR-PSOX)	CXCR6	Inflammatory liver disease, AS
CXCL17		
XCL1 (lymphotactin α)	XCR1	RA, IgA nephropathy, tumour responses
XCL2 (lymphotactin β)	XCR1	
CX_3CL1 (fractalkine)	CX_3CR1	Atherosclerosis, renal inflammatory disease, RA, IBD

Table 3. The CXC, XC and CX_3C Families of Chemokines and Chemokine Receptors

Chemokine and Receptor Binding

The chemokine repertoire produced by a particular cell and the local environmental conditions influencing this production, will determine the type(s) of leukocytes that will be recruited. CXC chemokines with a glutamic acid-leucine-arginine (ELR) residue preceding the CXC sequence are chemoattractant for neutrophils and promote degranulation, whereas non-ELR CXC chemokines are attractant for lymphocytes. Other chemokines such as many of the CC chemokines attract largely T cells and dendritic cells. The CX_3C chemokine attracts monocytes and natural killer cells in addition to some T cells.

Chemokines bind to 7 transmembrane domain G protein-coupled receptors. Ligand binding results in a conformational change in the receptor and allows guanosine diphosphate (GDP) to be exchanged for guanosine triphosphate (GTP) in the $G\alpha$ subunit. This subunit then dissociates from the $G\beta\gamma$ subunit and both subunits stimulate various distinct intracellular signalling pathways. There are more than 20 chemokine receptors and there is often more than one receptor for any one ligand and conversely, often more than one ligand for any given receptor. There is thought to be significant functional redundancy as a specific function may be initiated by more than one receptor/ligand pair. Adding to the complexity of chemokine system is the fact that many of the chemokine receptors form homo- and hetero-oligomers (40). This can have the effect of amplifying or inhibiting a particular response. Chemokine receptors may even cross talk, directly or

indirectly, with other signalling pathways further extending the number of possible permutations resulting in a particular signal. In view of this, there may be less functional redundancy than was originally suggested and the formation of oligomers may contribute to the specificity of a response. Adding to the broad spectrum of chemokine mediated responses are the presence of splice variants and extensive posttranslational modifications of the proteins.

At sites of inflammation chemokines are secreted by; injured tissues, resident and recruited leukocytes and cytokine activated endothelial cells. Soluble chemokine retention in the inflamed environment is achieved by binding to local cell surface or matrix glycosaminoglycans, thus creating a chemokine gradient. In this way, endothelial cells attract and bind leukocytes with the cognate chemokine receptor, rolling over the endothelial surface. Activation of this receptor induces integrin receptor expression on the leukocyte, which then interacts with integrin receptor ligands on the endothelial cell, such as intercellular cell adhesion molecule 1 (ICAM-1), resulting in firm adhesion of the leukocyte with subsequent diapedesis into the injured tissue. The two transmembrane chemokines, CXCL16 and CX_3CL1, are able to effect leukocyte adhesion directly by the association of the chemokine domain with its receptor. In addition, these chemokine cell adhesion molecules also stimulate integrin expression, promoting leukocyte adhesion in the same manner as the soluble chemokines (41). Resident leukocytes are activated by the local secretion of cytokines and chemokines, with

binding of leukocytes to chemokines bound to matrix glycosaminoglycans.

Circulating chemokines can also bind to "silent" or "decoy" chemokine receptors such as Duffy Antigen Receptor for Chemokines (DARC), D6 and CCXCKR (42). These receptors are not G protein coupled, despite having a 7 transmembrane domain phenotype. They are apparently non-signalling and are thought to be important for the transcytosis of chemokines. Chemokine binding to decoy receptors may also act as a chemokine reservoir although this function has not been conclusively proven.

Some chemokines, rather than being inflammatory, have a more homeostatic role. Production of these chemokines, for example by high endothelial venules (HEV), does not require activation of the source cell. These chemokines are often referred to as lymphoid chemokines as they are primarily involved in lymphoid tissue interactions such as homing of naïve T cells or the follicular localisation of B cells (43). Chemokines are important for both T and B cell activation and function. They play a role in all aspects of the immune response including emigration of cells from the bone marrow, homing of cells to the lymph nodes and spleen, the chemoattraction of naïve T cells to dendritic cells and the colocalisation of cells required to orchestrate a particular immune response.

CX_3CL1 (Fractalkine)

CX_3CL1 (fractalkine), or neurotactin as it was originally termed in the mouse, is the only known member of the CX_3C subgroup of chemokines and was first described in 1997 (35, 44). The full-length protein is transmembrane and has a total of 373 amino acids. It consists of a 76 amino acid extracellular chemokine domain attached to a long mucin stalk, a 19 amino acid transmembrane domain and a 37 amino acid intracellular tail, as shown in figure 1. It has just one known receptor, CX_3CR1.

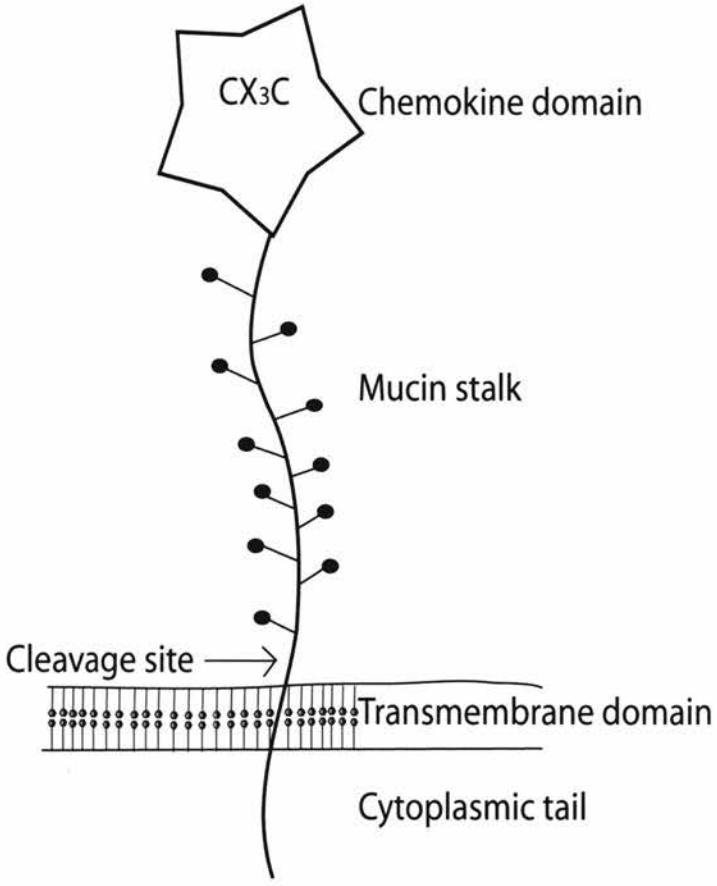

Figure 1. The structure of CX_3CL1.

CX_3CL1 in renal diseases

Despite numerous aetiologies, most renal diseases culminate in a common pathway of fibrosis often associated with a leukocyte, particularly a macrophage infiltration. Given that CX_3CL1 is chemotactic for macrophages, it is reasonable to assume that CX_3CL1/CX_3CR1 would play a role in both acute and chronic renal inflammation and fibrosis. Indeed this has been found to be the case in many differing renal pathologies. In 1998 Chen *et al* published the first experimental data showing that inhibition of CX_3CL1 with the viral protein vMIPII, a chemokine analogue encoded by the human herpes virus 8, attenuated the leukocytic infiltration and subsequent proteinuria in a rat model of anti-glomerular basement membrane (anti-GBM) glomerulonephritis (45). The same group also showed that an antibody to CX_3CR1 was even more effective at reducing the inflammatory response in the same model of anti-GBM disease (46). Since then a body of work has been published demonstrating the involvement of CX_3CL1/CX_3CR1 in numerous models of renal diseases and renal pathophysiology as highlighted below.

CX_3CL1 in the embryonic kidney

In the developing kidney Grone *et al* found CX_3CL1 in the nephrogenic blastema, around the S shaped structure, in the mesangium of the

developing glomerulus, in the venous and arterial endothelium, in the medial smooth muscle cells and in the distal tubule and collecting ducts (47). They also found CXCL10 and CXCL12 in the developing human kidney and suggested that chemokines may be involved in the fine-tuning of nephrogenesis and further hypothesised that the same chemokines may be important in the adult kidney, playing a role in tissue regeneration. Segerer *et al* looked more specifically at CX_3CR1 distribution and found that it was present in human fetal kidneys, between 8 and 17 weeks gestation, but with no clear pattern for specific areas of the developing nephron or different stages of development (48).

CX_3CL1 in renal inflammatory conditions

The expression of CX_3CL1 mRNA and CX_3CL1 protein secretion was investigated by Cockwell *et al*, in human biopsy specimens with vasculitic glomerulonephritis (predominantly glomerular inflammation), acute renal allograft rejection (predominantly tubulointerstitial inflammation), non-inflammatory glomerulonephritis (minimal change nephrotic syndrome) and normal renal tissue (49). They found that in the inflammatory conditions, CX_3CL1 localised to the inflamed compartment and correlated strongly with macrophage infiltration. Several studies have used the anti-thy1.1 antibody model of mesangial proliferative glomerulonephritis in rats to assess the role of CX_3CL1 in renal disease (50, 51). The first of these set out to examine why uni-nephrectomy prior to injection of the anti-thy1.1 antibody

results in more prolonged renal alterations. They found that uni-nephrectomised animals had no difference in complement deposition, mesangiolysis or expression of CCL2, CCL5, CCL17 or lymphotactin but there was a significant increase in CX_3CL1 production on day 14 when compared to sham operated rats. This was accompanied by an increase in CX_3CR1 mRNA expression. A further experiment using two injections of anti-thy1.1 antibody in non-nephrectomized rats also resulted in increased CX_3CL1 expression and worse renal injury suggesting that CX_3CL1 has a role in chronic injury. The second study using this model showed that activated mesangial cells were the major source of CX_3CL1 production and although increased mRNA was detected as early as 2 hours post injection, there was no significant increase in protein until 3 days later, whereas CCL2 production increased earlier and waned earlier, suggesting that CCR2+ and CX_3CR1+ leukocytes are recruited at different time points in this disease (51).

Despite several studies suggesting a pro-inflammatory role for CX_3CL1/CX_3CR1 in renal diseases in rats and humans, Haskell *et al* found no difference in the degree of proteinuria or renal injury in CX_3CR1-/- mice compared to wild type mice, following nephrotoxic serum induced glomerulonephritis (52). This could be due to a species-specific effect or because of differences in the experimental protocols.

In human biopsy specimens of class III and IV lupus nephritis, but not in the less severe class I or II nephritis, there was increased glomerular

production of CX_3CL1 with associated increased numbers of CD16+ monocytes, which characteristically have moderate to high CX_3CR1 expression (53). Furthermore the CX_3CL1 expression significantly correlated with the histopathologic activity index, a measure of the activity and chronicity of the inflammation and the CD16+ monocyte count correlated with the clinical disease severity. Inoue *et al* had earlier used a mouse model of lupus nephritis to show that glomerular CX_3CL1 was significantly increased and the use of a CX_3CL1 truncated analogue before or during the early stages of the renal inflammation reduced the glomerular hypercellularity, glomerulosclerosis, crescent formation and vasculitis when compared to control animals, by reducing the macrophage infiltration (54).

In 23 human biopsy samples of crescentic glomerulonephritis Furuichi *et al* found interstitial but not glomerular CX_3CL1, whereas CD16+ cells were found in both areas of the kidney (55). Interestingly, steroid treatment reduced the amount of CX_3CL1 but had no effect on the number of CD16+ cells, suggesting a more acute role for CX_3CL1 in crescent formation.

CX_3CL1 in haemolytic uraemic syndrome.

More recently CX_3CL1/CX_3CR1 has been implicated in the pathophysiology of haemolytic uraemic syndrome (HUS). Ramos *et al* noted a more than 50% decrease in circulating mononuclear leukocytes (monocytes, natural killer (NK) cells and NK Tcells) expressing CX_3CR1

in children with HUS and the lowest levels of circulating CX_3CR1^+ leukocytes correlated with the most severe renal failure (56). The authors postulated that CX_3CL1 on activated endothelial cells interacts with CX_3CR1^+ cells, removing them from the circulation and contributing to renal injury in this disease. A further study has expanded on this and found that one of the toxins responsible for HUS, Shiga toxin-2, does indeed stimulate endothelial cell CX_3CL1 expression and additionally the toxin triggers CX_3CL1 mediated leukocyte adhesion (57).

CX_3CL1 in transplantation.

The first studies to suggest a role for CX_3CL1 in transplant rejection were done in murine cardiac allograft models. CX_3CL1 was increased, particularly in vascular tissues and endothelium during rejection and treatment with an anti-CX_3CR1 antibody brought about a 7-fold increase in allograft survival (58). A further study found no difference in the graft survival times between $CX_3CR1^{-/-}$ and $CX_3CR1^{+/+}$ mice receiving heterotopic heart transplants with no immunosuppression, but in the presence of subtherapeutic levels of cyclosporin there was a significant improvement in graft survival in the knockout mice, which was associated with a decrease in infiltrating macrophages, natural killer cells and other leukocytes (52). Several studies have examined the role of CX_3CL1/CX_3CR1 in renal allograft rejection. The initial papers described CX_3CL1 detected by immunohistochemistry, on a proportion

of tubules in human acute rejection, compared to negligible staining in control kidneys (49, 59). CX_3CL1 was detected on both the basolateral and the apical membranes of these tubular epithelial cells (59). Segerer *et al* investigated the presence of CX_3CR1 in acute renal allograft rejection, again in humans, and found that CX_3CR1 staining correlated with a subset of infiltrating cells (48). Another study examined the gene expression of CX_3CL1 in 12 biopsies from laser dissected renal allografts with histological evidence of acute rejection and 10 control biopsies. They found a marked increase in both the tubular and glomerular expression of CX3CL1 mRNA in rejection, as quantified by real-time PCR but there was a large variation between samples (60). More recently Peng *et al* have used enzyme-linked immunosorbent assays (ELISA) to measure urinary CX_3CL1, CXCL9, CXCL10, CCL23, granzyme B and perforin levels in 215 renal allograft recipients and 80 healthy controls (61). They found that all the chemokines were increased in acute rejection but CX_3CL1 was the only good discriminator between acute rejection and acute tubular necrosis. Furthermore CX_3CL1 levels were the best predictors of steroid resistant rejection and graft loss. One final study examined CX_3CL1 staining by immunohistochemistry in hyperacute, acute and chronic renal allograft rejection and found markedly increased levels of CX_3CL1 in the tubulointersitium in chronic rejection in comparison to the other 2 groups. Moreover they found CX_3CL1 in more than 80% of tubules in

chronic rejection compared to less than 50% of acutely rejecting tubules (62).

A couple of studies have tried to identify possible genetic polymorphisms in CX_3CR1 that are associated with allograft rejection, one in cardiac transplantation and the other in renal transplantation, but both studies had negative results (63, 64).

CX_3CL1 in renal ischaemia-reperfusion injury.

Various groups have examined the role of CX_3CL1/CX_3CR1 in ischemia-reperfusion injury. Furuichi *et al* used CX_3CR1 knockout mice to show that there was no difference in the initial area of acute tubular necrosis, the number of infiltrating neutrophils or the number of infiltrating lymphocytes between these mice and the wild type mice following 60 minutes of ischemia with subsequent reperfusion (65). They did however find 40% fewer infiltrating macrophages on day 7 post ischemia, an effect that was lost by day 14. They found no difference in the expression of other chemokines, TGF-β levels or platelet accumulation between the two groups but found significantly lower levels of PDGF-β in the CX_3CR1 knockout mice at both 24 and 48 hours post-injury. PDGF is a recognised stimulant of fibroblast proliferation and extracellular matrix production. They also found that the deterioration in renal function at day 14 was 25% less in the knockout mice. Given that there were no significant early findings the authors concluded that CX_3CR1 was important for renal fibrosis but not for

acute tubular necrosis. These results are in contrast to those of Oh *et al* who demonstrated mainly endothelial localised CX_3CL1 following acute renal ischemia from as early as 8 hours post reperfusion (66). They also found decreased infiltrating macrophages at 24 hours in mice pre-treated with anti-CX_3CR1 antibody, though this effect was modest in comparison to the use of clodronate to inhibit macrophage infiltration. There was no effect of the anti-CX_3CR1 antibody on tubular cell apoptosis and the conclusion was therefore that CX_3CR1 was protective by inhibition of tubular necrosis. This group did not look beyond a 24 hour time-point.

In a more recent article, Li *et al* used $CX_3CR1^{+/GFP}$ mice and demonstrated that renal dendritic cells, positive for CD11b, CD11c and MHC II, comprised 85% of the GFP^+ cells (67). They induced ischemia and at 3 and 24 hours after reperfusion found an increase in inflammatory renal macrophages, ($F4/80^{lo}$, Ly-$6C^{hi}$, Gr-1^{int} and CX_3CR1^{lo}). At 3 hours the $F4/80^{lo}$ macrophages were Ly$6C^{high}$, representing immature monocytes recently emigrated from the bone marrow. By 24 hours there was down-regulated Ly6C expression. To further investigate the role of chemokines and chemokine receptors in ischemia reperfusion they used CCR2 knockout mice and in addition created chimeras using $CCR2^{-/-}$ and $CCR2^{+/+}$ cells transfused into $CCR2^{+/+}$ mice previously treated with bone marrow ablation. This technique confirmed that CCR2 promoted the macrophage infiltration and renal damage following ischemia reperfusion injury and this was

due to both CCR2 dependent monocyte emigration from bone marrow and to CCR2 dependent monocyte infiltration into injured kidney. Added to this finding was the fact that CX_3CR1 deficient mice also developed less tubular necrosis and mice were shown to require CX_3CR1 in addition to CCR2 for monocyte recruitment to the re-perfused kidney following ischemic damage. This finding was in keeping with the previous observations that CCR2 is essential for the emigration of monocytes from the bone marrow (28) and that CCR2, CCR5 and CX_3CR1 mediate the differential infiltration of monocyte subsets into atherosclerotic plaques (68, 69).

Chronic hypoxia has been postulated as a final common pathway to renal failure and is supported by a substantial literature (70). Hypoxia leads to tubular cell apoptosis and EMT, which in turn promote fibrosis and further ischemia. Hypoxia also results in the generation of reactive oxygen species in the tubulointerstitium and this has been shown to be the mechanism of increased CX_3CR1 expression in human renal fibroblasts (71). Koziolek *et al* examined human renal biopsy specimens and found markedly increased levels of CX_3CR1 in fibrotic kidneys compared to normal controls. Furthermore, they demonstrated over 4 times more CX_3CR1 positive cells than co-labelled infiltrating lymphocytes (CD3) or macrophages (CD68). They found that CX_3CR1 was also produced by renal tubular cells, dendritic cells and myofibroblasts. CX_3CR1 expression was not increased by pro-inflammatory or pro-fibrotic cytokines such as IL-1β, TNF-α, PDGF,

EGF, FGF-2 or TGF-β, but it was increased by hydrogen peroxide. The group went on to show that CX_3CL1 induced cell motility in renal fibroblasts, in much the same way as it induces vascular smooth muscle cell motility in atherosclerosis (72).

Regulation of CX_3CL1

The CX_3CL1 gene is found on chromosome 16 (35, 73). It is under the control of proinflammatory stress-responsive transcription factors such as Nuclear Factor-κB (NF-κB), Signal Transducer of Activated Transcription-1 (STAT-1) and Activating Protein-1 (AP-1) (74-77). CX_3CL1 is activated by inflammatory agents such as Tumour Necrosis Factor-alpha (TNF-α), Interleukin-1 (IL-1), lipopolysaccharide (LPS) and Interferon-gamma (IFN-γ) (35, 78, 79). Stimulation with TNF-α and IFN-γ is synergistic in several cell types including astrocytes and smooth muscle cells (80, 81).

NFκB and MAPK signalling pathways in CX_3CL1 activation.

In the resting state NFκB is found in the cytoplasm, bound to the inhibitory protein, inhibitor-kappa B-alpha (IκBα). Upon activation in response to various signals from cytokines and other molecules, IκB is phosphorylated, ubiquitinated and subsequently broken down in a proteosome-dependent manner. The unbound NFκB is then able to translocate to the nucleus, where it binds to specific promoter regions

and induces gene transcription. This mechanism has been studied in various cell types with regard to stimulation of CX_3CL1 gene transcription. Garcia *et al* used a dominant negative form of IκBα and various inhibitors of NFκB to demonstrate the role of NFκB induced transcription of CX_3CL1 in rat aortic endothelial cells (74). Chen *et al* specifically examined the intracellular signalling involved in TNF-α induced production of CX_3CL1 in rat mesangial cells and again found that NFκB induced transcription was one of the responsible mechanisms for CX_3CL1 production (76). Further stimulation of CX_3CL1 production, in various cell types, is achieved via Mitogen Activated Protein Kinases (MAPK) such as the extracellular signal-regulated kinases (ERK1/2), c-Jun N-terminal kinases and p38, which respond to extracellular stimuli, including TNF-α, IL1-β and LPS (76, 82, 83). MAPK intracellular signalling is involved in the regulation of various cell functions such as gene expression, cell proliferation, chemokine production, secretion of growth factors and cell survival. Chen *et al*, in addition to showing NFκB induced transcription of CX_3CL1 following TNF-α stimulation, also found that inhibitors of protein kinase C (PKC) and p42/44 mitogen activated protein kinase (MAPK) attenuated expression of CX_3CL1 mRNA and protein in mesangial cells and they demonstrated that AP-1 is also involved. More recently Wu *et al* discovered that connective tissue growth factor (CTGF) stimulates CX_3CL1 production in cultured human mesangial cells via the ERK1/2, phosphoinositol-3-

kinase (PI3K)/protein kinase B and NFκB pathways and another group demonstrated that IL-1β stimulation of astrocytes activated p38 and ERK1/2 to induce CX_3CL1 production (83, 84).

IFN-γ pathways in CX_3CL1 activation.

Interferon-gamma induced CX_3CL1 production is not mediated by NFκB but instead uses STAT-1 (85, 86). In some cells IL-1β is synergistic with IFN-γ to promote CX_3CL1 production (86). Interferon-γ is produced primarily by activated T lymphocytes, but is also secreted by natural killer cells, dendritic cells and natural killer T cells. It is the characteristic type 1 T helper cell cytokine. It binds to a heterodimeric receptor made up of interferon gamma receptors 1 and 2. (INF-γ additionally binds to cell surface heparan sulphate proteoglycans, which inhibit its biological activity.) Engagement of the cytokine activates the receptor associated Janus Activated Kinase-1 (JAK1), which acts as a tyrosine kinase and results in the phosphorylation of the cytoplasmic domain. This allows the recruitment of a STAT molecule, which is then tyrosine phosphorylated. The stimulated STAT molecules are released into the cytoplasm where they form dimers and translocate to the nucleus. STATs bind to specific Ges sites on the enhancer or promoter regions of genes and induce transcription. Although there are 4 JAK proteins and 7 STATs, to date only STAT-1 and JAK-1 are associated with IFN-γ induced activation of CX_3CL1 transcription (77, 87).

Signalling pathways repressing CX_3CL1 expression.

Several factors are known to negatively regulate CX_3CL1 production. Interferon- γ induced CX_3CL1 production in human umbilical vascular endothelial cells (HUVECs) is reversibly inhibited by hypoxia and this is associated with a concomitant increase in vascular endothelial growth factor (88).

The interleukin-6 receptor has a cytokine binding α subunit (IL-6Rα) and a transmembrane signalling gp130 subunit. IL-6Rα is produced by leukocytes. In activated neutrophils the soluble form of IL-6Rα (sIL-6Rα) is shed from the transmembrane form. In HUVECs sIL-6Rα inhibits IL-1 or IFN-γ induced CX_3CL1 expression, whereas it augments the expression of other chemokines and adhesion molecules such as CXCL8, E-selectin and VCAM-1 (89, 90).

A metabolite of prostaglandin D2, 15-Deoxy-$\Delta^{12,14}$-prostaglandin J_2 (15d-PGJ_2), is an agonist for peroxisome proliferator-activated receptor-γ (PPAR-γ). It inhibits endothelial CX_3CL1 expression, however this effect is likely to be independent of PPAR-γ, as other agonists did not have the same effect (91). The down-regulation of CX_3CL1 may be due to an inhibitory effect on NF-κB, AP-1 and STAT-1 (82).

Heparin inhibits IFN-γ induced CX_3CL1 expression but not IL-1β induced expression. This is due to heparin binding directly to IFN-γ and preventing binding to its receptor (77).

Cleavage of CX_3CL1

Garton *et al* in 2001 performed a pulse-chase experiment with CX_3CL1 and found that it was synthesised as a 50-75kDa protein that matured, most likely by glycosylation, to a 100kDa protein in the membrane. From this full-length protein, a soluble protein of approximately 85kDa was released and a 15-20kDa portion remained in the cell (92). Both this group and Tsou *et al* went on to show that CX_3CL1 is cleaved just proximal to the transmembrane domain inducibly by a disintegrin and metalloprotease-17 (ADAM-17), also known as tumour necrosis factor-α converting enzyme (TACE) (92, 93). This shedding of CX_3CL1 is stimulated by phorbol-12-myristate-13-acetate (PMA), which is a protein kinase C agonist. TACE cleaves numerous other proteins such as TNF-α, transforming growth factor-α (TGF-α), L-selectin and IL-6. CX_3CL1 is also constitutively cleaved by another metalloprotease ADAM-10 (94). There are thought to be numerous cleavage sites close to the proximal transmembrane domain and it is not clear if these have any physiological relevance. There are also other pathways involved in the cleavage of CX_3CL1 to lesser degrees, as inhibiting metalloproteases does not completely abrogate the ectodermal shedding of the chemokine (94, 95). More recently Dean and Overall have shown that CX_3CL1 is a substrate for the matrix metalloproteinase -2 (MMP2) (96). MMPs were initially thought to simply degrade extracellular matrix, however they are now known to contribute to the homeostatic regulation of the

extracellular environment and influence cell signalling pathways. MMP-2 cleaves CX_3CL1 in at least 4 regions and interestingly this cleavage is mainly in the chemokine domain, as shown in figure 2. Furthermore, a N-terminal truncation of the chemokine domain resulted in loss of chemotactic function and in fact acted as a potent antagonist of the CX_3CL1 receptor (96). The lysosomal cysteine protease cathepsin S has also been shown to cleave CX_3CL1 in neurological cells (97).

Subsequent work has provided evidence for the recycling of CX_3CL1 between the cell membrane and an intracellular compartment (98). This has been shown to protect CX_3CL1 from rapid cleavage at the membrane and provides a quickly accessible reservoir of full-length chemokine when required (99).

Figure 2. Cleavage of CX_3CL1.

A schematic of CX_3CL1 showing the various cleavage sites (arrows), by MMP-2 (1-4) or ADAM 10 and ADAM 17. (Taken from RA Dean and CM Overall. Molecular and Cellular Proteomics 6.3 (2007) 611-623.

CX_3CR1 – the receptor for CX_3CL1

CX_3CR1 is the only known chemokine receptor for CX_3CL1, although US28, the promiscuous cytomegaloviral receptor also binds to CX_3CL1, as it does to many other chemokines (100, 101). The gene for CX_3CR1 is on chromosome 3, in common with many other chemokine receptor genes. CX_3CR1 is expressed on natural killer cells, monocytes and subsets of CD3+ T cells, which are largely CD8+, as well as several types of intrinsic cells such as synovial cells, vascular smooth muscle cells and bowel epithelial cells (37, 81, 102-106). More recently, CX_3CR1 was found to be expressed on endothelial cells (107, 108). CX_3CR1 is also a co-receptor for the human immunodeficiency virus-1 (HIV-1), albeit a weaker co-receptor than CCR5 (103), although receptor isoforms, with extended N-terminal regions have been identified that are more potent HIV co-receptors than the standard CX_3CR1 isoform (109).

CX_3CL1 chemotaxis and cell adhesion.

CX_3CL1 chemotaxis involves signalling of receptor-coupled pertussis toxin sensitive G proteins (37). The cell adhesion properties of CX_3CL1 are somewhat more complex and are both G protein dependent and

independent (37, 108). CX_3CL1 promotes cell adhesion both directly by interaction with cells bearing CX_3CR1 and indirectly by up-regulating expression of integrins such as Intercellular Adhesion Molecule-1 (ICAM-1) (37-39, 41). The integrin independent mechanism does not follow the model of cell rolling, activation and subsequent capture and diapedesis, as shown in figure 3A, but rather involves the capture of circulating activated leukocytes bearing the CX_3CR1 receptor and the firm binding of these directly to CX_3CL1 (figure 3B) (38). Furthermore, CX_3CL1-dependent, integrin-independent cell adhesion does not require calcium or an opposing cell membrane, is G-protein independent and occurs under conditions of physiological flow with a slower off-rate than is seen with most chemokine and receptor interactions (37-39, 41, 110). The exact mechanism is not fully understood but cell adhesion critically requires the chemokine domain and it is proposed that the role of the mucin-like stalk is to provide a way of distancing the chemokine domain from the endothelial wall, promoting its contact with circulating leukocytes (111). However other authors have suggested that the unique structure of CX_3CL1 alone, with prominent exposure of the chemokine domain is not sufficient to explain its robust cell adhesion properties and that perhaps the mucin-like stalk may play a role that has still to be fully elucidated (37, 110). CX_3CL1 also increases expression of integrins such as ICAM-1 and Yang *et al* demonstrated that this effect in endothelial cells is mediated via pertussis toxin

sensitive CX_3CR1, which results in activation of the Jak2/Stat 5 pathway (112).

Finally, CX_3CR1 plays a pivotal role in the crawling of $CX_3CR1^{hi}Gr1^{lo}$ monocytes along the endothelium lining in a surveillance role, with rapid extravasation into injured tissues and initiation of the innate immune response (34).

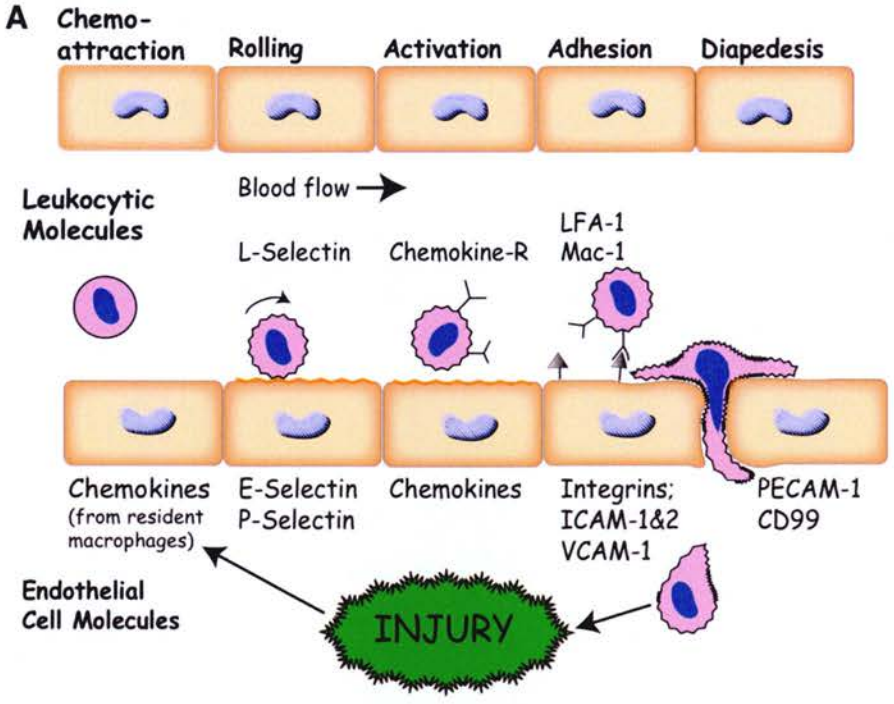
A
Chemo-attraction
Rolling
Activation
Adhesion
Diapedesis
Leukocytic Molecules
Blood flow
L-Selectin
Chemokine-R
LFA-1
Mac-1
Chemokines (from resident macrophages)
E-Selectin
P-Selectin
Chemokines
Integrins; ICAM-1&2 VCAM-1
PECAM-1 CD99
Endothelial Cell Molecules
INJURY

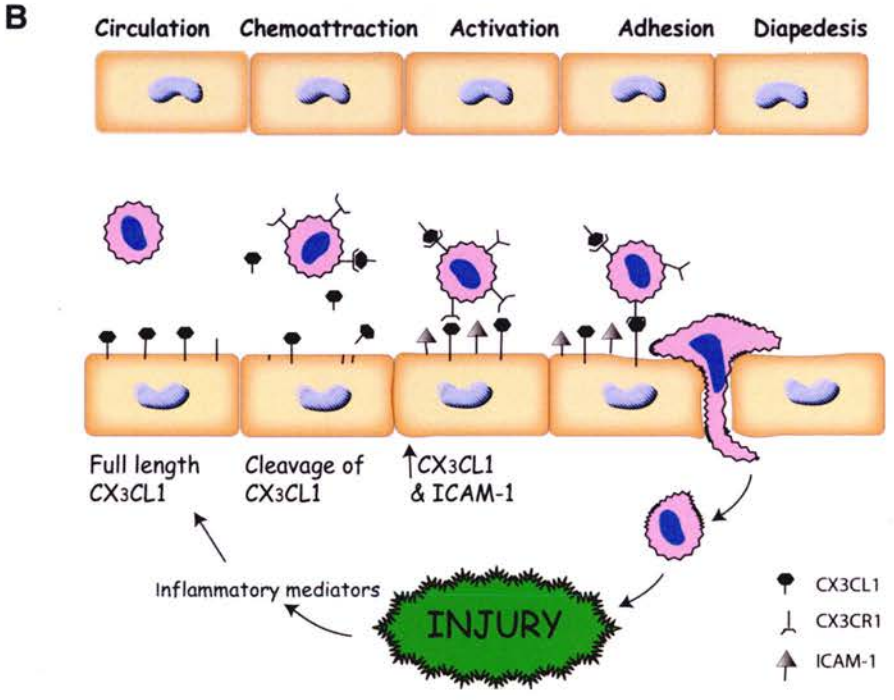
B
Circulation
Chemoattraction
Activation
Adhesion
Diapedesis
Full length CX3CL1
Cleavage of CX3CL1
CX3CL1 & ICAM-1
Inflammatory mediators
INJURY
CX3CL1
CX3CR1
ICAM-1

Figure 3. Mechanisms of leukocyte adhesion to the endothelial wall. A) The conventional method with leukocyte cell rolling followed by activation and subsequent interactions between selectins and integrins. After firmly adhering to the endothelium, the leukocyte diapedeses into the injured tissue. B) Circulating leukocytes expressing CX_3CR1 are stimulated by soluble CX_3CL1. These leukocytes then bind directly to transmembrane CX_3CL1 expressed by the endothelium before diapedesis into the tissues. Leukocytes may also bind to other adhesion molecules on the endothelial surface. Chemokine-R denotes chemokine receptor, E-selectin Endothelial-selectin, P-selectin platelet-selectin, LFA-1 lymphocyte function associated antigen-1, Mac-1 macrophage antigen-1, VCAM-1 vascular cell adhesion molecule-1, ICAM 1,2 intercellular adhesion molecule 1,2, PECAM-1 platelet cell adhesion molecule-1, CD99 cluster of differentiation 99.

CX_3CL1 in non-renal disease.

CX_3CL1 is expressed on both endothelial and epithelial cells, in addition to certain other cell types eg. mesangial cells, macrophages and dendritic cells (35, 113-116). It is found throughout the body and is particularly prominent in the nervous system where it is constitutively expressed in the olfactory bulb, cerebral cortex and hippocampal areas. It plays a role in neuronal migration and is implicated in the pathogenesis of neurodegenerative diseases, for example in a model of Parkinson's disease, CX_3CR1 deficient mice developed worse neurotoxicity (117-120). CX_3CL1 is up-regulated in a wide variety of inflammatory conditions including asthma, psoriasis, Crohn's disease, rheumatoid arthritis, atherosclerosis and transplant rejection (52, 58, 104, 105, 121-124). CX_3CL1 plays a prominent role in atherosclerosis,

along with CCL2. Studies using mice genetically modified to be deficient in either CX_3CL1 or CX_3CR1 revealed significantly less atherosclerosis compared to control animals under similar conditions (125-127). Furthermore, the knockout of both CX_3CR1 and CCR2 has an additive effect, supporting the concept of independent roles for each chemokine (125, 128). Tacke *et al* took this work further demonstrating that although both CX_3CR1^{hi} and CX_3CR1^{lo} monocyte subsets enter atherosclerotic plaques only $CCR2^{+}CX_3CR1^{lo}Ly6C^{hi}$ monocyes required CX_3CR1 for their entry into the plaques whereas $CCR2^{-}CX_3CR1^{hi}Ly6C^{lo}$ monocytes were partially dependent on CCR5 for their entry (68). Smooth muscle cell proliferation is another component of atherosclerosis and the CX_3CL1/CX_3CR1 axis is involved at several levels. CX_3CL1 is produced by aortic smooth muscle cells and promotes the adhesion of monocytes (81). Lucas *et al* showed that human aortic smooth muscle cells also produce CX_3CR1 and these cells are capable of migrating towards CX_3CL1 along a chemokine gradient, facilitating their accumulation within the atheroma (72). In addition to the association between atherosclerotic monocytes, smooth muscle cells and CX_3CL1, Schafer *et al* showed that CX_3CL1 contributes to *in vitro* platelet activation and adhesion, by increasing P-selectin expression, via a pertussis toxin sensitive pathway (129). This effect is blocked by aspirin, nitric oxide and sodium nitroprusside. Adenosine diphosphate (ADP) is also known to stimulate platelets and P-selectin production. Although blocking ADP with apyrase decreased the effect of CX_3CL1 stimulation

on P-selectin expression and platelet degranulation, it did not affect platelet adhesion, suggesting that co-stimulation of ADP and CX_3CL1 induces P-selectin expression. The same group went on to demonstrate that both soluble and membrane bound CX_3CL1 stimulate platelet degranulation and P-selectin expression and that platelets are critical for the CX_3CL1 induced adhesion of leukocytes to endothelial cells under high shear conditions (130) thus providing further weight to the argument for the importance of this chemokine in inflammation.

Protective effects of CX_3CL1/CX_3CR1.

CX_3CR1-mediated signals are essential for intraperitoneal bacterial clearance in a model of septic peritonitis induced by cecal ligation and puncture, in mice (131). In this model there was a similar degree of peritoneal leukocytic infiltration comparing wild type and CX_3CR1 knockout mice but there was a more than doubling of the mortality rate (75% v 33%) in the deficient mice. CX_3CL1 was found to stimulate the gene expression of IL-1β, TNF-α, IFN-γ and IL-12, which are pro-inflammatory cytokines. There was attenuated bactericidal phagocytosis by neutrophils and macrophages in the CX_3CR1 deficient mice associated with reduced intraperitoneal inducible nitric oxide synthase activity. This study provides evidence for the role of CX_3CL1/CX_3CR1 in the optimisation of bactericidal host defence. CX_3CL1 plays a significant role in wound healing and importantly, CX_3CR1 seems to have a substantial role in anti-tumour responses in mice, a function

which may well extrapolate into humans (132, 133). Ishida *et al* examined the role of CX_3CL1/CX_3CR1 in skin wound healing in mice (133). They found that both were increased following a skin injury and that CX_3CR1 knockout mice had delayed wound healing. This was due to a decreased macrophage infiltration in the knockout mice with subsequent decreased macrophage products such as TGF-β and vascular endothelial growth factor (VEGF). Furthermore there was also reduced neo-revascularisation. The reparative role of CX_3CL1/CX_3CR1 is not fully understood and there is obviously a close association between the processes involved in inflammation and those involved in subsequent repair or fibrosis.

Localisation of CX_3CL1 in renal injury

Using immunohistochemistry and in situ hybridisation Cockwell *et al* showed that CX_3CL1 is expressed in human renal biopsy specimens (49). Furthermore they demonstrated expression of CX_3CL1 within the renal glomerulus in glomerular pathology and in the renal tubules in acute allograft rejection, which is predominantly a tubular pathology. Chakravorty *et al* continued this work and again using immunohistochemistry showed that CX_3CL1 is expressed on both the basolateral and luminal surfaces of renal tubular epithelial cells in acute allograft rejection (figure 4) (59).

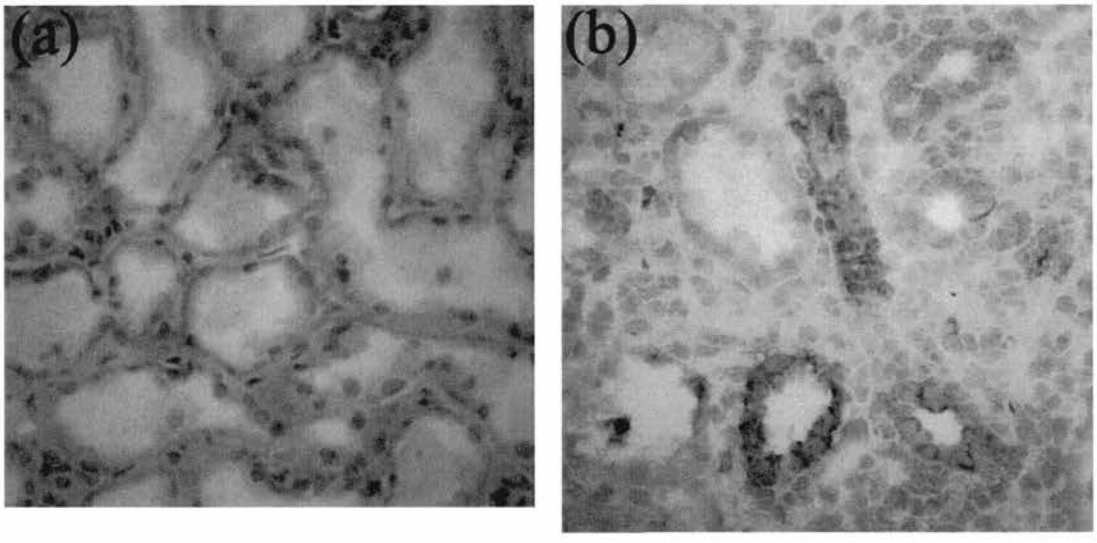

Figure 4. Immunohistochemical localisation of CX_3CL1. Normal kidney (a) and acute allograft rejection (b). Magnification x400. Taken from Chakravorty *et al.* Fractalkine expression on human renal tubular epithelial cells: potential role in mononuclear cell adhesion. J Exp Immunol 2002; 129: 150-159

It is widely acknowledged that although immunohistochemistry is a good technique for assessing the presence or absence of a particular protein in a specimen, it is not the optimal tool for assessing the precise subcellular localisation of the protein. Since the location of CX_3CL1 in renal tubular epithelial cells will have implications for its function, we sought to examine the exact intracellular location of CX_3CL1 in these cells, with a view to establishing the function of CX_3CL1 in renal tubules. Furthermore we made the assumption that CX_3CL1 would preferentially target a particular membrane in polarised renal tubular cells and investigated the mechanism(s) responsible for this.

Cell polarity and protein targeting

Epithelial cells form a barrier to the external environment but they also have important roles in the transfer of proteins in and out of cells. They are typically cuboidal or columnar in morphology with clearly defined apical and basal membranes, separated by tight junctions and this polarisation permits distinct functions to be carried out by the different membranes. Cell polarisation is widespread in biology and despite the extensive number of cell types exhibiting this phenomenon there are relatively few mechanisms responsible for its achievement. The three major contributory factors to cell polarity are i) protein sorting to a particular membrane, ii) cell signalling complexes and infrastructure associations with the cytosolic face of the particular membrane and iii) cell orientation in 3-dimensional space by stimuli from adjacent cells and extracellular matrix via adhesion receptors (134).

Cell polarity is essential for many cellular functions and a loss of polarity can be seen in many disease states such as cancer, where cells attain a mesenchymal phenotype allowing migration to other parts of the body before integrating into the new organ. Within the kidney tubules cell polarity is crucial to the maintenance of homeostasis as solutes are exchanged at both the apical and basal membranes in a finely regulated manner. Many renal diseases are due to protein mis-sorting or exchanger malfunction within the tubular cells, resulting in excessive or inadequate solute losses. Specific drugs target the receptors found on a particular tubular membrane for example amiloride targets

the epithelial sodium channel on the apical membrane, to increase urinary sodium losses.

Proteins are constructed in the endoplasmic reticulum (ER) and are then transported to the membrane via various organelles and vesicular intermediates as shown in figure 5. In addition, there is usually some degree of post-translational modification of the protein during the transport from the ER to the membrane. Vesicular intermediates are formed by three classes of proteins; coatomer protein complex-II sorts the newly formed protein into vesicles and mediates transport from the ER to the Golgi, coatomer protein complex-I mediates Golgi to ER transport and intra-Golgi transport and the adaptor protein (AP)-clathrin complex is responsible for transport between the Golgi, endosomes and the plasma membrane. Movement of vesicles between compartments is mediated by the actin and microtubule cytoskeleton. The fusion of vesicles with the plasma membrane is regulated by Rab GTPases, vesicle-tethering complexes and soluble N-ethyl-maleimide-sensitive fusion protein attachement-protein receptors (SNAREs). These mechanisms are generic to protein transport within the cell and are modified to sort proteins specifically to a particular membrane in polarised cells (fig 5).

One further possible route for protein transport is the transcytosis pathway whereby a protein is transported to one membrane initially, usually the basolateral membrane, and is then moved to the opposite membrane via early and recycling endosomes.

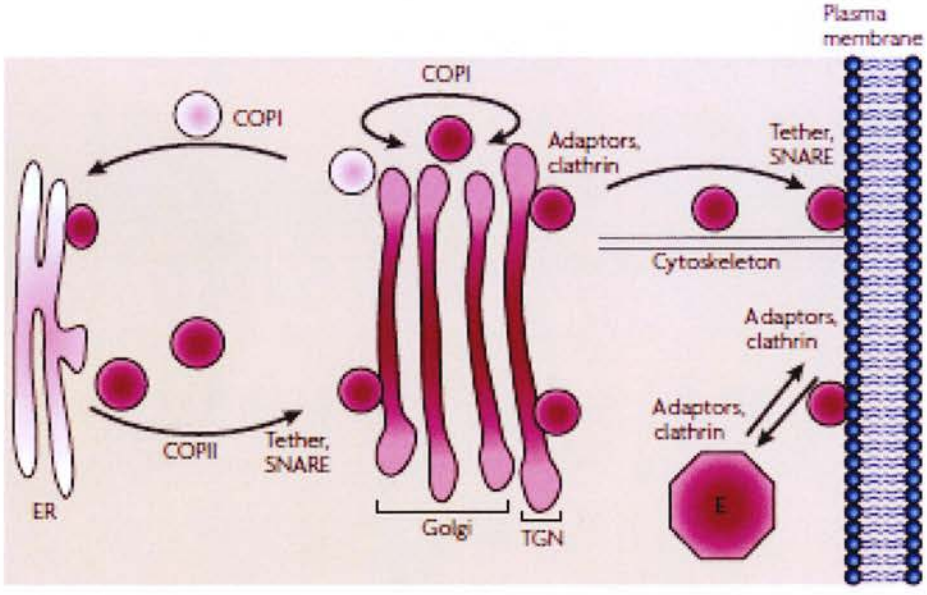

Figure 5. A generic post-translational pathway for protein trafficking to the plasma membrane.

ER – endoplasmic reticulum, COP- coatamer protein complex, SNARE-soluble N-ethyl-maleimide-sensitive fusion protein attachment-protein receptor, TGN- trans-Golgi network.

Coordinated protein sorting, targeting and distribution in polarized cells. Mellman I and Nelson WJ. Nature Reviews Molecular Cell Biology 2008, 9(11) 833-845.

The regulating mechanisms that direct a particular protein to a specific membrane appear to be limited despite the vast array of proteins synthesised by a cell. Essentially signalling codes are due to cytosolic domains, glycosylation of the protein, transmembrane domains or to an association with lipid rafts or caveolae. In general, apical sorting motifs are transmembrane or extracellular whereas basolateral sorting motifs

are more likely to be found in the cytoplasmic domain of the protein though there are exceptions to this for example rhodopsin and podocalyxin/Gp135 are apical proteins that use a cytosolic domain for membrane targeting (135, 136).

Protein targeting via a cytosolic domain.

Various cytosolic domains have been established as basolateral targeting motifs. Proteins such as the low density lipoprotein receptor (LDLR) and the H+K+ATPase transporter use tyrosine based motifs. The LDLR has two tyrosine motifs, one of which is important for endocytosis and the other directs traffic to the basolateral membrane (137). Other proteins have leucine or dileucine motifs that signal for basolateral transport. Just how these motifs direct protein transport is not understood. An association with AP-clathrin complexes is suggested however knockdown of clathrin with small interfering RNA (siRNA) affects the traffic of some proteins but not others and clearly other pathways are involved (138).

Protein targeting via a transmembrane domain.

Transmembrane signalling motifs commonly are due to an association with a glycosyl phosphoinositol (GPI) lipid anchor, such as those used by THY-1 or by direct association with lipid rafts in the plasma membrane. Lipid rafts are rich in glycosphingolipids, sphingomyelin and cholesterol. After sorting of GPI-anchored proteins in the Golgi complex, there is oligomerisation in the lipid rafts. GPI-anchored

proteins are preferentially sorted to the apical membrane. There is still only rudimentary information on just how apical clustering of proteins within lipid rafts results in delivery of the protein to this membrane.

Protein targeting via glycosylation of the protein.

The final trafficking pathway relies on glycosylation of the protein and this includes both N-linked and O-linked glycosylation. Numerous proteins use this mechanism and it is generally used to direct the protein to the apical membrane. In intestinal epithelial cells inhibition of O-glycosylation prevents the apical targeting of mucins and brush border glycoproteins (139, 140). Chemical inhibition of N-glycosylation and mutation or deletion of glycosylation residues has been used to show that this mechanism is also used for protein trafficking. The role of N-glycosylation in apical protein trafficking was further supported by a study by Scheiffele *et al*, in which they compared the secretion of growth hormone in MDCK cells. Growth hormone is a non-glycosylated protein, which is secreted to both the apical and basolateral membranes in MDCK cells in an approximate 1:2 ratio. When it is genetically modified to incorporate one N-glycosylation site it is preferentially targeted to the apical membrane and the addition of 2 glycosylation sites directs over 90% to the apical membrane (141). Chemical inhibition of N-glycosylation or mutagenesis of the glycosylation site(s) has implicated this process in the apical targeting of proteins such as erythropoietin, enteropeptidase, glycine transporter 2

(GLYT2), sialomucin endolyn and membrane dipeptidase (142-146). It seems that some proteins have just one crucial N-glycosylation site for example, erythropoietin, whereas others, such as GLYT2, have multiple sites and the loss of apical targeting is directly related to the number of disrupted glycosylation sites. Interestingly, the addition of N-glycans to proteins such as a truncated occludin and a chimeric ERGIC-53, which both normally reside in the Golgi, results in increased apical distribution (147). The exact mechanism involved in N-glycosylation directed apical targeting is not yet elucidated and glycosylation is also known to have effects on protein folding, regulation of intracellular transport and protein stability. It is possible that disruption of glycosylation causes protein mis-folding which then masks an apical signalling code.

The regulation of CX_3CL1 by other inflammatory pathways.

The role of CX_3CL1/CX_3CR1 in renal diseases is gradually emerging but clearly there is still much to learn. To date the well recognised stimulators of CX_3CL1, such as TNF-α and IFN-γ, have been investigated but there is little or no work studying other potential pathways for the activation of CX_3CL1 in the kidney. There are numerous inflammatory pathways at play in the pathogenesis of renal inflammation, with many points of interaction and cross-talk. Given the highly vascular nature of the kidney and its high blood flow, we questioned whether a common mediator of endothelial inflammation,

namely thromboxane A_2, (TXA_2) would have an effect on renal inflammation with particular reference its effect on CX_3CL1. Both TXA_2 and CX_3CL1 are present very early in the inflammatory process but no direct link between the two pathways has previously been shown in renal disease. We therefore chose to investigate this potential link more closely.

Thromboxane A2 and the Thromboxane Prostanoid Receptor

Thromboxane A_2, (TXA_2), is a prostanoid formed from the cyclooxygenase (COX) pathway metabolism of arachidonic acid, which is itself, derived from cell membrane lipids (figure 6). TXA_2 is a potent vasoconstrictor, induces platelet aggregation and is a smooth muscle cell mitogen (148). It is produced mainly by platelets but can also be synthesised by monocyte/macrophages, vascular smooth muscle cells, and endothelial cells. TXA_2 mediates its effects by binding to the thromboxane prostanoid receptor (TP), a G protein-coupled receptor expressed in diverse hematopoietic cell types involved in inflammation, including platelets, monocytes, T lymphocytes, and neutrophils, as well as in endothelial cells, fibroblasts and smooth muscle cells. The highest levels of TP mRNA are found in thymus, followed by spleen, lung and kidney.

Despite its very short half-life, of about 20-30 seconds, TXA_2 is extremely potent and acts on cells in close proximity to the TXA_2-synthesising cells as an autocoid in autocrine or paracrine systems. In aqueous solutions it

is rapidly hydrolysed to thromboxane B2 (TXB_2), which is inactive. TXA_2 is released early in inflammation and has long been implicated in the pathogenesis of atherosclerosis, as well as many other inflammatory conditions.

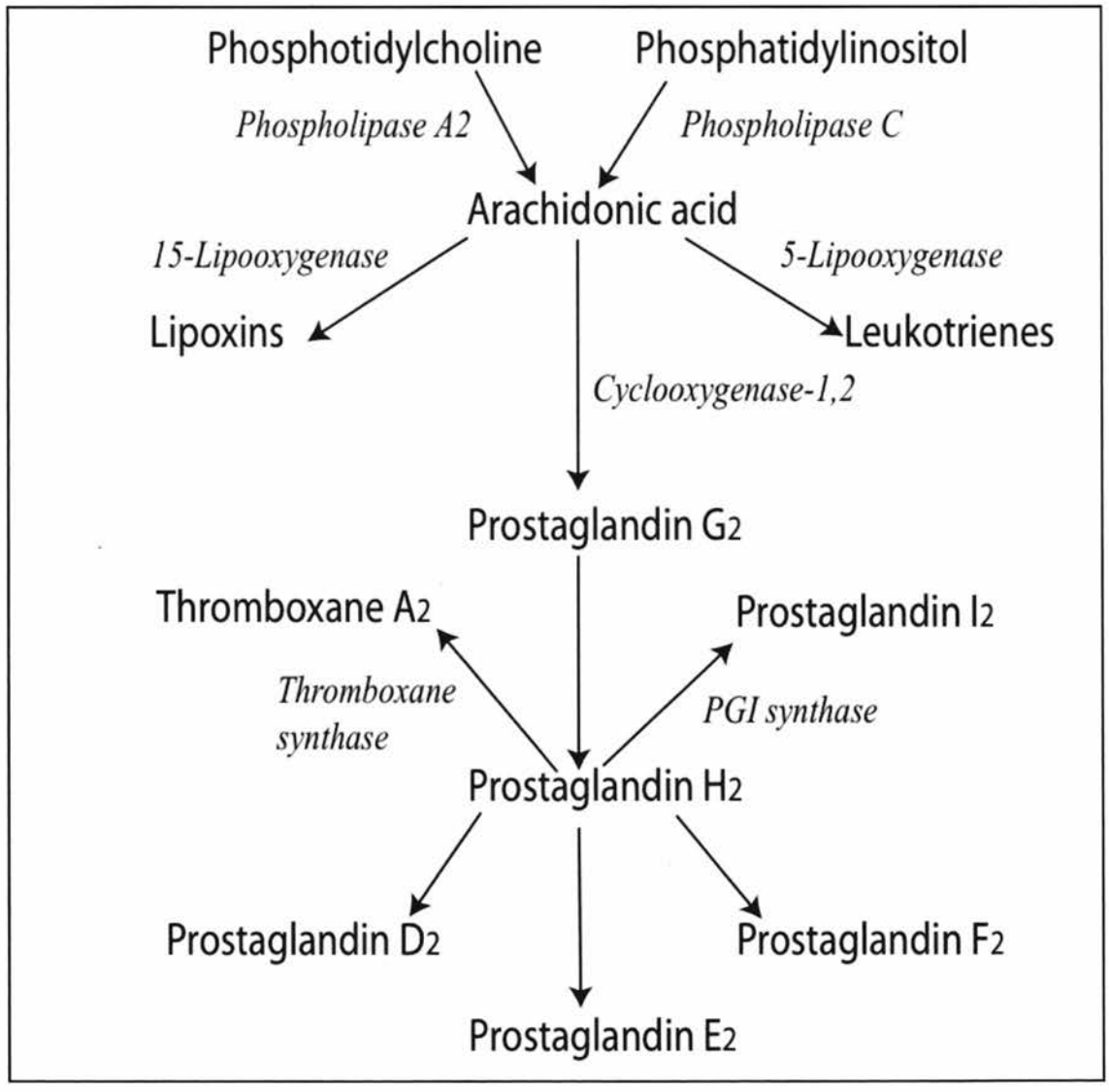

Figure 6. The Metabolism of Arachidonic Acid

Thromboxane A_2/Thromboxane Prostanoid Receptor Signalling

The thromboxane prostanoid receptor (TP) is a 7 transmembrane G protein coupled receptor. TP communicates with various families of G proteins but the major interactions are between TP and G_q and G_{13}. Platelets deficient in both these G proteins are completely unresponsive to TP stimulation. It is known that G_q is required for platelet aggregation whereas G_{13} is needed for the conformational change of platelets (149). The G proteins communicating with TP are tissue and cell type dependent. There are two alternatively spliced variants of TP, TPα and TPβ (150, 151). TPα was originally cloned from placenta whereas TPβ was cloned from umbilical vein endothelial cells. These two isoforms are thought to have identical ligand binding sites and differ only in their C-terminal tail regions. Although mRNAs for both splicing variants have been detected in most cells, the translated protein is not always expressed, for example, platelets only express TPα (152). In cells that express both isoforms differences in function have been noted, for example TPα activates adenylyl cyclase in CHO cells whereas TPβ inhibits this enzyme, and this may be explained by coupling of the two isoforms with different G proteins (153-155). Figure 7 demonstrates the downstream signalling induced by the coupling of TP with different G proteins.

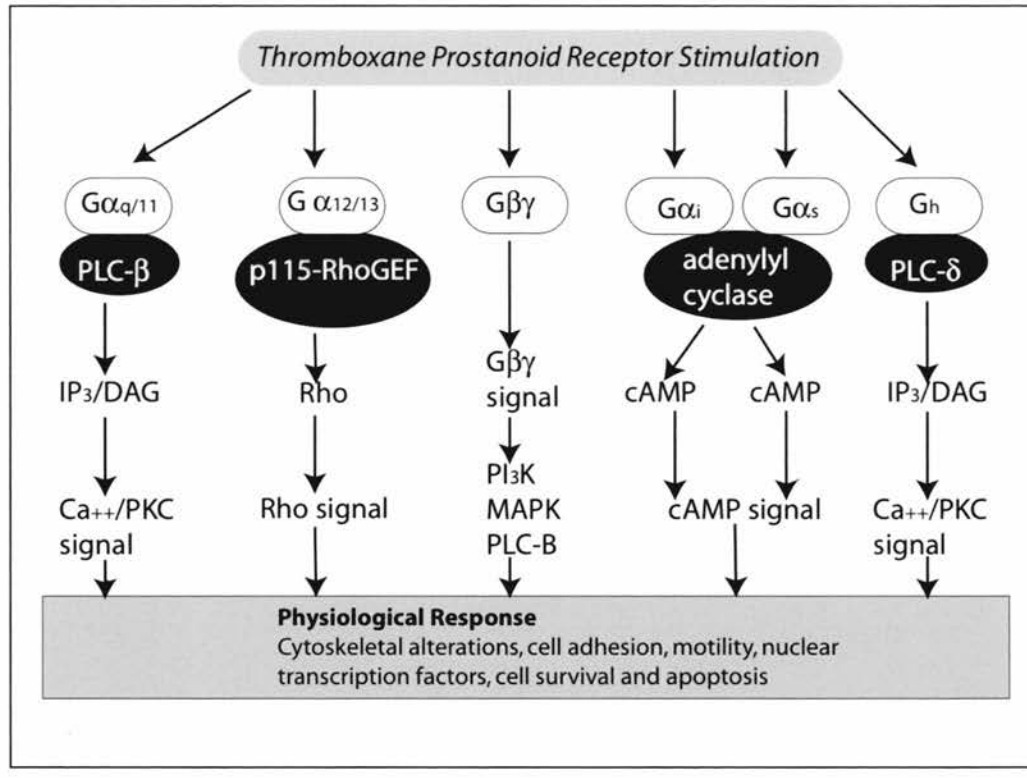

Figure 7. G protein coupling with the thromboxane prostanoid receptor and signal transduction.

PLC-phospholipase C, p115-RhoGEF- p115 guanine nucleotide exchange factor for Rho, IP_3- inositol 1,4,5-triphosphate, DAG- diacylglycerol, cAMP- cyclicAMP, PI3K-phosphatidylinositol 3-kinase, MAPK-mitogen activated kinase, PKC- protein kinase C.

Adapted from Nakahata N. Thromboxane A2: Physiology/pathophysiology, cellular signal transduction and pharmacology. Pharmacology & Therapeutics, 2008; 118, 18-35.

Thromboxane A_2/ Thromboxane Prostanoid Receptor and Renal Inflammation

Although the link between prostanoid secretion and renal injury has long been recognised the actual mechanisms by which this occurs are not well understood. Increased urinary levels of thromboxane metabolites are often found in kidney pathologies of diverse aetiologies. Early studies showed that in normal kidneys TXA_2 appears to regulate renal haemodynamics and sodium handling (156-159). In non-diseased animals an infusion of a TP agonist resulted in decreased glomerular filtration rate (GFR) in rats that was due to increased vascular resistance within the kidneys (156). TP stimulation in the kidney also directly affects mesangial cells resulting in cell contraction, which may contribute to the decrease in GFR (157). In both rat and human glomerular mesangial cells, prostanoids induce a change in the cellular ion fluxes, with an increase in inositol phosphates and intracellular calcium and the environment becomes profibrotic with increased production of extracellular matrix that is associated with increased mRNA for fibronectin, collagen and laminin (160). TP stimulation also results in increased PAI-1 production and tissue plasminogen activator by mesangial cells (161). Given the effects of PAI-1 on fibrinolysis and renal fibrosis discussed previously, this effect of TP stimulation adds a further potential mechanism for the promotion of glomerular thrombosis and renal fibrosis.

Numerous studies have used methods to block TP or TXA_2 synthesis to examine the impact of this pathway on disease models. Many of these studies, but not all, suggested a beneficial outcome of blocking the prostanoid pathway, for example pathway blockade resulted in lower levels of proteinuria in rodent models of nephrotic syndrome (162), anti-glomerular basement membrane disease (163), membranous nephropathy (164) and mesangioproliferative glomerulonephritis (165). This is not always accompanied by significant improvements in the histological appearances of the kidneys.

Following an ischaemic insult in rats, the use of a TXA_2 synthase inhibitor improved renal blood flow, GFR and urine volumes (166). Similarly, in a mouse model of acute renal failure induced by endotoxemic shock, blockade of TP resulted in attenuated decreases in renal blood flow and glomerular filtration rates but it did not effect overall survival at an early time-point (167). A human study of the use of ibuprofen or placebo in patients with sepsis showed no improvement in mortality rates or rates of acute renal failure, despite reduced thromboxane urine metabolites in the ibuprofen group (168).

In rat models of diabetic nephropathy, TP stimulation contributes to the development of albuminuria, increased glomerular and mesangial volumes and to the increased width of the glomerular basement membrane (169). Specific blockade of TP or the administration of a thromboxane synthase inhibitor resulted in attenuated

microalbuminuria, prevention of the increased glomerular volume and lower levels of markers of oxidative stress (169, 170).

There is increased TXA_2 production in lupus nephritis in both humans and mice (171, 172). This increase correlates with the degree of lupus activity as measured by proteinuria and histological changes on renal biopsy. Blockade of TXA_2 synthesis in mice and the use of a specific TP antagonist in humans have renoprotective effects and improved clinical outcomes (173, 174).

Numerous studies have examined the role of thromboxane in renal allografts and although there is an association between the prostanoid pathway and acute rejection, functional therapeutic interventions have not yet materialised. Coffman *et al* were the first to demonstrate that acute rejection is associated with increased levels of the inactive thromboxane metabolite TXB_2 and this has been corroborated by various other groups in both animal models and in humans (175-178). In a rat model of renal allograft rejection, a continuous infusion of a TXA_2 synthase inhibitor improved renal function and reduced urinary thromboxane metabolites but did not affect the cellular immune response to rejection. Furthermore, it seemed that the responses were temporary as by day 6 there was only partial reduction in urinary metabolites (176). Similarly, in a canine model of renal allograft rejection, selective inhibition of TXA_2 synthase improved renal blood flow and GFR but did not affect the histological changes of rejection (179). Staining for TXA_2 synthase is increased in humans during

episodes of acute rejection and directly correlates with a faster decline in renal function over 6 months (180). The TXA_2 synthase staining appears to co-localise with a macrophage infiltrate. Prostanoid stimulation contributes to the reduced blood flow seen in rejection but the exact role(s) of the thromboxane prostanoid pathway in renal allografts is still not clear and needs further elucidation.

Thromboxane A_2/ Thromboxane Prostanoid Receptor and Inflammation of Other Organs

In the central nervous system TP is expressed by astrocytes, astrocytoma cells and oligo dendrocytes (181-183). Stimulation of TP results in IL-6 secretion by astrocytes and enhanced proliferation and survival of oligodendrocytes. In the peripheral nervous system, TP stimulation elicits pulmonary and cardiovascular reflexes (184-186).

TP is implicated in the pathogenesis of asthma, both as a mediator in the allergic responses in asthma, as well as causing contraction of bronchial smooth muscle cells (187, 188).

TP is also involved in allergic responses in rhinitis and atopic dermatitis (189-191), in inflammatory tachycardia (192), in metastasis of tumour cells (193), in angiogenesis during tumour growth and chronic inflammation (194). In addition, it plays a role in modulating acquired immunity, by impairing the adhesion between dendritic cells and naïve, but not memory, T cells (195). TP stimulation causes contraction of

numerous types of smooth muscle cells including those found in the vasculature, intestine, uterus and bladder (196-199).

Thromboxane Prostanoid Receptor and Atherosclerosis (as a disease model)

Perhaps the disease for which there is the greatest information regarding the role of TP stimulation is atherosclerosis. Atherosclerosis is the end result of complex inflammatory processes involving interactions between the endothelial wall, platelets, lymphocytes and macrophages. Oxidative stress, cytokine activation, lipid deposition, leukocyte recruitment and smooth muscle cell proliferation all contribute to its pathogenesis. The initial lesion is the fatty streak, beneath the endothelium, which is made up mainly of lipid-laden macrophages, (foam cells), with some T cells. Progression of the fatty streak results in the formation of the atherosclerotic plaque or atheroma, an asymmetric thickening of the arterial intima consisting of foam cells, extracellular lipid droplets, smooth muscle cells, extracellular matrix and inflammatory leukocytes. The atheroma has the potential to rupture and induce thrombosis, with the consequential and often devastating, acute vascular events such as ischemic heart disease and cerebrovascular accident or stroke.

Ishizuka *et al,* found that stimulation of the TP on endothelial cells results in increased ICAM-1 expression, which promotes monocyte cell adhesion (200). Monocyte/macrophage infiltration is a very early

feature of atherogenesis, being present in the fatty streak. In addition, TP stimulation increases IL-1β induced VCAM-1 expression in aortic vascular smooth muscle cells, further promoting cell adhesion to the endothelial wall (201). In human ischemic atherosclerotic vessels, Katugampola *et al*, showed increased TP receptor density in both the aorta and in the epicardial coronary arteries (202). They also found that the angiotensin receptor blocking agent, losartan, competed for binding to the TP suggesting an association between the renin-angiotensin pathway and the prostanoid pathway.

The effects of TP stimulation on platelets have been well established. Platelet activation by TP leads to conformational change, aggregation and secretion of granule contents including; ADP, ATP, serotonin, calcium, von Willebrand factor, factor V and fibrinogen, with resultant increased thrombotic tendency. This further contributes to the pathogenesis of atherosclerosis and its clinical outcomes (202-204). Prostaglandin I_2 (PGI_2) is the biological opposite of TXA_2 and has platelet inhibitory and vasodilating properties (205). It is mainly produced by vascular endothelial cells and its synthesis is dependent on COX-2 and prostacyclin synthase. Both TXA_2 and PGI_2 have increased expression in atherosclerosis (206, 207). It is believed that changes to the equilibrium between TXA_2 and PGI_2 are critical for the development of thrombus rather than the absolute amounts of each mediator. In 2004 Kobayashi *et al* published work examining the individual contributions of TXA_2 and PGI_2 to the development of atherosclerosis (208). They

cross-bred apolipoprotein E knock-out (Apo E-/-) mice (genetically modified mice that develop atherosclerosis) with mice that were either deficient for TP or for the PGI receptor (IP). The TP deficient mice had markedly delayed atherogenesis with a significant decrease in ICAM-1 expression in the endothelial cells overlying the atheromatous lesions, whereas the IP deficient mice had accelerated atherogenesis with increased ICAM-1 expression. Furthermore, they found decreased/increased platelet reactivity in the TP deficient/IP deficient mice respectively and increased leukocyte adhesion in the IP deficient mice.

Therapeutic interventions that aim to block the production of TXA_2 are already in widespread use, both in cardiovascular disease and in other inflammatory conditions. As can be seen in figure 8, TXA_2 is produced via the COX-1 pathway, whereas PGI_2 is produced via the COX-2 pathway. As early as 1973, Bailey *et al* showed that non-steroidal anti-inflammatory drugs (NSAIDS) decreased atherosclerotic lesions in cholesterol fed rabbits (209). Further studies using pharmacological blockade of COX-1 have found similar results in various models of atherosclerosis (210-212). Low dose aspirin, which effectively blocks COX-1, is now used daily by millions of people to prevent atherosclerosis progression and to induce plaque stability where atheroma is already present. Recently many COX-2 inhibitors, which were used mainly for rheumatological conditions, were removed from

the market because of their undesirable side effects on the cardiovascular system, which were believed to be due to the selective depletion of PGI_2, altering the equilibrium between PGI_2 and TXA_2.

An alternative therapeutic option to blocking COX-1 is to block the TP receptor directly and various studies using TP antagonists have been reported. In 2005 Viles-Gonzales demonstrated atherosclerosis regression in S18886, (a TP antagonist), treated rabbits (213). In the same year Worth *et al* showed that S18886 inhibited the development of atherosclerosis in rabbits (214). Another TP antagonist and synthase inhibitor, BM-573, decreased the development and progression of atherosclerosis in low density lipoprotein receptor knockout mice (215). The same investigators also showed that TP blockade decreased macrophage infiltration, whilst increasing smooth muscle cell and collagen content of atherosclerotic plaques rendering them more stable (216). Furthermore, they found decreased levels of inflammatory cytokines including CCL2 and CD40L, in those mice treated with the TP antagonist.

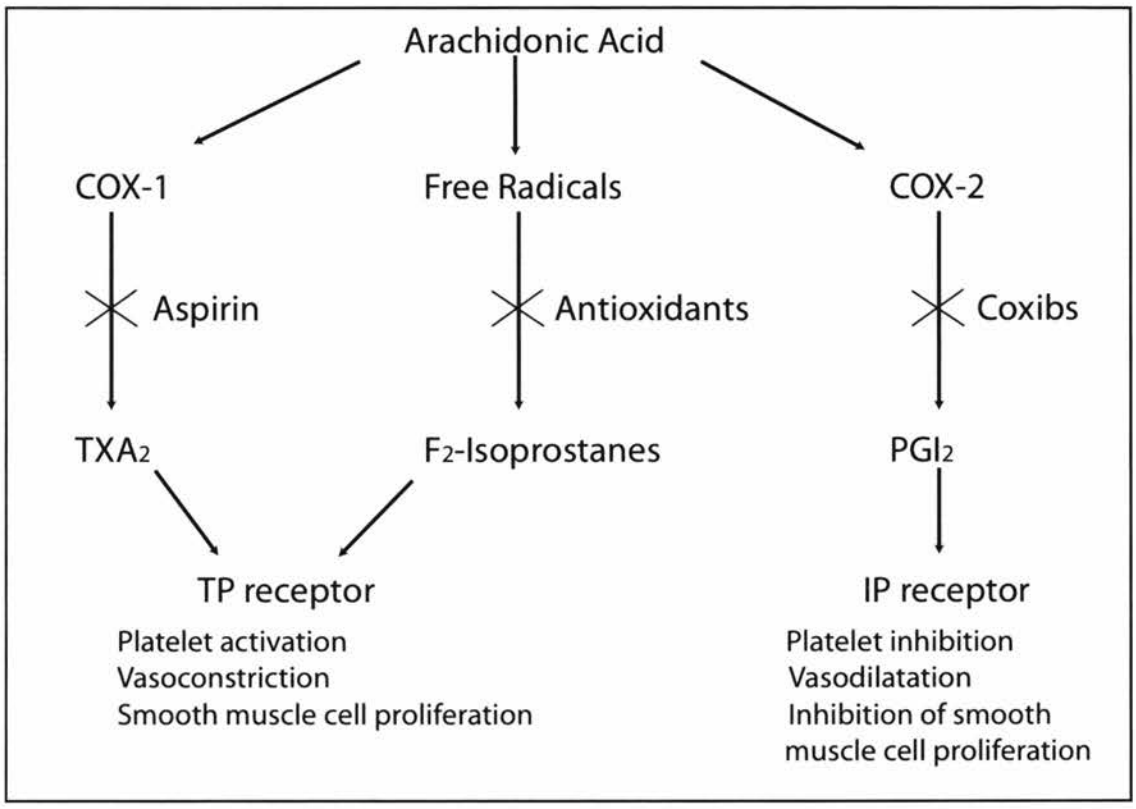

Figure 8. The Pharmacological Modulation of Thromboxane A_2 and Prostaglandin I_2.

COX–cyclooxygenase, TXA_2–thromboxane A_2, PGI_2–prostaglandin I_2, TP–thromboxane prostanoid, IP-prostaglandin I_2 receptor

Thromboxane Prostanoid Receptor Stimulation by Other Ligands

If the pathogenic effect of stimulation of TP is entirely from TXA_2 then, aspirin alone should prevent the formation of atherosclerotic plaques. If however it is the stimulation of the TP receptor *per se* that causes the inflammatory cascade then blocking the TP should provide greater therapeutic benefits than inhibiting COX-1, as COX-1 inhibition may not affect the production of other TP ligands. This latter hypothesis is

supported by a study that examined the effect of aspirin and S18886 in ApoE-/- mice. There were smaller aortic root atherosclerotic lesions and lower serum levels of ICAM-1 in the S18886 treated mice but not in the aspirin treated mice when compared to controls (217). These findings were supported in a further study using SC560, a selective COX-1 inhibitor and BM-573, a TP antagonist, in LDLR deficient mice, which are also predisposed to the development of atherosclerosis. Both agents individually reduced atherosclerosis formation but the effect was increased in mice treated with both agents simultaneously (216). A study in humans with coronary artery disease, all of whom were all treated with aspirin, showed improved endothelial function, as measured by flow mediated vasodilatation, after a single dose of S18886 (218).

Although TXA_2 is the most common ligand for TP, others are known about, the main group being the F2 isoprostanes, derived from the free radical oxidation of arachidonic acid (figure 7). The F2 isoprostanes, as well as being reliable markers of oxidative stress, increase platelet activation, induce mitogenesis of vascular smooth muscle cells, induce the proliferation of fibroblasts and endothelial cells and increase the expression of endothelin-1, a vasoconstrictor, in aortic endothelial cells all via TP stimulation (219, 220). Distinct F2 isoprostanes have been localised in human atherosclerotic lesions (221). In addition, Tang *et al* demonstrated that isoprostane F2α-III directly promotes atherogenesis

in both apoE-/- and LDL receptor-/- mouse models by activating TP (222).

Thromboxane Prostanoid Receptor Stimulation and Chemokines

There is accumulating data linking TP stimulation with chemokine activation. Over ten years ago, Schneider *et al* found that non-selective COX inhibition with indomethacin, stimulated the glomerular expression of both CCL2 and CCL5 mRNA in two different rat models of glomerulonephritis (mesangial proliferative and anti-GBM nephritis). This effect was not seen when they used selective COX-2 inhibition, implying that it was a COX-1 effect. The increase in chemokine mRNA was associated with increased chemokine activity and augmented recruitment of monocytes and macrophges to the glomeruli (223). A further study noted that CCL17 and CCL22 induced platelet aggregation, which could be inhibited by aspirin (224). Hoshino *et al* then used the TP antagonist AA-2414 in asthmatic patients and showed decreased CCL5 and CCL3 in the bronchial epithelium and submucosa, which was associated with less eosinophilic infiltration and improved clinical outcomes (225). A year later Ishizuka *et al* used U46619, a TP agonist, in human umbilical vascular endothelial cells (HUVECs) and found augmented CCL2 expression (226). This group demonstrated that TP stimulation induced NFκB and AP-1 binding activity through the protein kinase C system. The same group later used Ramatroban, a TP antagonist, in a rabbit model of arterial injury and showed dose-

dependent decreased plasma CCL2 levels and decreased mRNA for CCL2 in the injured aortas of the treated animals (227). Cyrus *et al* initially demonstrated that low dose aspirin decreased circulating levels of CCL2 in LDLR knockout mice (228) and then went on to show that a combination of a selective COX-1 inhibitor with a TP antagonist, in the same animal model, suppressed circulating CCL2 levels to a greater extent than each drug individually (215). Finally, the TXA_2 synthase inhibitor, ozagrel, was shown to reduce CCL2 and CXCL8 mRNA expression in a model of lung injury in guinea pigs, with an associated decreased inflammatory response (229). Similar data is also emerging regarding the links between stimulation of other prostanoid receptors such as the protaglandinF2 receptor and regulation of chemokines (230, 231).

Although there is currently no data linking the stimulation of the thromboxane prostanoid receptor and regulation of the chemokine CX_3CL1, given the preceding information and the fact that both TXA_2 and CX_3CL1 are active early in inflammation, in overlapping clinical scenarios, it seemed reasonable to hypothesise a possible association between the two that would add to the increasing complexity of the pathogenesis of inflammation.

Chapter 2. Hypotheses and Aims

Hypotheses

Hypothesis 1a: The chemokine CX_3CL1 is mainly on the basal membrane of renal tubular epithelial cells.

Hypothesis 1b: There are signalling pathways that direct CX_3CL1 to the basal membrane.

Hypothesis 1c: CX_3CL1 is immobile in the cell membrane.

Hypothesis 1d: CX_3CL1 is a cell adhesion molecule on renal tubular epithelial cells.

Hypothesis 2a: Stimulation of the thromboxane prostanoid receptor increases surface cell levels of CX_3CL1.

Hypothesis 2b: Stimulation of the thromboxane prostanoid receptor alters recycling of CX_3CL1.

Hypothesis 2c: Stimulation of the thromboxane prostanoid receptor inhibits cleavage of CX_3CL1.

Hypothesis 1a: The chemokine CX_3CL1 is mainly on the basal membrane of renal tubular epithelial cells. Previous studies have shown increased CX_3CL1 in some diseased renal tubules. The precise intracellular location of the chemokine will have implications for its function and this has not yet been unequivocally demonstrated in these cells. The close proximity of the peritubular capillaries to the basal membrane would allow circulating leukocytes to migrate towards the transmembrane CX_3CL1 and chemokine mediated adhesion would also

be possible. The apical surface of renal tubular epithelial cells is in contact with the urinary space and this is ordinarily devoid of leukocytes, hence apically expressed CX_3CL1 would not have any direct contact with cells expressing its receptor under normal conditions.

Hypothesis 1b: There are signalling pathways that direct CX_3CL1 to the basal membrane. Despite numerous proteins being trafficked to a specific membrane in polarised cells there are relatively few mechanisms employed.

Hypothesis 1c: CX_3CL1 is immobile in the cell membrane. CX_3CL1 acts as a chemoattraction agent and as a cell adhesion molecule in various cell types. To facilitate the cell adhesion properties, immobility with the membrane would allow CX_3CL1 to act as a firm anchor, capturing leukocytes in the vicinity. The counter argument to this is that a freely mobile membrane chemokine would offer some elasticity to the stress forces present and there would be less chance of accidental detachment of the leukocyte.

Hypothesis 1d: CX_3CL1 is a cell adhesion molecule on renal tubular epithelial cells. This function has been proved in other cell types.

Hypothesis 2a: Stimulation of the thromboxane prostanoid receptor increases surface cell levels of CX_3CL1. Stimulation of the TP receptor and chemokine release both occur early in inflammation. Both TP stimulation and CX_3CL1 have been implicated in the pathogenesis of very similar inflammatory conditions. The thromboxane prostanoid

pathway has been previously shown to regulate other chemokines. Leukocyte recruitment is required for the pathogenesis of inflammation. Therefore, stimulation of TP receptor is predicted to increase surface levels of CX_3CL1, to then promote the leukocytic infiltrate into the damaged tissue.

Hypothesis 2b: Stimulation of the thromboxane prostanoid receptor alters recycling of CX_3CL1. CX_3CL1 recycles from the cell surface to an intracellular compartment. An increase of CX_3CL1 at the cell surface could be due to less endocytosis ± more exocytosis. This increase could be achieved far more quickly than by new protein synthesis.

Hypothesis 2c: Stimulation of the thromboxane prostanoid receptor inhibits cleavage of CX_3CL1. CX_3CL1 is cleaved at the cell membrane by TACE and ADAM-10. Increased surface levels of CX_3CL1 could be obtained by inhibition of this cleavage.

Aims

Aim 1.1. To identify the precise intracellular location of CX_3CL1 in renal tubular cells.

Aim 1.2. To identify the mechanism responsible for directing CX_3CL1 to a particular membrane in renal tubular epithelial cells.

Aim 1.3. To evaluate the mobility of CX_3CL1 within the cell membrane.

Aim 1.4. To evaluate if CX_3CL1 in renal tubular epithelial cells acts as a cell adhesion molecule.

Aim 2.1. To evaluate the effect of TP stimulation on total cellular CX_3CL1 protein.

Aim 2.2. To evaluate the effect of TP stimulation on cell surface CX3CL1 levels.

Aim 2.3. To evaluate the effect of TP stimulation on trafficking of CX_3CL1.

Aim 2.4. To evaluate the effect of TP stimulation on cleavage of CX_3CL1.

Aim 2.5. To evaluate the signalling pathways used by TP in the regulation of CX_3CL1.

Chapter 3. Methods and Materials

Cells. HK-2 cells were a kind gift from Dr. Andras Kapus, (University of Toronto). Madin Derby Canine Kidney-II (MDCK) cells and ECV-304 cells were from American Type Culture Collection (Manassas, VA). MDCK cells stably expressing sodium-hydrogen exchanger 3 (NHE3) tagged with hemagglutinin (HA) were kindly provided by Dr. Sergio Grinstein, (University of Toronto). The preceding cells were cultured in DMEM and Ham's F12 (Wisent, Quebec), containing 5% fetal calf serum (FCS). MDCK cells are well-defined distal renal tubular epithelial cells that have been used extensively for decades to assess epithelial cell properties and function. They originated from an adult female cocker spaniel in 1958. They form columnar monolayers in culture with tight and gap junctions. They have provided an excellent model system for examining cell polarity and for the study of transporters and ion channels found on specific cell membranes (232-234). We genetically modified the MDCK cells such that they expressed CX3CL1, as described below, and confirmed that the cells maintained classical epithelial cell polarity as demonstrated by the labelling of E-cadherin (an important component of the adherens junction contributing to epithelial cell differentiation) and ZO-1 (a component of the intercellular tight junction) as shown in figure 1.

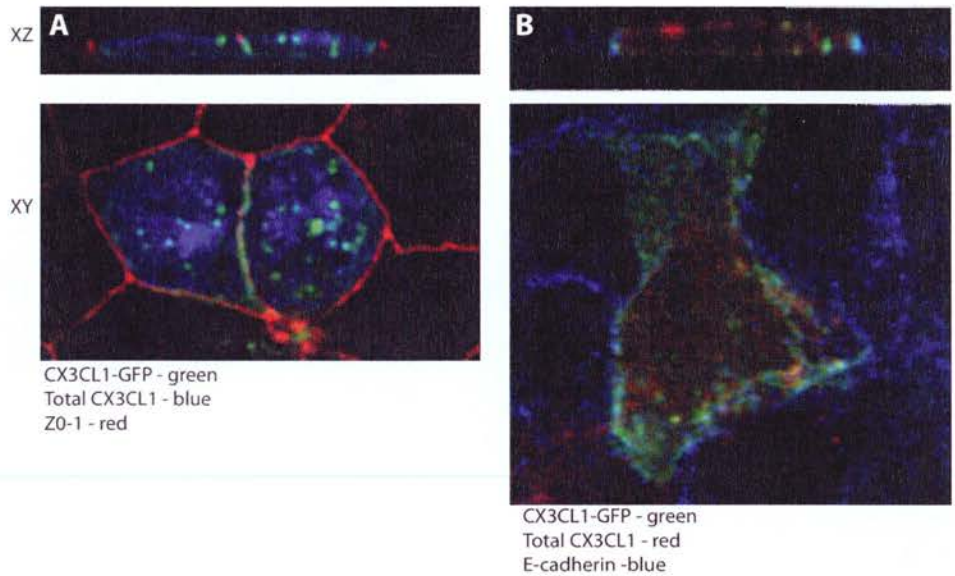

Figure 1. MDCK-CX_3CL1-GFP cells retain epithelial cell properties. A. MDCK-CX_3CL1-GFP cells were fixed and permeabilised and then labelled with an anti-CX_3CL1 Ab (1μg/ml) followed by a Cy-5 conjugated secondary Ab. They were simultaneously labelled with an anti-ZO-1 Ab (1.25μg/ml) followed by a Cy-3 conjugated secondary Ab. (B) After permeabilisation, MDCK-CX_3CL1-GFP cells were simultaneously labelled with an anti-CX_3CL1 Ab followed by a Cy-3 conjugated secondary Ab and an anti-E-cadherin Ab (1.25μg/ml) followed by a Cy-5 conjugated secondary Ab.

ECV-304 cells were originally reported to be immortalised endothelial cells of HUVEC origin but they are now acknowledged to be irrefutably derived from the T24 bladder epithelial carcinoma cell line (235, 236). The cells grow in flattened monolayers and form relatively tight intercellular junctions. They have been reported to express some endothelial markers such as Ulex europaeus agglutinin-1 51(UEA-1), HAM-56 and PHM-5 but they do not stain for von Willebrand factor,

which is a specific marker of endothelial cells and extensive testing, including DNA profiling and genetic analysis, has clearly identified the cells as being of epithelial T24 cell origin. (http://www.atcc.org/CulturesandProducts/CellBiology/MisidentifiedCellLines/tabid/683/Default.aspx -).

ECV-304 cells genetically manipulated to produce CX_3CL1 (ECV-CX_3CL1 cells) are known to have surface levels of CX_3CL1 that reflect those seen in primary activated vascular endothelial cells and for this reason they have been used repeatedly to study the distribution and cleavage of CX_3CL1 (35, 39, 93-95, 98, 237). This was our rationale for using these cells in experiments examining the effect of TP stimulation on cellular CX_3CL1 levels. Clearly they are not suitable for functional studies of endothelial cells but as none of the experiments described below specifically examined cell function, this was not deemed to be important. (In further experiments performed after the completion of the work in this thesis, primary endothelial cells were used to assess functional properties of endothelial cells following TP stimulation).

K562 erythroleukemia cells and K562 cells stably expressing CX_3CR1 (K562-CX_3CR1) were a gift from Dr. Dhavalkumar Patel, (University of North Carolina, Chapel Hill) and were cultured in RPMI supplemented with HEPES and 15% FCS. Primary human RTEC (Clonetics, Cambrex, Walkersville, MD) were a gift from Dr Jim Scholey (University of Toronto) and were cultured, according to the manufacturer's instructions, in renal epithelial cell basal medium (Clonetics) with the

following added to each 500ml; hEGF 0.5ml, hydrocortisone 0.5ml, epinephrine 0.5ml, insulin 0.5ml, triiodothyronine 0.5ml, transferrin 0.5ml, GA-1000 (gentamicin 30mg/ml and amphotericin B 15μg/ml) 0.5ml, FCS 2.5ml (238). The cell phenotype was not confirmed but could have been checked by performing immunofluorescent staining for gamma-glutamyl transpeptidase and alkaline phosphatase, as is routinely done by the company supplying the cells.

Human peripheral blood mononuclear cells (PBMC) were isolated from heparinised peripheral blood from healthy volunteers (239). Ten ml of heparinised blood was centrifuged at 2300rpm for 10 mins at room temperature. One ml of plasma was removed and the remaining blood and plasma was diluted to 30ml in Dulbecco's phosphate buffered saline (DPBS- Invitrogen). Ten ml of Ficoll Hypaque solution (density 1.077g/L - Sigma) was added to a 50ml Falcon tube and the diluted blood was gently overlaid prior to centrifugation at 1500rpm for 30 mins with no brake. The PBMCs were collected from the interphase of the PBS and the Ficoll solution and transferred to a new 50ml tube and diluted with DPBS to 40ml. This was followed by further centrifugation at 1000rpm for 8 mins. The supernatant was decanted and the cells were washed again to remove the platelets. The cells were resuspended in RPMI with 10%FBS. Cell density was assessed using a hemacytometer. Cell viability was assessed using the trypan blue exclusion method; 0.1mL of 0.4% solution of trypan blue (Invitrogen) in PBS was added to 1mL of cells, after determination of the cell density.

Cells were again counted using a hemacytometer and percentage viability was calculated as:

(1-[Number of blue cells + Number of total cells]) x100

The cell phenotype was not formally assessed but could have been checked by labelling the cells for markers of T cells (CD3), monocytes (CD14) and NK cells (NK1.1) and performing flow cytometry. As the same cells were used for the control and experimental conditions this was not deemed to be essential.

Constructs. DNA expression plasmids for CX_3CL1 or CX_3CL1 tagged with green fluorescent protein (CX_3CL1-GFP) were created as previously published and described below (37, 98, 240). cDNA for CX_3CL1 (GenBank registration no: **NM-002996**) was generated by PCR from vector pCAGG- Neo-CX_3CL1 (gift from Dr Dhavalkumar D. Patel lab, Department of Medicine, Duke University Medical Center, Durham, North Carolina 27710, USA). A plasmid encoding CX_3CL1-GFP was generated by PCR using 0.2mM of the forward primer 5′-CGGGTCGACTCAGCCATGGCTCCGATA and 5′-CTGAGGATCCCCACGGGCACCAGGAC together with 10mL of Tsg buffer (US biological), 5%DMSO, 200mM deoxynucleotide triphosphate, 50ng template DNA and 1mL Tsg DNA polymerase (1mL/5U) (US biological) made up to 100mL with autoclaved distilled water. Amplification was performed in a PTC-200 thermal cycler. An initial cycle of 95°C for 1 min was followed by 30 cycles of 95°C for 20 seconds,

60°C for 30 seconds and 72°C for 1.25 mins. There was a final cycle of 72°C for 10 mins. Amplified DNA was digested with Sal1 and BamH1 and cloned into the corresponding sites of pEGFP-N2 vector (BD Biosciences Clontech) with a CMV promoter. The nucleotide sequence of the full length CX_3CL1 (1194 base pairs) construct was verified by sequencing .

For the stable expression of CX_3CL1 in ECV-304 cells, the expression plasmid pCAGG- Neo-CX_3CL1 was transfected into the cells by Lipofectamine (GIBCO-BRL). Cells were selected with 500ug/ml of G418 for 1-2 weeks and the drug resistant cells were pooled and incubated with a murine anti-CX_3CL1 antibody. Cells were washed with PBS and were then stained with FITC-conjugated anti-mouse IgG. Flow cytometry was used to separate the cells expressing membrane bound CX_3CL1.

ECV-304 cells were transfected with CX_3CL1-GFP by electroporation (Gene Pulser II, Bio-Rad) and selected in 500ug/ml G418. CX_3CL1-GFP expression was determined by flow cytometry.

MDCK cells were stably transfected with these CX_3CL1 and CX_3CL1-GFP DNA expression plasmids using FuGENE™ (Roche, Indianapolis, IN) and selected in 500mg/mL G418 (Wisent, Quebec). CX_3CL1 and CX_3CL1-GFP expression was determined by western blot and immunofluorescence microscopy.

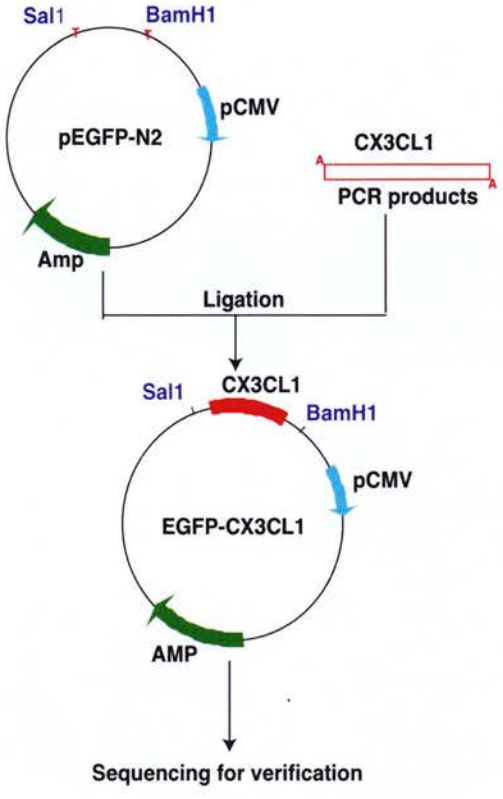

Figure 2. The generation of the CX3CL1-GFP construct.

The predicted transmembrane portion of CX_3CL1 ends at amino acid 360 (PSORT II). To investigate the potential role of a cytosolic domain motif in the targeting of CX_3CL1 to a specific membrane, a mutant DNA expression plasmid lacking amino acids 361-397, CX_3CL1-360, was generated by PCR using the common upstream primer 5'>GTGGAATTCTGCAGTCGACTC <3' and the downstream primer 5'> GCGGCCGCTCACATGGCCACCCCCAGGCAG <3'. In the downstream primer stop codons and NotI sites were introduced. PCR products were cloned into TOPO vector (Invitrogen, Burlington, ON) and the appropriate clones were selected by sequencing. Inserts were released by cutting with NotI and EcoRI, and subcloned into HA-

pcDNA3.1 (Invitrogen, Burlington, ON) with a CMV promoter. MDCK cells were transfected using FuGENE™and selected in 500μg/mL G418.

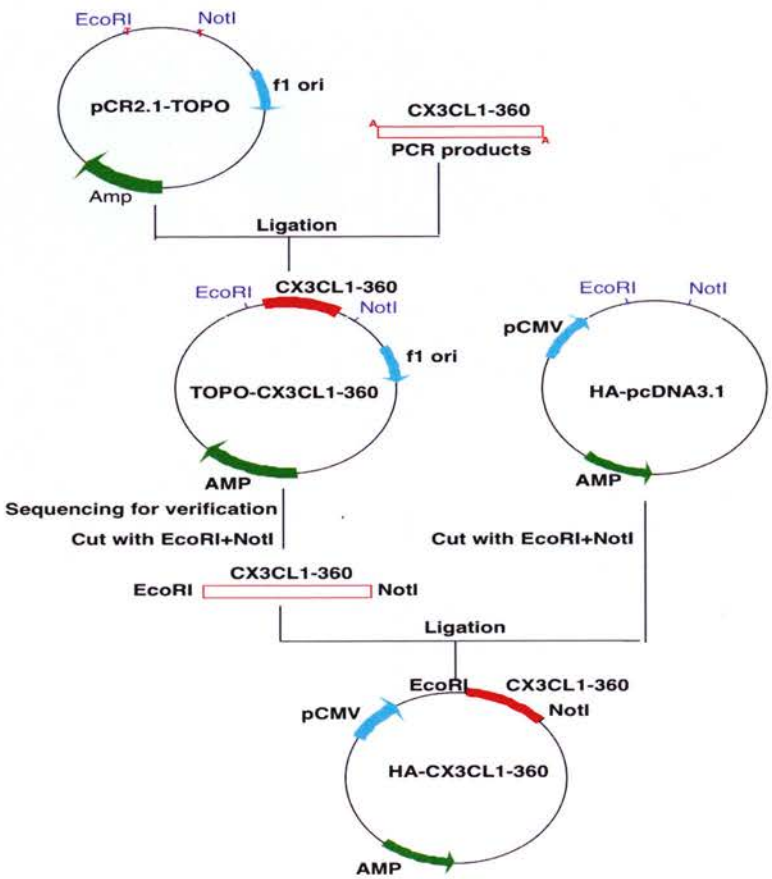

Figure 3. The generation of the CX3CL1-360 construct. Adapted from an unpublished figure by Min Riu Crow, with permission.

DNA expression plasmids encoding GFP-tagged-glycosyl phosphatidylinositol (GPI-GFP) and -FcIIa receptor (FcR-GFP) were a gift from Dr S. Grinstein (University of Toronto).

Antibodies and reagents. The following antibodies were used: goat anti-human CX_3CL1 directed against the chemokine region (R&D, Minneapolis, MN), goat anti-human CX_3CL1 against the carboxy

terminus (Santa Cruz, CA), anti-actin (Sressgen, Victoria, BC) rabbit anti-Erk (extracellular signal-related kinase) and rabbit anti-phospho-Erk (Cell Signaling, Danvers, MA) and anti-HA (Covance, Berkeley, CA). The following secondary antibodies were used: horseradish peroxidase-conjugated anti-mouse, anti-goat and anti-rabbit IgG, Cy3-conjugated anti-goat IgG, Cy5-conjugated anti-mouse IgG, phycoerythrin-conjugated anti-goat IgG and 18nm gold-labelled anti-goat IgG (Jackson Immunoresearch Laboratories, Bar Harbor, ME). TP agonists, U46619 and 1S-[1a,2b(5Z0,3a(1E,3S)4a]}-7-{3-[3-hydroxy-4(p-iodophenoxy)-1-butenyl]-7-oxabicyclo(155)hept-2-yl}-5-heptenoic acid (IBOP), as well as the specific TP antagonist, SQ29548 were from Biomol (Plymouth Meeting, PA). The Erk inhibitor, U0126 was from LC Laboratories (Woburn, MA). The metalloprotease inhibitors TAPI-2 and GM6001 were from Peptides International (Louisville, KY) and Chemicon International (Temecula, CA), respectively.

Tunicamycin, benzyl-2-acetamido-2-deoxy-α-D-galacto-pyranoside and methyl-β-cyclodextrin (MβCD) were from Sigma-Aldrich (St Louis, MO). Amplex Red kit was used to measure cholesterol levels (Molecular Probes, Eugene, Oregon). Cholera toxin B conjugated to Alexa fluor 555 was from Molecular Probes (Eugene, OR). Tumour necrosis factor-α was from R&D Systems (Minneapolis, MN). Mouse monoclonal Ab directed against human TACE was a kind gift of Dr. Roy Black (Amgen, Sherman Oaks, CA).

Immunohistochemistry. Renal transplant biopsy specimens were obtained in accordance with the guidelines of the Research Ethics Board of University Health Network (University of Toronto). Frozen 7μM sections were air-dried and fixed in acetone. After blocking with 5% donkey serum, sections were incubated with anti-CX_3CL1 Ab (1μg/ml), followed by Cy2-conjugated anti-goat IgG (1.5μg/ml).

Immunofluorescence staining of cultured cells was performed as previously described (241). MDCK cells expressing CX_3CL1 or CX_3CL1-GFP were grown to confluence on glass coverslips. To detect surface CX_3CL1, cells were washed with ice cold PBS and then fixed with 4% paraformaldehyde for 20 minutes at 4°C. The cells were washed with 100mM glycine in PBS for 10 mins. The cells were blocked with 5% donkey serum for 20 minutes and then they were then incubated with anti-CX_3CL1 Ab (1μg/ml) for 45 mins at room temperature, prior to further washing with PBS. A Cy3-conjugated secondary Ab (1.5 μg/ml) was added for 1 hour at room temperature. After final washing, the cells were mounted onto glass slides using DAKO medium (Dako Corp). To detect both surface and intracellular CX_3CL1, the same cells were permeabilised with 0.1 % Triton X-100 after labelling of the surface chemokine as described above. The cells were washed with PBS and were again blocked with 5% donkey serum and then incubated with anti-CX_3CL1 Ab (1μg/ml) at room temperature for 45 mins. Following

further washing, they were incubated with Cy5-conjugated secondary Ab (1.5μg/ml) for 1 hour at room temperature. In some experiments Alexa 488-conjugated phalloidin (0.6U/ml) was added with the secondary Ab to label F-actin. Cells were visualised using either a LSM 510 confocal microscope (Zeiss, Jena) or a spinning disk DMIRE2 confocal microscope (Leica, Wetzlar), equipped with an Hamamatsu Backthinned EM-CCD camera. Images were acquired using 100x oil immersion and the appropriate filters. Z stacks were constructed and images deconvolved using Volocity™ software (Improvision, Lexington, MA). All experiments included some cells without the application of a primary antibody but ideally an irrelevant isotype antibody of the same species as the primary antibody being investigated should also have been used to confirm the specificity of the results.

RNA Isolation and PCR. RNA was isolated from HK-2 cells using TRIzol (Life Technologies, Burlington, ON). Cells were grown to confluence on a $10cm^2$ culture dish and rinsed with ice cold PBS. One ml of TRIzol reagent was added and the cells were scraped prior to pipetting into a test tube and vortexing. The homogenised sample was incubated at room temperature for 5 minutes prior to the addition of 0.2ml of chloroform and the sample was vortexed for 15 secs. Samples were incubated at room temperature for 2-3 mins. The samples were then centrifuged at 10000g for 15 mins in the cold room (4°C).

Following this phase separation, the upper aqueous layer was transferred into a new tube. To precipitate the RNA, 0.5ml of isopropyl alcohol was added to the aqueous phase and the samples were incubated for 10mins at room temperature. The samples were centrifuged at 10,000g for 10 mins in at 4°C. The supernatant was discarded and the RNA pellet was washed with 75% ethanol.

RT-PCR for CX_3CL1 was performed using oligo(dT) and specific primers; sense primer 5'-CCTGGATGCAGCCTCACAGT and antisense primer 5'-GGACAATCCAAGGGAGAGGTG (9). Two microlitres of each of the DNA primers (10μM) were mixed with 10μL buffer (200mM Tris-HCl, 500mM KCl), 3μL $MgCl_2$ (50mM), 1μL taq (Tsg) DNA polymerase (5U/μL) (US Biological, Swampscott MA), 2μL deoxynucelotide triphosphate (10mM) and 50ng of the cDNA. Autoclaved, distilled water was added to give a final volume of 100μL. Amplification was performed in a PTC-200 thermal cycler. An initial denaturation (5 mins at 94°C) was followed by 40 PCR cycles, consisting of 1 min denaturation at 94°C, 1 min annealing at 58°C and an extension time of 5 minutes at 72°C, with a final extension of 10 minutes at 72°C. One microlitre of cDNA was size fractionated on a gel of 1% agarose in a Tris borate EDTA (TBE) buffer. The cDNA was visualised using ethidium bromide. Glyceraldehyde-3-phosphate dehydrogenase (GAPDH) cDNA was used as an internal control.

Immunoblotting. Cells were lysed with 1% TritonX-100 lysis solution (NaCl 150mM, HEPES 25mM, MES 25mM, EDTA 0.5mM, TritonX-100 1%, mammalian protease inhibitor 8%) on ice for 6 minutes. After centrifuging for 1 minute at 1300 rpm, an equal volume of 2x Laemmli solution (4% SDS, 20% glycerol, 10% 2-mercaptoethanol, 0.004% bromophenol blue, 0.125M Tris HCl) was added to each lysate and the samples were boiled for 5 minutes. Bradford assays were performed, according to published protocol and the manufacturers instructions, using Bio-Rad Protein Assay solution (242). One hundred micrograms of protein per lane were resolved by 10% SDS-polyacrylamide gel electrophoresis and transferred onto nitrocellulose membranes. The blots were blocked overnight at 4°C with 5% milk PBS/0.1% Tween 20. The blots were then incubated for 4 hours at room temperature with primary antibody (anti-CX_3CL1 antibody 0.2μg/ml, anti-Erk 0.01μg/ml, anti-phospho-Erk 0.2μg/ml, anti-GFP 1μg/ml, anti-TACE 0.5μg/ml or anti-ADAM10 antibody 2μg/ml). Anti-actin (1μg/ml) or anti-GAPDH (0.125μg/ml) antibodies were used to control for protein loading. Following extensive washes with PBS containing 0.1% Tween 20, the blots were incubated with anti-goat or anti-mouse IgG (0.8μg/ml) conjugated with horseradish peroxidase (HRP) for 1 hour at room temperature. Immunoreactive bands were visualised by enhanced chemiluminescence (Amersham Pharmaceuticals, UK) recorded on X-ray film.

To assess detergent resistance, cells were lysed with 1% TritonX-100 lysis solution as above, without scraping (241). The supernatant was removed and a volume of 4x Laemmli was added to effectively dilute to an equivalent of 1x Laemmli. 1x Laemmli solution was added to the remaining cells. The cells were scraped and then spun down to create a pellet. A total cell lysate was used to compare the TritonX-100 soluble and insoluble components.

For some experiments the band intensities of the immunoblots were quantified and mean values were calculated for at least 3 experiments.

Electron microscopy. MDCK-CX_3CL1 cells were grown to confluence on 25mm coverslips. The cells were fixed with 4% paraformaldehyde at 4°C for 30 mins, washed and then labelled with anti-CX_3CL1 Ab (1μg/ml) in PBS for 1 hour at room temperature. After further washing, cells were incubated with 18nm gold-labelled anti-goat IgG secondary antibody (1:20 dilution) for 1 hour at room temperature. The cells were again washed prior to enhancement of the gold particles with a Goldenhanced EM Kit (Nanoprobes, Yaphank, NY). Samples were dehydrated and then mounted on stubs. They were coated with carbon before analysis with an XL30environmental ESM (ESEM) from FEI (Hillboro, Oregon). Images were generated through the combination of signals from the

gaseous secondary electron detector and the backscatter electron detector.

Fluorescence recovery after photobleaching (FRAP). Experiments were performed as previously described (232, 243). MDCK-CX_3CL1-GFP cells or ECV-CX_3CL1-GFP cells were grown to confluence on 25mm coverslips. Cells were treated with 10μM GM6001 4 hours prior to the photobleaching to prevent constitutive cleavage of CX_3CL1. The coverslip was placed into an Attafluor chamber at 37°C and the cells were maintained in RPMI containing 5% fetal calf serum and 25mM HEPES.

To assess the lateral mobility of CX_3CL1 in the cell membrane of epithelial cells, the apical surface of the MDCK-CX_3CL1-GFP cells was brought into focus on a confocal microscope and two 2.5μm diameter areas of similar fluorescent intensity were selected per cell. After acquiring baseline measurements, one of the defined areas was irreversibly photobleached using a 30 milliwatt LASOS argon laser and the fluorescence of both selected areas was measured over time. Fractional fluorescence recovery of the bleached area was determined relative to pre-bleach measurements. The unbleached area was used to control for inadvertent bleaching during repeated image acquisition. Results are expressed as the mean fluorescence recovery for at least 5 experiments, with standard errors of the mean (SEM). This same

protocol was used in ECV-CX_3CL1 cells to assess the lateral mobility of CX_3CL1 following TP stimulation.

To assess the endocytosis of CX_3CL1 in ECV cells, cells were again grown to confluence on 25mm coverslips. Four hours prior to transfer into an Attafluor chamber, the cells were treated with 10μM GM6001, a metalloprotease inhibitor, to prevent potential shedding of cell surface CX_3CL1. The live cells were analysed by confocal microscopy and the entire juxtanuclear CX_3CL1 containing compartment was photobleached as described above. In other experiments, a 2μm region of the plasma membrane was irreversibly photobleached. Recovery of fluorescence of the bleached areas was recorded over time. The fluorescence of defined non-bleached areas of the plasma membrane of the same cell was also measured as a control to quantify the amount of bleaching induced by repeated image acquisition. The results are again expressed as the mean normalised fluorescence recovery, with standard errors of the mean.

Adhesion assays – renal tubular epithelial cells. Experiments were performed as described elsewhere with minor modifications as outlined (58). MDCK-CX_3CL1-GFP cells were grown to confluence on 25mm coverslips and pre-treated with 10μM TAPI-2 for 2 hours to maximize cell surface expression of CX_3CL1. K562-CX_3CR1 cells were labelled with cholera toxin B-555 (0.5μg/ml) for 20 mins at room temperature and $1x10^6$ cells were added to wells of either MDCK-WT or MDCK-CX_3CL1-

GFP cells with gentle rocking at 10 cycles per minute for 30 mins. Non-adherent cells were washed away and remaining cells were fixed and mounted onto slides. Using a Leica deconvolution microscope, at least 50 high power fields (x63) were examined to count the number of adhered cells. The data was graphed to show a normal distribution for each experiment.

Results are the mean of 4 separate experiments with SEMs and were compared using the Student's t-test. Cells were also examined using a spinning disk confocal microscope, after being fixed and mounted onto glass slides. Experiments were repeated using primary RTECs and peripheral blood mononuclear cells isolated from healthy volunteers as outlined above. The PBMCs were labelled with calcein-AM (15μM for 30 mins at 37°C) and $1x10^4$ PBMCs were added to 25mm coverslips with confluent primary RTEC for 30 mins with rocking at 10 cycles per minute. The cells were washed and fixed as above. In parallel experiments, a functional anti-CX3CL1 Ab (1μg/ml) was added to the wells 30 mins prior to the addition of the PBMCs.

Flow cytometry. ECV-CX_3CL1-GFP cells were grown on 10 cm dishes and treated with TP agonists, IBOP (100nM) or U46619 (20μM), for various time periods. Cells were lifted by briefly incubating with 5% EDTA at 4°C, washed and fixed in 4% paraformaldehyde. After further washing, cells were incubated with 5% donkey serum for 20 mins at

room temperature, followed by incubation with anti-CX_3CL1 Ab (1μg/ml) for 1 hr at room temperature. After further washing, cells were incubated with PE-conjugated donkey anti-goat IgG (2.5μg/ml) for 1 hr at room temperature. Cells were suspended in PBS and analysed using a fluorescence-activated cell scanner (FACScan; BD Biosciences, San Jose, CA). Experiments were done without the use of primary antibody in some cases but ideally an irrelevant isotype antibody of the same species as the experimental antibody should also have been used to confirm the specificity of the results.

The mean fluorescence intensity was normalised to control and given as a percentage. Repeated measures analysis of variance (ANOVA) was used to compare means for repeated tests such as the effect of TP stimulation for different time periods and one-way ANOVA was used to compare the means of independent groups, for example TP stimulation in the presence or absence of TAPI-2.

CX_3CL1 shedding experiments. Small interfering RNA (siRNA) directed against human ADAM-10, human TACE, and control non-targeting siRNA were purchased from Santa Cruz Biotechnology. ECV-CX_3CL1 cells were grown in two $75cm^2$ flasks with DMEM and 5% FBS until confluent. The cells were then trypsinised and washed with PBS. The cells were centrifuged and the cell pellet had 100μL of AMAXA kit V solution added plus 10μL of 10μM stock siRNA for TACE, ADAM-10 or

scrambled siRNA (=100pmol of siRNA). The cells were electroporated using program A23 of the AMAXA kit, (Amaxa, Gaithersburg, MD) on Day 0 and Day 2. After the first electroporation 0.5ml of DMEM with 5% FCS was added to the cuvette. Following resuspension, cells were added to 10cm culture dishes with 10ml of DMEM and incubated for 2 days before undergoing a second electroporation with siRNA. After the second electroporation, cells were plated in 6-well tissue culture plates at a density of $1x10^5$ cells/well and cultured for 48 h.

Two electroporations were done as it was found that after one the transfection rate was only 40-50%. By doing two electroporations this figure increased to 80%. Having started with approximately 10 million cells, around 30% were killed following the first electroporation.

Following electroporation cells were incubated with IBOP (2.5 μg/ml) for 30 min at 37°C, and conditioned medium collected. Cells were washed once with PBS and lysed by adding 0.5 ml RIPA buffer. Protease inhibitor cocktail (Sigma) was added (1:100) to both harvested conditioned medium and to cell lysis buffer to prevent protein degradation. Supernatants and cell lysates were cleared by centrifugation at 13,000 rpm at 4°C for 10 min. Using fresh samples, CX_3CL1 was detected in conditioned medium and cell lysates using a CX_3CL1 ELISA Kit (R&D Systems, Minneapolis, MN), according to the manufacturer's specifications. Three independent experiments were performed, and the data were expressed as the mean ± SEM of the

percentage of soluble CX_3CL1 released into the medium in relation to the total amount of CX_3CL1 (soluble and cell-associated).

Acid-stripping experiments. The rate of delivery of internalised CX_3CL1 back to the plasma membrane was assessed using previously published protocols as described below (98, 244). ECV-CX_3CL1-GFP cells were grown to confluence on 25mm coverslips. To prevent potential shedding of cell surface CX_3CL1, cells were treated with the metalloprotease inhibitor GM6001 (20μM) for 4 hours prior to incubating with anti-CX_3CL1 Ab (1μg/ml) for 1 h at 37°C (93). Cells were then washed with ice cold PBS. Membrane-associated Ab was removed by acid wash (0.15M NaCl, 50 mM glycine, 0.1% BSA, pH 2.5) on ice for 2 mins. Cells were then bathed in recovery solution (150mM NaCl, 20mM HEPES, 1mM $CaCl_2$, 5mM KCl, 1mM $MgCl_2$, pH 7.4) for 3 mins and were allowed to recover for time periods of 5-15 mins in the presence of TP agonist or in media alone. Cells were washed, fixed in 4% paraformaldehyde, and incubated with Cy3-conjugated secondary Ab (1.5μg/ml) for 1 hour at room temperature. After further washing, the cells were mounted onto glass slides using DAKO. Images were captured using a Leica DMIRE2 microscope and OpenLab software (Improvision Inc., Lexington, MA). Cell surface immunofluorescence intensity was measured using Volocity imaging software for at least 30 cells for each condition (Improvision, INC., Waltham, MA). The results

represent the mean of 3 experiments with SEMs. The data was graphed initially to demonstrate normal distribution and then the difference between means was analysed using the Student's t-test.

Statistical Analyses. All the results were reviewed and analysed by a University of Sydney statistician. For all techniques a minimum of 3 experiments were performed. The data were analysed by comparing the mean values using the Student's t-test for data with a normal distribution and using analysis of variance (ANOVA) for non-normally distributed data or repeated measures data. A value of $p<0.05$ was considered significant

Chapter 4. Results part 1

The Expression and Targeting of CX_3CL1 in Renal Tubular Epithelial Cells

1. CX_3CL1 is expressed in renal tubular epithelial cells (RTEC).

To define the functions of CX_3CL1 in RTEC, we first examined CX_3CL1 expression in five human renal allograft biopsy specimens. Three specimens had a histologic diagnosis of acute rejection and two of acute tubular necrosis. Cockwell *et al* have previously used immunohistochemistry to show CX_3CL1 expression in human renal biopsy specimens with acute allograft rejection (49). We used immunofluorescent probes to label the CX_3CL1. In all 5 specimens we detected CX_3CL1 expression in renal tubules, particularly on the apical surface, which was against our hypothesis of basal expression (Figure 1B, C &F-K). In addition to being expressed on tubular epithelium, CX_3CL1 expression was noted within glomeruli and on vascular endothelium, (Figure 1A, F &G), which is in keeping with Cockwell's previous published report (49). Again, similar to the previous report, we found that some tubules had more staining than others. We were unable to correlate the clinical severity with the degree of CX_3CL1 expression, as this information was not available. Further experiments were done using the addition of DAPI staining to facilitate orientation within the kidney. To verify the specificity of staining, we omitted primary anti-CX_3CL1 Ab from some experiments. When secondary

antibody alone was used, very little background immunofluorescence was observed (Figure 1D). At the Hospital for Sick Children in Toronto, where this work was performed, donor pre-implantation renal transplant biopsies are not taken routinely and therefore could not be used as an additional negative control. We did however repeat the experiments at a later date and included a normal renal biopsy specimen, which showed minimal staining for CX_3CL1 (Figure 1E). Using the same anti-CX_3CL1 Ab as the one used in our study, other investigators previously reported minimal immunohistochemical expression of CX_3CL1 in normal renal biopsy tissue (49, 59).

(Renal biopsy specimens were provided by Dr Andrew Herzenberg, staining was done by Michael Ho, pathology technician, and by Guang-Ying Liu and the microscopy was done by Anne Durkan.)

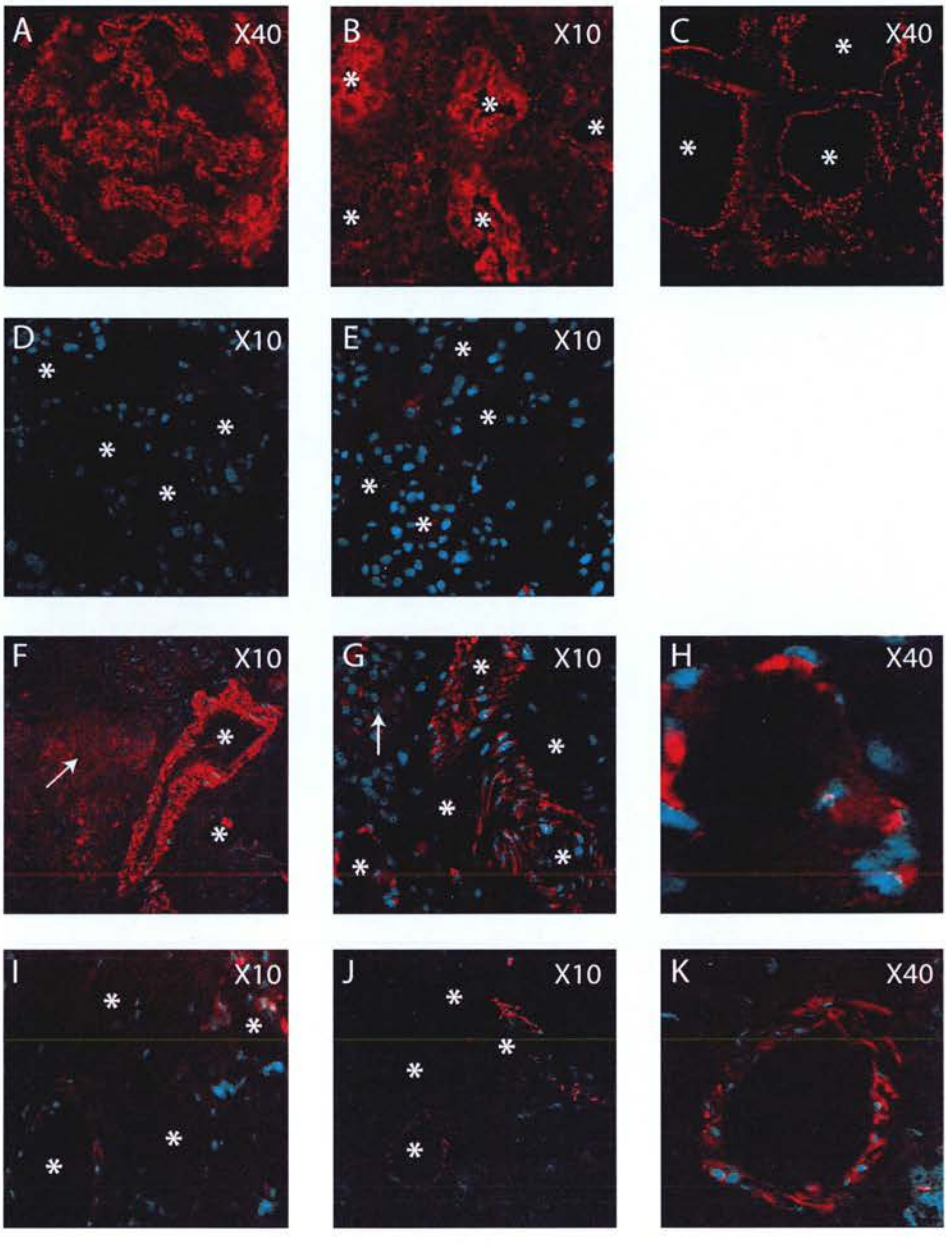

Figure 1. ***CX_3CL1 is expressed in human renal tubular epithelial cells.*** Immunofluorescent labelling of CX_3CL1 in human renal allograft biopsy specimens, with histologic diagnoses of acute tubular necrosis (A, C, D & F-H) and acute tubular rejection (B, I-K). Biopsy specimens were labelled with anti-CX_3CL1 Ab and Cy3 conjugated secondary Ab. A glomerulus is shown in figure 1A and tubules are shown

in figures 1 B and C. In experiments D-K DAPI was also used to label cell nuclei. No primary antibody was used in figure 1D and a normal kidney biopsy specimen was stained in figure 1E. * denotes tubular lumen and arrows mark glomeruli.

To examine the expression and subcellular distribution of CX_3CL1 more closely, we selected HK-2 cells, a human RTEC line, as we felt that this was the most appropriate to reflect the *in vivo* situation in human kidneys. Using RT-PCR, we detected CX_3CL1 mRNA (Figure 2A). To verify CX_3CL1 protein expression we performed immunofluorescence staining and again found the chemokine predominantly at the apical surface (Figure 2C&D). We encountered some difficulty with the HK-2 cells, as they tended to grow in flattened monolayers, rather than as tall cuboidal or columnar cells that are typical of epithelial cells. We needed to clearly demarcate the apical from the basolateral surface, particularly when using immunofluorescent microscopy to examine the cells. Using confocal microscopy we took multiple images in the XY plane at various depths through the cell, thus creating a Z stack, which is essentially a 3 dimensional reconstruction of the cell. The Z stacks created with the HK-2 cells were sub-optimal because of the flattened phenotype so we sought an alternative model to enable unequivocal differentiation of the apical membrane from the basolateral membrane.

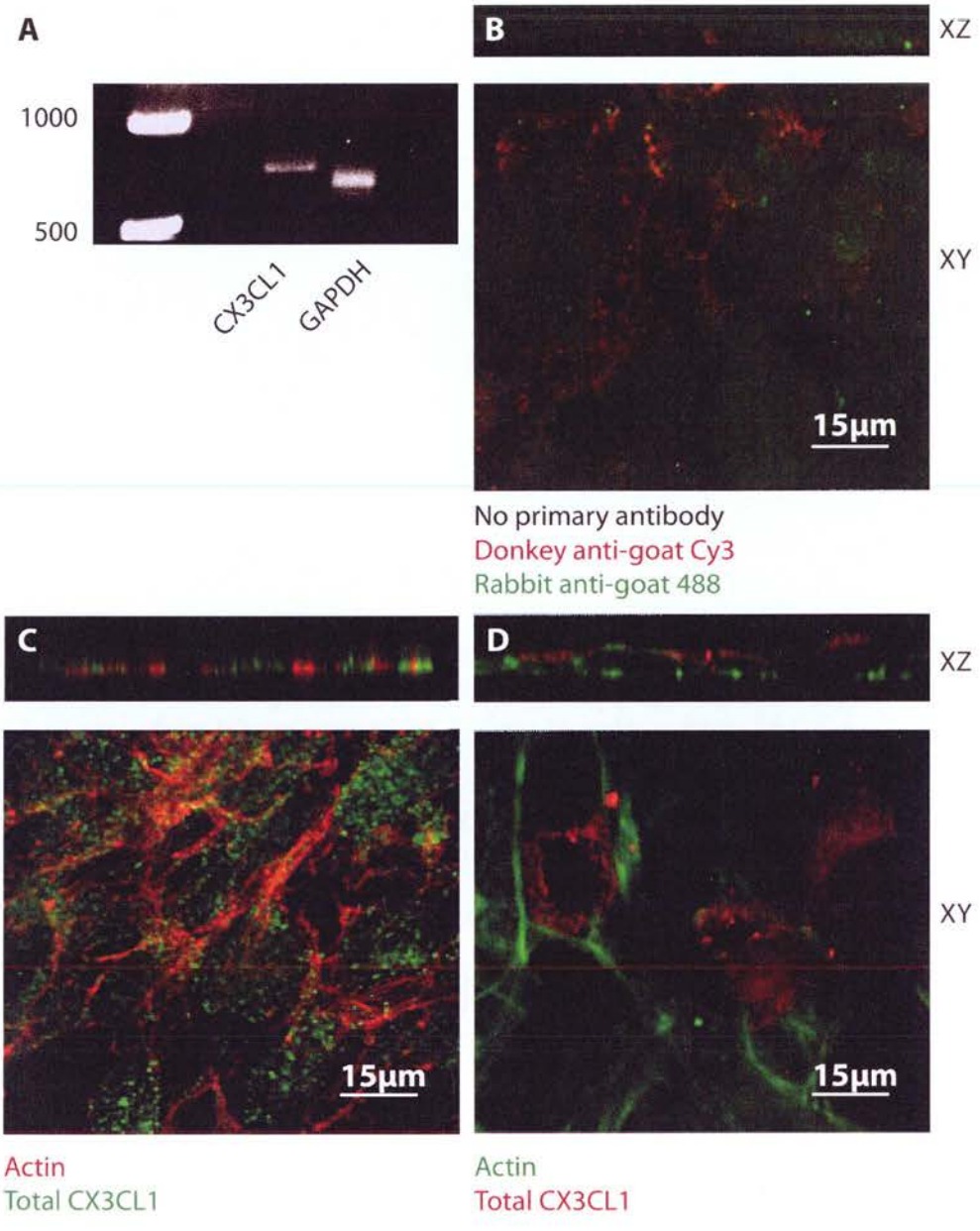

Figure 2. ***CX_3CL1 is expressed in HK-2 renal tubular epithelial cells.*** (A) Total RNA was isolated from HK-2 cells and CX_3CL1 amplified by RT-PCR using specific published primers. The PCR products were size-fractionated on 1% agarose. GAPDH is shown as a control. (B-C) Immunofluorescence staining of HK-2 cells using anti-CX_3CL1 antibody and a Cy2-conjugated secondary antibody. Actin was labelled with rhodamine-conjugated phalloidin in figure 2C. No primary antibody was used in

figure 2B as a negative control. (D) Immunofluorescence staining of HK-2 cells using anti-CX_3CL1 antibody and a Cy3-conjugated secondary antibody. Actin was labelled with Oregon green 488-conjugated phalloidin.

(The RT-PCR was done by Guiseppe Femia, a summer student and the immunofluorescence staining and microscopy was done by Anne Durkan.)

2. *CX_3CL1 is expressed in the apical membrane of RTEC.*

Madin Derby Canine Kidney II (MDCK) cells are renal tubular cells that have a classical cuboidal morphology typical of epithelial cells. They have been used extensively to study epithelial cell structure and function and because of their morphology permit clear differentiation of the apical and basolateral membranes (232, 245). In the absence of an anti-canine CX_3CL1 antibody, we initially stained the wild type cells with the anti-human CX_3CL1 Ab, followed by a fluorescent-conjugated secondary Ab. No CX_3CL1 was detected (Figure 3). This was confirmed using Western blotting to detect the protein (Figure 4A).

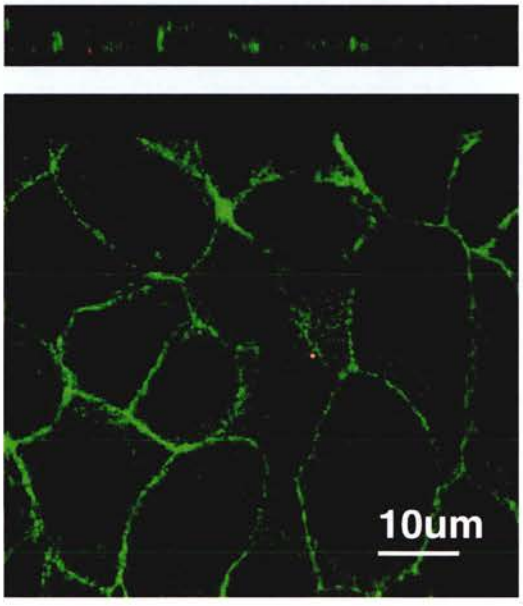

MDCK-WT cells
Surface CX3CL1- red
Total CX3CL1- blue
Actin - green

(Experiment done by Anne Durkan)

Figure 3. ***MDCK-WT cells do not stain for CX_3CL1.***

We therefore created a stable cell line of MDCK cells expressing full-length CX_3CL1 or CX_3CL1 with a GFP tag at the C-terminus, (MDCK-CX_3CL1 and MDCK-CX_3CL1-GFP respectively). The GFP tagged CX_3CL1 has been used previously by members of our laboratory in a different cell line with no effect on cellular levels or distribution of CX_3CL1 (98).

Using Western analysis and anti-CX_3CL1 Ab, both MDCK-CX_3CL1 and MDCK-CX_3CL1-GFP cells displayed bands of appropriate molecular weight (90kDa and 117kDa respectively) (Figure 4A). To confirm these findings cell lysates from control MDCK cells and from MDCK-CX_3CL1-GFP cells were probed with an anti-GFP antibody and again a band at molecular weight 117kDa was obtained from the MDCK-CX_3CL1-GFP cells (Figure 4B).

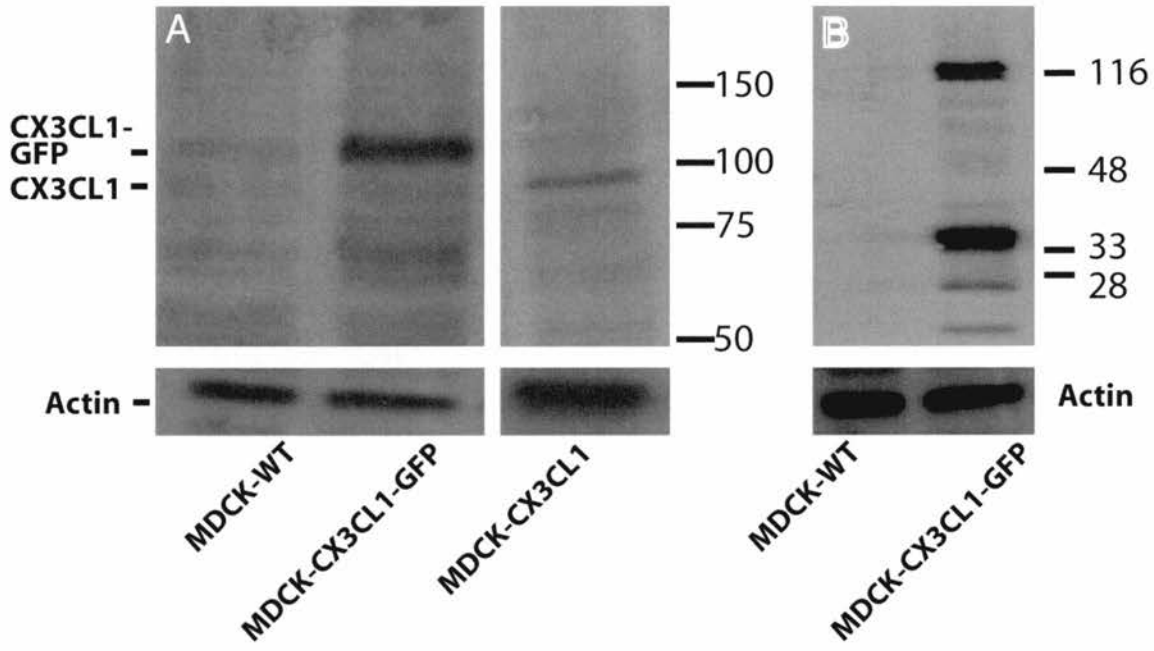

Figure 4. ***CX_3CL1 and CX_3CL1-GFP in MDCK cells.***

Western analysis was performed using cell lysates from MDCK-WT, MDCK-CX_3CL1 and MDCK-CX_3CL1-GFP cells. The lysates were labelled with anti-CX_3CL1 antibody (A) or anti-GFP antibody (B) and HRP conjugated secondary antibody.

(The stable MDCK-CX_3CL1 and MDCK-CX_3CL1-GFP cell lines created by Guang-Ying Liu. The Western analysis was done by Anne Durkan).

To assess the subcellular localization of CX_3CL1, MDCK-CX_3CL1-GFP cells were fixed and incubated with anti-CX_3CL1 Ab, which labelled only the apical surface (Figure 5F&J). To visualize intracellular CX_3CL1, the same cells were then permeabilised with 0.1% Triton X-100 and incubated with anti-CX_3CL1 Ab followed by a different secondary Ab. This confirmed an intracellular pool of CX_3CL1 in subapical vesicles, with a small proportion on the basolateral membrane (Figure 5D, E, H, I

L&M). To confirm that any labelling of MDCK-CX_3CL1-GFP cells with anti-CX_3CL1 Ab was specific for CX_3CL1, we incubated untransfected cells with the same Ab. In these experiments there was no immunofluorescence staining observed (Figure 3). Furthermore, incubation of MDCK-CX_3CL1-GFP cells with secondary Ab alone, after omitting the primary Ab, again yielded no immunofluorescence staining (Figure 5B). These data demonstrate that CX_3CL1 is expressed on the apical plasma membrane as well as within subapical vesicles and to a lesser degree on the basolateral membrane in RTEC. This was in keeping with previous immunohistochemistry results from kidney biopsy specimens (59).

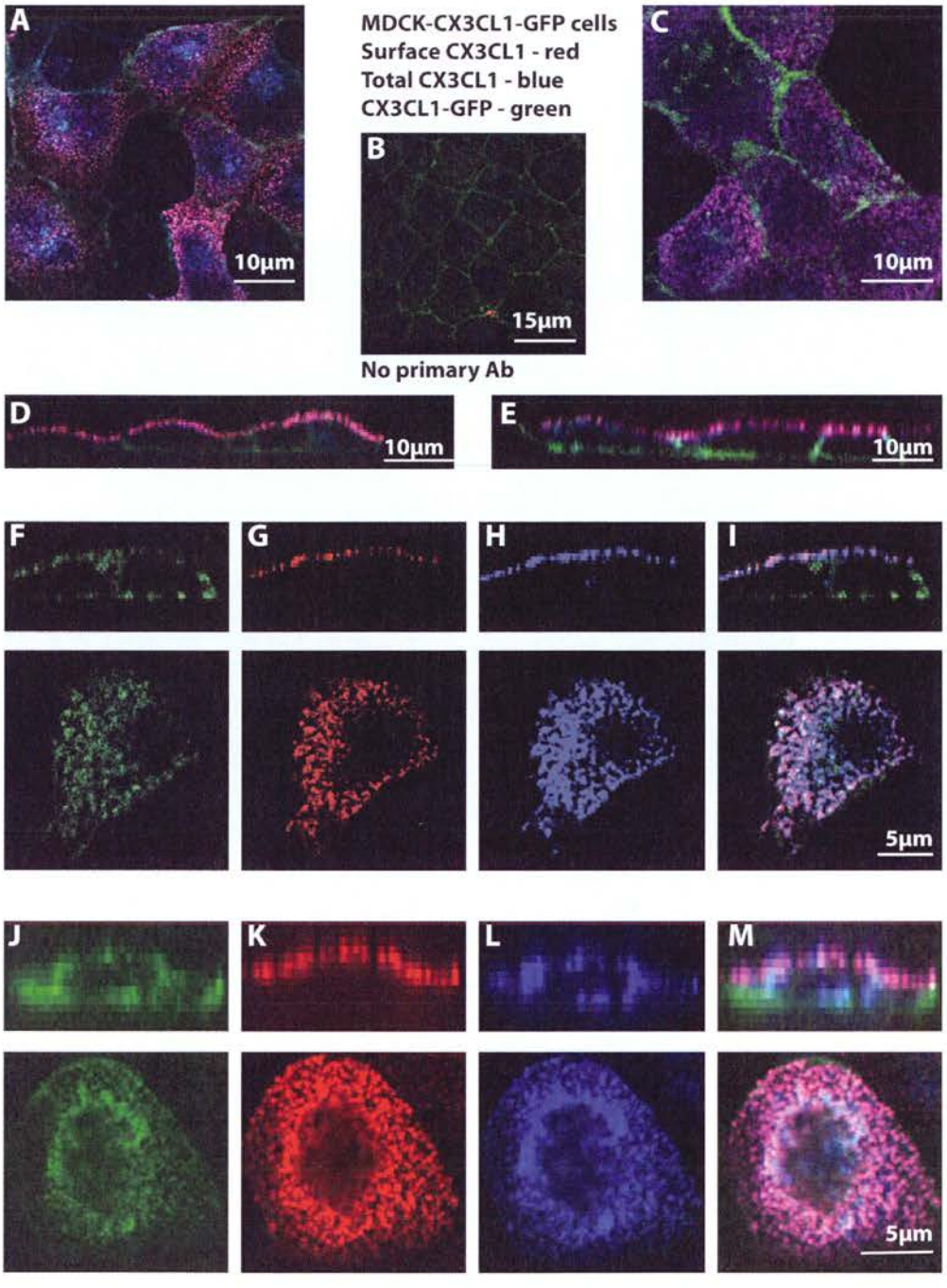

Figure 5. *CX_3CL1 is found largely on the apical surface and in subapical vesicles in MDCK-CX_3CL1-GFP cells, with only a small proportion on the basolateral membrane.* MDCK-CX_3CL1-GFP cells were fixed and labelled with an anti-CX_3CL1 Ab

applied to the apical surface, followed by a Cy-3 conjugated secondary Ab. The cells were then permeabilised and again labelled with an anti-CX_3CL1 Ab followed by a Cy-5 conjugated secondary Ab. Low power images of two different experiments in the XY plane (figures 5A&C) and in the XZ plane (figures 5D&E). Higher power images of single cells showing the apical and subapical distribution of CX_3CL1 (figures 5F-M). The XZ plane is shown above and the XY plane below. Control experiment using no primary Ab confirms the specificity of the Ab (figure 5B).
(Experiments done by Anne Durkan).

In MDCK-CX_3CL1-GFP cells, GFP is attached to the cytoplasmic tail of the chemokine. Since the tagged construct was recognised by the antibody directed against the extracellular domain of CX_3CL1, the protein expressed must traverse the apical membrane (Figures 5D, E, I & M). We also noted a second pool of GFP, present in the basolateral membrane (Figures 5D-F & J). This pool did not completely overlap with the total CX_3CL1 staining seen following permeabilisation of the cells (figures 5D, E, I & M). To determine the source of this we used a second anti-CX_3CL1 Ab that recognised the C-terminal region of CX_3CL1, rather than the chemokine domain against which the first Ab was directed. Following permeabilisation, the basolateral pool of GFP could be labelled by this C-terminal domain anti-CX_3CL1 Ab suggesting that at the very least the C-terminal domain of CX_3CL1 was present (Figure 6I-L). These results were confirmed in MDCK-CX3CL1 cells without the GFP tag (Figure 6E-H).

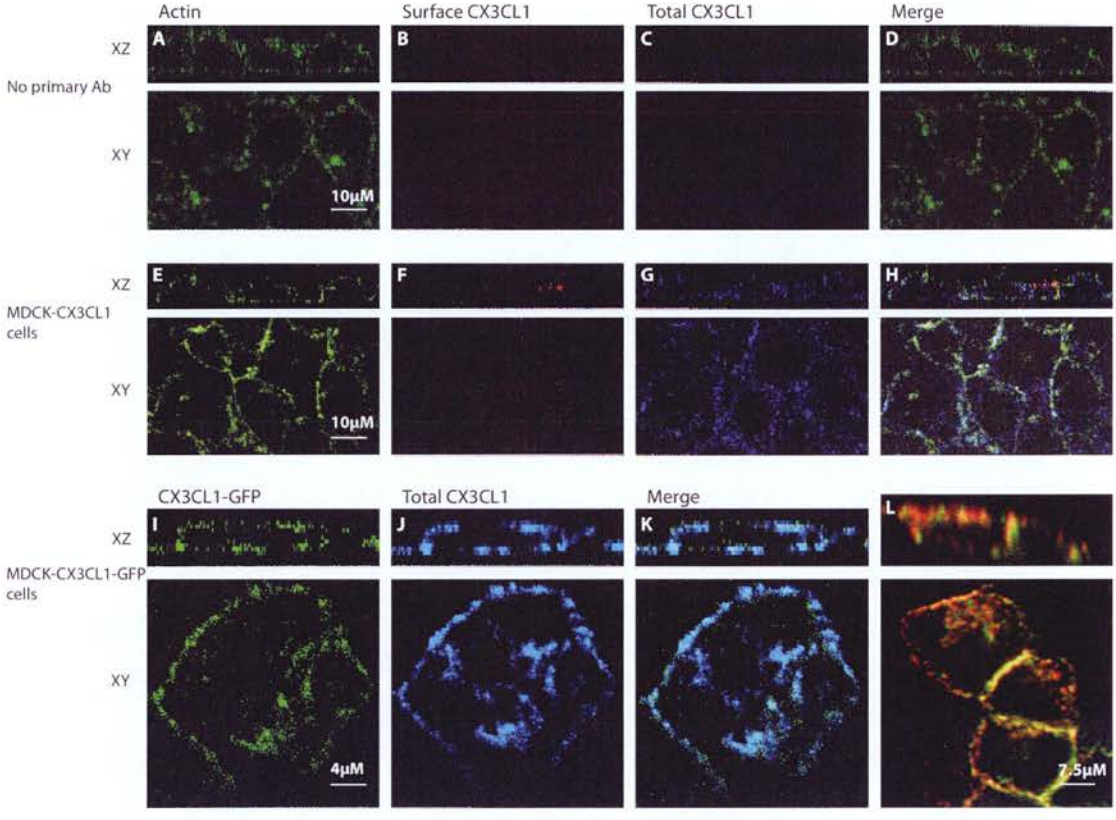

Figure 6. ***The entire basal pool of CX_3CL1 can be labelled with an antibody recognising the C-terminal of the protein.*** After fixation, MDCK-CX_3CL1 cells were labelled with a primary antibody recognising the C-terminal of CX_3CL1, followed by Cy-3 conjugated secondary Ab. The cells were permeabilised and re-labelled with the C-terminal Ab, followed by a Cy-5 conjugated secondary Ab (Fig 6E-H). As a negative control the primary Ab was omitted in some experiments (Fig 6A-D). The experiments were repeated in MDCK-CX_3CL1-GFP cells using only the permeabilised cells, as the previous experiments had demonstrated no surface CX_3CL1 staining (Fig 6I-K). In a repeat experiment the total CX_3CL1 was labelled with the anti-C-terminal CX_3CL1 Ab followed by a Cy-3 conjugated secondary Ab (Fig 6L).

(Experiments done by Anne Durkan).

It could be argued that the basolateral CX_3CL1 could not be properly labelled in our initial experiments as we used an apical application of an antibody directed against the chemokine (extracellular) domain. To investigate this, we grew MDCK-CX_3CL1-GFP cells on filters and after fixation, applied the Ab recognising the chemokine domain to the basal medium, with no Ab application to the apical medium. The cells were then labelled with a Cy-3 secondary Ab. The total CX_3CL1 content was labelled as previously following permeabilisation. This showed that there was very little basal surface staining of CX_3CL1, despite the basal application of the antibody (figure 7). (Unfortunately the format in which these images were stored does not allow further manipulation and I am unable to create a merged image, which would enhance the figure below).

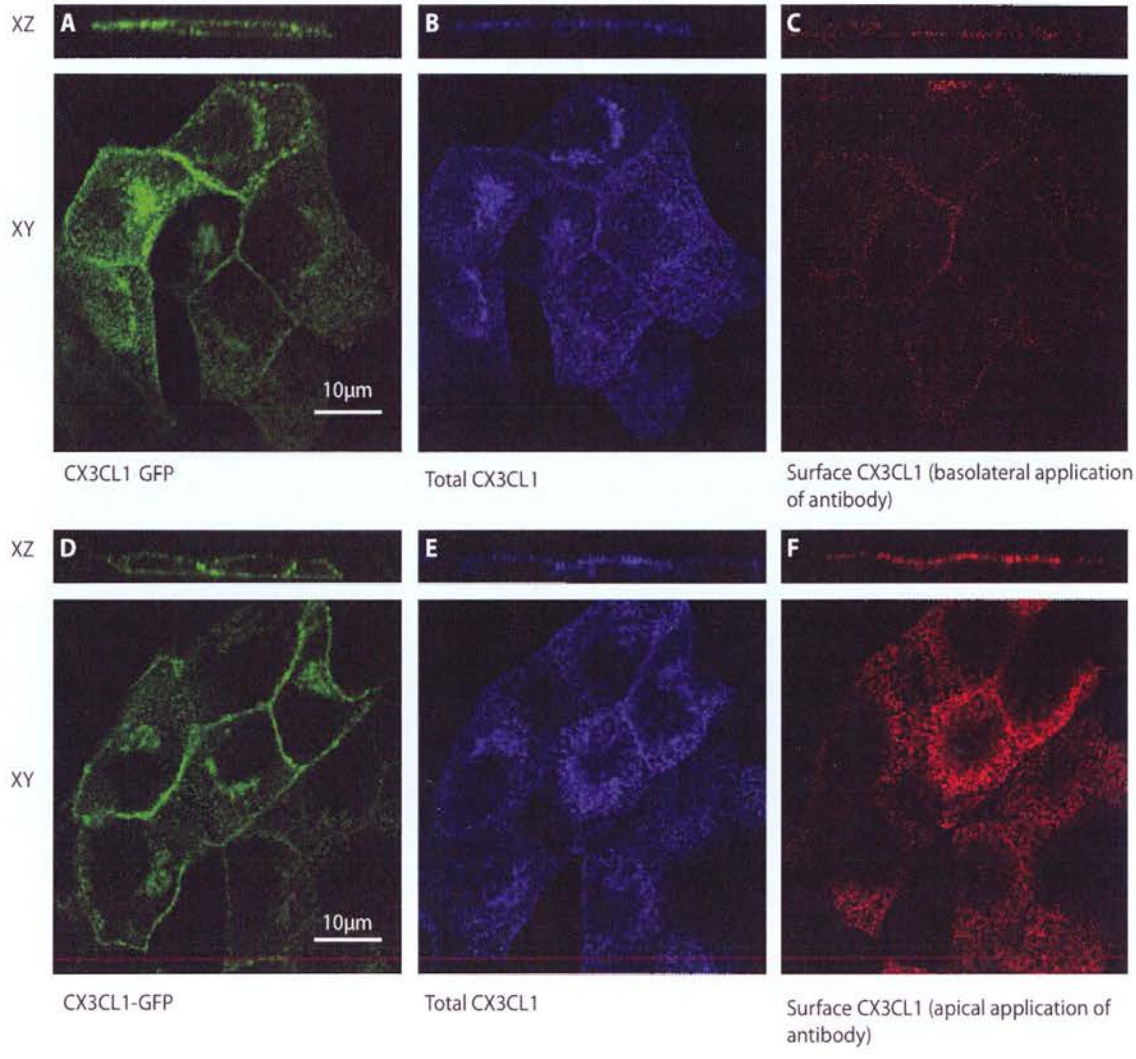

Figure 7. ***Basal application of the anti-CX_3CL1 Ab does not demonstrate significant basal full-length CX_3CL1.*** MDCK-CX_3CL1-GFP cells were grown on filters and after fixation, were labelled with an anti-CX_3CL1 Ab applied to the basal surface. This was followed by the application of a Cy-3 conjugated secondary Ab. The cells were then permeabilised and re-labelled with the anti-CX_3CL1 Ab. A Cy-5 secondary Ab was then applied (fig 7A-C). Control experiments used apical application of the anti-CX_3CL1 Ab (fig 7D-F).

(Experiments done by Anne Durkan).

We believe that basolateral GFP largely represents the intracellular portion of CX_3CL1, which remains after the extracellular segment has been proteolytically released. In agreement with this supposition is the Western analysis of MDCK-CX_3CL1-GFP cells using an anti-GFP Ab, which consistently revealed two separate bands. The molecular masses of these bands correlated with the full-length CX_3CL1-GFP fusion protein (Figure 4A&B) or a fusion protein corresponding to the intracellular region of CX_3CL1 together with GFP (~36 kDa; Figure 4B). To ensure that the GFP tag did not alter subcellular traffic of CX_3CL1, we examined MDCK cells expressing the untagged chemokine. After labelling both surface and total CX_3CL1 we found a similar distribution, primarily on the apical membrane but also in subapical vesicles (Figure 8). This was consistent with our findings using the anti-CX_3CL1 antibody directed against the C-terminal of CX_3CL1 (Fig 6E-H).

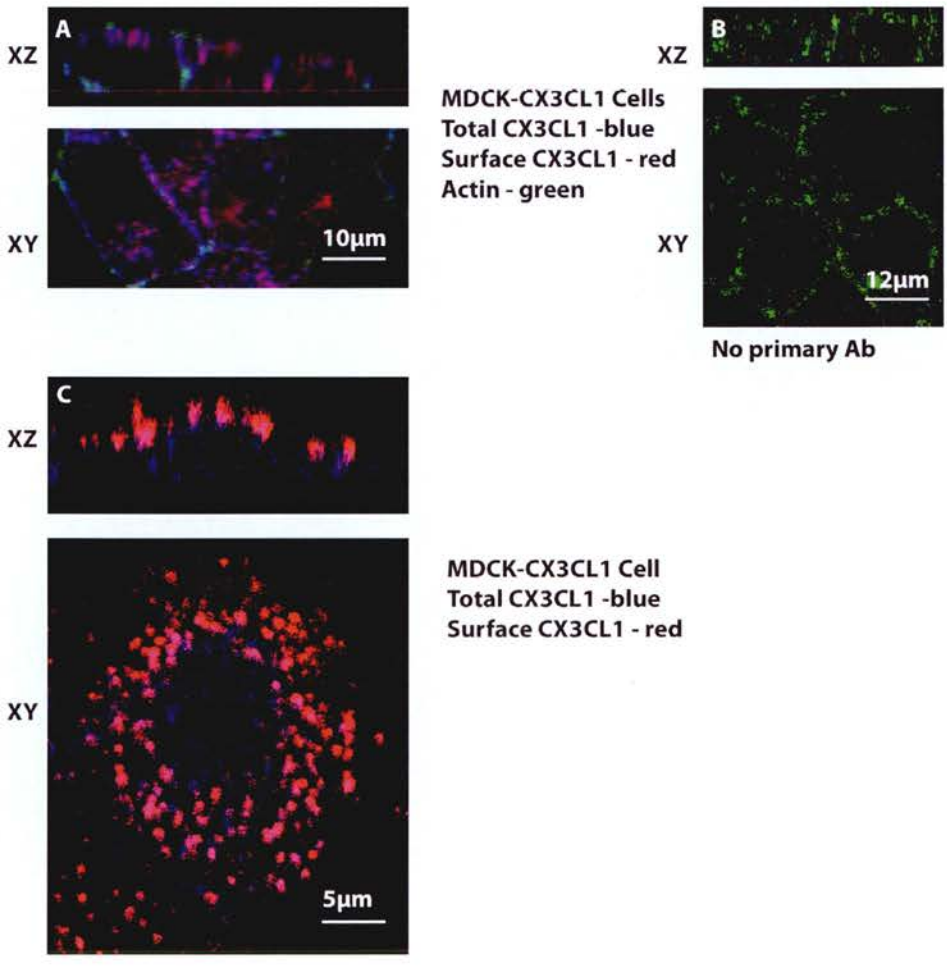

Figure 8. ***The distribution of CX_3CL1 is not affected by the addition of the GFP tag.*** MDCK-CX_3CL1 cells were fixed and labelled with anti-CX_3CL1 Ab, followed by a Cy-3 conjugated secondary Ab. The cells were permeabilised and then relabelled with an anti-CX_3CL1 Ab followed by a Cy-5 conjugated Ab. Figures 8A&C represent two different experiments. The specificity of the primary antibody was assessed by omission in some experiments (fig 8B).

(Experiments done by Anne Durkan).

Electron microscopy was then used to examine the apical microvilli. After labelling the surface CX_3CL1 of MDCK-CX_3CL1-GFP cells with a gold-conjugated Ab we subjected the cells to scanning electron microscopy. As shown in Figure 9, this provided further evidence that CX_3CL1 is associated with microvilli on the apical surface of RTEC.

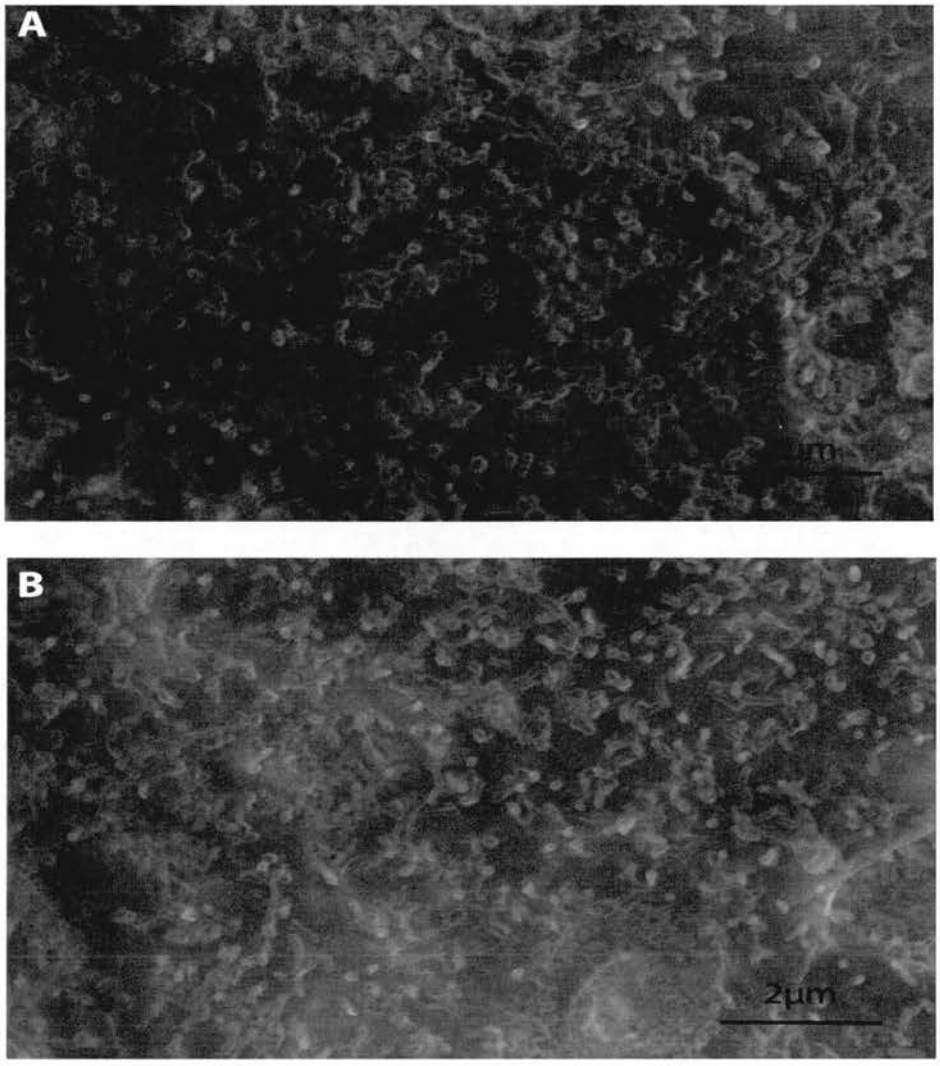

Figure 9. ***Electron microscopy of apical CX_3CL1 in MDCK-CX_3CL1-GFP cells.*** MDCK-CX_3CL1-GFP cells were labelled with anti-CX_3CL1 antibody and gold-conjugated secondary antibody and examined using scanning electron microscopy. Arrows show the association of the CX_3CL1 with apical microvilli (fig 9A). MDCK-WT cells were used as control cells (fig 9B).

(The cells were stained by Anne Durkan. The electron microscopy images were taken by technicians in the electron microscopy facility at the University of Toronto).

3. *CX_3CL1 is targeted to the apical membrane by N-glycosylation.*

Having been somewhat surprised by the apical distribution of CX_3CL1, we next investigated the signals that targeted the protein to this membrane in RTEC. Apical sorting of transmembrane proteins can be determined by signals conferred by the cytoplasmic tail of the protein (246, 247), by O- or N-glycosylation (248), or by membrane anchoring of the protein to lipid microdomains in the cell membrane, through GPI or by direct binding of the transmembrane domain of the protein to lipid rafts (249). We examined each of these potential mechanisms in turn.

There are various signalling mechanisms that are found in the cytosolic domain of proteins such as tyrosine-based signals, leucine or dileucine motifs and PDZ domains. To determine if any of these were important for the apical targeting of CX_3CL1, we generated a mutant construct lacking the cytoplasmic domain (CX_3CL1-360). (In the initial description of CX_3CL1 by Bazan *et al*, the predicted signal peptide amino acid sequence was numbered from -24 to -1 and therefore the cytoplasmic tail began at amino acid 361 (35)). To confirm the accuracy of the DNA expression plasmid, it was gene sequenced. We examined the distribution of CX_3CL1 in MDCK cells stably expressing "tail-less" CX_3CL1 using immunofluorescent microscopy but found that the protein was still directed to the apical membrane (Figure 10).

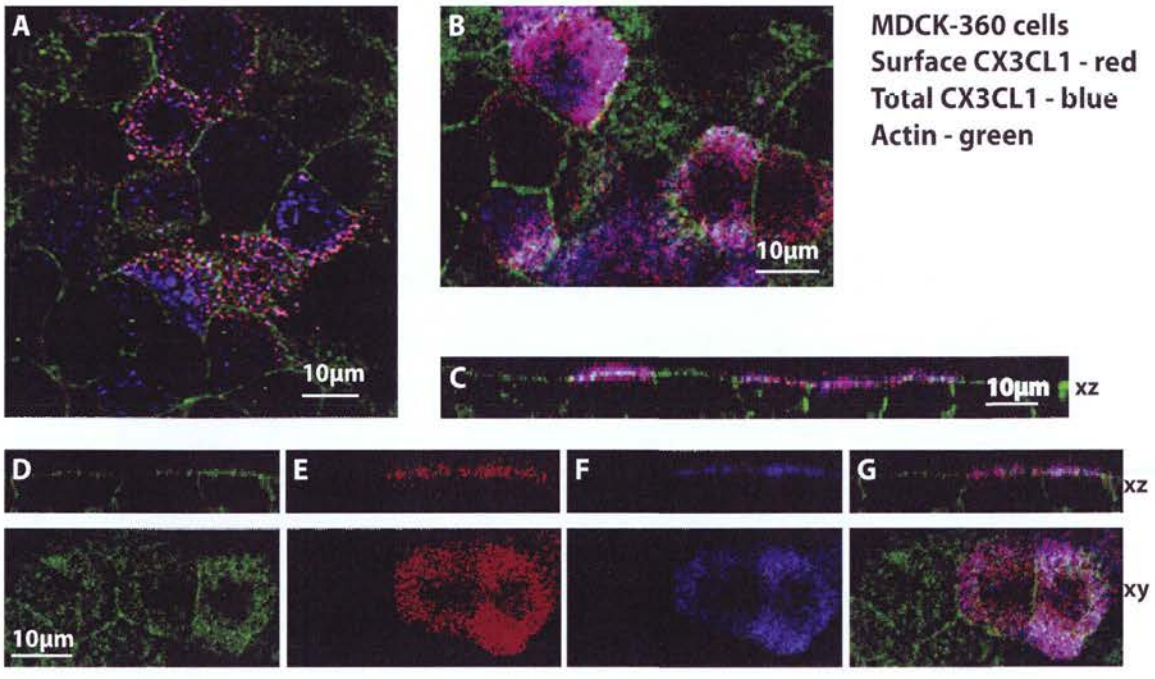

Figure 10. Deletion of the cytoplasmic tail of CX_3CL1 does not affect its apical distribution. MDCK cells expressing a mutant CX_3CL1 DNA expression plasmid that lacks the cytoplasmic tail (MDCK-CX_3CL1-360) were fixed, incubated with anti-CX_3CL1 antibody and a Cy3-conjugated secondary antibody, to visualise cell surface CX_3CL1. To further visualise intracellular CX_3CL1, the same cells were then permeabilised, labelled with anti-CX_3CL1 antibody and then Cy5-conjugated secondary antibody. After permeabilisation, cells were incubated with Alexa-488 conjugated phalloidin to label F-actin. Slides were examined using a spinning disk confocal microscope.

(The CX_3CL1-360 construct was created by Min Rui. The transfections, staining and microscopy were done by Anne Durkan.)

We next assessed the potential associations of CX_3CL1 with lipid rafts or caveolae. Lipid rafts are microdomains within the plasma membrane that are rich in cholesterol and sphingolipids. Caveolae are similarly rich in cholesterol and sphingolipids but also contain caveolin, hence the name. Partitioning of proteins into these microdomains is believed to have implications on the function of the protein, for example the cell adhesion molecule CD44 co-partitions with protein tyrosine kinases, which are required for its activation (250). Methyl-β-cyclodextrin (MβCD) selectively extracts cholesterol by directly binding to it and incorporating it in a cavity of cyclic oligmers of glucopyranoside (251). It has advantages over other methods of cholesterol binding in that it neither binds to the plasma membrane, nor does it become incorporated into the membrane. It has been used in several cell types to disrupt sphingolipid microdomains (252-254). Moreover, MβCD was used in MDCK cells to demonstrate the association of influenza virus haemagluttinin with lipid rafts to target to the apical plasma membrane (255). We therefore treated cells with MβCD to disrupt lipid rafts and caveolae in our MDCK-CX_3CL1-GFP cells. To ensure MβCD treatment was effective, we measured cholesterol spectrophotometrically, using a commercially available kit and compared the cell cholesterol levels with the provided standards (256). MβCD depleted total cellular cholesterol by 58 % (Figure 11A) but had no effect on apical targeting of CX_3CL1 (Figure 11B&F).

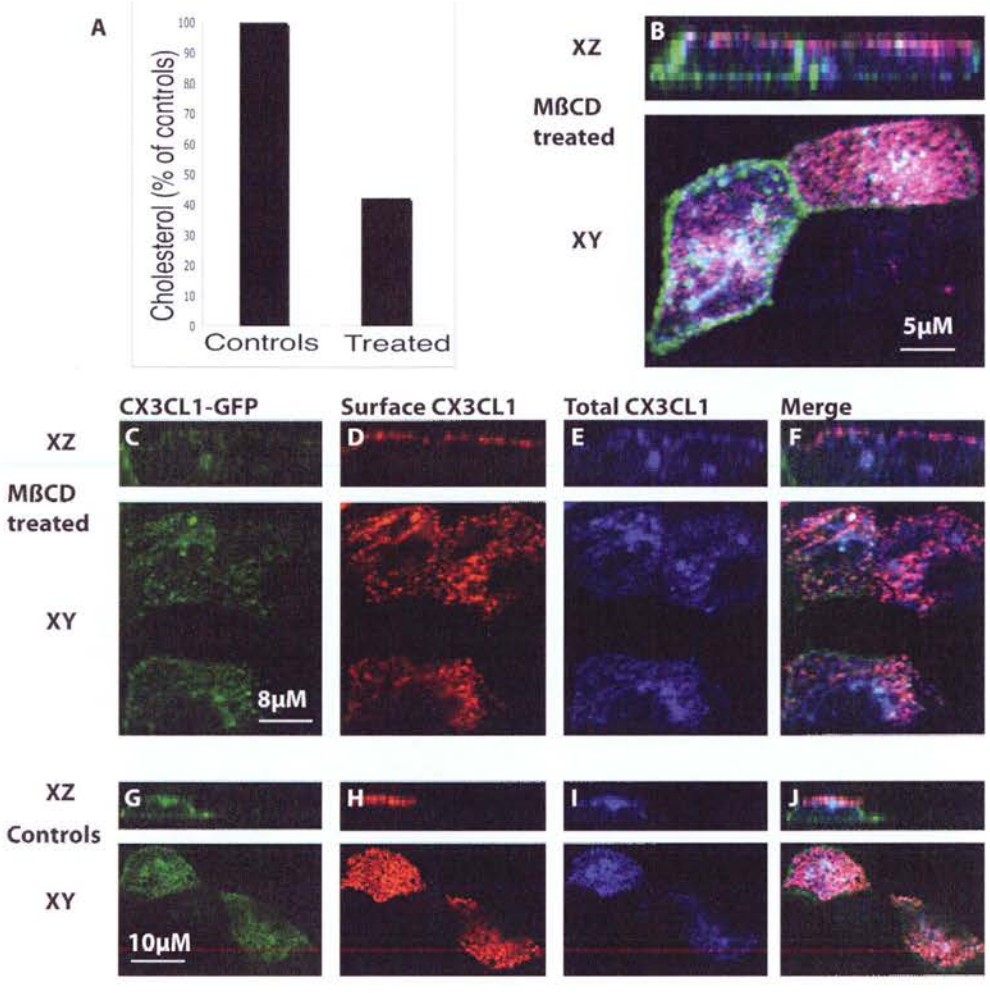

Figure 11. Apical targeting of CX_3CL1 is not disrupted by cholesterol depletion. To deplete cholesterol and disrupt lipid rafts, MDCK-CX_3CL1-GFP cells were incubated for 30 minutes at 37°C with methyl-β-cyclodextrin and the cholesterol content measured by spectrophotometry, using Amplex Red (Molecular Probes). Values for cholesterol content are expressed as a percentage of untreated controls and represent a mean of 3 experiments (Fig 11A). MDCK-CX_3CL1-GFP cells were incubated for 30 mins with methyl-β-cyclodextrin, prior to fixation and incubation with anti-CX_3CL1 Ab and a Cy-3 conjugated secondary Ab. Following permeabilisation the cells were re-incubated with the anti-CX_3CL1 Ab and a Cy-5 conjugated secondary Ab (Fig 11B-F).

Control cells were not pre-treated with MβCD. Slides were examined using a spinning disk confocal microscope.

(Experiments done by Anne Durkan).

We next examined glycosylation of CX_3CL1 as a determinant of apical targeting. O-glycosylation was inhibited with benzyl-2-acetamido-2-deoxy-α-D-galacto-pyranoside, which acts as a competitive inhibitor (257). Again, CX_3CL1 targeting to the apical membrane remained intact (Figure 12).

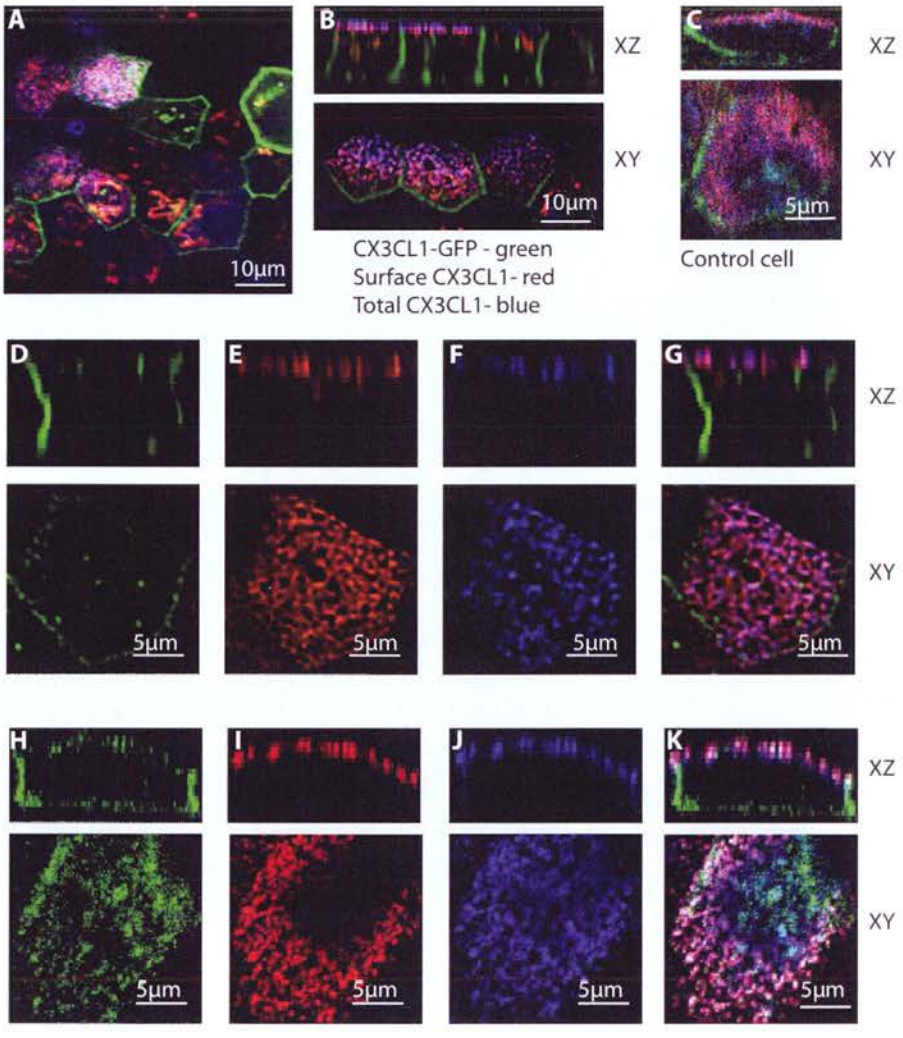

Figure 12. Inhibition of O-glycosylation does not affect the cellular distribution of CX_3CL1. MDCK-CX_3CL1-GFP cells were treated with benzyl-2-acetamido-2-deoxy-α-D-galacto-pyranoside to inhibit O-glycosylation. Surface CX_3CL1 was then labelled with an anti-CX_3CL1 Ab, followed by a Cy-3 conjugated secondary Ab (fig 12 E&I). Total CX_3CL1 was labelled, after permeabilisation, with the same anti-CX_3CL1 Ab and a Cy-5 conjugated secondary Ab (fig 12 F&J). The merged images are shown for several experiments (fig 12 A, B, G & K). In control experiments, no benzyl-2-acetamido-2-deoxy-α-D-galacto-pyranoside was used (fig 12C).

(Experiments done by Anne Durkan).

To inhibit N-glycosylation of CX_3CL1, we treated cells with 2.5μg/ml tunicamycin overnight. Tunicamycin is a homologous mix of antibiotics that prevents the formation of polyisoprenyl N-acetyl glucosaminyl pyrophosphate. This compound functions as a sugar donor in the N-glycosylation process and in this manner glycosylation is inhibited (258). Tunicamycin treatment resulted in intracellular retention of CX_3CL1 with virtually no expression observed on the apical surface (Figure 13D,H&L). These results were confirmed using both the antibody directed against the chemokine domain of CX_3CL1 and the antibody directed against the N-terminal domain. The dose of tunicamycin used was derived from the literature using studies that had treated MDCK cells with tunicamycin to inhibit N-glycosylation of various proteins. There was general consistency amongst the studies that 1-2.5μg/ml for 12-18 hours was sufficient to inhibit N-glycosylation (259-261). Titration assays were not done, though I accept the examiners comments that this would have been appropriate and improved the precision of the results. To verify the observed effects were not due to non-specific disruption of apical protein traffic, we evaluated the effects of tunicamycin on targeting of NHE3, an apical protein whose targeting does not require N-glycosylation. As expected, tunicamycin treatment did not affect the normal apical distribution of NHE3 (Figure 13M-P).

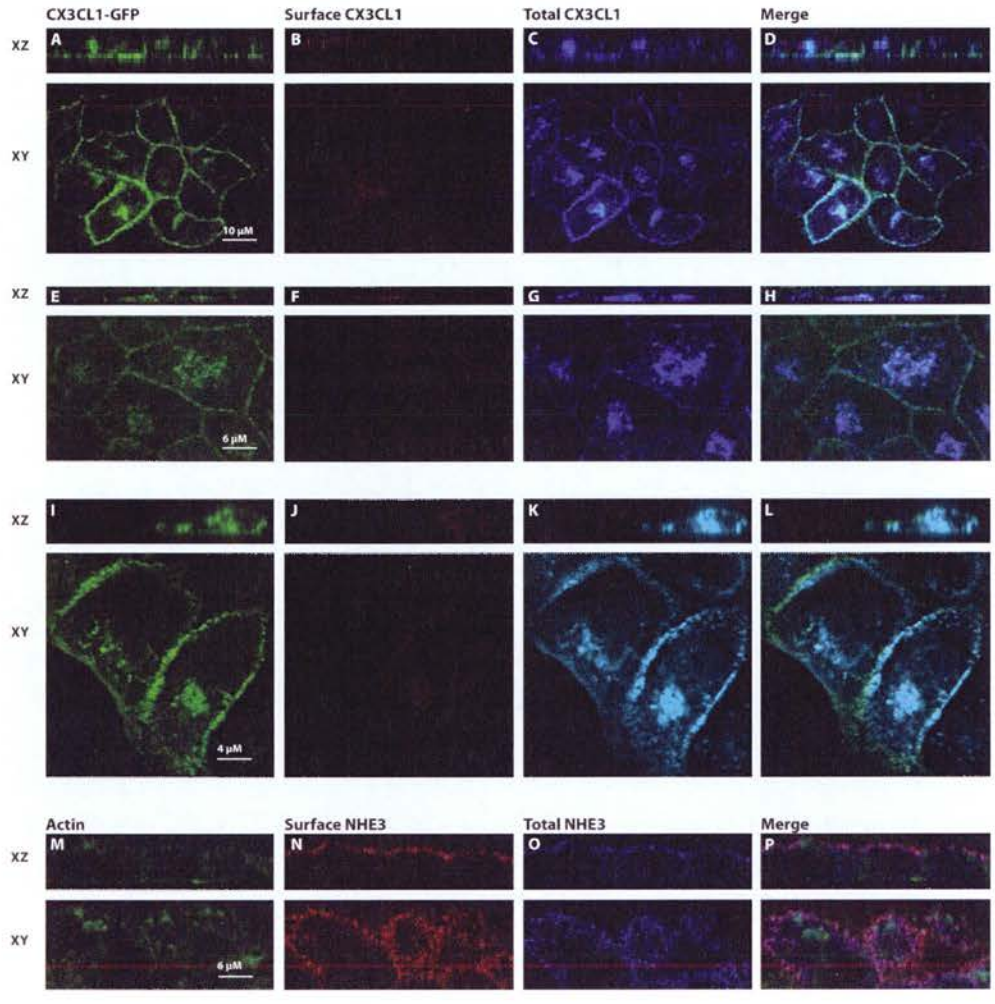

Figure 13. N-glycosylation of CX_3CL1 directs it to the apical membrane. MDCK-CX_3CL1-GFP cells were treated with tunicamycin to inhibit N-glycosylation. Surface CX_3CL1 was labelled with anti-CX_3CL1 Ab against the chemokine domain, followed by a Cy-3 conjugated Ab and total CX_3CL1 was labelled with a Cy-5 conjugated Ab (fig 13A-D and fig 13E-H). The experiments were repeated using an antibody directed against the C-terminal domain of CX_3CL1 (fig 13 I-L). As a negative control MDCK-NHE3 cells were also treated with tunicamycin. Surface NHE3 was labelled with a Cy-3 conjugated Ab, total NHE3 was labelled with a Cy-5 conjugated Ab and F-actin was labelled with phalloidin-488 (fig 13 M-P).

(Experiments done by Anne Durkan).

Collectively, these data indicate that the signals directing apical trafficking of CX_3CL1 are not conferred by the protein's cytoplasmic domain, O-glycosylation of the protein nor by associations with lipid rafts, but rather, apical localisation of CX_3CL1 is determined by N-glycosylation.

4. *CX_3CL1 is anchored to the apical membrane in RTEC.*

To determine whether CX_3CL1 is anchored in the luminal surface, we used fluorescence recovery after photobleaching (FRAP) to study the mobility characteristics of apical CX_3CL1-GFP in MDCK-CX_3CL1-GFP cells. FRAP has been extensively used to assess protein mobility within membranes (262, 263). It is a single cell technique utilising an intense laser beam to acutely photobleach a defined area of the cell membrane. The protein of interest is labelled with a fluorophore. Fluorescence recovery over time is then measured and this represents lateral movement of the unbleached fluorophore labelled protein within the cell membrane into the area of interest and movement away from the area of bleached protein. Figure 14A shows the cell before bleaching; 14B, immediately after bleaching; and 14C, 5 min after bleaching. As a control, MDCK cells were transfected with a DNA expression plasmid encoding GPI-GFP, which is freely mobile in the apical plasma membrane. A region of the apical membrane was similarly bleached and the recovery of fluorescence observed over time (Figure 14D-F). CX_3CL1-GFP recovered with significantly slower kinetics than GPI-GFP

(Figure 14G). For CX_3CL1-GFP, the bleached area recovered to 10.5± 4.3% of pre-bleached fluorescence intensity by 4 min, compared to 61.1±11.9% for GPI-GFP ($p<0.01$). As an additional control, MDCK cells were transfected with DNA encoding the single transmembrane protein, FcR-GFP. When FRAP was similarly performed, the bleached area in the membrane recovered significantly faster than CX_3CL1-GFP, with 4 min recovery of 51.5±6.1% for FcR-GFP ($p<0.01$) (Figure 14G). These data demonstrate that the ability of CX_3CL1 to diffuse laterally within the apical membrane is impeded, suggesting that transmembrane CX_3CL1 is immobile under basal conditions.

As discussed earlier, some single pass transmembrane proteins are tethered to the apical membrane by direct association with lipid rafts (264). To determine whether CX_3CL1 is anchored in such a manner we disrupted lipid rafts by treating cells with MβCD and repeated the FRAP experiments. However, this treatment only marginally increased the mobility of CX_3CL1 in the apical membrane and the effect was lost by 370 seconds (Figure 14G). To study whether apical CX_3CL1 is immobile because it is directly tethered to the actin cytoskeleton, we fractionated cellular proteins between two distinct fractions – TritonX-100 soluble and TritonX-100 insoluble, as previously described (241). In polarised epithelial cells, proteins directly anchored to the actin cytoskeleton, as well as those directly bound to the lipid component of the membrane, preferentially remain in the TritonX-100 insoluble

fraction. We found, however, that CX_3CL1 was largely soluble in TritonX-100 solution, suggesting that it is not directly tethered to the actin cytoskeleton (Figure 14H). Collectively, these data indicate that after sorting to the apical surface, CX_3CL1 is held immobile there, but this is not achieved by direct tethering to the actin cytoskeleton or by association with lipid rafts or caveolae.

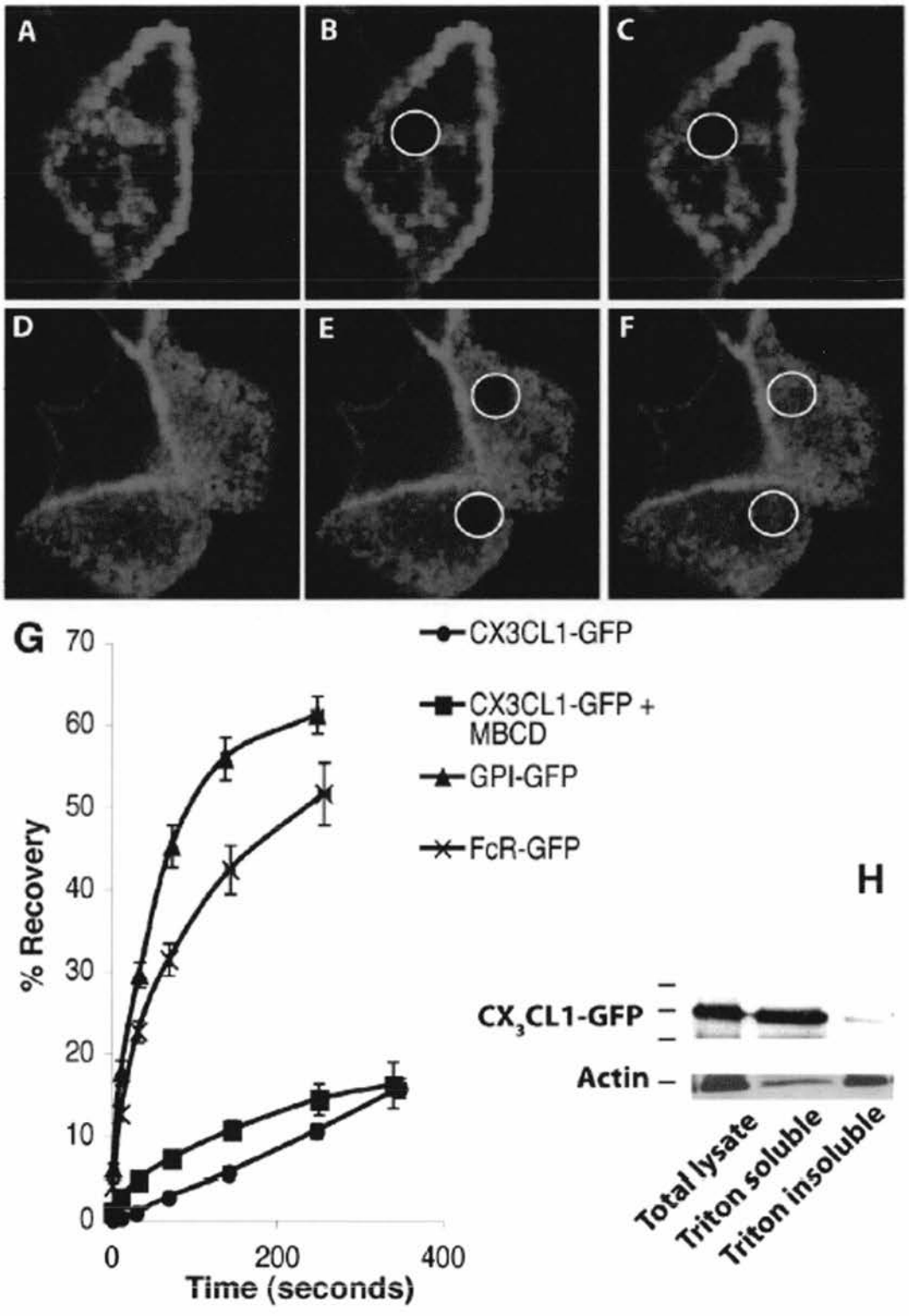
A
B
C
D
E
F
G
% Recovery
70
60
50
40
30
20
10
0
0
200
400
Time (seconds)
CX3CL1-GFP
CX3CL1-GFP + MBCD
GPI-GFP
FcR-GFP
H
CX3CL1-GFP
Actin
Total lysate
Triton soluble
Triton insoluble

Figure 14. ***CX_3CL1 is anchored to the apical membrane in renal tubular epithelial cells.*** To examine the mobility of CX_3CL1 in the apical membrane, FRAP was performed as described in 'Methods'. Using an argon laser and a scanning confocal microscope a 2.5μM region of the apical membrane expressing CX_3CL1-GFP was irreversibly photobleached (circles) and recovery of fluorescence monitored over time. (Fig 14A) MDCK-CX_3CL1-GFP cell before bleaching (fig 14B) shows the same cell immediately after photobleaching and (fig 14C) depicts the cell 5 mins later. Control areas of the same diameter in the plasma membrane were examined at each time point. (Figs14D-F) As a control, FRAP was similarly performed in MDCK cells expressing freely mobile glycosyl phosphatidylinositol conjugated to GFP (MDCK-GPI-GFP). (Fig 14D) MDCK-GPI-GFP cells before bleaching, (fig 14E) the same cell immediately after bleaching and (fig 14F) after 5 mins of recovery. (Fig 14G) As an additional control FRAP was performed in MDCK cells expressing the single transmembrane protein, Fc gamma IIa receptor tagged with GFP (FcR-GFP). Recovery of fluorescence after photobleaching of apical CX_3CL1-GFP, GPI-GFP, FcR-GFP or CX_3CL1-GFP after cholesterol depletion using methyl-β-cyclodextrin (MBCD) (Fig 14G). Points represent the mean ± SEM of recovery at serial time points from at least 6 experiments. (Fig 14H) Lysates from MDCK-CX_3CL1-GFP cells were obtained after separating into TritonX-100 soluble and TritonX-100 insoluble fractions, as described in the 'Methods' section. Western blotting was performed using anti-CX_3CL1 antibody and HRP-conjugated secondary antibody.

(Experiments done by Anne Durkan).

5. CX_3CL1 expressed on the apical surface of RTEC promotes adhesion of leukocytes.

Transmembrane CX_3CL1 can act as a cell adhesion molecule, facilitating the binding of leukocytes (39, 41). We therefore hypothesised that CX_3CL1 might perform a similar function when expressed on the apical surface of RTEC. These experiments were performed under low shear conditions to mimic the *in vivo* environment. K562 leukocytes do not constitutively express CX_3CR1 and therefore leukocytes that had been genetically modified to express the CX_3CL1 receptor were obtained in addition to unmodified cells. We found significant binding of K562-CX_3CR1 leukocytes to MDCK-CX_3CL1-GFP cells compared to MDCK-WT control cells (Figure 15A-D). When CX_3CL1 was present on the apical membrane, leukocyte adhesion was almost three times greater than when CX_3CL1 was absent (Figure 15G, $p<0.001$). There was minimal binding of control K562 leukocytes to either MDCK-WT or MDCK-CX_3CL1-GFP cells (Figure 15G).

Figure 15. ***CX_3CL1 on MDCK cells promotes binding of leukocytes bearing the receptor CX_3CR1.*** K562-leukocytes expressing the CX_3CR1 receptor (K562-CX_3CR1) were labelled with rhodamine-conjugated cholera toxin B to visualise them. One million K562-CX_3CR1 cells were added to MDCK-WT or MDCK-CX_3CL1-GFP monolayers, growing on 25mm cover slips, under conditions of low shear stress. After 20 minutes, the non-adherent cells were removed by washing and the remaining cells were fixed. Serial fields (x63) were examined, using a Leica deconvolution microscope, and the number of adherent leukocytes counted. K562-CX_3CR1 cells applied to MDCK-CX_3CL1-GFP cells, fluorescence images (A) and DIC images (B). K562-CX_3CR1 cells applied to MDCK-WT cells, fluorescence images (C) and DIC images (D). Photomicrographs of labelled K562-CX_3CR1 cells, (red), binding to MDCK-CX_3CL1-GFP monolayers. Images shown in x *versus* y (E) and x *versus* z (F) optical sections. (G) Graph depicting the number of K562-control cells or K562-CX_3CR1 leukocytes bound to either MDCK or MDCK-CX_3CL1-GFP cells. The values represent the mean number of adherent cells per high power field (x63). Values represent the mean of at least 3 experiments ± SEM (*$p<0.001$). (The number of adherent cells per field was plotted to prove the normal distribution of the data and comparisons between means was analysed using the Student's t-test).
(Experiments done by Anne Durkan).

To verify that any observed responses were not an idiosyncratic feature of transformed cell lines, we performed the same experiment using both primary epithelial and primary leukocytic cells. Human peripheral blood mononuclear cells (PBMC) were isolated from the heparinized blood of healthy volunteers. PBMC contain multiple leukocyte subsets, including CD8+ T cells, monocytes and NK cells, all of which express the CX_3CR1 receptor. PBMC efficiently adhered to the apical surface of

monolayers of primary human RTEC. When primary RTEC were pre-incubated with a function-blocking anti-CX_3CL1 Ab, binding of PBMC was inhibited significantly (Figure 16). Collectively, these data suggest that CX_3CL1 expressed on the luminal surface of RTEC promotes the adhesion of leukocytes that bear the complementary receptor CX_3CR1. Our results are in keeping with a previous report in which blockade of CX_3CL1/CX_3CR1 impaired binding of THP-1 monocytic cells to primary proximal RTEC (59).

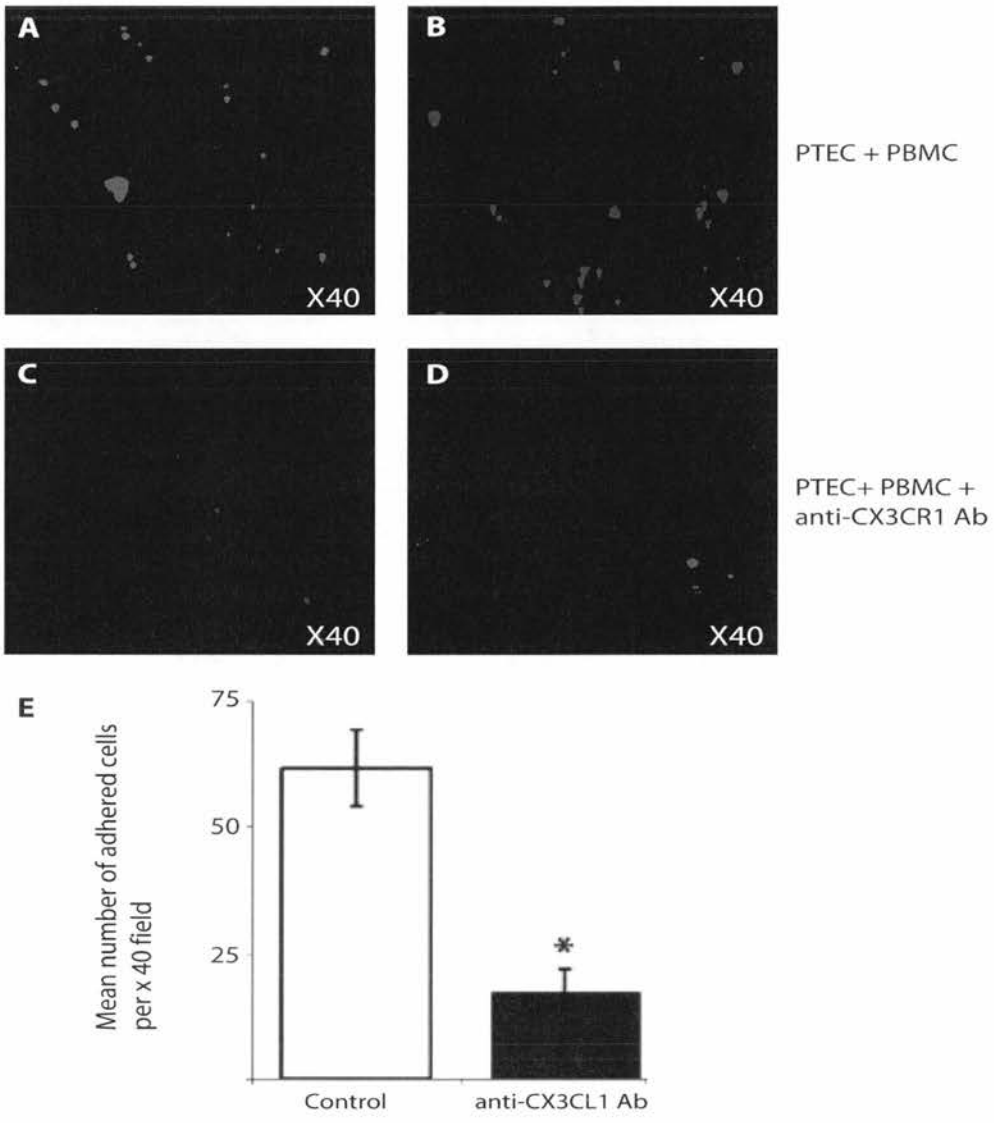

Figure 16. ***CX_3CR1-expressing leukocytes adhere to CX_3CL1 in the apical membrane of renal tubular epithelial cells.*** Adhesion assays were repeated using primary RTEC and human peripheral blood mononuclear cells (PBMC) that were isolated from the blood of healthy volunteers and labelled with Calcein-AM (A&B). In parallel experiments, primary RTEC monolayers were pre-incubated with function blocking anti-CX_3CL1 Ab (1μg/ml) for 30 min before addition of PBMC (C&D). A graph depicting the mean

number of adherent PBMCs per x40 field. Experiments were performed six times for each condition and the means compared with controls using the Student's t-test (*$p<0.0001$ *versus* control). Note that the original images were lost in a laboratory move. The images shown in A-D above were re-done in 2010 and the numbers shown in the graph do not reflect these images.

(The original experiments were done by Todd Alexander after being requested for publication. The repeat staining and adhesion assays were done by Jerry Pan and the microscopy was done by Anne Durkan).

Chapter 5. Results Part 2

The Regulation of CX_3CL1 by Thromboxane Prostanoid Receptor Stimulation

1. ***Stimulation of the TP receptor decreases surface and total expression of CX_3CL1.*** TXA_2 has a very short half-life of about 30 seconds and, thus, for these studies we used two distinct and stable pharmacologic agonists of TP, namely, U46619 and IBOP (265, 266). Both of these agonists have been used extensively in previous studies in numerous cell types including ECV-304 cells. The dose of 20μM of U46619 was chosen based on studies that had used between 1 and 20μM in cells to induce platelet aggregation, phosphoinositide hydrolysis and inhibition of monocyte adhesion (265, 267-270). Mean EC_{50} values of 4.8nM, 82nM and 30nM have been found for shape change in human platelets, human platelet aggregation and phosphoinositide hydrolysis in CHO cells respectively (271). Bishop-Bailey *et al* used 10μM U46619 and did not induce endothelial cell toxicity or affect cell viability (268). The IBOP dose used in our experiments was 100nM and again this was taken from published studies in the scientific literature. Yan *et al* used 50nM IBOP for 15 minutes in HEK cells to induce phosphorylation of ERK and glycogen synthase kinase-3 (272). They also induced HEK cell aggregation and changes to the cell shape. Gao *et al* found that 100nM IBOP resulted in a 4-5 times increase in phosphorylation of

ERK in ECV-304 cells (273). Gallet *et al* also used 100nM IBOP to induce phosphorylation of ERK in Hek-293 cells and Kinsella *et al* used the same dose to assess thromboxane prostanoid receptor binding in human erythroleukaemia cells (274, 275). Platelet aggregation is induced by IBOP with an EC_{50} value of 0.34nM (276) and in HEK-293 cells ERK activation is induced with an EC_{50} value of 0.16nM for the TPα receptor and 0.6nM for the TPβ receptor (277). The dose used of SQ29548, a specific TP antagonist, was also taken from previously published studies. Numerous studies had used 10μM SQ29548 to antagonise the TP receptor in endothelial and epithelial cells (226, 277). Human platelet aggregation induced by U46619 was inhibited by SQ29548 with an IC_{50} of 0.06μM (278).

To evaluate the effect of stimulation of the TP receptor on CX_3CL1 expression, cells were treated with the TP receptor agonist U46619 for various time periods and immunoblotting of whole cell lysates was performed. The total expression of CX_3CL1 fell after just 10 min of TP stimulation, with lowest levels observed by 30-60 min (figure 1A). Total levels of CX_3CL1 recovered to near baseline values by 4 h (figure 1A). To verify these results, cells were treated with the second TP agonist, IBOP, and similar results were obtained (figures 1B&C).

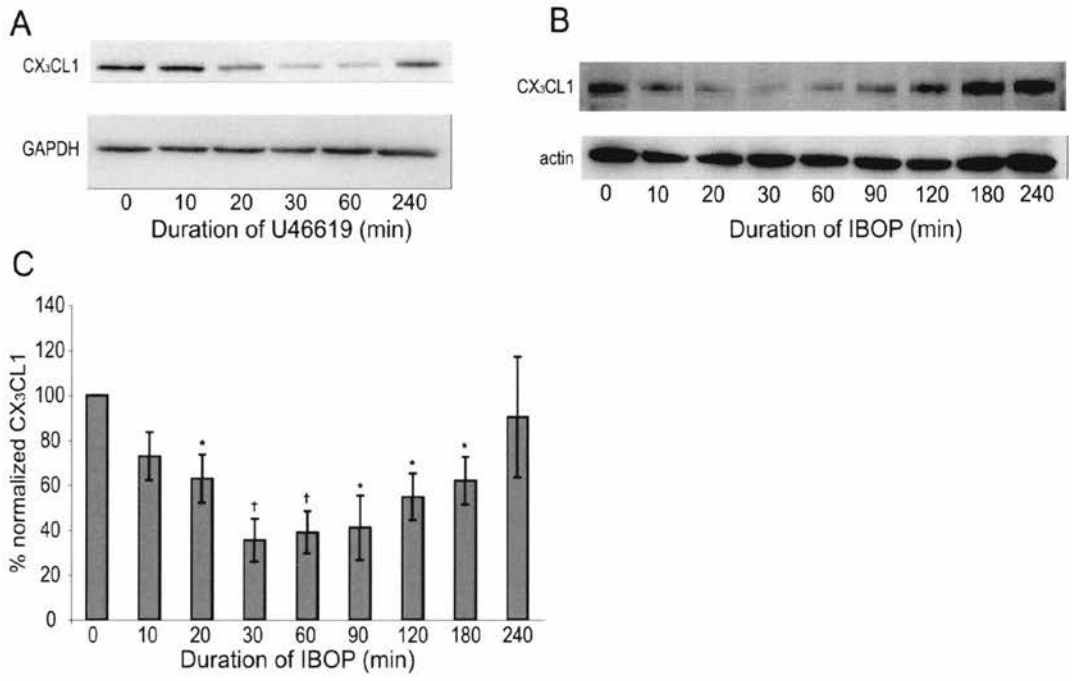

Figure 1. Stimulation of TP results in an early decrease in total cellular CX_3CL1. ECV-CX_3CL1-GFP cells were incubated with 20μM U46619 for various time periods. Cell lysates were harvested and immunoblotting performed using anti-CX_3CL1 Ab and HRP conjugated secondary Ab. To control for protein loading, blots were stripped and re-probed with anti-GAPDH Ab and HRP-conjugated secondary Ab (fig 1A). Cells were incubated with 100nM IBOP and immunoblotting performed as in 1A. To control for protein loading, blots were stripped and re-probed with anti-actin Ab and HRP-conjugated secondary Ab (fig 1B). Experiments were performed as in 1B. Band intensities for CX_3CL1 were quantified and normalized to actin (fig 1C). Values represent mean values ± SEM for 4 separate experiments. *, $p = 0.05$. †, $p < 0.01$ vs untreated. (Experiments done by Anne Durkan).

To assess the effect of TP activation specifically on cell surface levels of CX_3CL1, cells were treated with TP agonist and surface CX_3CL1 was

measured by flow cytometry. There was again an initial decrease in surface CX_3CL1 levels, with full recovery to baseline by 4 hours of TP receptor stimulation (figure 2).

Figure 2. Stimulation of TP results in a decrease in surface CX_3CL1. ECV-CX_3CL1-GFP cells were incubated with 20μM U46619 for varying time periods, labelled with anti-CX_3CL1 Ab and PE-conjugated secondary Ab, and cell surface CX_3CL1 expression was measured using flow cytometry. The result shown is representative of 8 separate experiments. The data for all the experiments was analysed using ANOVA. *, $p<0.001$ compared to control for timepoints 10, 30 and 60 mins. (Experiments done by Anne Durkan and the flow cytometry analysis performed by the technicians of the flow facility at the University of Toronto).

To ensure that any observed effects were specific to stimulation of TP, cells were incubated with IBOP together with the specific TP antagonist, SQ29548 and analysed by both Western blotting and flow cytometry (figure 3). SQ29548 abrogated the rapid decrease in CX_3CL1 expression following TP stimulation.

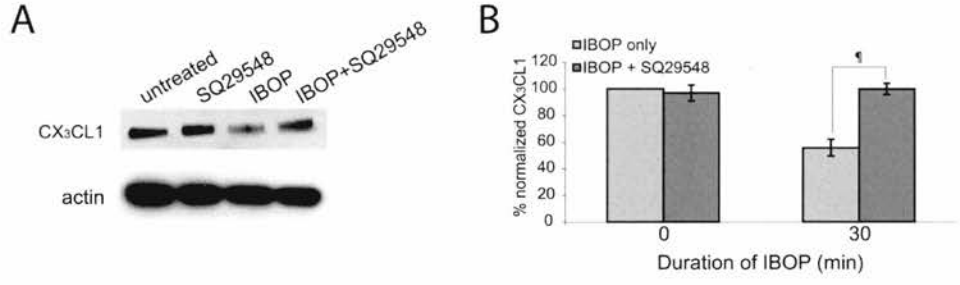

Figure 3. The effect of TP stimulation on total CX_3CL1 is abrogated by the TP antagonist, SQ29548. Cells were incubated with IBOP (100nM for 30 mins) in the presence or absence of TP antagonist, SQ29548 (10μM). Cell lysates were harvested and immunoblotting performed using anti-CX_3CL1 Ab and HRP conjugated secondary Ab. To control for protein loading, blots were stripped and re-probed with anti-GAPDH Ab and HRP-conjugated secondary Ab (figure 3A). Experiments were

performed as in 3A. Band intensities for CX_3CL1 were quantified and normalized to actin (figure 3B). Values represent mean values ± SEM for 3 separate experiments.

¶, $p < 0.05$.

(Experiments done by Anne Durkan and Soumitra Tole).

2. ***Stimulation of the TP receptor induces cleavage of CX_3CL1 by TACE.***

Since both total and surface levels of CX_3CL1 decreased following TP stimulation, we hypothesised that CX_3CL1 was inducibly cleaved from the plasma membrane, a process mediated by the metalloprotease, TACE (92, 93). To test this hypothesis, we compared the subcellular distribution of CX_3CL1 with that of TACE. We initially stimulated the cells with phorbol-12 myristate 13-acetate (PMA) 100ng/ml, a protein kinase C agonist and a known activator of TACE and other proteins (92). There was poor co-localisation of TACE and CX_3CL1 at the baseline but after 5 mins of stimulation with PMA there was significant co-localisation of the two proteins. We then went on to stimulate the cells with U46619. By labelling the proteins with different fluorescent antibodies we could then assess co-localisation using specific software. In resting cells CX_3CL1 and TACE expressed on the cell surface did not co-localise (Pearson's coefficient = 0.429 ± 0.042; $p > 0.05$). After 5 min of TP stimulation there was co-localisation of the two proteins, yielding a statistically significant Pearson's correlation coefficient greater than 0.5, ($r=0.645 \pm 0.031$, $p<0.01$) (figure 4).

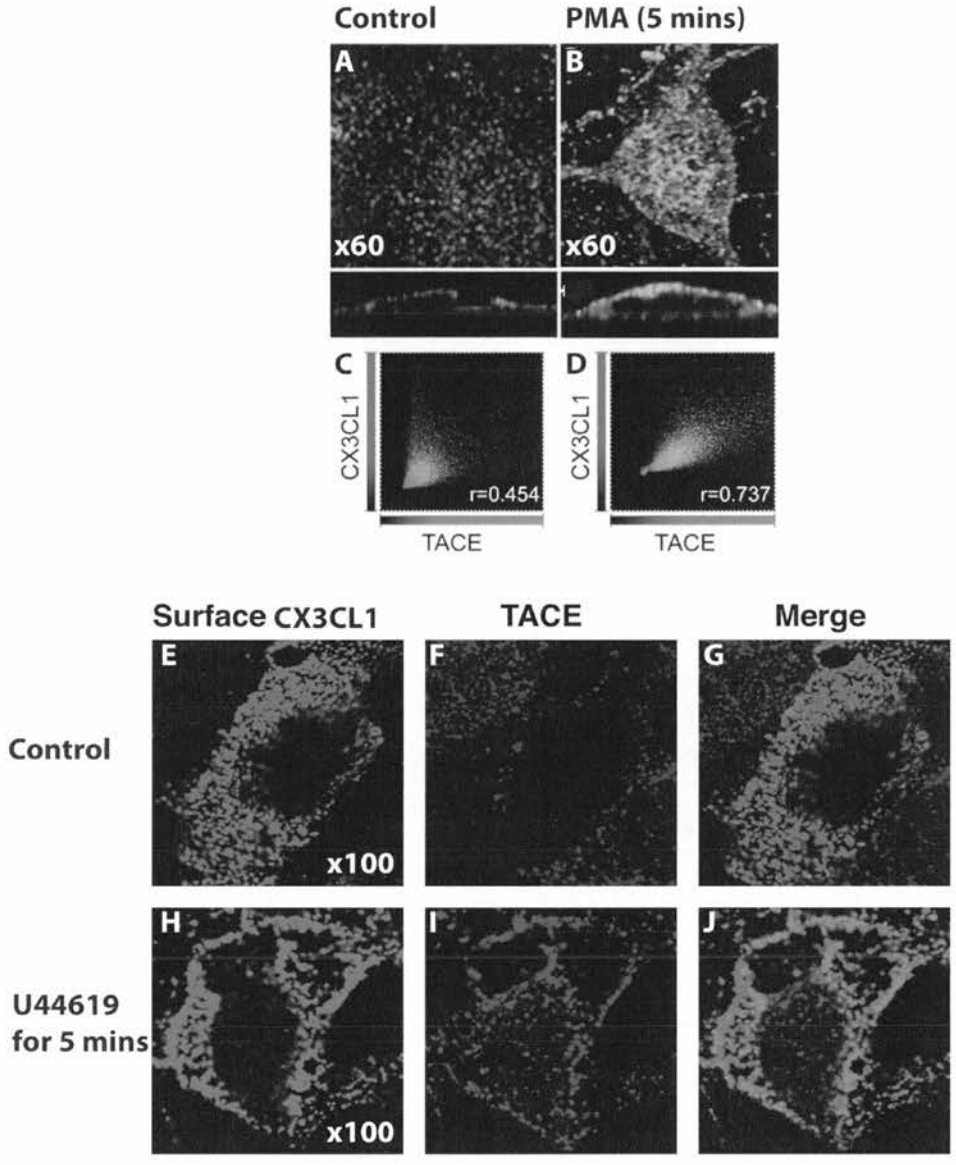

Figure 4. TP stimulation induces co-localisation of TACE with CX_3CL1. ECV-CX_3CL1 cells were treated with control medium (A) or PMA 100ng/ml (B) for 5 min. Cells were fixed with 4% paraformaldehyde, washed, and permeabilised with 0.1% triton. Cells were washed again and labeled with goat anti-human CX_3CL1 Ab and M220 mouse anti-human TACE Ab. Cells were washed and incubated with Cy3-conjugated anti-goat IgG and Cy2-conjugated anti-mouse IgG secondary antibodies to visualise CX_3CL1 and TACE respectively. Slides were examined using a spinning

disk confocal microscope (100x). The degree of co-localization between CX_3CL1/Cy3 and TACE/Cy2 was determined using OpenLab 5.0 co-localization software, before (C) and after (D) treatment with PMA. A minimum of 25 cells for each condition were examined in this manner. Experiments were repeated using U46619 (20μM) to stimulate the cells for 5 mins. After labeling with goat anti-human CX_3CL1 Ab and M220 mouse anti-human TACE Ab, the cells were labeled with a Cy-3 conjugated anti-goat Ab and a Cy-5 conjugated anti-mouse secondary Ab (E-J). Slides were visualised as in the previous experiments.
(Experiments A-D done by Guang-Ying Liu and Anne Durkan. Experiments E-J done by Anne Durkan).

In mammalian cells, TACE becomes activated when its cytoplasmic tail is phosphorylated by the intracellular signalling molecule extracellular-regulated kinase (Erk) (279-281). Stimulation of TP results in the activation of various second messenger systems including inositol triphosphate, cAMP, small G proteins, protein kinase C (PKC) and protein kinase A (PKA) depending on the G protein to which it couples and the cell involved (282). Furthermore, stimulation of TP has been reported to phosphorylate Erk 1/2 (270, 283). We therefore hypothesised that stimulation of TP resulted in the activation and phosphorylation of Erk, which then activated TACE. To examine whether this was the case, cells were stimulated with TP agonists, U46619 or IBOP and the phosphorylation of Erk determined by Western blot of cell lysates. There was rapid phosphorylation of Erk in the stimulated cells (Figure 5A-C). Following stimulation of TP

for 4-6 hours there was a return to baseline levels of phosphorylated Erk (Figure 5A). To verify this finding we simultaneously used the Erk inhibitor, U0126, with TP stimulation. U0126 is a chemically synthesised compound that is highly selective in its inhibition of MEK1 and MEK2, also called mitogen-activated protein kinase (MAPK)/Erk kinase. MEK1/2 are upstream of Erk and stimulate its enzymatic activity (284). Concurrent use of U0126 with TP stimulation prevented the loss of surface CX_3CL1 (Figure 6).

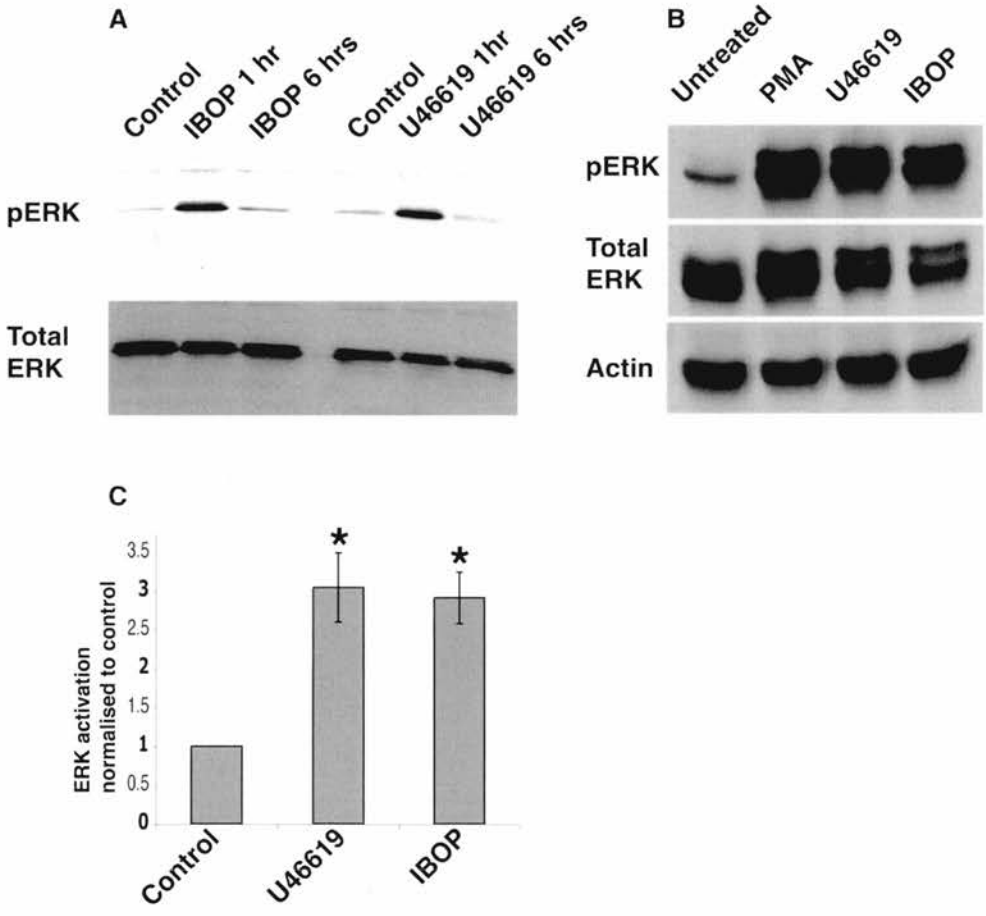

Figure 5. Stimulation of TP activates phosphorylation of ERK. ECV-CX_3CL1 cells were incubated with PMA (100ng/ml), U46619 (20μM), or IBOP (100nM) for 1 hr or

6 hrs (A) or 30 min (B). Cell lysates were harvested and immunoblotting performed using anti-phospho-Erk Ab and HRP conjugated secondary Ab. Blots were stripped and re-probed with anti-Erk Ab and anti-actin Ab to control for protein loading. Figure 5C, Experiments were performed as in (*B*). Band intensities for phospho-Erk were quantified and normalised to total Erk. Values represent mean values ± SEM for 3 separate experiments. $^{*}p < 0.01$.

Experiments done by Anne Durkan (A) and Soumitra Tole (B).

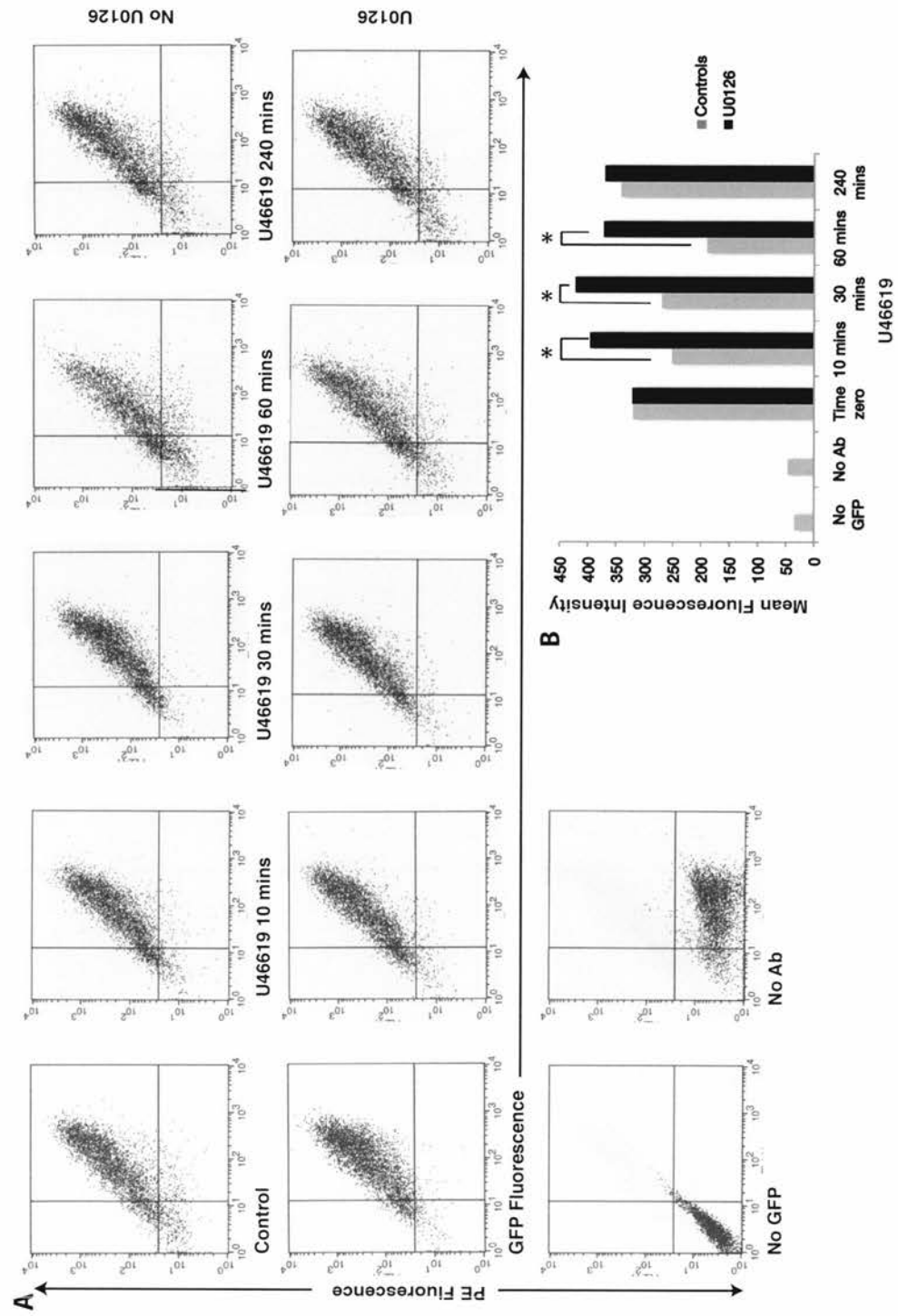

Figure 6. U0126, a specific inhibitor of MAPK/Erk kinase, abrogates the effect of TP stimulation on surface CX_3CL1 levels. ECV-CX_3CL1-GFP cells were incubated with

U46619 for various time periods in the presence or absence of U0126 (10μM). Cells were fixed, labelled with anti-CX_3CL1 Ab and PE-conjugated secondary Ab, and analysed by flow cytometry. Representative individual dot plots are shown (fig 6A) with a graph for the mean of 4 separate experiments (fig 6B). The results of the 4 experiments were analysed by ANOVA ($* p < 0.001$).

(The experiments done by Anne Durkan).

We further inhibited TACE activity using the matrix metalloprotease inhibitor, TAPI-2 (93). In the presence of TAPI-2, total levels of CX_3CL1 did not decrease in response to TP stimulation (Figure 7).

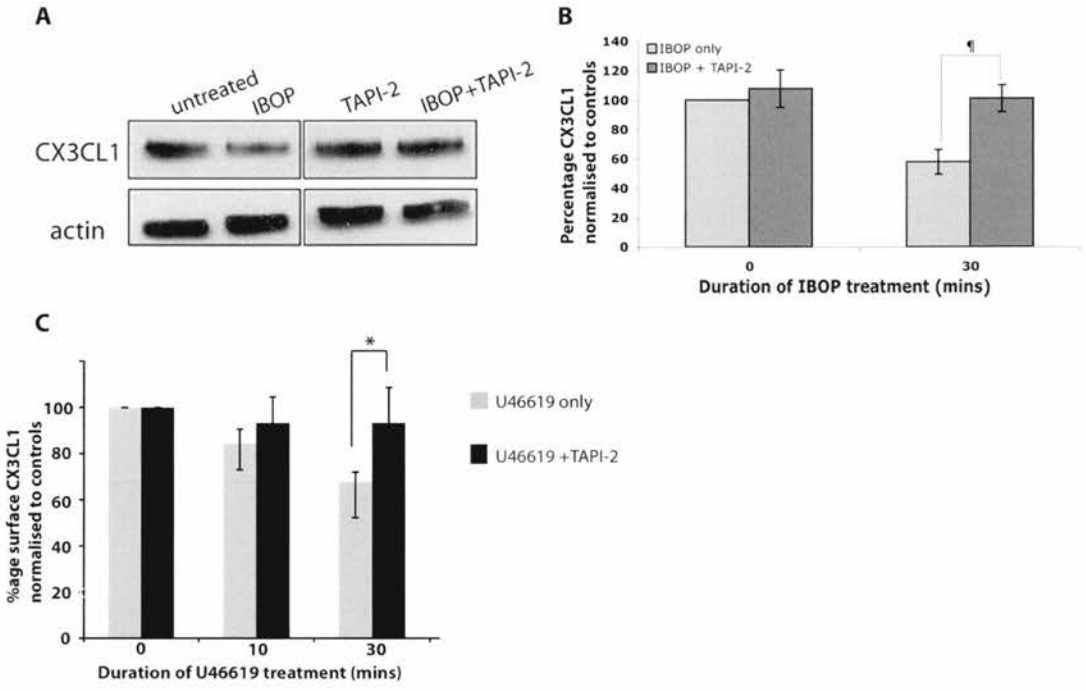

Figure 7. TAPI-2, an inhibitor of TACE attenuates the effect of TP stimulation on cellular CX_3CL1 levels. ECV-CX_3CL1-GFP cells were incubated with IBOP in the presence or absence of metalloprotease inhibitor, TAPI-2, and immunoblotting performed using anti-CX_3CL1 Ab and HRP-conjugated secondary Ab (figure 7A). Experiments were performed as in 7A. Band intensities for CX_3CL1 were quantified and normalised to actin (figure 7B). Values represent mean values ± SEM for 4 separate experiments. ¶, $p < 0.02$. (C) ECV-CX_3CL1-GFP cells were incubated with U46619 in the presence or absence of TAPI-2. Cells were labelled with anti-CX_3CL1 Ab followed by a PE-conjugated secondary Ab and surface fluorescence was measured using flow cytometry and normalised to control fluorescence. Results represent the mean of 3 separate experiments ± SEM and statistical analysis was done using ANOVA (figure 7C). * $p<0.001$

(Western blot done by Soumitra Tole and flow cytometry staining done by Anne Durkan).

Although TAPI-2 inhibits TACE activity, its actions are not entirely specific, as it also inhibits activation of ADAM10, a closely-related metalloprotease which constitutively cleaves CX_3CL1 (94). To determine whether TP stimulation promotes proteolytic shedding of CX_3CL1 by TACE and/or by ADAM10, we used siRNA to selectively knock down expression of each of these metalloproteases. As demonstrated in figure 8A, expression of TACE and ADAM10 was efficiently knocked down using the corresponding siRNA. There were also some off target effects as the use of ADAM-10 siRNA also reduced the amount of TACE in comparison to the scrambled and mock siRNA. We tried to minimise the off target effects by using a minimum amount of siRNA (100pmol) to prevent saturation of the RNAi cellular machinery. We also used a commercially available siRNA which contained a pool of 3 target specific 19-25 nucleotide siRNAs designed to knock down gene expression of TACE or ADAM-10 (285, 286). The AMAXA nucleofection kit was used to avoid the need for a viral vector and it is also promoted as being less harmful to the cells although we found that approximately 30-40% cells died after the first electroporation, but given a transfection rate of around 80% after two electroporations and a starting number of approximately 10 million cells, there were ample surviving cells with which to do the experiments.

Following siRNA transfection, we then used ELISA to measure the levels of soluble CX_3CL1 generated, and to thereby ascertain the relative contribution of each protease to TP-induced shedding of CX_3CL1 from the cell surface (93). In the presence of control, non-targeting siRNA, TP stimulation significantly increased levels of soluble CX_3CL1 (figure 8B). Similarly, when ADAM10 expression was knocked down, stimulation of TP also resulted in significant generation of soluble CX_3CL1 (figure 8B). However, when TACE expression was inhibited, TP stimulation did not result in proteolytic release of transmembrane CX_3CL1 from the plasma membrane (figure 8B). (Arbitrary units were used for the results of this experiment, as there was significant variability in the absolute amounts of soluble CX_3CL1 found in different experiments).

Collectively, these data suggest that TP stimulation induces rapid activation of TACE, and subsequent cleavage of CX_3CL1 from the plasma membrane.

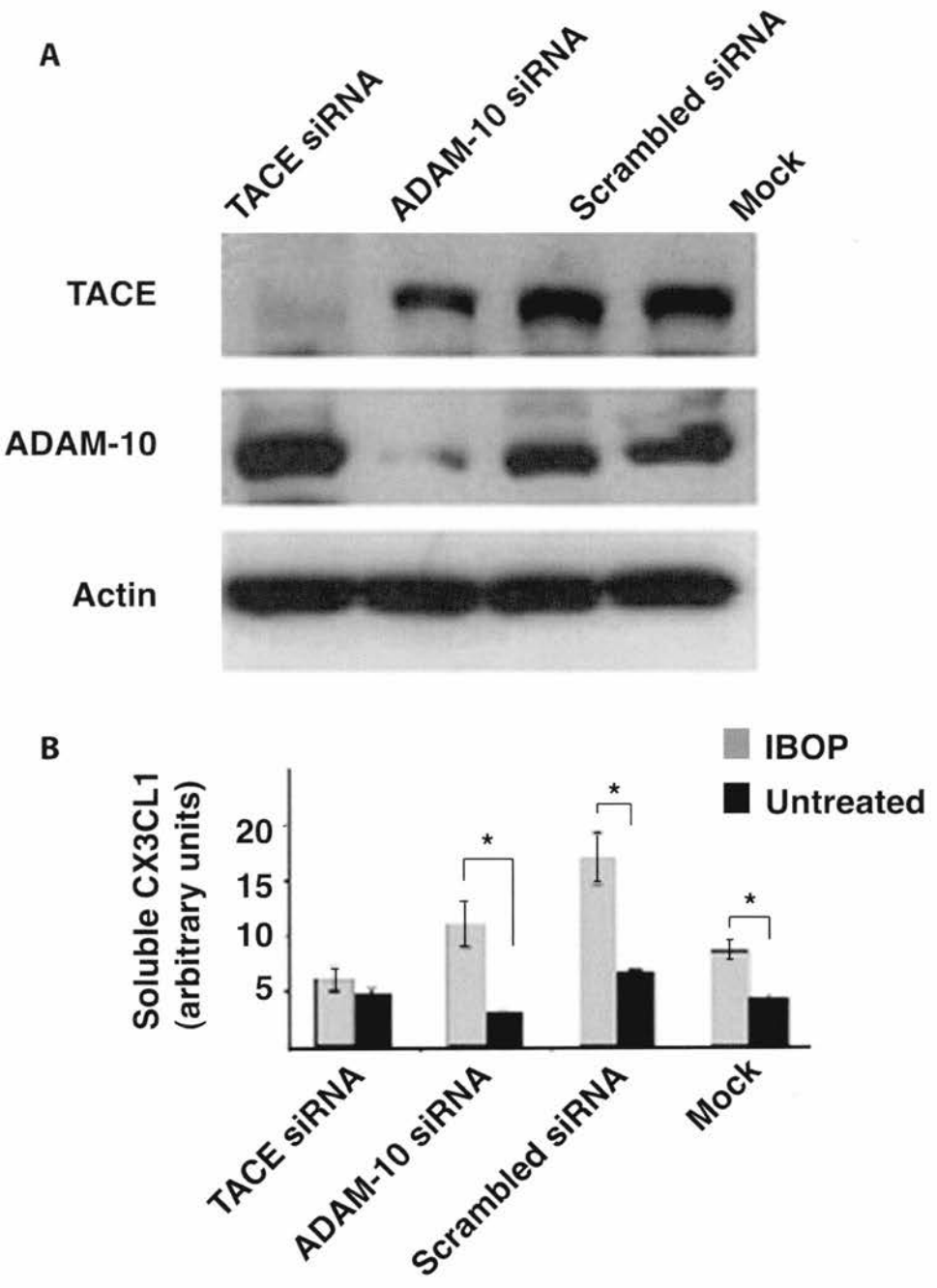

Figure 8. Knock down of TACE and ADAM-10 gene expression using siRNA results in attenuated response of CX_3CL1 to TP stimulation. ECV-CX_3CL1 cells were electroporated with TACE siRNA, ADAM10 siRNA, or control, non-targeting (scrambled) siRNA by nucleofection on Days 0 and 2. After 48 h, cell lysates were

harvested. Immunoblotting was performed using specific Ab directed against TACE and ADAM10. To control for protein loading, blots were stripped and re-probed with Ab directed against actin (figure 8A). Cells were electroporated with TACE siRNA, ADAM10 siRNA, or control, non-targeting (scrambled) siRNA, as described in 8A. Forty-eight hours after the second electroporation, cells were incubated with IBOP (2.5 μg/ml) for 30 min at 37°C, conditioned medium collected, and cell lysates harvested. Protease inhibitor cocktail was added to conditioned medium and to cell lysis buffer to prevent protein degradation. Supernatants and cell lysates were cleared by centrifugation. Using fresh samples, CX_3CL1 was measured using a CX_3CL1 ELISA Kit (R&D Systems), according to the manufacturer's specifications. Three independent experiments were performed and the data were expressed as the mean ± SEM of the percentage of soluble CX_3CL1 released into the conditioned medium in relation to the total amount of CX_3CL1 (soluble and cell-associated) (figure 8B). $^*p < 0.03$. (Experiments done by Yi-Wei Huang).

3. ***Stimulation of TP does not alter recycling of CX_3CL1 to and from the cell surface.*** Co-workers in my research group have previously shown that CX_3CL1 rapidly recycles between the plasma membrane and a juxtanuclear compartment (98). We therefore questioned whether stimulation of TP might affect this process, shifting the distribution of the chemokine from the superficial to the intracellular pool. To examine endocytosis of CX_3CL1 we used fluorescence recovery after photobleaching (FRAP). To prevent inadvertent shedding of CX_3CL1 from the cell surface, ECV-CX_3CL1-GFP cells were pre-incubated with metalloprotease inhibitor, TAPI-2. The entire juxtanuclear CX_3CL1-containing intracellular compartment was irreversibly photobleached and recovery of fluorescence, an index of the rate of internalisation of CX_3CL1 from the plasma membrane, was recorded over time. Fluorescence of the plasma membrane pool, which remained largely unaffected by the bleaching procedure, was also monitored. Figure 9A depicts an ECV-CX_3CL1-GFP cell prior to bleaching, and figures 9B and 9C illustrate the same cell immediately after and 5 min after bleaching, respectively. The plasmalemmal fluorescence decreased as the juxtanuclear fluorescence recovered, consistent with delivery of unbleached CX_3CL1-GFP from the former to the latter compartment. The rate of recovery of endomembrane fluorescence was quantified (figure 9D). In ten similar experiments, the juxtanuclear CX_3CL1-GFP compartment recovered to 21.5 ± 3.1% of its original fluorescence by

170 seconds. When TP was stimulated, the rate and degree of recovery of fluorescence did not change (figure 9D).

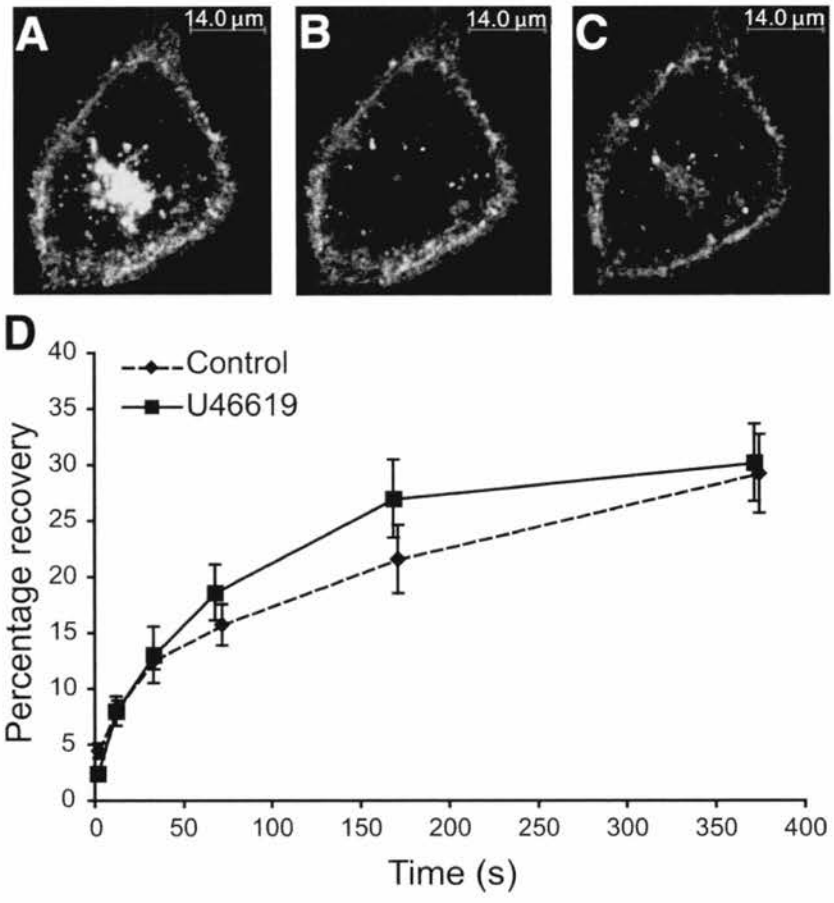

Figure 9. Stimulation of the TP receptor does not alter the rate of endocytosis of CX_3CL1. ECV-CX_3CL1-GFP cells were grown on glass coverslips and incubated for 4 hrs with TAPI-2 (10 µM) to prevent inadvertent shedding of CX_3CL1 from the cell surface. Cells were incubated with U46619 for 30 min, and using an argon laser and scanning confocal microscope, the entire juxtanuclear CX_3CL1-containing compartment was irreversibly photobleached, and recovery of fluorescence was determined at 5-200 s intervals. To control for inadvertent photobleaching associated with serial image acquisition, non-bleached areas in the plasma membrane were serially observed in parallel. Fig 9A represents a cell before bleaching, fig 9B depicts the same cell immediately after photobleaching, and fig 9C depicts the cell 5 minutes

later. At each timepoint, the ratio of the fluorescence intensity of the internal compartment to the mean control membrane fluorescence intensity was calculated. Each point represents mean values ± SEM for at least 6 separate experiments (fig 9D). (Experiments done by Anne Durkan).

To test whether TP stimulation had any effect on the rate of delivery of internalised CX_3CL1 back to the plasma membrane, the endomembrane pool was loaded by incubation with CX_3CL1 Ab at 37 °C for 1 hour. Antibody bound to the surface was stripped by a short exposure to an acidic solution. The cells were allowed to recover for varying periods of time and the re-insertion of CX_3CL1 in the plasma membrane was determined by quantifying the reappearance of Ab using immunofluorescence microscopy (98). For these experiments, cells were pre-treated with metalloprotease inhibitor, GM6001, to prevent rapid proteolytic shedding of CX_3CL1 from the cell surface. As shown in figure 10, fluorescence at the cell surface increased progressively after acid stripping, confirming that CX_3CL1 within the endomembrane compartment undergoes exocytosis to the plasma membrane. Stimulation of TP using IBOP had no effect on the rate of exocytosis of internalised CX_3CL1 (figures 10C-E).

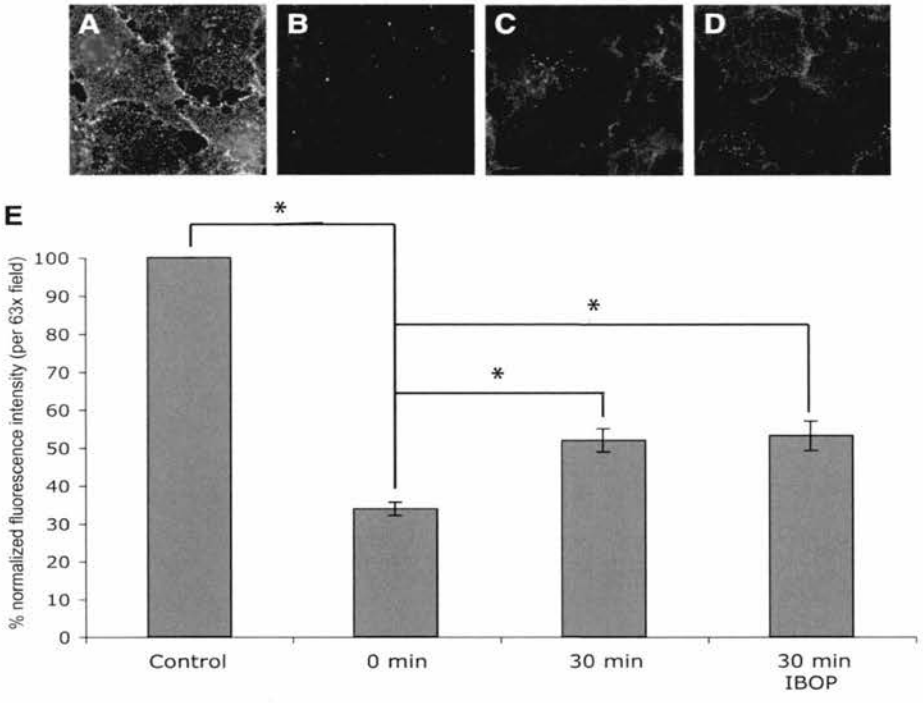

Figure 10. TP stimulation does not alter the rate of delivery of internalised CX_3CL1 back to the plasma membrane. ECV-CX_3CL1 cells were incubated with anti-CX_3CL1 Ab at 37 °C for 1 h, then membrane-associated Ab was removed by acid wash (pH 2.5) at 4°C for 2 min. Cells were allowed to recover for 30 min in the presence or absence of IBOP, then washed, fixed and stained with Cy3-conjugated secondary Ab. In all experiments, cells were pre-incubated with metalloprotease inhibitor, TAPI-2 (10 μM), to prevent cleavage of CX_3CL1 from the cell surface. Shown are immunofluorescent images of cells before acid-stripping (fig 10A), of cells immediately after acid stripping (fig 10B), of cells 30 min after recovering from acid shock (fig 10C), and of cells 30 min after recovering from acid shock in the presence of IBOP (fig 10D). Cell surface immunofluorescence was quantified using Volocity software. Results represent mean values of at least 30 fields per condition from 3 separate experiments (fig 10E). The data was initially graphed to prove a normal distribution and then differences between means was compared using the Student's t test. *, $p < 0.02$ (Experiments done by Anne Durkan and Soumitra Tole).

In summary we found that stimulation of TP resulted in decreased total and surface CX_3CL1, with a maximal effect at 30-60 minutes and full recovery of cellular levels of CX_3CL1 by 4 hours. TP stimulation had no effect on the recycling of CX_3CL1 but it did activate TACE via phosphorylation of Erk, which induced cleavage of surface CX_3CL1. We hypothesised that this would result in functional changes for the cell with decreased leukocyte adhesion and this will be discussed further in the next chapter as the experiments were done after the experimental work for this thesis was finished.

Chapter 6. Discussion

This work was designed to examine the intracellular location and function of CX_3CL1 in polarised renal tubular epithelial cells and to examine the effect of thromboxane prostanoid receptor stimulation on the regulation of CX_3CL1.

The presence and function of CX_3CL1 in endothelial cells have been well described (37, 41, 98, 111). In the kidney, an important role for CX_3CL1 has been found in diseases involving glomerular inflammation and endothelial injury (46, 49, 50, 55, 59). Importantly, CX_3CL1 is also up-regulated in renal tubulointerstitial inflammation, most notably in acute allograft rejection suggesting that CX_3CL1 also functions in renal tubular epithelial cells (287). The specific localisation of the chemokine in these cells (apical *vs* basolateral) has been somewhat unclear (59). We initially demonstrated mainly apical CX_3CL1 in human renal biopsy specimens with tubular disease. In keeping with previous studies, we also found that not all tubules stained for CX_3CL1 but we were unable to correlate clinical severity with our immunofluorescence results as ethical permission had not been obtained. We accept the examiners comments that more images including H&E stains of the biopsies would be helpful but we were unable to obtain these due to the untimely and tragic death of the pathologist involved.

We next moved to a cell-line model to examine the precise location of CX_3CL1. Our original model used HK-2 cells, which are a human renal tubular cell line but these cells tend to grow in flattened monolayers, which meant it was very difficult to differentiate the apical from the basal membrane using fluorescent confocal microscopy. We therefore switched to MDCK-2 cells, a canine renal tubular cell line that has typical epithelial cell morphology. These cells do not constitutively express CX_3CL1 therefore we transfected CX_3CL1±GFP into the wild type cells and created stable cell lines. We did not perform extensive functional cell testing after transfection, but the cells were shown to retain epithelial cell morphology as demonstrated by ZO-1 and E-cadherin immunofluorescence staining.

Unexpectedly, we found that transmembrane CX_3CL1 was expressed on the apical, but not the basolateral surface of RTEC. We had anticipated basolateral CX_3CL1 as this could then attract circulating leukocytes from the peritubular capillaries into areas of injury. The apical pattern of expression seen mirrors that found in epithelial cells of biliary ductules (288), but differs markedly from that of intestinal epithelial cells, where CX_3CL1 is largely expressed in the basolateral membrane and in regions of intercellular contact (289, 290). In the intestine, as in the kidney, expression of CX_3CL1 is highly enhanced in disease states marked by active inflammation (121, 290, 291).

We next examined how CX_3CL1 is sorted to the apical membrane. Polarised cells are ubiquitous in biology and allow proteins to be

differentially trafficked to either the apical or basolateral membrane. Despite the diversity of polarised cells and synthesised proteins, there are relatively few intrinsic protein sorting signals to direct the protein to the desired destination. The sorting determinant may lie within any domain of the protein. Basolateral membrane proteins use largely motifs in the cytoplasmic domain such as tyrosine based motifs, for example the low density lipoprotein receptor, or (di)leucine based motifs, for example the IgG Fc receptor (247, 292). Apically sorted proteins use signals mainly in the extracellular or transmembrane domains, but some proteins, such as rhodopsin and the cystic fibrosis transmembrane regulator (CFTR) use cytoplasmic domain signals, for example the CFTR uses a PDZ domain signal (136, 246). By genetically deleting the cytoplasmic tail of CX_3CL1 we excluded an apical targeting signal in this region. Other transmembrane proteins, such as Thy-1, apically target through direct or indirect associations with lipid rafts (293). Lipid rafts are rich in sphingolipids and cholesterol and are disrupted by extracting cholesterol (294). However when we disrupted any potential association with rafts by extracting cholesterol we found no change in the distribution of CX_3CL1. Although we did not completely deplete the cholesterol content of the cell, we feel that it was sufficiently reduced to affect a difference in surface staining of CX_3CL1 if an association with lipid rafts had been the mechanism responsible for apical targeting.

Carbohydrate modification of the protein backbone may also direct trafficking of transmembrane proteins, as is the case for sucrase

isomaltase, which requires O-glycosylation for apical targeting (248). CX_3CL1 has 26 O-glycosylation sites in the mucin stalk. However, when we inhibited O-glycosylation, CX_3CL1 still trafficked to the apical membrane. We did not perform any formal testing to check that inhibition of O-glycosylation was complete and this would have added to the robustness of the result.

For other proteins, such as endolyn and the glycine transporter GLYT2, N-glycosylation is the crucial determinant of apical targeting (143, 145). CX_3CL1 has a single N-glycosylation site, located in the chemokine domain (35). Our studies indicate that glycosylation of this site is the key signal which directs CX_3CL1 to the apical membrane. We used tunicamycin, an antibiotic mixture to inhibit N-glycosylation as this has been used widely for this purpose (147, 295-297). Tunicamycin prevents the formation of the sugar donor compound required for glycosylation (258). We did not perform a titration assay for the dose of tunicamycin as we used a dose previously given to inhibit N-glycosylation in cultured kidney epithelial cells, but accept that this would have been useful to identify the minimum concentration required for inhibition (295). Furthermore, to confirm our findings that N-glycosylation was indeed responsible for the apical targeting of CX_3CL1, we could have performed genetic modification to delete or mutate the N-glycosylation site. As with other proteins that require glycosylation for apical targeting, it is not known whether the oligosaccharides are recognised directly by the sorting machinery of the membrane or if glycosylation

results in a conformational change in the protein which then exposes a sorting motif (134).

We postulated that after translocating to the apical membrane, CX_3CL1 would become anchored there, positioning it to act as a cellular adhesion molecule (39, 41, 58, 298). Firm anchoring of the chemokine within the membrane would allow it to tether passing cells that express the receptor, CX_3CR1. Our experiments indicate that CX_3CL1 is indeed immobile, similar to other adhesion molecules, such as CD44 and ICAM(264, 299, 300). Interestingly, subsequent experiments by our group have shown that although CX_3CL1 is relatively immobile in the basal state, upon stimulation of TP, CX_3CL1 becomes more freely mobile within the cell membrane (301).

We next considered how CX_3CL1 might be physically anchored to the apical membrane. Some adhesion molecules, including CD44, are tethered to the cell membrane by direct association with lipid rafts, whereas some cell adhesion molecules, such as VCAM-1, ICAM-2, CD43 and also CD44 bind to the ERM proteins (ezrin, moesin and radixin) which act as cross-linkers between the plasma membrane and actin filaments (264, 302, 303). ICAM-1 on the other hand is known to be directly associated with α-actinin (304). We, initially, examined the effect of cholesterol depletion and disruption of rafts on apical tethering of CX_3CL1. Disruption of lipid rafts did not increase the lateral mobility of CX_3CL1, in contrast to previous work with CD44, suggesting that this is not how CX_3CL1 is held immobile (264). Moreover, CX_3CL1 mainly

segregated with the detergent-soluble, rather than the detergent-insoluble, cellular fraction, further refuting a direct association with lipid rafts or the presence of a glycosylphosphatidylinositol (GPI) anchor (294). These data also suggest that CX_3CL1 is only weakly anchored to the actin cytoskeleton. As CX_3CL1 was largely detergent soluble we did not proceed with experiments to examine potential associations with the ERM proteins or α-actinin but these could have been done using immunoprecipitation and Western blotting.

A recent model of membrane fluidity proposes that transmembrane proteins might be corralled into discrete regions of the membrane, with the actin cytoskeleton acting as a fence and the proteins anchored to the cytoskeleton acting as pickets. Movement between compartments would require the protein to "hop" over the fence (305). Such a mechanism might account for the limited lateral mobility of CX_3CL1. Alternatively, CX_3CL1 could be indirectly anchored to the actin cytoskeleton by one or more TritonX-100 soluble adaptor protein(s). It is also conceivable that since CX_3CL1 is expressed in so many different cell types, like CD44 it may have different TritonX-100 solubilities, and perhaps varying mobility characteristics, according to the type of cell in which the protein in present (306). More work is clearly required to clarify exactly how CX_3CL1 is held immobile in the apical membrane of epithelial cells. Initial studies could try to establish the region of CX_3CL1 that is responsible for its immobility. We have already created a mutant CX_3CL1 with no cytosolic tail (CX_3CL1-360), the mobility of

which could be investigated using the FRAP technique implemented in our experiments. Further studies could examine the role of the transmembrane region of CX_3CL1. Hermand *et al* published their work showing that the transmembrane domain is crucial for clustering of CX_3CL1 within the membrane after our thesis experiments had been completed (307). This was the first work to show that, like several other cell adhesion molecules, CX_3CL1 did indeed cluster and that this improved the adhesive potency of the chemokine.

Although our studies demonstrate that CX_3CL1 is targeted and anchored within the apical membrane, the key question is what role it might play there. CX_3CL1 in intestinal epithelium has been shown to recruit leukocytes in inflammation and to regulate cell survival and wound repair (39, 106, 290). In intestinal epithelium CX_3CL1 is predominantly expressed on the basolateral surface, where it is in direct contact with CX_3CR1-expressing host leukocytes, including macrophages, lymphocytes, and dendritic cells. In the lamina propria, basolateral CX_3CL1 tethers dendritic cells to intestinal epithelium. Adherent dendritic cells then form transepithelial protrusions, which they extend into the gut lumen facilitating immunosurveillance and defence against entero-invasive bacteria (289).

In contrast, no such immunosurveillance was thought to occur within the kidney or the intrahepatic biliary tree. However the recent work of Soos *et al* elegantly demonstrated a network of CX_3CR1+ dendritic cells

extending throughout the renal interstitium, encasing Bowman's capsule and present within the glomerular extracellular matrix (308). No protrusions into the urinary space were seen and this was attributed to either the urine being normally sterile or to an inadequate experimental technique. In biliary ductular epithelial cells, CX_3CL1 is expressed both apically and basolaterally (288, 291, 309). CX_3CL1 on the apical surface of regenerating biliary epithelial cells has been shown to facilitate repair of the biliary tree following acute injury, presumably by recruiting hepatic stem cells, which express CX_3CR1 (291). In RTEC, a similar role has been proposed for the cell adhesion molecule CD44. CD44 is normally expressed on the basolateral membrane, where it participates in cell-matrix interactions. However, following renal tubulointerstitial injury, CD44 is expressed apically, where it is thought to promote regeneration and repair (310, 311). Our experiments demonstrate that CX_3CL1 is also expressed on the apical surface of RTEC. We have further found that CX_3CL1 on the apical membrane promotes tethering of leukocytes that bear the complementary receptor. During tubulointerstitial renal inflammation tight junctions break down, potentially allowing leukocytes to escape into the urinary space. We postulate that apical CX_3CL1 facilitates recruitment and retention of these leukocytes, redirecting them to the site of injury. In this manner CX_3CL1 may play an important role in tubulointerstitial nephritis, pyelonephritis and renal allograft rejection, diseases processes in which the production of CX_3CL1 is markedly increased (9, 49, 59, 60). As with

biliary epithelial cells, CX_3CL1 may also participate in the regeneration of tubules following inflammatory injury. In a model of ischemia-reperfusion injury to the kidney, there was an initial increase in endothelial cell levels of CX_3CL1 and this was later followed by increased tubular expression of the chemokine, which was found to be protective to the kidney (65). This may well reflect the biphasic nature of the CX_3CL1/CX_3CR1 axis, in that it is implicated both in acute inflammation and in subsequent repair. To examine the role of renal tubular cell CX_3CL1 more closely specific tubulointerstitial injury could be induced in CX_3CL1 knockout mice and the effects on acute and chronic histology and function compared with wild type mice. The nature of the inflammatory infiltrate would be predicted to be different between the two groups assuming that CX_3CL1/CX_3CR1 plays an important role in leukocyte recruitment in this condition.

Having demonstrated the location and a potential role of CX_3CL1 in RTEC, we next investigated the possible regulation of CX_3CL1 by stimulation of the thromboxane prostanoid receptor. Given that both thromboxane A_2 and CX_3CL1 are upregulated early in inflammation, we hypothesised that there was a direct link between the two inflammatory agents. For these studies, we used CX_3CL1-expressing ECV-304 cells. As discussed earlier, these cells were initially thought to be from a human endothelial cell line but were subsequently proved to be a bladder epithelial carcinoma cell. However, they have been used

extensively to study the distribution, cleavage and function of the CX_3CL1, because the surface levels of chemokine mirror those seen in cytokine-activated primary vascular endothelial cells (35, 39, 93, 94, 98, 237). The cells are suitable for preliminary studies but the experiments should then be repeated with primary cells and ideally with *in vivo* studies.

We found that TP stimulation acutely reduces total and surface expression of CX_3CL1, reaching a nadir at 30-60 minutes, and regaining baseline levels of CX_3CL1 after 4 hours. Although there are no comparative published studies of the acute effects of TP stimulation on cell surface molecules, several groups have investigated the effects of long-term TP stimulation on cell surface expression of vascular adhesion molecules and found augmented expression of vascular adhesion molecule-1 (VCAM-1), intercellular adhesion molecule-1 (ICAM-1), and endothelial adhesion molecule-1 (ELAM-1; E-selectin) (312, 313). However in these studies, adhesion molecule levels were examined only after sustained periods of TP stimulation (4 to 24 hr), and the resultant increase in expression likely reflected enhanced transcription and new protein synthesis (312, 313). Supporting this is the finding, in one study, that inhibition of nuclear factor (NF)-κB-induced transcription prevented increased expression of ICAM-1 and ELAM-1 at the level of both mRNA and protein (312). Genetically modified mice lacking both TP and apo-E, have a significant reduction in ICAM-1 expression again underscoring the role of TP in promoting adhesion molecule expression

(208). The effects of prolonged TP stimulation on the expression of the chemokine, CCL2 (monocyte chemoattractant protein-1; MCP-1) have also been determined. After 6 hours of TP stimulation, expression of the CCL2 was enhanced, again through the actions of protein kinase C and NF-κB-induced transcription (226). To our knowledge, no other study has examined how TP activation acutely modulates cell surface expression of an adhesion molecule or a chemokine. We did not perform experiments after 4 hours of TP stimulation to allow any comparison with the published literature. A further limitation of this work is that in a clinical scenario there is more likely to be sustained TP stimulation following an acute insult and therefore the effects of this on CX_3CL1 may be more clinically relevant.

It has previously been demonstrated that CX_3CL1 undergoes recycling between the cell membrane and a juxtanuclear compartment in ECV cells (98). Moreover, the overall exposure of CX_3CL1 at the cell surface reflects the balance between recycling and shedding or cleavage of the soluble chemokine. Therefore, the initial decrease in CX_3CL1 expression at the plasma membrane could potentially be achieved through three distinct mechanisms: a) increased endocytosis of CX_3CL1 from the cell surface, b) decreased traffic of internalised CX_3CL1 back to the plasma membrane, and/or c) increased shedding of CX_3CL1 from the cell surface. We systematically established that TP stimulation did not acutely alter the rate of traffic of the chemokine between the cell surface and the intracellular endocytic compartment, but rather it enhanced

shedding of the chemokine from the cell surface by the metalloprotease, TACE. Previous studies have shown that CX_3CL1 is cleaved by TACE or ADAM-10 (92-94) and therefore to delineate precisely which of the two enzymes was responsible for the shedding of CX_3CL1 we used siRNA against both TACE and ADAM-10 and demonstrated that TACE was the crucial enzyme involved in the TP stimulated cleavage of CX_3CL1, however we did see some off-target effects, despite trying to minimise these with our experimental protocol.

There are several methods by which we could have further established TACE as the responsible enzyme for the TP induced cleavage of full-length CX_3CL1. The first of these would be to use a commercially available kit to measure TACE activity. Indeed we did try this but despite the best efforts of myself and several other members of the laboratory team, we could not get consistent, reproducible results and eventually abandoned this assay. Other investigators have used a mutant dominat negative form of TACE to inhibit TACE activity in cell cultures (314, 315). A potential future model could use a TACE knockout mouse to assess any effect of TP stimulation on CX_3CL1, but this was outside of our planned study. However, adding to our evidence that TACE is indeed the agent responsible for the TP induced cleavage of CX_3CL1 is the finding that blocking the activation of TACE by inhibiting Erk activation also prevented shedding of CX_3CL1. These results are supported by work demonstrating that one of the mechanisms of action of TP stimulation is activation of protein kinase C

and consequent Erk phosphorylation (273, 316-319). Moreover, others have shown that Erk phosphorylates the cytoplasmic tail of TACE at positions Thr 735 and Ser 819, resulting in conformational change and consequent activation of the protease (279-281). Blocking this phosphorylation prevents activation of TACE and ectodomain shedding of its biologic substrates, including TNF-∝ and L-selectin (279-281). Thus we have demonstrated that TP stimulation results in phosphorylation of Erk, which then phosphorylates TACE, activating the enzyme and inducing cleavage of transmembrane CX_3CL1. In summary, our experiments demonstrated that TP stimulation causes rapid loss of CX_3CL1 from the cell surface, by promoting TACE-induced shedding, rather than by altering the recycling dynamics of the chemokine.

Other members of the research team continued this work, as we were aware that we had not answered a functional question regarding the effect of TP stimulation on CX_3CL1. The full length transmembrane CX_3CL1 acts as a cell adhesion molecule and because TP activation caused rapid loss of surface CX_3CL1, we predicted that it would result in decreased adhesion of leukocytes expressing CX_3CR1, the only known receptor for CX_3CL1. However the opposite was found to be true and there was in fact increased cell adhesion after only 20 to 30 min of TP stimulation (301). Ishizuka *et al* have demonstrated by several methods that stimulation of TP results in increased expression of ICAM-1, VCAM-1 and E-selectin by stimulated human vascular endothelial

cells (HUVECs) (200, 312, 320) and we therefore wondered whether TP stimulation might cause a rapid increase in cell surface adhesion molecules other than CX_3CL1, which would account for the increased cell adhesion seen. Although ECV-304 cells do not have VCAM-1, E-Selectin or PECAM-1, they do have ICAM-1 (321). However further experiments demonstrated no increased binding of leukocytes to control untransfected ECV-304 cells stimulated with TP agonist, suggesting that the enhanced binding to ECV-CX_3CL1 cells was specifically due to the presence of CX_3CL1 itself. To ensure that observed results were not an idiosyncratic feature of the cell line used, the experiments were repeated using primary human vascular endothelial cells. Once again, TP stimulation induced rapid shedding of CX_3CL1 from endothelial cells, yet still enhanced binding of leukocytes. In the experiments by Ishizuka *et al* TP agonists were used for 6 hours to assess E-selectin expression and for 24 hours to assess ICAM-1 and VCAM-1 expression (312). Again, it is entirely feasible that the increased cell adhesion molecule expression was due to new protein synthesis as the effect could be abrogated by the inhibition of NFκB induced transcription, and this would explain why we did not see the same increase in our more acute experiments.

Given that TP stimulation promoted loss of CX_3CL1 from the cell surface, yet enhanced the adhesion of cells expressing CX_3CR1, it was hypothesized that TP stimulation must somehow also increase the avidity of the remaining available CX_3CL1 for its receptor. Other cell

adhesion molecules such as ICAM-1 are known to cluster in the cell membrane following stimulation (322). It therefore seemed reasonable to postulate that mobilization of plasmalemmal CX_3CL1 and subsequent clustering of the chemokine within the cell membrane could promote adhesion of appropriate leukocytes. In this way, the avidity of adhesive interactions between leukocytes and membrane-bound CX_3CL1 would be strengthened. To verify this prediction, FRAP experiments in the presence of TP agonists were performed and accordingly, it was found that CX_3CL1 was relatively immobile within the cell membrane under basal conditions, but it became highly mobile following stimulation of TP. This observation of poor resting state membrane mobility is supported by our previous work, in the first half of this thesis, using MDCK cells, in which we found that plasmalemmal CX_3CL1 is similarly immobile under basal conditions. The expression of CX_3CL1 at sites of contact with adherent leukocytes was then examined using quantitative immunofluorescence. Following stimulation with TP there was indeed clustering of CX_3CL1 at contact interfaces with bound leukocytes. At the time that these experiments were performed there was no published literature regarding the clustering of CX_3CL1, though since then Hermand *et al* have published the results of their work examining the aggregation of CX_3CL1 using the techniques of bioluminescence resonance energy transfer (BRET) and homogeneous time-resolved fluorescence (HTRF) (307). They found that CX_3CL1 clustered within the cell membrane in human embryonic kidney (HEK) cells and that this

phenomenon was mainly due to the transmembrane region of the protein, though they were unable to establish the exact sequence motif involved. They suggested that the aggregation of CX_3CL1 in the cell membrane corresponded to oligomerisation of the protein. Importantly they found that clustering of CX_3CL1 increased its adhesive properties for cells bearing CX_3CR1. To our knowledge, there are no prior descriptions of regulation of CX_3CL1 expression and mobility by a G protein-coupled receptor.

Given the timeframe of events that we have investigated, it is conceivable that early in the inflammatory cascade, stimulation of TP induces shedding of membrane-anchored CX_3CL1 to release the soluble chemoattractant molecule, thereby recruiting circulating leukocytes. This is then followed by a period where the balance is subtly altered to facilitate adhesion of recruited leukocytes to the area of vascular or tissue injury.

In summary this work demonstrates that CX_3CL1 is apically expressed, utilising N-glycosylation to traffic to this membrane, in renal tubular epithelial cells. CX_3CL1 is relatively immobile in the cell membrane under basal conditions and is able to adhere to cells expressing CX_3CR1. Stimulation of the thromboxane prostanoid receptor results in an acute reduction in surface and total CX_3CL1 levels and this is due to enhanced cleavage of the full-length protein by TACE.

Future studies should aim to examine the *in vivo* implications of TP regulation on CX_3CL1 regulation. These could be achieved with the various genetically modified mouse models that are already available such as the TP knockout mouse, the CX_3CL1 knockout mouse and the TACE knockout mouse. The use of these mice could be combined with specific disease states such as experimental models of ischaemic reperfusion injury. The nature of the inflammatory infiltrate, especially the type and number of monocyte/macrophages could also be affected by the amount of CX_3CL1 either secreted or present on the cell membrane following injury and this may represent an area for potential therapeutic intervention.

Chapter 7. References

1. Liu, Y. 2006. Renal fibrosis: new insights into the pathogenesis and therapeutics. *Kidney Int* 69:213-217.
2. Kriz, W., and LeHir, M. 2005. Pathways to nephron loss starting from glomerular diseases-insights from animal models. *Kidney Int* 67:404-419.
3. Christensen, E.I., and Verroust, P.J. 2008. Interstitial fibrosis: tubular hypothesis versus glomerular hypothesis. *Kidney Int* 74:1233-1236.
4. Wang, S.N., and Hirschberg, R. 1999. Tubular epithelial cell activation and interstitial fibrosis. The role of glomerular ultrafiltration of growth factors in the nephrotic syndrome and diabetic nephropathy. *Nephrol Dial Transplant* 14:2072-2074.
5. Wang, S.N., Lapage, J., and Hirschberg, R. 1999. Glomerular ultrafiltration and apical tubular action of IGF-I, TGF-beta, and HGF in nephrotic syndrome. *Kidney Int* 56:1247-1251.
6. Hirschberg, R., and Wang, S. 2005. Proteinuria and growth factors in the development of tubulointerstitial injury and scarring in kidney disease. *Curr Opin Nephrol Hypertens* 14:43-52.
7. Zoja, C., Donadelli, R., Colleoni, S., Figliuzzi, M., Bonazzola, S., Morigi, M., and Remuzzi, G. 1998. Protein overload stimulates RANTES production by proximal tubular cells depending on NF-kappa B activation. *Kidney Int* 53:1608-1615.
8. Donadelli, R., Abbate, M., Zanchi, C., Corna, D., Tomasoni, S., Benigni, A., Remuzzi, G., and Zoja, C. 2000. Protein traffic activates NF-kB gene signaling and promotes MCP-1-dependent interstitial inflammation. *Am J Kidney Dis* 36:1226-1241.
9. Donadelli, R., Zanchi, C., Morigi, M., Buelli, S., Batani, C., Tomasoni, S., Corna, D., Rottoli, D., Benigni, A., Abbate, M., et al. 2003. Protein overload induces fractalkine upregulation in proximal tubular cells through nuclear factor kappaB- and p38 mitogen-activated protein kinase-dependent pathways. *J Am Soc Nephrol* 14:2436-2446.
10. Ketteler, M., Noble, N.A., and Border, W.A. 1995. Transforming growth factor-beta and angiotensin II: the missing link from glomerular hyperfiltration to glomerulosclerosis? *Annu Rev Physiol* 57:279-295.
11. Wolf, G., and Neilson, E.G. 1993. Angiotensin II as a renal growth factor. *J Am Soc Nephrol* 3:1531-1540.
12. Orth, S.R., Weinreich, T., Bonisch, S., Weih, M., and Ritz, E. 1995. Angiotensin II induces hypertrophy and hyperplasia in adult human mesangial cells. *Exp Nephrol* 3:23-33.
13. Ma, L., and Fogo, A.B. 2001. Role of angiotensin II in glomerular injury. *Semin Nephrol* 21:544-553.

14. Wang, W., Huang, X.R., Canlas, E., Oka, K., Truong, L.D., Deng, C., Bhowmick, N.A., Ju, W., Bottinger, E.P., and Lan, H.Y. 2006. Essential role of Smad3 in angiotensin II-induced vascular fibrosis. *Circ Res* 98:1032-1039.
15. Eddy, A.A., and Neilson, E.G. 2006. Chronic kidney disease progression. *J Am Soc Nephrol* 17:2964-2966.
16. Ma, L.J., Yang, H., Gaspert, A., Carlesso, G., Barty, M.M., Davidson, J.M., Sheppard, D., and Fogo, A.B. 2003. Transforming growth factor-beta-dependent and -independent pathways of induction of tubulointerstitial fibrosis in beta6(-/-) mice. *Am J Pathol* 163:1261-1273.
17. Fukuda, N., Tahira, Y., Matsuda, H., and Matsumoto, K. 2009. Transforming growth factor-beta as a treatment target in renal diseases. *J Nephrol* 22:708-715.
18. Yang, J., Zhang, X., Li, Y., and Liu, Y. 2003. Downregulation of Smad transcriptional corepressors SnoN and Ski in the fibrotic kidney: an amplification mechanism for TGF-beta1 signaling. *J Am Soc Nephrol* 14:3167-3177.
19. Schiffer, M., Bitzer, M., Roberts, I.S., Kopp, J.B., ten Dijke, P., Mundel, P., and Bottinger, E.P. 2001. Apoptosis in podocytes induced by TGF-beta and Smad7. *J Clin Invest* 108:807-816.
20. Border, W.A., and Noble, N.A. 1993. Cytokines in kidney disease: the role of transforming growth factor-beta. *Am J Kidney Dis* 22:105-113.
21. Seo, J.Y., Park, J., Yu, M.R., Kim, Y.S., Ha, H., and Lee, H.B. 2009. Positive feedback loop between plasminogen activator inhibitor-1 and transforming growth factor-beta1 during renal fibrosis in diabetes. *Am J Nephrol* 30:481-490.
22. Yokoi, H., Sugawara, A., Mukoyama, M., Mori, K., Makino, H., Suganami, T., Nagae, T., Yahata, K., Fujinaga, Y., Tanaka, I., et al. 2001. Role of connective tissue growth factor in profibrotic action of transforming growth factor-beta: a potential target for preventing renal fibrosis. *Am J Kidney Dis* 38:S134-138.
23. Iwano, M., Plieth, D., Danoff, T.M., Xue, C., Okada, H., and Neilson, E.G. 2002. Evidence that fibroblasts derive from epithelium during tissue fibrosis. *J Clin Invest* 110:341-350.
24. Zeisberg, E.M., Potenta, S.E., Sugimoto, H., Zeisberg, M., and Kalluri, R. 2008. Fibroblasts in kidney fibrosis emerge via endothelial-to-mesenchymal transition. *J Am Soc Nephrol* 19:2282-2287.
25. Wang, W., Huang, X.R., Li, A.G., Liu, F., Li, J.H., Truong, L.D., Wang, X.J., and Lan, H.Y. 2005. Signaling mechanism of TGF-beta1 in prevention of renal inflammation: role of Smad7. *J Am Soc Nephrol* 16:1371-1383.
26. Swirski, F.K., Nahrendorf, M., Etzrodt, M., Wildgruber, M., Cortez-Retamozo, V., Panizzi, P., Figueiredo, J.L., Kohler, R.H., Chudnovskiy, A., Waterman, P., et al. 2009. Identification of

splenic reservoir monocytes and their deployment to inflammatory sites. *Science* 325:612-616.
27. Geissmann, F., Jung, S., and Littman, D.R. 2003. Blood monocytes consist of two principal subsets with distinct migratory properties. *Immunity* 19:71-82.
28. Serbina, N.V., and Pamer, E.G. 2006. Monocyte emigration from bone marrow during bacterial infection requires signals mediated by chemokine receptor CCR2. *Nat Immunol* 7:311-317.
29. Liu, K., Waskow, C., Liu, X., Yao, K., Hoh, J., and Nussenzweig, M. 2007. Origin of dendritic cells in peripheral lymphoid organs of mice. *Nat Immunol* 8:578-583.
30. Yona, S., and Jung, S. 2010. Monocytes: subsets, origins, fates and functions. *Curr Opin Hematol* 17:53-59.
31. Nahrendorf, M., Swirski, F.K., Aikawa, E., Stangenberg, L., Wurdinger, T., Figueiredo, J.L., Libby, P., Weissleder, R., and Pittet, M.J. 2007. The healing myocardium sequentially mobilizes two monocyte subsets with divergent and complementary functions. *J Exp Med* 204:3037-3047.
32. Arnold, L., Henry, A., Poron, F., Baba-Amer, Y., van Rooijen, N., Plonquet, A., Gherardi, R.K., and Chazaud, B. 2007. Inflammatory monocytes recruited after skeletal muscle injury switch into antiinflammatory macrophages to support myogenesis. *J Exp Med* 204:1057-1069.
33. Karlmark, K.R., Weiskirchen, R., Zimmermann, H.W., Gassler, N., Ginhoux, F., Weber, C., Merad, M., Luedde, T., Trautwein, C., and Tacke, F. 2009. Hepatic recruitment of the inflammatory Gr1+ monocyte subset upon liver injury promotes hepatic fibrosis. *Hepatology* 50:261-274.
34. Auffray, C., Fogg, D., Garfa, M., Elain, G., Join-Lambert, O., Kayal, S., Sarnacki, S., Cumano, A., Lauvau, G., and Geissmann, F. 2007. Monitoring of blood vessels and tissues by a population of monocytes with patrolling behavior. *Science* 317:666-670.
35. Bazan, J.F., Bacon, K.B., Hardiman, G., Wang, W., Soo, K., Rossi, D., Greaves, D.R., Zlotnik, A., and Schall, T.J. 1997. A new class of membrane-bound chemokine with a CX3C motif. *Nature* 385:640-644.
36. Matloubian, M., David, A., Engel, S., Ryan, J.E., and Cyster, J.G. 2000. A transmembrane CXC chemokine is a ligand for HIV-coreceptor Bonzo. *Nat Immunol* 1:298-304.
37. Imai, T., Hieshima, K., Haskell, C., Baba, M., Nagira, M., Nishimura, M., Kakizaki, M., Takagi, S., Nomiyama, H., Schall, T.J., et al. 1997. Identification and molecular characterization of fractalkine receptor CX3CR1, which mediates both leukocyte migration and adhesion. *Cell* 91:521-530.
38. Haskell, C.A., Cleary, M.D., and Charo, I.F. 1999. Molecular uncoupling of fractalkine-mediated cell adhesion and signal

transduction. Rapid flow arrest of CX3CR1-expressing cells is independent of G-protein activation. *J Biol Chem* 274:10053-10058.
39. Fong, A.M., Robinson, L.A., Steeber, D.A., Tedder, T.F., Yoshie, O., Imai, T., and Patel, D.D. 1998. Fractalkine and CX3CR1 mediate a novel mechanism of leukocyte capture, firm adhesion, and activation under physiologic flow. *J Exp Med* 188:1413-1419.
40. Salanga, C.L., O'Hayre, M., and Handel, T. 2009. Modulation of chemokine receptor activity through dimerization and crosstalk. *Cell Mol Life Sci* 66:1370-1386.
41. Goda, S., Imai, T., Yoshie, O., Yoneda, O., Inoue, H., Nagano, Y., Okazaki, T., Imai, H., Bloom, E.T., Domae, N., et al. 2000. CX3C-chemokine, fractalkine-enhanced adhesion of THP-1 cells to endothelial cells through integrin-dependent and -independent mechanisms. *J Immunol* 164:4313-4320.
42. Horne, K., and Woolley, I.J. 2009. Shedding light on DARC: the role of the Duffy antigen/receptor for chemokines in inflammation, infection and malignancy. *Inflamm Res* 58:431-435.
43. Mackay, C.R. 2001. Chemokines: immunology's high impact factors. *Nat Immunol* 2:95-101.
44. Pan, Y., Lloyd, C., Zhou, H., Dolich, S., Deeds, J., Gonzalo, J.A., Vath, J., Gosselin, M., Ma, J., Dussault, B., et al. 1997. Neurotactin, a membrane-anchored chemokine upregulated in brain inflammation. *Nature* 387:611-617.
45. Chen, S., Bacon, K.B., Li, L., Garcia, G.E., Xia, Y., Lo, D., Thompson, D.A., Siani, M.A., Yamamoto, T., Harrison, J.K., et al. 1998. In vivo inhibition of CC and CX3C chemokine-induced leukocyte infiltration and attenuation of glomerulonephritis in Wistar-Kyoto (WKY) rats by vMIP-II. *J Exp Med* 188:193-198.
46. Feng, L., Chen, S., Garcia, G.E., Xia, Y., Siani, M.A., Botti, P., Wilson, C.B., Harrison, J.K., and Bacon, K.B. 1999. Prevention of crescentic glomerulonephritis by immunoneutralization of the fractalkine receptor CX3CR1 rapid communication. *Kidney Int* 56:612-620.
47. Grone, H.J., Cohen, C.D., Grone, E., Schmidt, C., Kretzler, M., Schlondorff, D., and Nelson, P.J. 2002. Spatial and temporally restricted expression of chemokines and chemokine receptors in the developing human kidney. *J Am Soc Nephrol* 13:957-967.
48. Segerer, S., Hughes, E., Hudkins, K.L., Mack, M., Goodpaster, T., and Alpers, C.E. 2002. Expression of the fractalkine receptor (CX3CR1) in human kidney diseases. *Kidney Int* 62:488-495.
49. Cockwell, P., Chakravorty, S.J., Girdlestone, J., and Savage, C.O. 2002. Fractalkine expression in human renal inflammation. *J Pathol* 196:85-90.
50. Ito, Y., Kawachi, H., Morioka, Y., Nakatsue, T., Koike, H., Ikezumi, Y., Oyanagi, A., Natori, Y., Natori, Y., Nakamura, T., et al. 2002. Fractalkine expression and the recruitment of CX3CR1+

cells in the prolonged mesangial proliferative glomerulonephritis. *Kidney Int* 61:2044-2057.

51. Chen, Y.M., Hu-Tsai, M.I., Lin, S.L., Tsai, T.J., and Hsieh, B.S. 2003. Expression of CX3CL1/fractalkine by mesangial cells in vitro and in acute anti-Thy1 glomerulonephritis in rats. *Nephrol Dial Transplant* 18:2505-2514.
52. Haskell, C.A., Hancock, W.W., Salant, D.J., Gao, W., Csizmadia, V., Peters, W., Faia, K., Fituri, O., Rottman, J.B., and Charo, I.F. 2001. Targeted deletion of CX(3)CR1 reveals a role for fractalkine in cardiac allograft rejection. *J Clin Invest* 108:679-688.
53. Yoshimoto, S., Nakatani, K., Iwano, M., Asai, O., Samejima, K., Sakan, H., Terada, M., Harada, K., Akai, Y., Shiiki, H., et al. 2007. Elevated levels of fractalkine expression and accumulation of CD16+ monocytes in glomeruli of active lupus nephritis. *Am J Kidney Dis* 50:47-58.
54. Inoue, A., Hasegawa, H., Kohno, M., Ito, M.R., Terada, M., Imai, T., Yoshie, O., Nose, M., and Fujita, S. 2005. Antagonist of fractalkine (CX3CL1) delays the initiation and ameliorates the progression of lupus nephritis in MRL/lpr mice. *Arthritis Rheum* 52:1522-1533.
55. Furuichi, K., Wada, T., Iwata, Y., Sakai, N., Yoshimoto, K., Shimizu, M., Kobayashi, K., Takasawa, K., Kida, H., Takeda, S., et al. 2001. Upregulation of fractalkine in human crescentic glomerulonephritis. *Nephron* 87:314-320.
56. Ramos, M.V., Fernandez, G.C., Patey, N., Schierloh, P., Exeni, R., Grimoldi, I., Vallejo, G., Elias-Costa, C., Del Carmen Sasiain, M., Trachtman, H., et al. 2007. Involvement of the fractalkine pathway in the pathogenesis of childhood hemolytic uremic syndrome. *Blood* 109:2438-2445.
57. Zanchi, C., Zoja, C., Morigi, M., Valsecchi, F., Liu, X.Y., Rottoli, D., Locatelli, M., Buelli, S., Pezzotta, A., Mapelli, P., et al. 2008. Fractalkine and CX3CR1 mediate leukocyte capture by endothelium in response to Shiga toxin. *J Immunol* 181:1460-1469.
58. Robinson, L.A., Nataraj, C., Thomas, D.W., Howell, D.N., Griffiths, R., Bautch, V., Patel, D.D., Feng, L., and Coffman, T.M. 2000. A role for fractalkine and its receptor (CX3CR1) in cardiac allograft rejection. *J Immunol* 165:6067-6072.
59. Chakravorty, S.J., Cockwell, P., Girdlestone, J., Brooks, C.J., and Savage, C.O. 2002. Fractalkine expression on human renal tubular epithelial cells: potential role in mononuclear cell adhesion. *Clin Exp Immunol* 129:150-159.
60. Pietrzyk, M.C., Banas, B., Wolf, K., Rummele, P., Woenckhaus, M., Hoffmann, U., Kramer, B.K., and Fischereder, M. 2004. Quantitative gene expression analysis of fractalkine using laser microdissection in biopsies from kidney allografts with acute rejection. *Transplant Proc* 36:2659-2661.

61. Peng, W., Chen, J., Jiang, Y., Wu, J., Shou, Z., He, Q., Wang, Y., Chen, Y., and Wang, H. 2008. Urinary fractalkine is a marker of acute rejection. *Kidney Int* 74:1454-1460.
62. Cao, G., Lu, Y., Gao, R., Xin, Y., Teng, D., Wang, J., and Li, Y. 2006. Expression of fractalkine, CX3CR1, and vascular endothelial growth factor in human chronic renal allograft rejection. *Transplant Proc* 38:1998-2000.
63. Simeoni, E., Vassalli, G., Seydoux, C., Ramsay, D., Noll, G., von Segesser, L.K., and Fleury, S. 2005. CCR5, RANTES and CX3CR1 polymorphisms: possible genetic links with acute heart rejection. *Transplantation* 80:1309-1315.
64. Abdi, R., Tran, T.B., Sahagun-Ruiz, A., Murphy, P.M., Brenner, B.M., Milford, E.L., and McDermott, D.H. 2002. Chemokine receptor polymorphism and risk of acute rejection in human renal transplantation. *J Am Soc Nephrol* 13:754-758.
65. Furuichi, K., Gao, J.L., and Murphy, P.M. 2006. Chemokine receptor CX3CR1 regulates renal interstitial fibrosis after ischemia-reperfusion injury. *Am J Pathol* 169:372-387.
66. Oh, D.J., Dursun, B., He, Z., Lu, L., Hoke, T.S., Ljubanovic, D., Faubel, S., and Edelstein, C.L. 2008. Fractalkine receptor (CX3CR1) inhibition is protective against ischemic acute renal failure in mice. *Am J Physiol Renal Physiol* 294:F264-271.
67. Li, L., Huang, L., Sung, S.S., Vergis, A.L., Rosin, D.L., Rose, C.E., Jr., Lobo, P.I., and Okusa, M.D. 2008. The chemokine receptors CCR2 and CX3CR1 mediate monocyte/macrophage trafficking in kidney ischemia-reperfusion injury. *Kidney Int* 74:1526-1537.
68. Tacke, F., Alvarez, D., Kaplan, T.J., Jakubzick, C., Spanbroek, R., Llodra, J., Garin, A., Liu, J., Mack, M., van Rooijen, N., et al. 2007. Monocyte subsets differentially employ CCR2, CCR5, and CX3CR1 to accumulate within atherosclerotic plaques. *J Clin Invest* 117:185-194.
69. Combadiere, C., Potteaux, S., Rodero, M., Simon, T., Pezard, A., Esposito, B., Merval, R., Proudfoot, A., Tedgui, A., and Mallat, Z. 2008. Combined inhibition of CCL2, CX3CR1, and CCR5 abrogates Ly6C(hi) and Ly6C(lo) monocytosis and almost abolishes atherosclerosis in hypercholesterolemic mice. *Circulation* 117:1649-1657.
70. Nangaku, M. 2006. Chronic hypoxia and tubulointerstitial injury: a final common pathway to end-stage renal failure. *J Am Soc Nephrol* 17:17-25.
71. Koziolek, M.J., Schmid, H., Cohen, C.D., Blaschke, S., Hemmerlein, B., Zapf, A., Muller, G.A., and Strutz, F. 2007. Potential role of fractalkine receptor expression in human renal fibrogenesis. *Kidney Int* 72:599-607.
72. Lucas, A.D., Bursill, C., Guzik, T.J., Sadowski, J., Channon, K.M., and Greaves, D.R. 2003. Smooth muscle cells in human atherosclerotic plaques express the fractalkine receptor CX3CR1

and undergo chemotaxis to the CX3C chemokine fractalkine (CX3CL1). *Circulation* 108:2498-2504.

73. Nomiyama, H., Imai, T., Kusuda, J., Miura, R., Callen, D.F., and Yoshie, O. 1998. Human chemokines fractalkine (SCYD1), MDC (SCYA22) and TARC (SCYA17) are clustered on chromosome 16q13. *Cytogenet Cell Genet* 81:10-11.
74. Garcia, G.E., Xia, Y., Chen, S., Wang, Y., Ye, R.D., Harrison, J.K., Bacon, K.B., Zerwes, H.G., and Feng, L. 2000. NF-kappaB-dependent fractalkine induction in rat aortic endothelial cells stimulated by IL-1beta, TNF-alpha, and LPS. *J Leukoc Biol* 67:577-584.
75. Ahn, S.Y., Cho, C.H., Park, K.G., Lee, H.J., Lee, S., Park, S.K., Lee, I.K., and Koh, G.Y. 2004. Tumor necrosis factor-alpha induces fractalkine expression preferentially in arterial endothelial cells and mithramycin A suppresses TNF-alpha-induced fractalkine expression. *Am J Pathol* 164:1663-1672.
76. Chen, Y.M., Lin, S.L., Chen, C.W., Chiang, W.C., Tsai, T.J., and Hsieh, B.S. 2003. Tumor necrosis factor-alpha stimulates fractalkine production by mesangial cells and regulates monocyte transmigration: down-regulation by cAMP. *Kidney Int* 63:474-486.
77. Hatakeyama, M., Imaizumi, T., Tamo, W., Yamashita, K., Yoshida, H., Fukuda, I., and Satoh, K. 2004. Heparin inhibits IFN-gamma-induced fractalkine/CX3CL1 expression in human endothelial cells. *Inflammation* 28:7-13.
78. Harrison, J.K., Jiang, Y., Wees, E.A., Salafranca, M.N., Liang, H.X., Feng, L., and Belardinelli, L. 1999. Inflammatory agents regulate in vivo expression of fractalkine in endothelial cells of the rat heart. *J Leukoc Biol* 66:937-944.
79. Imaizumi, T., Matsumiya, T., Fujimoto, K., Okamoto, K., Cui, X., Ohtaki, U., Hidemi, Yoshida, and Satoh, K. 2000. Interferon-gamma stimulates the expression of CX3CL1/fractalkine in cultured human endothelial cells. *Tohoku J Exp Med* 192:127-139.
80. Yoshida, H., Imaizumi, T., Fujimoto, K., Matsuo, N., Kimura, K., Cui, X., Matsumiya, T., Tanji, K., Shibata, T., Tamo, W., et al. 2001. Synergistic stimulation, by tumor necrosis factor-alpha and interferon-gamma, of fractalkine expression in human astrocytes. *Neurosci Lett* 303:132-136.
81. Ludwig, A., Berkhout, T., Moores, K., Groot, P., and Chapman, G. 2002. Fractalkine is expressed by smooth muscle cells in response to IFN-gamma and TNF-alpha and is modulated by metalloproteinase activity. *J Immunol* 168:604-612.
82. Imaizumi, T., Yoshida, H., and Satoh, K. 2004. Regulation of CX3CL1/fractalkine expression in endothelial cells. *J Atheroscler Thromb* 11:15-21.
83. Sheng, W.S., Hu, S., Ni, H.T., Rock, R.B., and Peterson, P.K. 2009. WIN55,212-2 inhibits production of CX3CL1 by human

astrocytes: involvement of p38 MAP kinase. *J Neuroimmune Pharmacol* 4:244-248.

84. Wu, S.H., Lu, C., Dong, L., and Chen, Z.Q. 2008. Signal transduction involved in CTGF-induced production of chemokines in mesangial cells. *Growth Factors* 26:192-200.
85. Fujimoto, K., Imaizumi, T., Yoshida, H., Takanashi, S., Okumura, K., and Satoh, K. 2001. Interferon-gamma stimulates fractalkine expression in human bronchial epithelial cells and regulates mononuclear cell adherence. *Am J Respir Cell Mol Biol* 25:233-238.
86. Isozaki, T., Otsuka, K., Sato, M., Takahashi, R., Wakabayashi, K., Yajima, N., Miwa, Y., and Kasama, T. 2011. Synergistic induction of CX3CL1 by interleukin-1beta and interferon-gamma in human lung fibroblasts: involvement of signal transducer and activator of transcription 1 signaling pathways. *Transl Res* 157:64-70.
87. Lombardi, A., Cantini, G., Piscitelli, E., Gelmini, S., Francalanci, M., Mello, T., Ceni, E., Varano, G., Forti, G., Rotondi, M., et al. 2008. A new mechanism involving ERK contributes to rosiglitazone inhibition of tumor necrosis factor-alpha and interferon-gamma inflammatory effects in human endothelial cells. *Arterioscler Thromb Vasc Biol* 28:718-724.
88. Yamashita, K., Imaizumi, T., Hatakeyama, M., Tamo, W., Kimura, D., Kumagai, M., Yoshida, H., and Satoh, K. 2003. Effect of hypoxia on the expression of fractalkine in human endothelial cells. *Tohoku J Exp Med* 200:187-194.
89. Modur, V., Li, Y., Zimmerman, G.A., Prescott, S.M., and McIntyre, T.M. 1997. Retrograde inflammatory signaling from neutrophils to endothelial cells by soluble interleukin-6 receptor alpha. *J Clin Invest* 100:2752-2756.
90. Matsumiya, T., Imaizumi, T., Fujimoto, K., Cui, X., Shibata, T., Tamo, W., Kumagai, M., Tanji, K., Yoshida, H., Kimura, H., et al. 2001. Soluble interleukin-6 receptor alpha inhibits the cytokine-Induced fractalkine/CX3CL1 expression in human vascular endothelial cells in culture. *Exp Cell Res* 269:35-41.
91. Imaizumi, T., Matsumiya, T., Tamo, W., Shibata, T., Fujimoto, K., Kumagai, M., Yoshida, H., Cui, X.F., Tanji, K., Hatakeyama, M., et al. 2002. 15-Deoxy-D12,14-prostaglandin J2 inhibits CX3CL1/fractalkine expression in human endothelial cells. *Immunol Cell Biol* 80:531-536.
92. Garton, K.J., Gough, P.J., Blobel, C.P., Murphy, G., Greaves, D.R., Dempsey, P.J., and Raines, E.W. 2001. Tumor necrosis factor-alpha-converting enzyme (ADAM17) mediates the cleavage and shedding of fractalkine (CX3CL1). *J Biol Chem* 276:37993-38001.
93. Tsou, C.L., Haskell, C.A., and Charo, I.F. 2001. Tumor necrosis factor-alpha-converting enzyme mediates the inducible cleavage of fractalkine. *J Biol Chem* 276:44622-44626.
94. Hundhausen, C., Misztela, D., Berkhout, T.A., Broadway, N., Saftig, P., Reiss, K., Hartmann, D., Fahrenholz, F., Postina, R.,

Matthews, V., et al. 2003. The disintegrin-like metalloproteinase ADAM10 is involved in constitutive cleavage of CX3CL1 (fractalkine) and regulates CX3CL1-mediated cell-cell adhesion. *Blood* 102:1186-1195.

95. Hundhausen, C., Schulte, A., Schulz, B., Andrzejewski, M.G., Schwarz, N., von Hundelshausen, P., Winter, U., Paliga, K., Reiss, K., Saftig, P., et al. 2007. Regulated shedding of transmembrane chemokines by the disintegrin and metalloproteinase 10 facilitates detachment of adherent leukocytes. *J Immunol* 178:8064-8072.
96. Dean, R.A., and Overall, C.M. 2007. Proteomics discovery of metalloproteinase substrates in the cellular context by iTRAQ labeling reveals a diverse MMP-2 substrate degradome. *Mol Cell Proteomics* 6:611-623.
97. Clark, A.K., Yip, P.K., Grist, J., Gentry, C., Staniland, A.A., Marchand, F., Dehvari, M., Wotherspoon, G., Winter, J., Ullah, J., et al. 2007. Inhibition of spinal microglial cathepsin S for the reversal of neuropathic pain. *Proc Natl Acad Sci U S A* 104:10655-10660.
98. Liu, G.Y., Kulasingam, V., Alexander, R.T., Touret, N., Fong, A.M., Patel, D.D., and Robinson, L.A. 2005. Recycling of the membrane-anchored chemokine, CX3CL1. *J Biol Chem* 280:19858-19866.
99. Huang, Y.W., Su, P., Liu, G.Y., Crow, M.R., Chaukos, D., Yan, H., and Robinson, L.A. 2009. Constitutive endocytosis of the chemokine CX3CL1 prevents its degradation by cell surface metalloproteases. *J Biol Chem* 284:29644-29653.
100. Casarosa, P., Waldhoer, M., LiWang, P.J., Vischer, H.F., Kledal, T., Timmerman, H., Schwartz, T.W., Smit, M.J., and Leurs, R. 2005. CC and CX3C chemokines differentially interact with the N terminus of the human cytomegalovirus-encoded US28 receptor. *J Biol Chem* 280:3275-3285.
101. Boomker, J.M., van Luyn, M.J., The, T.H., de Leij, L.F., and Harmsen, M.C. 2005. US28 actions in HCMV infection: lessons from a versatile hijacker. *Rev Med Virol* 15:269-282.
102. Foussat, A., Coulomb-L'Hermine, A., Gosling, J., Krzysiek, R., Durand-Gasselin, I., Schall, T., Balian, A., Richard, Y., Galanaud, P., and Emilie, D. 2000. Fractalkine receptor expression by T lymphocyte subpopulations and in vivo production of fractalkine in human. *Eur J Immunol* 30:87-97.
103. Combadiere, C., Salzwedel, K., Smith, E.D., Tiffany, H.L., Berger, E.A., and Murphy, P.M. 1998. Identification of CX3CR1. A chemotactic receptor for the human CX3C chemokine fractalkine and a fusion coreceptor for HIV-1. *J Biol Chem* 273:23799-23804.
104. Wong, B.W., Wong, D., and McManus, B.M. 2002. Characterization of fractalkine (CX3CL1) and CX3CR1 in human

coronary arteries with native atherosclerosis, diabetes mellitus, and transplant vascular disease. *Cardiovasc Pathol* 11:332-338.
105. Blaschke, S., Koziolek, M., Schwarz, A., Benohr, P., Middel, P., Schwarz, G., Hummel, K.M., and Muller, G.A. 2003. Proinflammatory role of fractalkine (CX3CL1) in rheumatoid arthritis. *J Rheumatol* 30:1918-1927.
106. Brand, S., Sakaguchi, T., Gu, X., Colgan, S.P., and Reinecker, H.C. 2002. Fractalkine-mediated signals regulate cell-survival and immune-modulatory responses in intestinal epithelial cells. *Gastroenterology* 122:166-177.
107. Schafer, A., Schulz, C., Fraccarollo, D., Tas, P., Leutke, M., Eigenthaler, M., Seidl, S., Heider, P., Ertl, G., Massberg, S., et al. 2007. The CX3C chemokine fractalkine induces vascular dysfunction by generation of superoxide anions. *Arterioscler Thromb Vasc Biol* 27:55-62.
108. Yang, X.P., Mattagajasingh, S., Su, S., Chen, G., Cai, Z., Fox-Talbot, K., Irani, K., and Becker, L.C. 2007. Fractalkine upregulates intercellular adhesion molecule-1 in endothelial cells through CX3CR1 and the Jak Stat5 pathway. *Circ Res* 101:1001-1008.
109. Garin, A., Tarantino, N., Faure, S., Daoudi, M., Lecureuil, C., Bourdais, A., Debre, P., Deterre, P., and Combadiere, C. 2003. Two novel fully functional isoforms of CX3CR1 are potent HIV coreceptors. *J Immunol* 171:5305-5312.
110. Haskell, C.A., Cleary, M.D., and Charo, I.F. 2000. Unique role of the chemokine domain of fractalkine in cell capture. Kinetics of receptor dissociation correlate with cell adhesion. *J Biol Chem* 275:34183-34189.
111. Fong, A.M., Erickson, H.P., Zachariah, J.P., Poon, S., Schamberg, N.J., Imai, T., and Patel, D.D. 2000. Ultrastructure and function of the fractalkine mucin domain in CX(3)C chemokine domain presentation. *J Biol Chem* 275:3781-3786.
112. You, J.J., Yang, C.H., Huang, J.S., Chen, M.S., and Yang, C.M. 2007. Fractalkine, a CX3C chemokine, as a mediator of ocular angiogenesis. *Invest Ophthalmol Vis Sci* 48:5290-5298.
113. Lucas, A.D., Chadwick, N., Warren, B.F., Jewell, D.P., Gordon, S., Powrie, F., and Greaves, D.R. 2001. The transmembrane form of the CX3CL1 chemokine fractalkine is expressed predominantly by epithelial cells in vivo. *Am J Pathol* 158:855-866.
114. Papadopoulos, E.J., Sassetti, C., Saeki, H., Yamada, N., Kawamura, T., Fitzhugh, D.J., Saraf, M.A., Schall, T., Blauvelt, A., Rosen, S.D., et al. 1999. Fractalkine, a CX3C chemokine, is expressed by dendritic cells and is up-regulated upon dendritic cell maturation. *Eur J Immunol* 29:2551-2559.
115. Kanazawa, N., Nakamura, T., Tashiro, K., Muramatsu, M., Morita, K., Yoneda, K., Inaba, K., Imamura, S., and Honjo, T. 1999. Fractalkine and macrophage-derived chemokine: T cell-

attracting chemokines expressed in T cell area dendritic cells. *Eur J Immunol* 29:1925-1932.

116. Greaves, D.R., Hakkinen, T., Lucas, A.D., Liddiard, K., Jones, E., Quinn, C.M., Senaratne, J., Green, F.R., Tyson, K., Boyle, J., et al. 2001. Linked chromosome 16q13 chemokines, macrophage-derived chemokine, fractalkine, and thymus- and activation-regulated chemokine, are expressed in human atherosclerotic lesions. *Arterioscler Thromb Vasc Biol* 21:923-929.
117. Cardona, A.E., Pioro, E.P., Sasse, M.E., Kostenko, V., Cardona, S.M., Dijkstra, I.M., Huang, D., Kidd, G., Dombrowski, S., Dutta, R., et al. 2006. Control of microglial neurotoxicity by the fractalkine receptor. *Nat Neurosci* 9:917-924.
118. Nishiyori, A., Minami, M., Ohtani, Y., Takami, S., Yamamoto, J., Kawaguchi, N., Kume, T., Akaike, A., and Satoh, M. 1998. Localization of fractalkine and CX3CR1 mRNAs in rat brain: does fractalkine play a role in signaling from neuron to microglia? *FEBS Lett* 429:167-172.
119. Schwaeble, W.J., Stover, C.M., Schall, T.J., Dairaghi, D.J., Trinder, P.K., Linington, C., Iglesias, A., Schubart, A., Lynch, N.J., Weihe, E., et al. 1998. Neuronal expression of fractalkine in the presence and absence of inflammation. *FEBS Lett* 439:203-207.
120. Harrison, J.K., Jiang, Y., Chen, S., Xia, Y., Maciejewski, D., McNamara, R.K., Streit, W.J., Salafranca, M.N., Adhikari, S., Thompson, D.A., et al. 1998. Role for neuronally derived fractalkine in mediating interactions between neurons and CX3CR1-expressing microglia. *Proc Natl Acad Sci U S A* 95:10896-10901.
121. Brand, S., Hofbauer, K., Dambacher, J., Schnitzler, F., Staudinger, T., Pfennig, S., Seiderer, J., Tillack, C., Konrad, A., Goke, B., et al. 2006. Increased expression of the chemokine fractalkine in Crohn's disease and association of the fractalkine receptor T280M polymorphism with a fibrostenosing disease Phenotype. *Am J Gastroenterol* 101:99-106.
122. Raychaudhuri, S.P., Jiang, W.Y., and Farber, E.M. 2001. Cellular localization of fractalkine at sites of inflammation: antigen-presenting cells in psoriasis express high levels of fractalkine. *Br J Dermatol* 144:1105-1113.
123. Sawai, H., Park, Y.W., He, X., Goronzy, J.J., and Weyand, C.M. 2007. Fractalkine mediates T cell-dependent proliferation of synovial fibroblasts in rheumatoid arthritis. *Arthritis Rheum* 56:3215-3225.
124. El-Shazly, A., Berger, P., Girodet, P.O., Ousova, O., Fayon, M., Vernejoux, J.M., Marthan, R., and Tunon-de-Lara, J.M. 2006. Fraktalkine produced by airway smooth muscle cells contributes to mast cell recruitment in asthma. *J Immunol* 176:1860-1868.

125. Lesnik, P., Haskell, C.A., and Charo, I.F. 2003. Decreased atherosclerosis in CX3CR1-/- mice reveals a role for fractalkine in atherogenesis. *J Clin Invest* 111:333-340.
126. Teupser, D., Pavlides, S., Tan, M., Gutierrez-Ramos, J.C., Kolbeck, R., and Breslow, J.L. 2004. Major reduction of atherosclerosis in fractalkine (CX3CL1)-deficient mice is at the brachiocephalic artery, not the aortic root. *Proc Natl Acad Sci U S A* 101:17795-17800.
127. Combadiere, C., Potteaux, S., Gao, J.L., Esposito, B., Casanova, S., Lee, E.J., Debre, P., Tedgui, A., Murphy, P.M., and Mallat, Z. 2003. Decreased atherosclerotic lesion formation in CX3CR1/apolipoprotein E double knockout mice. *Circulation* 107:1009-1016.
128. Saederup, N., Chan, L., Lira, S.A., and Charo, I.F. 2008. Fractalkine deficiency markedly reduces macrophage accumulation and atherosclerotic lesion formation in CCR2-/- mice: evidence for independent chemokine functions in atherogenesis. *Circulation* 117:1642-1648.
129. Schafer, A., Schulz, C., Eigenthaler, M., Fraccarollo, D., Kobsar, A., Gawaz, M., Ertl, G., Walter, U., and Bauersachs, J. 2004. Novel role of the membrane-bound chemokine fractalkine in platelet activation and adhesion. *Blood* 103:407-412.
130. Schulz, C., Schafer, A., Stolla, M., Kerstan, S., Lorenz, M., von Bruhl, M.L., Schiemann, M., Bauersachs, J., Gloe, T., Busch, D.H., et al. 2007. Chemokine fractalkine mediates leukocyte recruitment to inflammatory endothelial cells in flowing whole blood: a critical role for P-selectin expressed on activated platelets. *Circulation* 116:764-773.
131. Ishida, Y., Hayashi, T., Goto, T., Kimura, A., Akimoto, S., Mukaida, N., and Kondo, T. 2008. Essential involvement of CX3CR1-mediated signals in the bactericidal host defense during septic peritonitis. *J Immunol* 181:4208-4218.
132. Yu, Y.R., Fong, A.M., Combadiere, C., Gao, J.L., Murphy, P.M., and Patel, D.D. 2007. Defective antitumor responses in CX3CR1-deficient mice. *Int J Cancer* 121:316-322.
133. Ishida, Y., Gao, J.L., and Murphy, P.M. 2008. Chemokine receptor CX3CR1 mediates skin wound healing by promoting macrophage and fibroblast accumulation and function. *J Immunol* 180:569-579.
134. Mellman, I., and Nelson, W.J. 2008. Coordinated protein sorting, targeting and distribution in polarized cells. *Nat Rev Mol Cell Biol* 9:833-845.
135. Yu, C.Y., Chen, J.Y., Lin, Y.Y., Shen, K.F., Lin, W.L., Chien, C.L., ter Beest, M.B., and Jou, T.S. 2007. A bipartite signal regulates the faithful delivery of apical domain marker podocalyxin/Gp135. *Mol Biol Cell* 18:1710-1722.

136. Chuang, J.Z., and Sung, C.H. 1998. The cytoplasmic tail of rhodopsin acts as a novel apical sorting signal in polarized MDCK cells. *J Cell Biol* 142:1245-1256.
137. Matter, K., Hunziker, W., and Mellman, I. 1992. Basolateral sorting of LDL receptor in MDCK cells: the cytoplasmic domain contains two tyrosine-dependent targeting determinants. *Cell* 71:741-753.
138. Deborde, S., Perret, E., Gravotta, D., Deora, A., Salvarezza, S., Schreiner, R., and Rodriguez-Boulan, E. 2008. Clathrin is a key regulator of basolateral polarity. *Nature* 452:719-723.
139. Huet, G., Kim, I., de Bolos, C., Lo-Guidice, J.M., Moreau, O., Hemon, B., Richet, C., Delannoy, P., Real, F.X., and Degand, P. 1995. Characterization of mucins and proteoglycans synthesized by a mucin-secreting HT-29 cell subpopulation. *J Cell Sci* 108 (Pt 3):1275-1285.
140. Alfalah, M., Jacob, R., Preuss, U., Zimmer, K.P., Naim, H., and Naim, H.Y. 1999. O-linked glycans mediate apical sorting of human intestinal sucrase-isomaltase through association with lipid rafts. *Curr Biol* 9:593-596.
141. Scheiffele, P., Peranen, J., and Simons, K. 1995. N-glycans as apical sorting signals in epithelial cells. *Nature* 378:96-98.
142. Kitagawa, Y., Sano, Y., Ueda, M., Higashio, K., Narita, H., Okano, M., Matsumoto, S., and Sasaki, R. 1994. N-glycosylation of erythropoietin is critical for apical secretion by Madin-Darby canine kidney cells. *Exp Cell Res* 213:449-457.
143. Martinez-Maza, R., Poyatos, I., Lopez-Corcuera, B., E, N.u., Gimenez, C., Zafra, F., and Aragon, C. 2001. The role of N-glycosylation in transport to the plasma membrane and sorting of the neuronal glycine transporter GLYT2. *J Biol Chem* 276:2168-2173.
144. Zheng, X., Lu, D., and Sadler, J.E. 1999. Apical sorting of bovine enteropeptidase does not involve detergent-resistant association with sphingolipid-cholesterol rafts. *J Biol Chem* 274:1596-1605.
145. Potter, B.A., Ihrke, G., Bruns, J.R., Weixel, K.M., and Weisz, O.A. 2004. Specific N-glycans direct apical delivery of transmembrane, but not soluble or glycosylphosphatidylinositol-anchored forms of endolyn in Madin-Darby canine kidney cells. *Mol Biol Cell* 15:1407-1416.
146. Pang, S., Urquhart, P., and Hooper, N.M. 2004. N-glycans, not the GPI anchor, mediate the apical targeting of a naturally glycosylated, GPI-anchored protein in polarised epithelial cells. *J Cell Sci* 117:5079-5086.
147. Gut, A., Kappeler, F., Hyka, N., Balda, M.S., Hauri, H.P., and Matter, K. 1998. Carbohydrate-mediated Golgi to cell surface transport and apical targeting of membrane proteins. *EMBO J* 17:1919-1929.

148. Fitzgerald, G.A., Catella, F., and Oates, J.A. 1987. Eicosanoid biosynthesis in human cardiovascular disease. *Hum Pathol* 18:248-252.
149. Offermanns, S., Laugwitz, K.L., Spicher, K., and Schultz, G. 1994. G proteins of the G12 family are activated via thromboxane A2 and thrombin receptors in human platelets. *Proc Natl Acad Sci U S A* 91:504-508.
150. Hirata, M., Hayashi, Y., Ushikubi, F., Yokota, Y., Kageyama, R., Nakanishi, S., and Narumiya, S. 1991. Cloning and expression of cDNA for a human thromboxane A2 receptor. *Nature* 349:617-620.
151. Raychowdhury, M.K., Yukawa, M., Collins, L.J., McGrail, S.H., Kent, K.C., and Ware, J.A. 1994. Alternative splicing produces a divergent cytoplasmic tail in the human endothelial thromboxane A2 receptor. *J Biol Chem* 269:19256-19261.
152. Habib, A., FitzGerald, G.A., and Maclouf, J. 1999. Phosphorylation of the thromboxane receptor alpha, the predominant isoform expressed in human platelets. *J Biol Chem* 274:2645-2651.
153. Hirata, T., Ushikubi, F., Kakizuka, A., Okuma, M., and Narumiya, S. 1996. Two thromboxane A2 receptor isoforms in human platelets. Opposite coupling to adenylyl cyclase with different sensitivity to Arg60 to Leu mutation. *J Clin Invest* 97:949-956.
154. Vezza, R., Habib, A., and FitzGerald, G.A. 1999. Differential signaling by the thromboxane receptor isoforms via the novel GTP-binding protein, Gh. *J Biol Chem* 274:12774-12779.
155. Ashton, A.W., and Ware, J.A. 2004. Thromboxane A2 receptor signaling inhibits vascular endothelial growth factor-induced endothelial cell differentiation and migration. *Circ Res* 95:372-379.
156. Baylis, C. 1987. Effects of administered thromboxanes on the intact, normal rat kidney. *Ren Physiol* 10:110-121.
157. Mene, P., and Dunn, M.J. 1986. Contractile effects of TxA2 and endoperoxide analogues on cultured rat glomerular mesangial cells. *Am J Physiol* 251:F1029-1035.
158. Wilcox, C.S., Welch, W.J., and Snellen, H. 1991. Thromboxane mediates renal hemodynamic response to infused angiotensin II. *Kidney Int* 40:1090-1097.
159. Welch, W.J., Wilcox, C.S., and Folger, W.H. 1991. Mechanism of renal vasoconstriction with thromboxane mimetic: engagement of tubuloglomerular feedback. *Adv Prostaglandin Thromboxane Leukot Res* 21B:693-696.
160. Spurney, R.F., Middleton, J.P., Raymond, J.R., and Coffman, T.M. 1994. Modulation of thromboxane receptor activation in rat glomerular mesangial cells. *Am J Physiol* 267:F467-478.
161. Coffman, T.M., Spurney, R.F., Mannon, R.B., and Levenson, R. 1998. Thromboxane A2 modulates the fibrinolytic system in glomerular mesangial cells. *Am J Physiol* 275:F262-269.

162. Remuzzi, G., Imberti, L., Rossini, M., Morelli, C., Carminati, C., Cattaneo, G.M., and Bertani, T. 1985. Increased glomerular thromboxane synthesis as a possible cause of proteinuria in experimental nephrosis. *J Clin Invest* 75:94-101.
163. Nagao, T., Ito, M., Nagamatsu, T., and Suzuki, Y. 1994. Effect of DP-1904, a thromboxane A2 synthetase inhibitor, on crescentic nephritis in rats. *Eur J Pharmacol* 259:233-242.
164. Zoja, C., Benigni, A., Verroust, P., Ronco, P., Bertani, T., and Remuzzi, G. 1987. Indomethacin reduces proteinuria in passive Heymann nephritis in rats. *Kidney Int* 31:1335-1343.
165. Takahashi, K., Schreiner, G.F., Yamashita, K., Christman, B.W., Blair, I., and Badr, K.F. 1990. Predominant functional roles for thromboxane A2 and prostaglandin E2 during late nephrotoxic serum glomerulonephritis in the rat. *J Clin Invest* 85:1974-1982.
166. Masumura, H., Kunitada, S., Irie, K., Ashida, S., and Abe, Y. 1991. A thromboxane A2 synthase inhibitor, DP-1904, prevents rat renal injury. *Eur J Pharmacol* 193:321-327.
167. Boffa, J.J., Just, A., Coffman, T.M., and Arendshorst, W.J. 2004. Thromboxane receptor mediates renal vasoconstriction and contributes to acute renal failure in endotoxemic mice. *J Am Soc Nephrol* 15:2358-2365.
168. Bernard, G.R., Wheeler, A.P., Russell, J.A., Schein, R., Summer, W.R., Steinberg, K.P., Fulkerson, W.J., Wright, P.E., Christman, B.W., Dupont, W.D., et al. 1997. The effects of ibuprofen on the physiology and survival of patients with sepsis. The Ibuprofen in Sepsis Study Group. *N Engl J Med* 336:912-918.
169. Craven, P.A., Melhem, M.F., and DeRubertis, F.R. 1992. Thromboxane in the pathogenesis of glomerular injury in diabetes. *Kidney Int* 42:937-946.
170. Xu, S., Jiang, B., Maitland, K.A., Bayat, H., Gu, J., Nadler, J.L., Corda, S., Lavielle, G., Verbeuren, T.J., Zuccollo, A., et al. 2006. The thromboxane receptor antagonist S18886 attenuates renal oxidant stress and proteinuria in diabetic apolipoprotein E-deficient mice. *Diabetes* 55:110-119.
171. Kelley, V.E., Sneve, S., and Musinski, S. 1986. Increased renal thromboxane production in murine lupus nephritis. *J Clin Invest* 77:252-259.
172. Patrono, C., Ciabattoni, G., Remuzzi, G., Gotti, E., Bombardieri, S., Di Munno, O., Tartarelli, G., Cinotti, G.A., Simonetti, B.M., and Pierucci, A. 1985. Functional significance of renal prostacyclin and thromboxane A2 production in patients with systemic lupus erythematosus. *J Clin Invest* 76:1011-1018.
173. Salvati, P., Lamberti, E., Ferrario, R., Ferrario, R.G., Scampini, G., Pugliese, F., Barsotti, P., and Patrono, C. 1995. Long-term thromboxane-synthase inhibition prolongs survival in murine lupus nephritis. *Kidney Int* 47:1168-1175.

174. Pierucci, A., Simonetti, B.M., Pecci, G., Mavrikakis, G., Feriozzi, S., Cinotti, G.A., Patrignani, P., Ciabattoni, G., and Patrono, C. 1989. Improvement of renal function with selective thromboxane antagonism in lupus nephritis. *N Engl J Med* 320:421-425.
175. Coffman, T.M., Yarger, W.E., and Klotman, P.E. 1985. Functional role of thromboxane production by acutely rejecting renal allografts in rats. *J Clin Invest* 75:1242-1248.
176. Coffman, T.M., Ruiz, P., Sanfilippo, F., and Klotman, P.E. 1989. Chronic thromboxane inhibition preserves function of rejecting rat renal allografts. *Kidney Int* 35:24-30.
177. Ruiz, P., Coffman, T.M., Klotman, P.E., and Sanfilippo, F. 1989. Association of chronic thromboxane inhibition with reduced in situ cytotoxic T cell activity in rejecting rat renal allografts. *Transplantation* 48:660-666.
178. Tonshoff, B., Busch, C., Schweer, H., Scharer, K., and Seyberth, H.W. 1993. In vivo prostanoid formation during acute renal allograft rejection. *Nephrol Dial Transplant* 8:631-636.
179. Mangino, M.J., Brunt, E.M., Von Doersten, P., and Anderson, C.B. 1989. Effects of the thromboxane synthesis inhibitor CGS-12970 on experimental acute renal allograft rejection. *J Pharmacol Exp Ther* 248:23-28.
180. Ramos, E.L., Barri, Y.M., Croker, B.P., Clapp, W.L., Peterson, J.C., and Wilcox, C.S. 1995. Thromboxane synthase expression in renal transplant patients with rejection. *Transplantation* 59:490-494.
181. Obara, Y., Kurose, H., and Nakahata, N. 2005. Thromboxane A2 promotes interleukin-6 biosynthesis mediated by an activation of cyclic AMP-response element-binding protein in 1321N1 human astrocytoma cells. *Mol Pharmacol* 68:670-679.
182. Honma, S., Saika, M., Ohkubo, S., Kurose, H., and Nakahata, N. 2006. Thromboxane A2 receptor-mediated G12/13-dependent glial morphological change. *Eur J Pharmacol* 545:100-108.
183. Blackman, S.C., Dawson, G., Antonakis, K., and Le Breton, G.C. 1998. The identification and characterization of oligodendrocyte thromboxane A2 receptors. *J Biol Chem* 273:475-483.
184. Orr, J.A., Ernst, M., Carrithers, J., and Shirer, H.W. 1990. Cardiopulmonary responses to HCl infusion are mediated by thromboxane A2 but not by serotonin. *Respir Physiol* 80:203-217.
185. Karla, W., Shams, H., Orr, J.A., and Scheid, P. 1992. Effects of the thromboxane A2 mimetic, U46,619, on pulmonary vagal afferents in the cat. *Respir Physiol* 87:383-396.
186. Kenagy, J., VanCleave, J., Pazdernik, L., and Orr, J.A. 1997. Stimulation of group III and IV afferent nerves from the hindlimb by thromboxane A2. *Brain Res* 744:175-178.
187. Martin, C., Uhlig, S., and Ullrich, V. 2001. Cytokine-induced bronchoconstriction in precision-cut lung slices is dependent upon cyclooxygenase-2 and thromboxane receptor activation. *Am J Respir Cell Mol Biol* 24:139-145.

188. Dogne, J.M., de Leval, X., Benoit, P., Delarge, J., and Masereel, B. 2002. Thromboxane A2 inhibition: therapeutic potential in bronchial asthma. *Am J Respir Med* 1:11-17.
189. Tanaka, K., Roberts, M.H., Yamamoto, N., Sugiura, H., Uehara, M., Mao, X.Q., Shirakawa, T., and Hopkin, J.M. 2002. Genetic variants of the receptors for thromboxane A2 and IL-4 in atopic dermatitis. *Biochem Biophys Res Commun* 292:776-780.
190. Nagai, H., Teramachi, H., and Tuchiya, T. 2006. Recent advances in the development of anti-allergic drugs. *Allergol Int* 55:35-42.
191. Shirasaki, H., Kikuchi, M., Seki, N., Kanaizumi, E., Watanabe, K., and Himi, T. 2007. Expression and localization of the thromboxane A2 receptor in human nasal mucosa. *Prostaglandins Leukot Essent Fatty Acids* 76:315-320.
192. Takayama, K., Yuhki, K., Ono, K., Fujino, T., Hara, A., Yamada, T., Kuriyama, S., Karibe, H., Okada, Y., Takahata, O., et al. 2005. Thromboxane A2 and prostaglandin F2alpha mediate inflammatory tachycardia. *Nat Med* 11:562-566.
193. Nie, D., Lamberti, M., Zacharek, A., Li, L., Szekeres, K., Tang, K., Chen, Y., and Honn, K.V. 2000. Thromboxane A(2) regulation of endothelial cell migration, angiogenesis, and tumor metastasis. *Biochem Biophys Res Commun* 267:245-251.
194. Michel, F., Silvestre, J.S., Waeckel, L., Corda, S., Verbeuren, T., Vilaine, J.P., Clergue, M., Duriez, M., and Levy, B.I. 2006. Thromboxane A2/prostaglandin H2 receptor activation mediates angiotensin II-induced postischemic neovascularization. *Arterioscler Thromb Vasc Biol* 26:488-493.
195. Kabashima, K., Murata, T., Tanaka, H., Matsuoka, T., Sakata, D., Yoshida, N., Katagiri, K., Kinashi, T., Tanaka, T., Miyasaka, M., et al. 2003. Thromboxane A2 modulates interaction of dendritic cells and T cells and regulates acquired immunity. *Nat Immunol* 4:694-701.
196. Yamamoto, K., Ebina, S., Nakanishi, H., and Nakahata, N. 1995. Thromboxane A2 receptor-mediated signal transduction in rabbit aortic smooth muscle cells. *Gen Pharmacol* 26:1489-1498.
197. Schultheiss, G., and Diener, M. 1999. Inhibition of spontaneous smooth muscle contractions in rat and rabbit intestine by blockers of the thromboxane A2 pathway. *Zentralbl Veterinarmed A* 46:123-131.
198. Wilhelmsson, L., Wikland, M., and Wiqvist, N. 1981. PGH2, TxA2 and PGI2 have potent and differentiated actions on human uterine contractility. *Prostaglandins* 21:277-286.
199. Palea, S., Toson, G., Pietra, C., Trist, D.G., Artibani, W., Romano, O., and Corsi, M. 1998. Pharmacological characterization of thromboxane and prostanoid receptors in human isolated urinary bladder. *Br J Pharmacol* 124:865-872.
200. Ishizuka, T., Suzuki, K., Kawakami, M., Hidaka, T., Matsuki, Y., and Nakamura, H. 1996. Thromboxane A2 receptor blockade

suppresses intercellular adhesion molecule-1 expression by stimulated vascular endothelial cells. *Eur J Pharmacol* 312:367-377.
201. Bayat, H., Xu, S., Pimentel, D., Cohen, R.A., and Jiang, B. 2008. Activation of thromboxane receptor upregulates interleukin (IL)-1beta-induced VCAM-1 expression through JNK signaling. *Arterioscler Thromb Vasc Biol* 28:127-134.
202. Katugampola, S.D., and Davenport, A.P. 2001. Thromboxane receptor density is increased in human cardiovascular disease with evidence for inhibition at therapeutic concentrations by the AT(1) receptor antagonist losartan. *Br J Pharmacol* 134:1385-1392.
203. Ally, A.I., and Horrobin, D.F. 1980. Thromboxane A2 in blood vessel walls and its physiological significance: relevance to thrombosis and hypertension. *Prostaglandins Med* 4:431-438.
204. Dorn, G.W., 2nd, Liel, N., Trask, J.L., Mais, D.E., Assey, M.E., and Halushka, P.V. 1990. Increased platelet thromboxane A2/prostaglandin H2 receptors in patients with acute myocardial infarction. *Circulation* 81:212-218.
205. de Leval, X., Hanson, J., David, J.L., Masereel, B., Pirotte, B., and Dogne, J.M. 2004. New developments on thromboxane and prostacyclin modulators part II: prostacyclin modulators. *Curr Med Chem* 11:1243-1252.
206. FitzGerald, G.A., Smith, B., Pedersen, A.K., and Brash, A.R. 1984. Increased prostacyclin biosynthesis in patients with severe atherosclerosis and platelet activation. *N Engl J Med* 310:1065-1068.
207. Belton, O., Byrne, D., Kearney, D., Leahy, A., and Fitzgerald, D.J. 2000. Cyclooxygenase-1 and -2-dependent prostacyclin formation in patients with atherosclerosis. *Circulation* 102:840-845.
208. Kobayashi, T., Tahara, Y., Matsumoto, M., Iguchi, M., Sano, H., Murayama, T., Arai, H., Oida, H., Yurugi-Kobayashi, T., Yamashita, J.K., et al. 2004. Roles of thromboxane A(2) and prostacyclin in the development of atherosclerosis in apoE-deficient mice. *J Clin Invest* 114:784-794.
209. Bailey, J.M., and Butler, J. 1973. Anti-inflammatory drugs in experimental atherosclerosis. I. Relative potencies for inhibiting plaque formation. *Atherosclerosis* 17:515-522.
210. Paul, A., Calleja, L., Camps, J., Osada, J., Vilella, E., Ferre, N., Mayayo, E., and Joven, J. 2000. The continuous administration of aspirin attenuates atherosclerosis in apolipoprotein E-deficient mice. *Life Sci* 68:457-465.
211. Pratico, D., Tillmann, C., Zhang, Z.B., Li, H., and FitzGerald, G.A. 2001. Acceleration of atherogenesis by COX-1-dependent prostanoid formation in low density lipoprotein receptor knockout mice. *Proc Natl Acad Sci U S A* 98:3358-3363.
212. Belton, O.A., Duffy, A., Toomey, S., and Fitzgerald, D.J. 2003. Cyclooxygenase isoforms and platelet vessel wall interactions in

the apolipoprotein E knockout mouse model of atherosclerosis. *Circulation* 108:3017-3023.

213. Viles-Gonzalez, J.F., Fuster, V., Corti, R., Valdiviezo, C., Hutter, R., Corda, S., Anand, S.X., and Badimon, J.J. 2005. Atherosclerosis regression and TP receptor inhibition: effect of S18886 on plaque size and composition--a magnetic resonance imaging study. *Eur Heart J* 26:1557-1561.
214. Worth, N.F., Berry, C.L., Thomas, A.C., and Campbell, J.H. 2005. S18886, a selective TP receptor antagonist, inhibits development of atherosclerosis in rabbits. *Atherosclerosis* 183:65-73.
215. Cyrus, T., Yao, Y., Ding, T., Dogne, J.M., and Pratico, D. 2007. A novel thromboxane receptor antagonist and synthase inhibitor, BM-573, reduces development and progression of atherosclerosis in LDL receptor deficient mice. *Eur J Pharmacol* 561:105-111.
216. Cyrus, T., Yao, Y., Ding, T., Dogne, J.M., and Pratico, D. 2007. Thromboxane receptor blockade improves the antiatherogenic effect of thromboxane A2 suppression in LDLR KO mice. *Blood* 109:3291-3296.
217. Cayatte, A.J., Du, Y., Oliver-Krasinski, J., Lavielle, G., Verbeuren, T.J., and Cohen, R.A. 2000. The thromboxane receptor antagonist S18886 but not aspirin inhibits atherogenesis in apo E-deficient mice: evidence that eicosanoids other than thromboxane contribute to atherosclerosis. *Arterioscler Thromb Vasc Biol* 20:1724-1728.
218. Belhassen, L., Pelle, G., Dubois-Rande, J.L., and Adnot, S. 2003. Improved endothelial function by the thromboxane A2 receptor antagonist S 18886 in patients with coronary artery disease treated with aspirin. *J Am Coll Cardiol* 41:1198-1204.
219. Comporti, M., Signorini, C., Arezzini, B., Vecchio, D., Monaco, B., and Gardi, C. 2008. F2-isoprostanes are not just markers of oxidative stress. *Free Radic Biol Med* 44:247-256.
220. Delanty, N., Reilly, M., Pratico, D., FitzGerald, D.J., Lawson, J.A., and FitzGerald, G.A. 1996. 8-Epi PGF2 alpha: specific analysis of an isoeicosanoid as an index of oxidant stress in vivo. *Br J Clin Pharmacol* 42:15-19.
221. Pratico, D., Iuliano, L., Mauriello, A., Spagnoli, L., Lawson, J.A., Rokach, J., Maclouf, J., Violi, F., and FitzGerald, G.A. 1997. Localization of distinct F2-isoprostanes in human atherosclerotic lesions. *J Clin Invest* 100:2028-2034.
222. Tang, M., Cyrus, T., Yao, Y., Vocun, L., and Pratico, D. 2005. Involvement of thromboxane receptor in the proatherogenic effect of isoprostane F2alpha-III: evidence from apolipoprotein E- and LDL receptor-deficient mice. *Circulation* 112:2867-2874.
223. Schneider, A., Harendza, S., Zahner, G., Jocks, T., Wenzel, U., Wolf, G., Thaiss, F., Helmchen, U., and Stahl, R.A. 1999. Cyclooxygenase metabolites mediate glomerular monocyte

chemoattractant protein-1 formation and monocyte recruitment in experimental glomerulonephritis. *Kidney Int* 55:430-441.
224. Abi-Younes, S., Si-Tahar, M., and Luster, A.D. 2001. The CC chemokines MDC and TARC induce platelet activation via CCR4. *Thromb Res* 101:279-289.
225. Hoshino, M., Sim, J., Shimizu, K., Nakayama, H., and Koya, A. 1999. Effect of AA-2414, a thromboxane A2 receptor antagonist, on airway inflammation in subjects with asthma. *J Allergy Clin Immunol* 103:1054-1061.
226. Ishizuka, T., Sawada, S., Sugama, K., and Kurita, A. 2000. Thromboxane A2 (TXA2) receptor blockade suppresses monocyte chemoattractant protein-1 (MCP-1) expression by stimulated vascular endothelial cells. *Clin Exp Immunol* 120:71-78.
227. Ishizuka, T., Matsumura, K., Matsui, T., Takase, B., and Kurita, A. 2003. Ramatroban, a thromboxane A2 receptor antagonist, prevents macrophage accumulation and neointimal formation after balloon arterial injury in cholesterol-fed rabbits. *J Cardiovasc Pharmacol* 41:571-578.
228. Cyrus, T., Sung, S., Zhao, L., Funk, C.D., Tang, S., and Pratico, D. 2002. Effect of low-dose aspirin on vascular inflammation, plaque stability, and atherogenesis in low-density lipoprotein receptor-deficient mice. *Circulation* 106:1282-1287.
229. Ishitsuka, Y., Moriuchi, H., Isohama, Y., Tokunaga, H., Hatamoto, K., Kurita, S., Irikura, M., Iyama, K., and Irie, T. 2009. A selective thromboxane A2 (TXA2) synthase inhibitor, ozagrel, attenuates lung injury and decreases monocyte chemoattractant protein-1 and interleukin-8 mRNA expression in oleic acid-induced lung injury in guinea pigs. *J Pharmacol Sci* 111:211-215.
230. Wallace, A.E., Sales, K.J., Catalano, R.D., Anderson, R.A., Williams, A.R., Wilson, M.R., Schwarze, J., Wang, H., Rossi, A.G., and Jabbour, H.N. 2009. Prostaglandin F2alpha-F-prostanoid receptor signaling promotes neutrophil chemotaxis via chemokine (C-X-C motif) ligand 1 in endometrial adenocarcinoma. *Cancer Res* 69:5726-5733.
231. Sales, K.J., Maldonado-Perez, D., Grant, V., Catalano, R.D., Wilson, M.R., Brown, P., Williams, A.R., Anderson, R.A., Thompson, E.A., and Jabbour, H.N. 2009. Prostaglandin F(2alpha)-F-prostanoid receptor regulates CXCL8 expression in endometrial adenocarcinoma cells via the calcium-calcineurin-NFAT pathway. *Biochim Biophys Acta* 1793:1917-1928.
232. Alexander, R.T., Furuya, W., Szaszi, K., Orlowski, J., and Grinstein, S. 2005. Rho GTPases dictate the mobility of the Na/H exchanger NHE3 in epithelia: role in apical retention and targeting. *Proc Natl Acad Sci U S A* 102:12253-12258.
233. Alexander, R.T., and Grinstein, S. 2009. Tethering, recycling and activation of the epithelial sodium-proton exchanger, NHE3. *J Exp Biol* 212:1630-1637.

234. Lang, F., and Paulmichl, M. 1995. Properties and regulation of ion channels in MDCK cells. *Kidney Int* 48:1200-1205.
235. Takahashi, K., Sawasaki, Y., Hata, J., Mukai, K., and Goto, T. 1990. Spontaneous transformation and immortalization of human endothelial cells. *In Vitro Cell Dev Biol* 26:265-274.
236. Brown, J., Reading, S.J., Jones, S., Fitchett, C.J., Howl, J., Martin, A., Longland, C.L., Michelangeli, F., Dubrova, Y.E., and Brown, C.A. 2000. Critical evaluation of ECV304 as a human endothelial cell model defined by genetic analysis and functional responses: a comparison with the human bladder cancer derived epithelial cell line T24/83. *Lab Invest* 80:37-45.
237. Chapman, G.A., Moores, K.E., Gohil, J., Berkhout, T.A., Patel, L., Green, P., Macphee, C.H., and Stewart, B.R. 2000. The role of fractalkine in the recruitment of monocytes to the endothelium. *Eur J Pharmacol* 392:189-195.
238. Reich, H., Tritchler, D., Herzenberg, A.M., Kassiri, Z., Zhou, X., Gao, W., and Scholey, J.W. 2005. Albumin activates ERK via EGF receptor in human renal epithelial cells. *J Am Soc Nephrol* 16:1266-1278.
239. Robinson, L.A., Tu, L., Steeber, D.A., Preis, O., Platt, J.L., and Tedder, T.F. 1998. The role of adhesion molecules in human leukocyte attachment to porcine vascular endothelium: implications for xenotransplantation. *J Immunol* 161:6931-6938.
240. Fong, A.M., Alam, S.M., Imai, T., Haribabu, B., and Patel, D.D. 2002. CX3CR1 tyrosine sulfation enhances fractalkine-induced cell adhesion. *J Biol Chem* 277:19418-19423.
241. Hayashi, H., Szaszi, K., and Grinstein, S. 2002. Multiple modes of regulation of Na+/H+ exchangers. *Ann N Y Acad Sci* 976:248-258.
242. Bradford, M.M. 1976. A rapid and sensitive method for the quantitation of microgram quantities of protein utilizing the principle of protein-dye binding. *Anal Biochem* 72:248-254.
243. Lippincott-Schwartz, J., Presley, J.F., Zaal, K.J., Hirschberg, K., Miller, C.D., and Ellenberg, J. 1999. Monitoring the dynamics and mobility of membrane proteins tagged with green fluorescent protein. *Methods Cell Biol* 58:261-281.
244. van Kerkhof, P., Sachse, M., Klumperman, J., and Strous, G. 2001. Growth hormone receptor ubiquitination coincides with recruitment to clathrin-coated membrane domains. *J Biol Chem* 276:3778-3784.
245. Simmons, N.L. 1982. Cultured monolayers of MDCK cells: a novel model system for the study of epithelial development and function. *Gen Pharmacol* 13:287-291.
246. Ostedgaard, L.S., Randak, C., Rokhlina, T., Karp, P., Vermeer, D., Ashbourne Excoffon, K.J., and Welsh, M.J. 2003. Effects of C-terminal deletions on cystic fibrosis transmembrane conductance regulator function in cystic fibrosis airway epithelia. *Proc Natl Acad Sci U S A* 100:1937-1942.

247. Matter, K., and Mellman, I. 1994. Mechanisms of cell polarity: sorting and transport in epithelial cells. *Curr Opin Cell Biol* 6:545-554.
248. Naim, H.Y., Joberty, G., Alfalah, M., and Jacob, R. 1999. Temporal association of the N- and O-linked glycosylation events and their implication in the polarized sorting of intestinal brush border sucrase-isomaltase, aminopeptidase N, and dipeptidyl peptidase IV. *J Biol Chem* 274:17961-17967.
249. Lisanti, M.P., Sargiacomo, M., Graeve, L., Saltiel, A.R., and Rodriguez-Boulan, E. 1988. Polarized apical distribution of glycosyl-phosphatidylinositol-anchored proteins in a renal epithelial cell line. *Proc Natl Acad Sci U S A* 85:9557-9561.
250. Ilangumaran, S., Briol, A., and Hoessli, D.C. 1998. CD44 selectively associates with active Src family protein tyrosine kinases Lck and Fyn in glycosphingolipid-rich plasma membrane domains of human peripheral blood lymphocytes. *Blood* 91:3901-3908.
251. Ilangumaran, S., and Hoessli, D.C. 1998. Effects of cholesterol depletion by cyclodextrin on the sphingolipid microdomains of the plasma membrane. *Biochem J* 335 (Pt 2):433-440.
252. Ohtani, Y., Irie, T., Uekama, K., Fukunaga, K., and Pitha, J. 1989. Differential effects of alpha-, beta- and gamma-cyclodextrins on human erythrocytes. *Eur J Biochem* 186:17-22.
253. Klein, U., Gimpl, G., and Fahrenholz, F. 1995. Alteration of the myometrial plasma membrane cholesterol content with beta-cyclodextrin modulates the binding affinity of the oxytocin receptor. *Biochemistry* 34:13784-13793.
254. Yancey, P.G., Rodrigueza, W.V., Kilsdonk, E.P., Stoudt, G.W., Johnson, W.J., Phillips, M.C., and Rothblat, G.H. 1996. Cellular cholesterol efflux mediated by cyclodextrins. Demonstration Of kinetic pools and mechanism of efflux. *J Biol Chem* 271:16026-16034.
255. Keller, P., and Simons, K. 1998. Cholesterol is required for surface transport of influenza virus hemagglutinin. *J Cell Biol* 140:1357-1367.
256. Amundson, D.M., and Zhou, M. 1999. Fluorometric method for the enzymatic determination of cholesterol. *J Biochem Biophys Methods* 38:43-52.
257. Kuan, S.F., Byrd, J.C., Basbaum, C., and Kim, Y.S. 1989. Inhibition of mucin glycosylation by aryl-N-acetyl-alpha-galactosaminides in human colon cancer cells. *J Biol Chem* 264:19271-19277.
258. Tkacz, J.S., and Lampen, O. 1975. Tunicamycin inhibition of polyisoprenyl N-acetylglucosaminyl pyrophosphate formation in calf-liver microsomes. *Biochem Biophys Res Commun* 65:248-257.
259. Marzolo, M.P., Bull, P., and Gonzalez, A. 1997. Apical sorting of hepatitis B surface antigen (HBsAg) is independent of N-

glycosylation and glycosylphosphatidylinositol-anchored protein segregation. *Proc Natl Acad Sci U S A* 94:1834-1839.
260. Green, R.F., Meiss, H.K., and Rodriguez-Boulan, E. 1981. Glycosylation does not determine segregation of viral envelope proteins in the plasma membrane of epithelial cells. *J Cell Biol* 89:230-239.
261. Roth, M.G., Fitzpatrick, J.P., and Compans, R.W. 1979. Polarity of influenza and vesicular stomatitis virus maturation in MDCK cells: lack of a requirement for glycosylation of viral glycoproteins. *Proc Natl Acad Sci U S A* 76:6430-6434.
262. Kenworthy, A.K., Nichols, B.J., Remmert, C.L., Hendrix, G.M., Kumar, M., Zimmerberg, J., and Lippincott-Schwartz, J. 2004. Dynamics of putative raft-associated proteins at the cell surface. *J Cell Biol* 165:735-746.
263. Thebault, S., Alexander, R.T., Tiel Groenestege, W.M., Hoenderop, J.G., and Bindels, R.J. 2009. EGF increases TRPM6 activity and surface expression. *J Am Soc Nephrol* 20:78-85.
264. Oliferenko, S., Paiha, K., Harder, T., Gerke, V., Schwarzler, C., Schwarz, H., Beug, H., Gunthert, U., and Huber, L.A. 1999. Analysis of CD44-containing lipid rafts: Recruitment of annexin II and stabilization by the actin cytoskeleton. *J Cell Biol* 146:843-854.
265. Thomas, D.W., Mannon, R.B., Mannon, P.J., Latour, A., Oliver, J.A., Hoffman, M., Smithies, O., Koller, B.H., and Coffman, T.M. 1998. Coagulation defects and altered hemodynamic responses in mice lacking receptors for thromboxane A2. *J Clin Invest* 102:1994-2001.
266. Thomas, D.W., Rocha, P.N., Nataraj, C., Robinson, L.A., Spurney, R.F., Koller, B.H., and Coffman, T.M. 2003. Proinflammatory actions of thromboxane receptors to enhance cellular immune responses. *J Immunol* 171:6389-6395.
267. Walsh, M.T., Foley, J.F., and Kinsella, B.T. 2000. The alpha, but not the beta, isoform of the human thromboxane A2 receptor is a target for prostacyclin-mediated desensitization. *J Biol Chem* 275:20412-20423.
268. Bishop-Bailey, D., and Hla, T. 1999. Endothelial cell apoptosis induced by the peroxisome proliferator-activated receptor (PPAR) ligand 15-deoxy-Delta12, 14-prostaglandin J2. *J Biol Chem* 274:17042-17048.
269. Kumar, A., Kingdon, E., and Norman, J. 2005. The isoprostane 8-iso-PGF2alpha suppresses monocyte adhesion to human microvascular endothelial cells via two independent mechanisms. *FASEB J* 19:443-445.
270. Miyosawa, K., Sasaki, M., Ohkubo, S., and Nakahata, N. 2006. Different pathways for activation of extracellular signal-regulated kinase through thromboxane A2 receptor isoforms. *Biol Pharm Bull* 29:719-724.

271. Tymkewycz, P.M., Jones, R.L., Wilson, N.H., and Marr, C.G. 1991. Heterogeneity of thromboxane A2 (TP-) receptors: evidence from antagonist but not agonist potency measurements. *Br J Pharmacol* 102:607-614.
272. Yan, W., and Tai, H.H. 2006. Glycogen synthase kinase-3 phosphorylation, T-cell factor signaling activation, and cell morphology change following stimulation of thromboxane receptor alpha. *J Pharmacol Exp Ther* 317:267-274.
273. Gao, Y., Tang, S., Zhou, S., and Ware, J.A. 2001. The thromboxane A2 receptor activates mitogen-activated protein kinase via protein kinase C-dependent Gi coupling and Src-dependent phosphorylation of the epidermal growth factor receptor. *J Pharmacol Exp Ther* 296:426-433.
274. Gallet, C., Blaie, S., Levy-Toledano, S., and Habib, A. 2003. Thromboxane-induced ERK phosphorylation in human aortic smooth muscle cells. *Adv Exp Med Biol* 525:71-73.
275. Kinsella, B.T., O'Mahony, D.J., and FitzGerald, G.A. 1994. Phosphorylation and regulated expression of the human thromboxane A2 receptor. *J Biol Chem* 269:29914-29919.
276. Mayeux, P.R., Morinelli, T.A., Williams, T.C., Hazard, E.S., Mais, D.E., Oatis, J.E., Baron, D.A., and Halushka, P.V. 1991. Differential effect of pH on thromboxane A2/prostaglandin H2 receptor agonist and antagonist binding in human platelets. *J Biol Chem* 266:13752-13758.
277. Gallet, C., Blaie, S., Levy-Toledano, S., and Habib, A. 2003. Epidermal-growth-factor receptor and metalloproteinases mediate thromboxane A2-dependent extracellular-signal-regulated kinase activation. *Biochem J* 371:733-742.
278. Ogletree, M.L., and Allen, G.T. 1992. Interspecies differences in thromboxane receptors: studies with thromboxane receptor antagonists in rat and guinea pig smooth muscles. *J Pharmacol Exp Ther* 260:789-794.
279. Diaz-Rodriguez, E., Montero, J.C., Esparis-Ogando, A., Yuste, L., and Pandiella, A. 2002. Extracellular signal-regulated kinase phosphorylates tumor necrosis factor alpha-converting enzyme at threonine 735: a potential role in regulated shedding. *Mol Biol Cell* 13:2031-2044.
280. Fan, H., Turck, C.W., and Derynck, R. 2003. Characterization of growth factor-induced serine phosphorylation of tumor necrosis factor-alpha converting enzyme and of an alternatively translated polypeptide. *J Biol Chem* 278:18617-18627.
281. Soond, S.M., Everson, B., Riches, D.W., and Murphy, G. 2005. ERK-mediated phosphorylation of Thr735 in TNFalpha-converting enzyme and its potential role in TACE protein trafficking. *J Cell Sci* 118:2371-2380.

282. Huang, J.S., Ramamurthy, S.K., Lin, X., and Le Breton, G.C. 2004. Cell signalling through thromboxane A2 receptors. *Cell Signal* 16:521-533.
283. Kobayashi, H., Honma, S., Nakahata, N., and Ohizumi, Y. 2000. Involvement of phosphatidylcholine-specific phospholipase C in thromboxane A2-induced activation of mitogen-activated protein kinase in astrocytoma cells. *J Neurochem* 74:2167-2173.
284. Crews, C.M., Alessandrini, A., and Erikson, R.L. 1992. The primary structure of MEK, a protein kinase that phosphorylates the ERK gene product. *Science* 258:478-480.
285. Liu, W.H., and Chang, L.S. 2010. Suppression of ADAM17-mediated Lyn/Akt pathways induces apoptosis of human leukemia U937 cells: Bungarus multicinctus protease inhibitor-like protein-1 uncovers the cytotoxic mechanism. *J Biol Chem* 285:30506-30515.
286. Hoy, B., Lower, M., Weydig, C., Carra, G., Tegtmeyer, N., Geppert, T., Schroder, P., Sewald, N., Backert, S., Schneider, G., et al. 2010. Helicobacter pylori HtrA is a new secreted virulence factor that cleaves E-cadherin to disrupt intercellular adhesion. *EMBO Rep* 11:798-804.
287. Cockwell, P., Calderwood, J.W., Brooks, C.J., Chakravorty, S.J., and Savage, C.O. 2002. Chemoattraction of T cells expressing CCR5, CXCR3 and CX3CR1 by proximal tubular epithelial cell chemokines. *Nephrol Dial Transplant* 17:734-744.
288. Isse, K., Harada, K., Zen, Y., Kamihira, T., Shimoda, S., Harada, M., and Nakanuma, Y. 2005. Fractalkine and CX3CR1 are involved in the recruitment of intraepithelial lymphocytes of intrahepatic bile ducts. *Hepatology* 41:506-516.
289. Niess, J.H., Brand, S., Gu, X., Landsman, L., Jung, S., McCormick, B.A., Vyas, J.M., Boes, M., Ploegh, H.L., Fox, J.G., et al. 2005. CX3CR1-mediated dendritic cell access to the intestinal lumen and bacterial clearance. *Science* 307:254-258.
290. Muehlhoefer, A., Saubermann, L.J., Gu, X., Luedtke-Heckenkamp, K., Xavier, R., Blumberg, R.S., Podolsky, D.K., MacDermott, R.P., and Reinecker, H.C. 2000. Fractalkine is an epithelial and endothelial cell-derived chemoattractant for intraepithelial lymphocytes in the small intestinal mucosa. *J Immunol* 164:3368-3376.
291. Efsen, E., Grappone, C., DeFranco, R.M., Milani, S., Romanelli, R.G., Bonacchi, A., Caligiuri, A., Failli, P., Annunziato, F., Pagliai, G., et al. 2002. Up-regulated expression of fractalkine and its receptor CX3CR1 during liver injury in humans. *J Hepatol* 37:39-47.
292. Matter, K., Yamamoto, E.M., and Mellman, I. 1994. Structural requirements and sequence motifs for polarized sorting and endocytosis of LDL and Fc receptors in MDCK cells. *J Cell Biol* 126:991-1004.

293. Powell, S.K., Lisanti, M.P., and Rodriguez-Boulan, E.J. 1991. Thy-1 expresses two signals for apical localization in epithelial cells. *Am J Physiol* 260:C715-720.
294. Rajendran, L., and Simons, K. 2005. Lipid rafts and membrane dynamics. *J Cell Sci* 118:1099-1102.
295. Touret, N., Martin-Orozco, N., Paroutis, P., Furuya, W., Lam-Yuk-Tseung, S., Forbes, J., Gros, P., and Grinstein, S. 2004. Molecular and cellular mechanisms underlying iron transport deficiency in microcytic anemia. *Blood* 104:1526-1533.
296. Bonen, D.K., Nassir, F., Hausman, A.M., and Davidson, N.O. 1998. Inhibition of N-linked glycosylation results in retention of intracellular apo[a] in hepatoma cells, although nonglycosylated and immature forms of apolipoprotein[a] are competent to associate with apolipoprotein B-100 in vitro. *J Lipid Res* 39:1629-1640.
297. Savage, K.E., and Baur, P.S. 1983. Effect of tunicamycin, an inhibitor of protein glycosylation, on division of tumour cells in vitro. *J Cell Sci* 64:295-306.
298. Kerfoot, S.M., Lord, S.E., Bell, R.B., Gill, V., Robbins, S.M., and Kubes, P. 2003. Human fractalkine mediates leukocyte adhesion but not capture under physiological shear conditions; a mechanism for selective monocyte recruitment. *Eur J Immunol* 33:729-739.
299. Constantin, G., Majeed, M., Giagulli, C., Piccio, L., Kim, J.Y., Butcher, E.C., and Laudanna, C. 2000. Chemokines trigger immediate beta2 integrin affinity and mobility changes: differential regulation and roles in lymphocyte arrest under flow. *Immunity* 13:759-769.
300. Brough, D., Bhatti, F., and Irvine, R.F. 2005. Mobility of proteins associated with the plasma membrane by interaction with inositol lipids. *J Cell Sci* 118:3019-3025.
301. Tole, S., Durkan, A.M., Huang, Y.W., Liu, G.Y., Leung, A., Jones, L.L., Taylor, J.A., and Robinson, L.A. 2010. Thromboxane prostanoid receptor stimulation induces shedding of the transmembrane chemokine CX3CL1 yet enhances CX3CL1-dependent leukocyte adhesion. *Am J Physiol Cell Physiol* 298:C1469-1480.
302. Yonemura, S., Hirao, M., Doi, Y., Takahashi, N., Kondo, T., Tsukita, S., and Tsukita, S. 1998. Ezrin/radixin/moesin (ERM) proteins bind to a positively charged amino acid cluster in the juxta-membrane cytoplasmic domain of CD44, CD43, and ICAM-2. *J Cell Biol* 140:885-895.
303. Barreiro, O., Yanez-Mo, M., Serrador, J.M., Montoya, M.C., Vicente-Manzanares, M., Tejedor, R., Furthmayr, H., and Sanchez-Madrid, F. 2002. Dynamic interaction of VCAM-1 and ICAM-1 with moesin and ezrin in a novel endothelial docking structure for adherent leukocytes. *J Cell Biol* 157:1233-1245.

304. Carpen, O., Pallai, P., Staunton, D.E., and Springer, T.A. 1992. Association of intercellular adhesion molecule-1 (ICAM-1) with actin-containing cytoskeleton and alpha-actinin. *J Cell Biol* 118:1223-1234.
305. Suzuki, K., Ritchie, K., Kajikawa, E., Fujiwara, T., and Kusumi, A. 2005. Rapid hop diffusion of a G-protein-coupled receptor in the plasma membrane as revealed by single-molecule techniques. *Biophys J* 88:3659-3680.
306. Neame, S.J., Uff, C.R., Sheikh, H., Wheatley, S.C., and Isacke, C.M. 1995. CD44 exhibits a cell type dependent interaction with triton X-100 insoluble, lipid rich, plasma membrane domains. *J Cell Sci* 108 (Pt 9):3127-3135.
307. Hermand, P., Pincet, F., Carvalho, S., Ansanay, H., Trinquet, E., Daoudi, M., Combadiere, C., and Deterre, P. 2008. Functional adhesiveness of the CX3CL1 chemokine requires its aggregation. Role of the transmembrane domain. *J Biol Chem* 283:30225-30234.
308. Soos, T.J., Sims, T.N., Barisoni, L., Lin, K., Littman, D.R., Dustin, M.L., and Nelson, P.J. 2006. CX3CR1+ interstitial dendritic cells form a contiguous network throughout the entire kidney. *Kidney Int* 70:591-596.
309. Bisset, L.R., and Schmid-Grendelmeier, P. 2005. Chemokines and their receptors in the pathogenesis of allergic asthma: progress and perspective. *Curr Opin Pulm Med* 11:35-42.
310. Xie, Y., Nishi, S., Fukase, S., Nakamura, H., Chen, X., Imai, N., Sakatsume, M., Saito, A., Ueno, M., Narita, I., et al. 2004. Different type and localization of CD44 on surface membrane of regenerative renal tubular epithelial cells in vivo. *Am J Nephrol* 24:188-197.
311. Asselman, M., Verhulst, A., Van Ballegooijen, E.S., Bangma, C.H., Verkoelen, C.F., and De Broe, M.E. 2005. Hyaluronan is apically secreted and expressed by proliferating or regenerating renal tubular cells. *Kidney Int* 68:71-83.
312. Ishizuka, T., Kawakami, M., Hidaka, T., Matsuki, Y., Takamizawa, M., Suzuki, K., Kurita, A., and Nakamura, H. 1998. Stimulation with thromboxane A2 (TXA2) receptor agonist enhances ICAM-1, VCAM-1 or ELAM-1 expression by human vascular endothelial cells. *Clin Exp Immunol* 112:464-470.
313. Mitsuhashi, M., Tanaka, A., Fujisawa, C., Kawamoto, K., Itakura, A., Takaku, M., Hironaka, T., Sawada, S., and Matsuda, H. 2001. Necessity of thromboxane A2 for initiation of platelet-mediated contact sensitivity: dual activation of platelets and vascular endothelial cells. *J Immunol* 166:617-623.
314. Solomon, K.A., Pesti, N., Wu, G., and Newton, R.C. 1999. Cutting edge: a dominant negative form of TNF-alpha converting enzyme inhibits proTNF and TNFRII secretion. *J Immunol* 163:4105-4108.

315. Gschwind, A., Hart, S., Fischer, O.M., and Ullrich, A. 2003. TACE cleavage of proamphiregulin regulates GPCR-induced proliferation and motility of cancer cells. *EMBO J* 22:2411-2421.
316. Citro, S., Ravasi, S., Rovati, G.E., and Capra, V. 2005. Thromboxane prostanoid receptor signals through Gi protein to rapidly activate extracellular signal-regulated kinase in human airways. *Am J Respir Cell Mol Biol* 32:326-333.
317. Miggin, S.M., and Kinsella, B.T. 2002. Regulation of extracellular signal-regulated kinase cascades by alpha- and beta-isoforms of the human thromboxane A(2) receptor. *Mol Pharmacol* 61:817-831.
318. Wei, J., Yan, W., Li, X., Chang, W.C., and Tai, H.H. 2007. Activation of thromboxane receptor alpha induces expression of cyclooxygenase-2 through multiple signaling pathways in A549 human lung adenocarcinoma cells. *Biochem Pharmacol* 74:787-800.
319. Yan, W., Ding, Y., and Tai, H.H. 2006. 14-3-3zeta interacts with human thromboxane receptors and is involved in the agonist-induced activation of the extracellular-signal-regulated kinase. *Biochem Pharmacol* 71:624-633.
320. Ishizuka, T., Suzuki, K., Kawakami, M., Kawaguchi, Y., Hidaka, T., Matsuki, Y., and Nakamura, H. 1994. DP-1904, a specific inhibitor of thromboxane A2 synthesizing enzyme, suppresses ICAM-1 expression by stimulated vascular endothelial cells. *Eur J Pharmacol* 262:113-123.
321. Lidington, E.A., Moyes, D.L., McCormack, A.M., and Rose, M.L. 1999. A comparison of primary endothelial cells and endothelial cell lines for studies of immune interactions. *Transpl Immunol* 7:239-246.
322. Burbach, B.J., Medeiros, R.B., Mueller, K.L., and Shimizu, Y. 2007. T-cell receptor signaling to integrins. *Immunol Rev* 218:65-81.

Appendix 1. Permissions to reprint

Copyright Clearance Center

1 PAYMENT 2 REVIEW 3 CONFIRMATION

Step 3: Order Confirmation

Thank you for your order! A confirmation for your order will be sent to your account email address. If you have questions about your order, you can call us at 978-646-2600, M-F between 8:00 AM and 6:00 PM (Eastern), or write to us at info@copyright.com.

Confirmation Number: 2204216
Order Date: 08/24/2009

If you pay by credit card, your order will be finalized and your card will be charged within 24 hours. If you pay by invoice, you can change or cancel your order until the invoice is generated.

Payment Information

Anne Durkan
amdurkan@yahoo.co.uk
+61 (2)80214622
Payment Method: CC ending in 1058

Order Details

JOURNAL OF THE AMERICAN SOCIETY OF NEPHROLOGY
Order detail ID: 30980632

Permission Status: Granted

ISBN/ISSN: 1046-6673
Publication year: 2007
Publisher: AMERICAN SOCIETY OF NEPHROLOGY
Rightsholder: American Society of Nephrology
Author/Editor: Durkan AM, Alexander RT, Liu G-Y, Rui M, Femia G, Robinson LA.

Permission type: Republish into a book, journal, newsletter...
Requested use: Dissertation
Republication title: THE EXPRESSION OF CX3CL1 (FRACTALKINE) IN RENAL TUBULAR EPITHELIAL CELLS AND THE REGULATION OF CX3CL1 BY STIMULATION OF THE THROMBOXANE PROSTANOID RECEPTOR
Republishing organization: UNIVERSITY OF EDINBURGH
Organization status: Non-profit 501(c)(3)
Republication date: 09/30/2009
Circulation/Distribution: 2
Type of content: Full article/chapter
Description of requested content: The expression and targeting of cx3cl1 (fractalkine) in renal tubular epithelial cells
Page range(s): 74-83
Translating to: No Translation
Requested content's publication date: 01/01/2007
Your reference: ANNE'S THESIS, CHAPTER 7

$ 3.00

Order Total: $ 3.00

About Us | Contact Us | Careers | Privacy Policy | Terms & Conditions
Site Index | Copyright Labs

Copyright Clearance Center

I hereby give my permission for Anne Durkan to include in her thesis the paper titled "The Expression and Targeting of CX3CL1 (Fractalkine) in Renal Tubular Epithelial Cells", which was published in the Journal of the American Society of Nephrology in January 2007.

Ming Pei — Aug 24. 2009

Print name — Date

Signature

I hereby give my permission for Anne Durkan to include in her thesis the paper titled "The Expression and Targeting of CX3CL1 (Fractalkine) in Renal Tubular Epithelial Cells", which was published in the Journal of the American Society of Nephrology in January 2007.

Guang-Ying Liu	September 14, 2009
Print name	Date

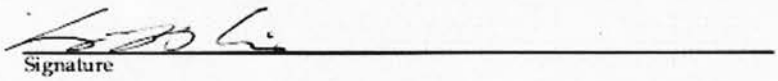

Signature

I hereby give my permission for Anne Durkan to include in her thesis the paper titled "The Expression and Targeting of CXCL1 (Fractalkine) in Renal Tubular Epithelial Cells", which was published in the Journal of the American Society of Nephrology in January 2007.

Giuseppe Remuzzi 01/09/09

Print name Date

Signature

I hereby give my permission for Anne Durkan to include in her thesis the paper titled "The Expression and Targeting of CX3CL1 (Fractalkine) in Renal Tubular Epithelial Cells", which was published in the Journal of the American Society of Nephrology in January 2007.

R TODD ALEXANDER — AUGUST 25TH, 2009

Print name — Date

Signature

I hereby give my permission for Anne Durkan to include in her thesis the paper titled "The Expression and Targeting of CX3CL1 (Fractalkine) in Renal Tubular Epithelial Cells", which was published in the Journal of the American Society of Nephrology in January 2007.

Dr. Lisa Robinson — August 24, 2009

Print name — Date

Signature

Appendix 2. Published papers

Expression and Targeting of CX_3CL1 (Fractalkine) in Renal Tubular Epithelial Cells

Anne M. Durkan,*† R. Todd Alexander,*† Guang-Ying Liu,† Min Rui,† Giuseppe Femia,† and Lisa A. Robinson*†

*Division of Nephrology and †Research Institute, Hospital for Sick Children, Toronto, Ontario, Canada

The chemokine CX_3CL1 plays a key role in glomerulonephritis and can act as both chemoattractant and adhesion molecule. CX_3CL1 also is upregulated in tubulointerstitial injury, but little is known about the subcellular distribution and function of CX_3CL1 in renal tubular epithelial cells (RTEC). Unexpectedly, it was found that CX_3CL1 is expressed predominantly on the apical surface of tubular epithelium in human renal transplant biopsy specimens with acute rejection or acute tubular necrosis. For studying the targeting of CX_3CL1 in polarized RTEC, MDCK cells that expressed untagged or green fluorescent protein–tagged CX_3CL1 were generated. The chemokine was present on the apical membrane and in subapical vesicles. Apical targeting of CX_3CL1 was not due to signals that were conferred by its intracellular domain, to associations with lipid rafts, or to O-glycosylation but, rather, depended on N-linked glycosylation of the protein. With the use of fluorescence recovery after photobleaching, it was found that CX_3CL1 is immobile in the apical membrane. However, CX_3CL1 partitioned with the triton-soluble rather than -insoluble cellular fraction, indicating that it is not associated directly with the actin cytoskeleton or with lipid rafts. Accordingly, disruption of rafts through cholesterol depletion did not render CX_3CL1 mobile. For exploration of potential functions of apical CX_3CL1, binding of CX_3CR1-expressing leukocytes to polarized RTEC was examined. Leukocyte adhesion to the luminal surface was enhanced significantly when CX_3CL1 was present. These data demonstrate that CX_3CL1 is expressed preferentially on the apical membrane of RTEC and suggest a novel function for the chemokine in recruitment and retention of leukocytes in tubulointerstitial inflammation.

J Am Soc Nephrol 18: 74–83, 2007. doi: 10.1681/ASN.2006080862

Renal tubulointerstitial inflammation is characterized by recruitment of circulating leukocytes to the site of injury. Traffic signals for leukocyte migration are provided by chemokines, a family of small molecular weight proteins (1). Among the chemokines, CX_3CL1 (fractalkine) has a unique role in the inflammatory cascade because of its structure: an extracellular chemokine domain and mucin stalk, tethered to a transmembrane region and a 37–amino acid cytoplasmic tail. Transmembrane CX_3CL1 is cleaved proximal to the membrane by metalloproteinases of the A disintegrin and metalloproteinase (ADAM) family to release a soluble species (2–5). Soluble CX_3CL1 acts as a chemoattractant, whereas the transmembrane protein acts as a cell adhesion molecule for monocytes, natural killer (NK) cells, and subsets of $CD8^+$ T cells, all of which express CX_3CR1, the receptor for CX_3CL1. In this way, CX_3CL1 and CX_3CR1 promote leukocyte infiltration at sites of injury (2,6,7). *In vivo*, CX_3CL1 is strongly implicated in inflammation, including allograft rejection and, most notably, atherogenesis (8–13).

Numerous organs express CX_3CL1, including brain, lung, heart, intestine, and kidney (10,14–17). In humans and rodents, CX_3CL1 expression is prominent in renal glomerular disease, particularly in endothelial and mesangial cells (18–20). The role of CX_3CL1 in mediating glomerular injury is well described in animal models of systemic lupus erythematosus nephritis, mesangioproliferative glomerulonephritis, and crescentic glomerulonephritis (21–23). In these disease processes, blockade of either CX_3CL1 or CX_3CR1 prevents renal injury and leukocyte infiltration (21–23). Little is known, however, regarding the role of CX_3CL1 in tubulointerstitial renal disease. Expression of CX_3CL1 clearly is enhanced in tubulointerstitial injury, including that associated with tubular protein overload and acute allograft rejection (19,24,25). However, knowledge regarding the subcellular distribution and function of CX_3CL1 in renal tubular epithelial cells (RTEC) is rudimentary.

We demonstrate here that CX_3CL1 is present on the apical membrane of RTEC, where it is anchored firmly. We further demonstrate that CX_3CL1 is targeted to the apical membrane *via* N-glycosylation of the chemokine. The implications of apical targeting of CX_3CL1 for the pathogenesis of tubulointerstitial inflammation are discussed.

Materials and Methods

Cells and Constructs

HK-2 cells were a gift from Dr. Andras Kapus, (University of Toronto, Toronto, ON, Canada). MDCK cells were from American Type Culture Collection (Manassas, VA). MDCK cells that stably expressed sodium-hydrogen exchanger 3 (NHE3) tagged with hemagglutinin (HA) were provided by Dr. Sergio Grinstein (University of Toronto).

Received August 15, 2006. Accepted October 19, 2006.

Published online ahead of print. Publication date available at www.jasn.org.

Address correspondence to: Dr. Lisa A. Robinson, Division of Nephrology, Hospital for Sick Children, 555 University Avenue, Toronto, ON, Canada. Phone: 416-813-7654 ext. 1745; Fax: 416-813-6271; E-mail: lisa.robinson@sickkids.ca

ISSN: 1046-6673/1801-0074

The preceding cells were cultured in DMEM and Ham's F12 (Wisent, St-Bruno, Quebec, Canada) that contained 5% FCS. K562 erythroleukemia cells and K562 cells that stably expressed CX_3CR1 (K562-CX_3CR1) were from Dr. Dhavalkumar Patel (University of North Carolina, Chapel Hill, NC) and were cultured in RPMI supplemented with HEPES and 15% FCS. Primary human RTEC (Clonetics, Cambrex, Walkersville, MD) were a gift from Dr. Jim Scholey (University of Toronto) and were cultured according to the manufacturer's instructions (26). CX_3CL1 expression in these cells was verified by Western blotting (27). Human peripheral blood mononuclear cells (PBMC) were isolated from heparinized peripheral blood from healthy volunteers (28).

DNA constructs for CX_3CL1 or CX_3CL1 tagged with green fluorescent protein (CX_3CL1-GFP) were created as described previously (6,27,29). MDCK cells were stably transfected with these constructs using FuGENE (Roche, Indianapolis, IN) and selected in 500 μg/ml G418 (Wisent).

The predicted transmembrane portion of CX_3CL1 ends at amino acid 360 (PSORT II). A mutant construct that lacked amino acids 361 to 397, CX_3CL1–360, was generated by PCR using the common upstream primer 5′-GTGGAATTCTGCAGTCGACTC-3′ and the downstream primer 5′-GCGGCCGCTCACATGGCCACCCCCAGGCAG-3′. In the downstream primer, stop codons and NotI sites were introduced. PCR products were cloned into TOPO vector (Invitrogen, Burlington, ON, Canada) and sequenced. Inserts were released by cutting with NotI and EcoRI and subcloned into HA-pcDNA3.1 (Invitrogen). MDCK cells were transfected using FuGENE and selected in 500 μg/ml G418 (MDCK-CX_3CL1–360). DNA constructs that encoded GFP-tagged glycosyl phosphatidylinositol (GPI-GFP) and FcRIIa receptor (FcR-GFP) were a gift from Dr. S. Grinstein (University of Toronto) (30,31).

Antibodies and Reagents

The following antibodies were used: Goat anti-human CX_3CL1 directed against the extracellular chemokine region (R&D Systems, Minneapolis, MN) (19,32), goat anti-human CX_3CL1 against the intracellular carboxy terminus (Santa Cruz Biotechnology, Santa Cruz, CA), anti-actin (Sressgen, Victoria, BC, Canada), and anti-HA (Covance, Berkeley, CA). Cy3- and horseradish peroxidase–conjugated anti-goat IgG, anti-mouse IgG, and 18 nm gold-labeled anti-goat IgG were from Jackson Immunoresearch Laboratories (Bar Harbor, ME). Tunicamycin, benzyl-2-acetamido-2-deoxy-α-D-galacto-pyranoside, and methyl-β-cyclodextrin (MβCD) were from Sigma-Aldrich (St. Louis, MO). Amplex Red kit was used to measure cholesterol levels (Molecular Probes, Eugene, OR). Cholera toxin B conjugated to Alexa fluor 555 was from Molecular Probes. The metalloprotease inhibitors TAPI-2 and GM6001 were from Peptides International (Louisville, KY) and Chemicon International (Temecula, CA), respectively. TNF-α was from R&D Systems.

Immunohistochemistry

Renal transplant biopsy specimens were obtained in accordance with the guidelines of the Research Ethics Board of University Health Network (University of Toronto). Frozen 7-μM sections were air-dried and fixed in acetone. After blocking with 5% donkey serum, sections were incubated with anti-CX_3CL1 antibody (Ab), followed by Cy3-conjugated anti-goat IgG.

Immunofluorescence staining of cultured cells was performed as described previously (33). For detection of surface CX_3CL1, cells were fixed and labeled with anti-CX_3CL1 Ab and Cy3-conjugated secondary Ab. For detection of surface and intracellular CX_3CL1, the same cells were permeabilized with 0.1% Triton X-100 and incubated again with anti-CX_3CL1 Ab and Cy5-conjugated secondary Ab. In some experiments, Alexa 488–conjugated phalloidin was added with the secondary Ab to label F-actin. Cells were visualized using either an LSM 510 confocal microscope (Zeiss, Toronto, ON, Canada) or a spinning disk DMIRE2 confocal microscope (Leica Microsystems, Toronto, ON, Canada), equipped with an Hamamatsu backthinned EM-CCD camera. Images were acquired using 100× oil immersion and the appropriate filters. Z stacks were constructed and images deconvolved using Velocity software (Improvision, Lexington, MA).

PCR

RNA was isolated from HK-2 cells using Trizol (Life Technologies, Burlington, ON, Canada), and reverse transcriptase–PCR for CX_3CL1 was performed using oligo(dT) and specific primers (24). PCR products were size-fractionated on 1% agarose in TBE gels and stained with ethidium bromide.

Immunoblotting

SDS-PAGE and immunoblotting were performed using anti-CX_3CL1 Ab (0.2 μg/ml) (27,34). Immunoreactive bands were visualized by enhanced chemiluminescence (Amersham Biosciences UK Limited, Buckinghamshire, UK) recorded on x-ray film. Detergent resistance was assessed as described previously (34). Triton-soluble and -insoluble components were compared with total cell lysate.

Electron Microscopy

Scanning electron microscopy (EM) was performed as described previously using anti-CX_3CL1 Ab (1 μg/ml) and 18 nm of gold-labeled anti-goat IgG secondary antibody (34).

Fluorescence Recovery after Photobleaching

Experiments were performed as described previously (34,35). Briefly, the apical surface was brought into focus on a confocal microscope, and two 2.5-μm diameter areas of similar fluorescence intensity were selected per cell. After acquisition of baseline measurements, one defined area was photobleached irreversibly, and fluorescence of both areas was measured over time. Fractional fluorescence recovery of the bleached area was determined relative to prebleach measurements. The unbleached area was used to control for inadvertent bleaching during repeated image acquisition. Results are expressed as the mean fluorescence recovery for at least six experiments, with SEM.

Adhesion Assays

Experiments were performed as described elsewhere with minor modifications (10). Briefly, MDCK-CX_3CL1-GFP cells were grown to confluence on 25-mm coverslips and pretreated with 10 μM TAPI-2 for 2 h to maximize cell surface expression of CX_3CL1. K562-CX_3CR1 cells were labeled with cholera toxin B-555, and 1×10^6 cells were added to wells of either MDCK or MDCK-CX_3CL1-GFP cells with gentle rocking at 10 cycles/min. Nonadherent cells were washed away, and remaining cells were fixed and mounted onto slides. Using a Leica deconvolution microscope, we examined at least 50 high-power fields (×63) to count the number of adhered cells. Results are the mean of three separate experiments with SEM and were compared using paired t test. Cells also were examined using a spinning disk confocal microscope.

Results

CX_3CL1 Is Expressed in RTEC

To define the functions of CX_3CL1 in RTEC, we first examined CX_3CL1 expression in five human renal allograft biopsy specimens. Three specimens had histologic diagnosis of acute

rejection and two of acute tubular necrosis. In all five specimens, we detected CX_3CL1 expression in renal tubules, particularly on the apical surface (Figure 1, A and B). In addition to being expressed on tubular epithelium, modest CX_3CL1 expression was noted within the glomeruli and on vascular endothelium (data not shown). This is in keeping with a previously published report (19). To verify the specificity of staining, we omitted primary anti-CX_3CL1 Ab from some experiments. When the secondary Ab alone was used, very little background immunofluorescence was observed (data not shown). At our institution, donor preimplantation renal transplant biopsies are not performed routinely and therefore could not be used as an additional negative control. However, using the same anti-CX_3CL1 Ab as the one used in our study, other investigators previously reported minimal immunohistochemical expression of CX_3CL1 in normal renal biopsy tissue (19,32). We then examined expression and subcellular distribution of CX_3CL1 in HK-2 cells, a human RTEC line. Using reverse transcriptase–PCR, we detected CX_3CL1 mRNA (Figure 1C). To verify CX_3CL1 protein expression, we performed immunofluorescence staining and again found the chemokine predominantly at the apical surface (Figure 1D).

CX_3CL1 Is Expressed in the Apical Membrane of RTEC

Because HK-2 cells, unlike other tubular epithelial lines, grow in flattened monolayers, we adopted another approach,

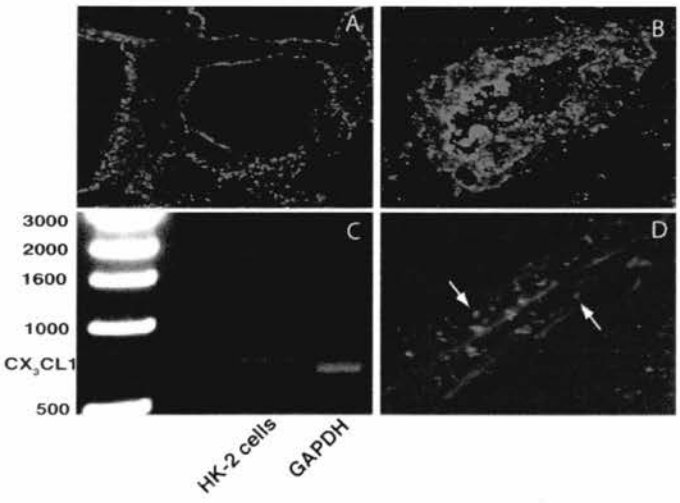

Figure 1. CX_3CL1 is expressed in human renal tubular epithelial cells (RTEC). Immunofluorescent labeling of CX_3CL1 in human renal allograft biopsy specimens, with histologic diagnoses of acute tubular rejection (A) and acute tubular necrosis (B). Samples were labeled with anti-CX_3CL1 antibody (Ab) and Cy3-conjugated secondary Ab. (C) Total RNA was isolated from HK-2 cells, and CX_3CL1 was amplified by reverse transcriptase–PCR using specific published primers. The PCR products were size-fractionated on 1% agarose. Glyceraldehyde-3-phosphate dehydrogenase (GAPDH) is shown as a control. (D) Immunofluorescence staining of HK-2 cells using anti-CX_3CL1 Ab and a Cy2-conjugated secondary Ab. Actin was labeled with rhodamine-conjugated phalloidin. Arrows demonstrate CX_3CL1 labeling on the apical surface of cells.

stably expressing full-length CX_3CL1 or CX_3CL1-GFP in MDCK cells, a renal cell line with cuboidal morphology that is typical of epithelial cells, facilitating distinction between apical and basolateral surfaces. Using Western analysis and anti-CX_3CL1 Ab, MDCK-CX_3CL1 and MDCK-CX_3CL1-GFP cells each displayed a single band of appropriate molecular weight (Figure 2A). For assessment of the subcellular localization of CX_3CL1, MDCK-CX_3CL1-GFP cells (Figure 2B) were fixed and incubated with anti-CX_3CL1 Ab, which labeled only the apical surface (Figure 2C). For visualization of intracellular CX_3CL1, the same cells then were permeabilized and incubated with anti-CX_3CL1 Ab followed by a different secondary Ab. This confirmed an intracellular pool of CX_3CL1 in subapical vesicles (Figure 2D). To confirm that any labeling of MDCK-CX_3CL1-GFP cells with anti-CX_3CL1 Ab was specific for CX_3CL1, we incubated untransfected MDCK cells with the same Ab. In this instance, no immunofluorescence staining was observed (data not shown). To control further for any background staining of Cy3- or Cy5-conjugated secondary Ab used, we also performed experiments in which the primary Ab was omitted. Once again, incubation with secondary Ab alone yielded no immunofluorescence labeling (data not shown). Collectively, these results demonstrate that CX_3CL1 is expressed on the apical plasma membrane as well as within subapical vesicles.

In MDCK-CX_3CL1-GFP cells, GFP is attached to the cytoplasmic tail of the chemokine. Because the tagged construct was recognized by the Ab directed against the extracellular domain of CX_3CL1, the protein expressed must traverse the apical membrane (Figure 2, B and E). We also noted a second pool of GFP, present in the basolateral membrane (Figure 2B). After permeabilization, the basolateral pool of GFP could be labeled by an anti-CX_3CL1 Ab directed against the intracellular domain of the chemokine (data not shown). We believe that basolateral GFP represents the intracellular portion of CX_3CL1 that remains after the extracellular segment has been proteolytically released. Accordingly, Western analysis of MDCK-CX_3CL1-GFP cells using anti-GFP Ab consistently revealed two separate bands. The molecular masses of these bands correlated with full-length CX_3CL1-GFP fusion protein (Figure 2A) or a fusion protein corresponding to the intracellular region of CX_3CL1 together with GFP (35 kD; data not shown). To ensure that the GFP tag did not alter subcellular traffic of CX_3CL1, we examined MDCK cells that expressed the untagged chemokine and found a similar distribution (Figure 2F).

We used scanning EM to confirm that CX_3CL1 is expressed on the apical membrane of RTEC. As shown in Figure 2G, CX_3CL1 is associated with microvilli on the apical surface.

CX_3CL1 Is Targeted to the Apical Membrane by N-Glycosylation

We next investigated the signals that target CX_3CL1 to the apical membrane. Apical sorting of transmembrane proteins can be determined by signals that are conferred by the cytoplasmic tail of the protein (36,37), by O- or N-glycosylation (38), or by membrane anchoring of the protein through GPI or directly to lipid rafts (39). We examined each of these potential mechanisms.

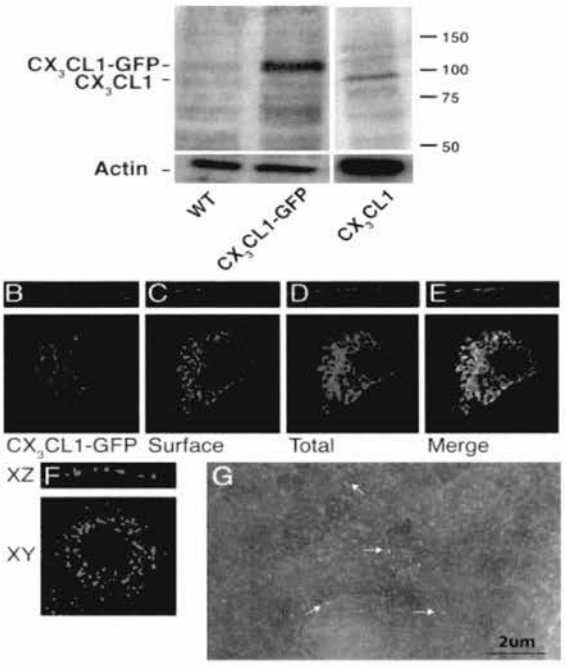

Figure 2. CX_3CL1 is expressed on the apical surface of RTEC. (A) Western analysis was performed using cell lysates from control wild-type MDCK cells (WT), MDCK-CX_3CL1-GFP, and MDCK-CX_3CL1 cells, using anti-CX_3CL1 Ab and horseradish peroxidase (HRP)-conjugated secondary Ab. For MDCK-CX_3CL1-GFP and MDCK-CX_3CL1 cells, bands of predicted molecular weight were obtained, namely 116 and 90 kD, respectively. (B through E) Immunofluorescence labeling of MDCK-CX_3CL1-GFP cells was performed as in Materials and Methods, and cells were examined by spinning disk confocal microscopy. (B) Spinning disk confocal image of MDCK-CX_3CL1-GFP cells. (C) For visualization of CX_3CL1 at the cell surface, MDCK-CX_3CL1-GFP cells were fixed before incubation with anti-CX_3CL1 Ab and Cy3-conjugated anti-goat IgG secondary Ab. (D) For visualization of both surface and intracellular CX_3CL1, cells were fixed and permeabilized before incubation with anti-CX_3CL1 Ab and Cy5-conjugated secondary Ab. (E) Merged images B through D. Images are shown as x *versus* y and x *versus* z optical sections. (F) Examination of the subcellular distribution of untagged CX_3CL1. For visualization of cell surface CX_3CL1, MDCK-CX_3CL1 cells were fixed, then incubated with anti-CX_3CL1 Ab, followed by Cy3-conjugated anti-goat IgG secondary Ab. For visualization of any intracellular CX_3CL1 present, the same cells then were permeabilized and incubated again with anti-CX_3CL1 Ab followed by Cy5-conjugated secondary Ab. (G) MDCK-CX_3CL1-GFP cells were labeled with anti-CX_3CL1 Ab and gold-conjugated secondary Ab and examined using scanning electron microscopy. Arrows show the association of the CX_3CL1 with apical microvilli. Reverse-phase images are shown. Magnification, ×100 in B through E.

To determine whether the cytosolic tail of CX_3CL1 mediates apical targeting, we generated a mutant construct that lacked the cytoplasmic domain (CX_3CL1–360). We examined the distribution of CX_3CL1 in MDCK cells that stably expressed "tailless" CX_3CL1 but found that the protein still was directed to the apical membrane (Figure 3A).

We next assessed potential associations of CX_3CL1 with lipid rafts. We treated cells with MβCD to extract cholesterol, thereby disrupting lipid rafts (40). To ensure that MβCD treatment was effective, we measured cholesterol spectrophotometrically (41). MβCD depleted total cellular cholesterol by 58% ($P < 0.05$; Figure 3B) but had no effect on apical targeting of CX_3CL1 (Figure 3C).

We next examined glycosylation of CX_3CL1 as a determinant of apical targeting. O-glycosylation was inhibited with benzyl-2-acetamido-2-deoxy-α-D-galacto-pyranoside. Again, CX_3CL1 targeting to the apical membrane remained intact (Figure 3D). To inhibit N-glycosylation of CX_3CL1, we treated cells with tunicamycin. This treatment resulted in intracellular retention of CX_3CL1 with virtually no expression observed on the apical surface (Figure 3E). To verify that the observed effects were not due to nonspecific disruption of apical protein traffic, we evaluated the effects of tunicamycin on NHE3, a protein that does not require N-glycosylation for its apical targeting. As expected, tunicamycin treatment did not affect the normal apical distribution of NHE3 (Figure 3F).

Collectively, these data indicate that the signals that direct apical trafficking of CX_3CL1 are not conferred by the protein's cytoplasmic domain, O-glycosylation of the protein, or associations with lipid rafts. Rather, apical localization of CX_3CL1 is determined by N-glycosylation.

CX_3CL1 Is Anchored to the Apical Membrane in RTEC

To determine whether CX_3CL1 is anchored in the luminal surface, we used fluorescence recovery after photobleaching to study the mobility characteristics of apical CX_3CL1-GFP in MDCK-CX_3CL1-GFP cells (see Materials and Methods) (Figure 4, A [before bleaching], B [immediately after bleaching], and C [5 min after bleaching]). As a control, MDCK cells were transfected with a DNA construct that encoded GPI-GFP, which is freely mobile in the apical plasma membrane. A region of the apical membrane was bleached similarly, and the recovery of fluorescence was observed over time (Figure 4, D through F). CX_3CL1-GFP recovered with significantly slower kinetics than GPI-GFP (Figure 4G). For CX_3CL1-GFP, the bleached area recovered to 10.5 ± 4.3% of prebleached fluorescence intensity by 4 min, compared with 61.1 ± 11.9% for GPI-GFP ($P < 0.01$). As an additional control, MDCK cells were transfected with DNA that encoded the single transmembrane protein FcR-GFP. When fluorescence recovery after photobleaching was performed similarly, the bleached area in the membrane recovered significantly faster than CX_3CL1-GFP, with 4-min recovery of 51.5 ± 6.1% for FcR-GFP ($P < 0.01$; Figure 4G). These data demonstrate that the ability of CX_3CL1 to diffuse laterally within the apical membrane is impeded, and, therefore, transmembrane CX_3CL1 is immobile.

Some single-pass transmembrane proteins are tethered to the apical membrane by direct association with lipid rafts (42). To determine whether CX_3CL1 is anchored in such a manner, we disrupted lipid rafts by treating cells with MβCD. However, this treatment did not mobilize CX_3CL1 in the apical membrane (Figure 4G). To study whether apical CX_3CL1 is immobile because it is tethered directly to the actin cytoskeleton, we

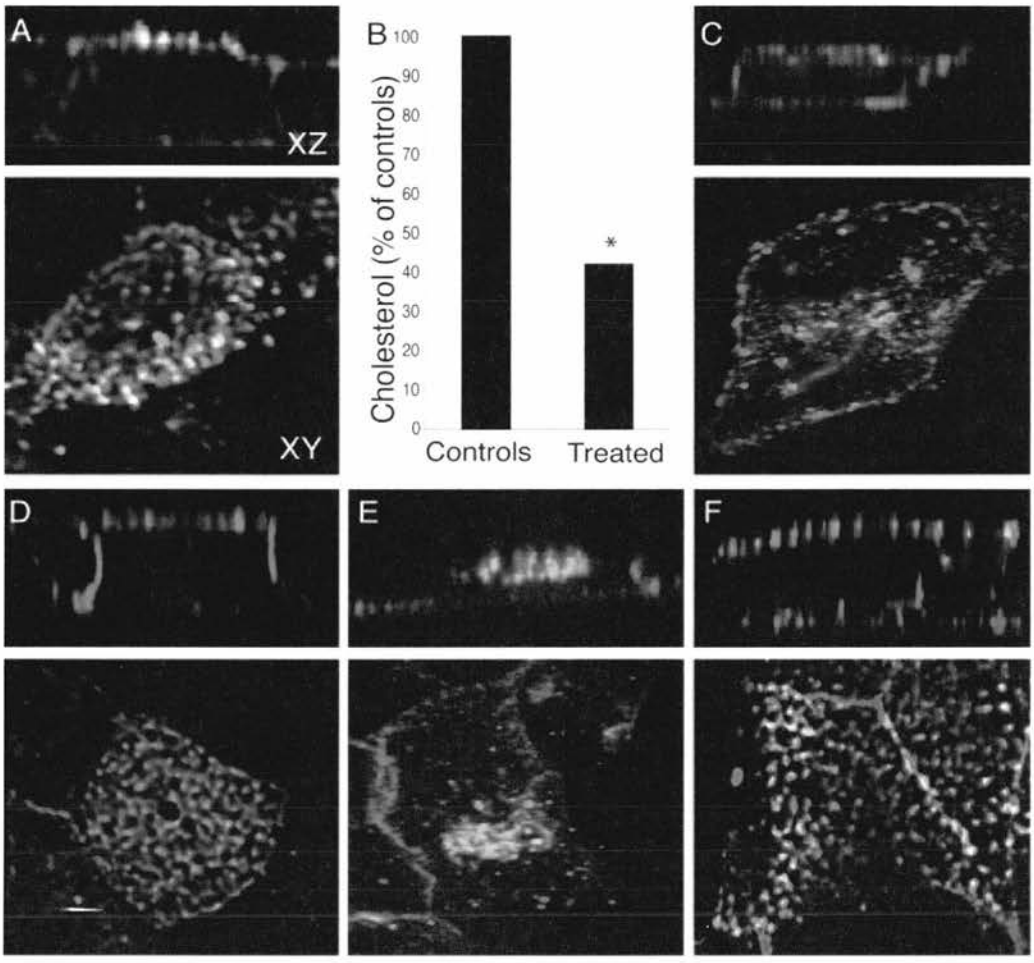

Figure 3. Targeting of CX_3CL1 to the apical membrane of RTEC. (A) MDCK cells that expressed a mutant CX_3CL1 construct that lacks the cytoplasmic tail (MDCK-CX_3CL1–360) were fixed and then incubated with anti-CX_3CL1 Ab and a Cy3-conjugated secondary Ab to visualize cell surface CX_3CL1. For further visualization of intracellular CX_3CL1, the same cells then were permeabilized and then labeled with anti-CX_3CL1 Ab and then Cy5-conjugated secondary Ab. After permeabilization, cells were incubated with Alexa 488–conjugated phalloidin to label F-actin. Slides were examined using a spinning disk confocal microscope. Images are shown as x *versus* y and x *versus* z optical sections. (B) For depletion of cholesterol and disruption of lipid rafts, MDCK-CX_3CL1-GFP cells were incubated for 30 min at 37°C with methyl-β-cyclodextrin (MβCD), and the cholesterol content was measured by spectrophotometry using Amplex Red (Molecular Probes). Values for cholesterol content are expressed as a percentage of untreated controls and represent a mean of three experiments ($^*P < 0.05$). (C) MDCK-CX_3CL1-GFP cells were incubated for 30 min with MβCD before fixation and incubation with antibodies as in A. (D) MDCK-CX_3CL1-GFP cells were labeled with anti-CX_3CL1 Ab, as in A, after treatment with benzyl-2-acetamido-2-deoxy-α-D-galacto-pyranoside overnight to inhibit O-glycosylation. (E) MDCK-CX_3CL1-GFP cells were labeled with anti-CX_3CL1 Ab as in A after overnight treatment with tunicamycin to inhibit N-glycosylation. (F) MDCK cells that expressed HA-tagged NHE3 (MDCK-NHE3) were incubated overnight with tunicamycin. The cells then were fixed and incubated with anti-HA Ab and then Cy3-conjugated secondary Ab. For visualization of intracellular NHE3, the same cells were permeabilized and then incubated with anti-HA Ab and then Cy5-conjugated secondary Ab. After permeabilization, the cells also were incubated with Alexa 488–conjugated phalloidin to label F-actin.

fractionated cellular proteins between two distinct fractions—triton soluble and triton insoluble—as described previously (33). In polarized epithelial cells, proteins that were anchored directly to the actin cytoskeleton preferentially remain in the triton-insoluble fraction. We found, however, that CX_3CL1 largely was soluble in triton solution, suggesting that it is not tethered directly to the actin cytoskeleton (Figure 4H). These data also confirm that CX_3CL1 is not associated with lipid rafts (Figures 3C and 4G). Collectively, these data indicate that after sorting to the apical surface, CX_3CL1 is held immobile there, but this is not achieved by direct tethering to the actin cytoskeleton or by association with lipid rafts.

CX_3CL1 Expressed on the Apical Surface of RTEC Promotes Adhesion of Leukocytes

CX_3CL1 can act as a cell adhesion molecule, facilitating the binding of leukocytes (7,43). We therefore hypothesized that CX_3CL1 might perform a similar function when expressed on

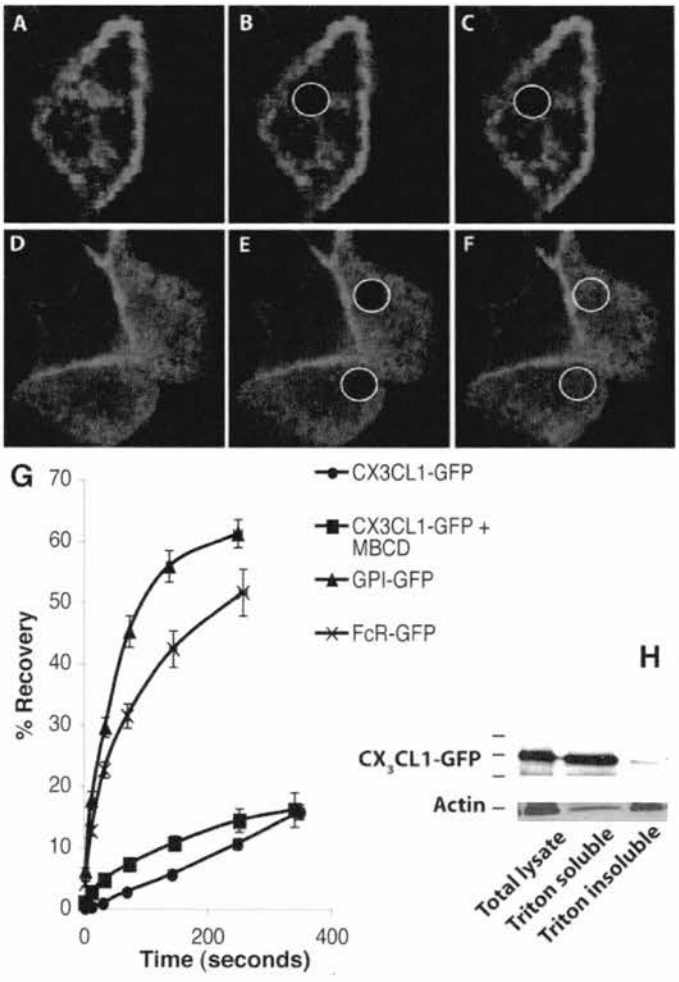

Figure 4. CX_3CL1 is anchored to the apical membrane in RTEC. For examination of the mobility of CX_3CL1 in the apical membrane, fluorescence recovery after photobleaching (FRAP) was performed as described in Materials and Methods. Using an argon laser and a scanning confocal microscope, a 2.5-μM region of the apical membrane that expressed CX_3CL1-GFP was photobleached irreversibly (circles), and recovery of fluorescence was monitored over time. (A) MDCK-CX_3CL1-GFP cell before bleaching. (B) The same cell immediately after photobleaching. (C) The same cell 5 min later. Control areas of the same diameter in the plasma membrane were examined at each time point. (D through F) As a control, FRAP was performed similarly in MDCK cells that expressed freely mobile glycosyl phosphatidylinositol conjugated to GFP (MDCK-GPI-GFP). (D) MDCK-GPI-GFP cells before bleaching. (E) The same cell immediately after bleaching. (F) The same cell after 5 min of recovery. (G) As an additional control, FRAP was performed in MDCK cells that expressed the single transmembrane protein FcγIIa receptor tagged with GFP (FcR-GFP). Recovery of fluorescence after photobleaching of apical CX_3CL1-GFP, GPI-GFP, FcR-GFP, and CX_3CL1-GFP after cholesterol depletion was done with MβCD. Points represent the mean ± SEM of recovery at serial time points from at least six experiments. (H) Lysates from MDCK-CX_3CL1-GFP cells were obtained after separation into triton-soluble and triton-insoluble fractions, as described in Materials and Methods. Western blotting was performed using anti-CX_3CL1 Ab and HRP-conjugated secondary Ab.

the apical surface of RTEC. Under the low-shear conditions used, there was minimal binding of control K562 leukocytes to either MDCK or MDCK-CX_3CL1-GFP cells (data not shown). We found significant binding of K562-CX_3CR1 leukocytes to MDCK-CX_3CL1-GFP cells (Figure 5, A and B). When CX_3CL1 was present on the apical membrane, leukocyte adhesion was almost three times greater than when CX_3CL1 was absent ($P < 0.001$; Figure 5C).

To verify that any observed responses were not an idiosyncratic feature of transformed cell lines, we performed the same experiments using primary, untransfected cells. Human PBMC

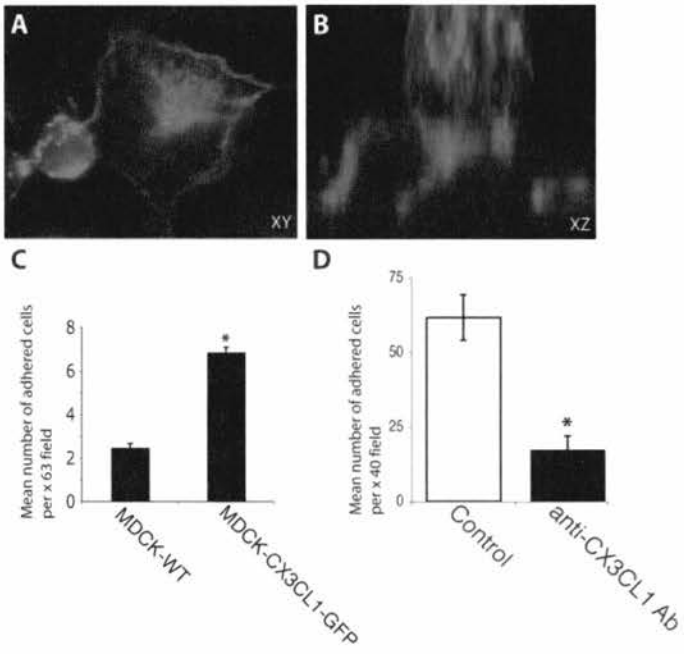

Figure 5. CX_3CR1-expressing leukocytes adhere to CX_3CL1 in the apical membrane of RTEC. K562 cells that expressed the CX_3CR1 receptor (K562-CX_3CR1) were labeled with rhodamine-conjugated cholera toxin B to visualize them. K562-CX_3CR1 cells (1×10^6) were added to MDCK or MDCK-CX_3CL1-GFP monolayers, growing on 25-mm cover slips, under conditions of low-shear stress. After 20 min, nonadherent cells were removed by washing, and the remaining cells were fixed. Serial fields (×63) were examined, using a Leica deconvolution microscope, and the number of adherent cells were counted. (A and B) Photomicrographs of labeled K562-CX_3CR1 cells (red) binding to MDCK-CX_3CL1-GFP monolayers. Images shown in x *versus* y (A) and x *versus* z (B) optical sections. (C) Graph depicting the number of K562-CX_3CR1 leukocytes bound to either MDCK or MDCK-CX_3CL1-GFP cells. Values represent the mean number of adherent cells per high-power field (×63). Values represent the mean of three experiments ± SEM (*$P < 0.001$). (D) Adhesion assays were repeated using primary RTEC and human peripheral blood mononuclear cells (PBMC) that were isolated from the blood of healthy volunteers. In parallel experiments, primary RTEC monolayers were preincubated with function-blocking anti-CX_3CL1 Ab (1 μg/ml) for 30 min before addition of PBMC. Values represent the mean number of adherent PBMC per ×40 field. Experiments were performed six times for each condition (*$P < 0.0001$ *versus* control).

were isolated from heparinized blood of healthy volunteers. PBMC contain multiple leukocyte subsets, including $CD8^+$ T lymphocytes, monocytes, and NK cells, all of which express the CX_3CR1 receptor. PBMC efficiently adhered to the apical surface of monolayers of primary human RTEC. When primary RTEC were preincubated with function-blocking anti-CX_3CL1 Ab, binding of PBMC was inhibited significantly (Figure 5D). Collectively, these data suggest that CX_3CL1 expressed on the luminal surface of RTEC promotes adhesion of leukocytes that bear the complementary receptor CX_3CR1. Our results are in keeping with previous reports in which blockade of CX_3CL1/CX_3CR1 impaired binding of THP-1 monocytic cells to primary proximal RTEC (32).

Discussion

The expression and the function of CX_3CL1 in endothelial cells have been well described (6,7,27,43). In the kidney, an important role for CX_3CL1 has been found in diseases that involve glomerular inflammation and endothelial injury (19,20,22,23). CX_3CL1 also is upregulated in renal tubulointerstitial inflammation, most notably in acute allograft rejection (19), but the specific localization of the chemokine (apical *versus* basolateral) has been somewhat unclear (32). The purpose of these studies, therefore, was to ascertain the subcellular distribution and targeting of CX_3CL1 in polarized tubular epithelial cells. Unexpectedly, we found that transmembrane CX_3CL1 was expressed predominantly on the apical surface of RTEC. This pattern of expression mirrors that found in epithelial cells of biliary ductules (44) but differs markedly from that of intestinal epithelial cells, where CX_3CL1 largely is expressed in the basolateral membrane and in regions of intercellular contact (45,46). In the intestine, as in the kidney, expression of CX_3CL1 is highly enhanced in disease states that are marked by active inflammation (14,45,47).

We next examined how CX_3CL1 is sorted to the apical membrane. In polarized cells, several signals can sort transmembrane proteins to either the basolateral or the apical membrane. The sorting determinant may lie in the cytoplasmic, transmembrane, or extracellular domain of the protein. Sorting signals in the cytoplasmic tail include PDZ domains and dileucine motifs, used by the cystic fibrosis transmembrane regulator and the IgG Fc receptor, respectively (36,37). By deleting the cytoplasmic tail of CX_3CL1, we excluded an apical targeting signal in this region. Other transmembrane proteins, such as Thy-1, apically target through direct or indirect associations with lipid rafts (48). However, when we disrupted any potential association with rafts by extracting cholesterol, we found no change in the distribution of CX_3CL1.

Carbohydrate modification of the protein backbone also may direct trafficking of transmembrane proteins, as is the case for sucrase isomaltase, which requires O-glycosylation for apical targeting (38). CX_3CL1 has 26 O-glycosylation sites in the mucin stalk. However, when we inhibited O-glycosylation, CX_3CL1 still trafficked to the apical membrane. For other proteins, such as endolyn and the glycine transporter GLYT2, N-glycosylation is the crucial determinant of apical targeting (49,50). CX_3CL1 has a single N-glycosylation site, located in the chemokine domain (2). Our studies indicate that glycosylation of this site is the key signal that directs CX_3CL1 to the apical membrane.

We postulated that after translocating to the apical membrane, CX_3CL1 would become anchored there, positioning it to act as a cellular adhesion molecule (7,10,43,51). Firm anchoring of the chemokine within the membrane would allow it to tether passing cells that express the receptor CX_3CR1. Our experiments indicate that CX_3CL1 indeed is immobile, similar to another adhesion molecule, CD44 (42,52).

We next considered how CX_3CL1 might be physically anchored to the apical membrane. Some adhesion molecules, including CD44, are tethered to the cell membrane by direct association with lipid rafts. We therefore examined the effect of cholesterol depletion and disruption of rafts on apical tethering of CX_3CL1. Disruption of lipid rafts did not increase the lateral mobility of CX_3CL1. Moreover, CX_3CL1 segregated with the detergent-soluble, rather than -insoluble, cellular fraction, further refuting a direct association with lipid rafts. These data also suggest that CX_3CL1 is not anchored directly to the actin cytoskeleton. A recent model of membrane fluidity proposed that transmembrane proteins might be fenced into discrete regions of the membrane (53). Such a mechanism might account for the limited lateral mobility of CX_3CL1. Alternatively, CX_3CL1 could be anchored indirectly to the actin cytoskeleton by one or more triton-soluble adaptor proteins (54).

Although our studies demonstrate that CX_3CL1 is targeted and anchored within the apical membrane, the key question is what role it might play there. CX_3CL1 in intestinal epithelium has been shown to recruit leukocytes in inflammation and to regulate cell survival and wound repair (7,45,55). In intestinal epithelium, CX_3CL1 is expressed predominantly on the basolateral surface, where it is in direct contact with CX_3CR1-expressing host leukocytes, including macrophages, lymphocytes, and dendritic cells. In the lamina propria, basolateral CX_3CL1 tethers dendritic cells to intestinal epithelium. Adherent dendritic cells then form transepithelial protrusions, which they extend into the gut lumen, facilitating immunosurveillance and defense against enteroinvasive bacteria (46). In contrast, no such immunosurveillance is known to occur within the kidney or the intrahepatic biliary tree. In biliary ductular epithelial cells, CX_3CL1 is expressed both apically and basolaterally (44,47). CX_3CL1 on the apical surface of regenerating biliary epithelial cells has been implicated in repair of the biliary tree after acute injury, presumably by recruiting hepatic stem cells, which express CX_3CR1 (47). In RTEC, a similar role has been proposed for CD44. CD44 normally is expressed on the basolateral membrane, where it participates in cell–matrix interactions. However, after renal tubulointerstitial injury, CD44 is expressed apically, where it is thought to promote regeneration and repair (56,57).

Conclusion

We have found that CX_3CL1 on the apical membrane promotes tethering of leukocytes that bear the complementary receptor. During tubulointerstitial renal inflammation, tight junctions break down, potentially allowing leukocytes to es-

cape into the urinary space. We postulate that apical CX_3CL1 facilitates recruitment and retention of these leukocytes, redirecting them to the site of injury. In this manner, CX_3CL1 may play an important role in tubulointerstitial nephritis, pyelonephritis, and renal allograft rejection, disease processes in which expression of CX_3CL1 is highly upregulated. As with biliary epithelial cells, CX_3CL1 also may participate in regeneration of tubules after inflammatory injury. Further work is needed to ascertain the *in vivo* functions of CX_3CL1 located on the apical membrane of RTEC.

Acknowledgments

A.M.D. was supported through a studentship through the Hospital for Sick Children Research Training Centre. R.T.A. was supported by the Canadian Child Health Clinician Scientist Program.

We thank Bob Temkin and Michael Ho for technical assistance. We are grateful to Drs. Sergio Grinstein and Andrew Herzenberg for reagents and helpful discussions.

Disclosures

None.

References

1. Moser B, Wolf M, Walz A, Loetscher P: Chemokines: Multiple levels of leukocyte migration control. *Trends Immunol* 25: 75–84, 2004
2. Bazan JF, Bacon KB, Hardiman G, Wang W, Soo K, Rossi D, Greaves DR, Zlotnick A, Schall TJ: A new class of membrane-bound chemokine with a CX3C motif. *Nature* 385: 640–644, 1997
3. Garton KJ, Gough PJ, Blobel CP, Murphy G, Greaves DR, Dempsey PJ, Raines EW: Tumor necrosis factor-alpha-converting enzyme (ADAM17) mediates the cleavage and shedding of fractalkine (CX3CL1). *J Biol Chem* 276: 37993–38001, 2001
4. Hundhausen C, Misztela D, Berkhout TA, Broadway N, Saftig P, Reiss K, Hartmann D, Fahrenholz F, Postina R, Matthews V, Kallen K-J, Rose-John S, Ludwig A: The disintegrin-like metalloproteinase ADAM-10 is involved in constitutive cleavage of CX3CL1 (fractalkine) and regulates CX3CL1-mediated cell-cell adhesion. *Blood* 102: 1186–1195, 2003
5. Tsou C-L, Haskell CA, Charo IF: Tumor necrosis factor-alpha-converting enzyme mediates the inducible cleavage of fractalkine. *J Biol Chem* 276: 44622–44626, 2001
6. Imai T, Hieshima K, Haskell C, Baba M, Nagira M, Nishimura M, Kakizaki M, Takagi S, Nomiyama H, Schall TJ, Yoshie O: Identification and molecular characterization of fractalkine receptor, CX3CR1, which mediates both leukocyte migration and adhesion. *Cell* 91: 521–530, 1997
7. Fong AM, Robinson LA, Steeber DA, Tedder TF, Yoshie O, Imai T, Patel DD: Fractalkine and CX3CR1 mediate a novel mechanism of leukocyte capture, firm adhesion, and activation under physiologic flow. *J Exp Med* 188: 1413–1419, 1998
8. Cybulsky MI, Hegele RA: The fractalkine receptor CX3CR1 is a key mediator of atherogenesis. *J Clin Invest* 111: 1118–1120, 2003
9. Eriksson EE: Mechanisms of leukocyte recruitment to atherosclerotic lesions: Future prospects. *Curr Opin Lipidol* 15: 553–558, 2004
10. Robinson LA, Nataraj C, Thomas DW, Howell DN, Griffiths R, Bautch V, Patel DD, Feng L, Coffman TM: A role for fractalkine and its receptor (CX3CR1) in cardiac allograft rejection. *J Immunol* 165: 6067–6072, 2000
11. Robinson LA, Nataraj C, Thomas DW, Cosby JM, Griffiths R, Bautch V, Patel DD, Coffman TM: The chemokine CX3CL1 regulates NK cell activity in vivo. *Cell Immunol* 225: 122–130, 2003
12. Schafer A, Schulz C, Eigenthaler M, Fraccarollo D, Kobsar A, Gawaz M, Ertl G, Walter U, Bauersachs J: Novel role of the membrane-bound chemokine fractalkine in platelet activation and adhesion. *Blood* 103: 407–412, 2004
13. Umehara H, Bloom E, Okazaki T, Domae N, Imai T: Fractalkine and vascular injury. *Trends Immunol* 22: 602–607, 2001
14. Brand S, Hofbauer K, Dambacher J, Schnitzler F, Staudinger T, Pfennig S, Seiderer T, Tillack C, Konrad A, Goke B, Ochsenkuhn T, Lohse P: Increased expression of the chemokine fractalkine in Crohn's disease and association of the fractalkine receptor T280M polymorphism with a fibrostenosing disease phenotype. *Am J Gastroenterol* 101: 99–106, 2006
15. Rimaniol AC, Till SJ, Garcia G, Capel F, Godot V, Balabanian K, Durand-Gasselin I, Varga E, Simonneau G, Emilie D, Durham SR, Humbert M: The CX3C chemokine fractalkine in allergic asthma and rhinitis. *J Allergy Clin Immunol* 112: 1139–1146, 2003
16. Schwaeble WJ, Stover CM, Schall TJ, Dairaghi DJ, Trinder PK, Linington C, Iglesias A, Schubart A, Lynch NJ, Weihe E, Schafer MK: Neuronal expression of fractalkine in the presence and absence of inflammation. *FEBS Lett* 439: 203–207, 1998
17. Wong BW, Wong D, McManus BM: Characterization of fractalkine (CX3CL1) and CX3CR1 in human coronary arteries with native atherosclerosis, diabetes mellitus, and transplant vascular disease. *Cardiovasc Pathol* 11: 332–338, 2002
18. Chen YM, Lin SL, Chen CW, Chiang W, Tsai TJ, Hsieh BW: Tumor necrosis factor-alpha stimulates fractalkine production by mesangial cells and regulates monocyte transmigration: Down-regulation by cAMP. *Kidney Int* 63: 474–486, 2003
19. Cockwell P, Chakravorty SJ, Girdlestone J, Savage CO: Fractalkine expression in human renal inflammation. *J Pathol* 196: 85–90, 2002
20. Furuichi K, Wada T, Iwata Y, Sakai N, Yoshimoto K, Shimizu M, Kobayashi K, Takasawa K, Kida H, Takeda S, Matsushima K, Yokoyama H: Upregulation of fractalkine in human crescentic glomerulonephritis. *Nephron* 87: 314–320, 2001
21. Inoue A, Hasegawa H, Kohno M, Ito M, Terada M, Imai T, Yoshie O, Nose M, Fujita S: Antagonist of fractalkine (CX3CL1) delays the initiation and ameliorates the progression of lupus nephritis in MRL/lpr mice. *Arthritis Rheum* 52: 1522–1533, 2005
22. Ito Y, Kawachi H, Morioka Y, Nakatsue T, Koike H, Ikezumi Y, Oyanagi A, Natori Y, Nakamura T, Gejyo F, Shimizu F: Fractalkine expression and the recruitment of CX3CR1+ cells in the prolonged mesangial proliferative glomerulonephritis. *Kidney Int* 61: 2044–2057, 2002

23. Feng L, Chen S, Garcia GE, Xia Y, Siani M, Botti P, Wilson CB, Harrison JK, Bacon KB: Prevention of crescentic glomerulonephritis by immunoneutralization of the fractalkine receptor CX3CR1. *Kidney Int* 56: 612–620, 1999
24. Donadelli R, Zanchi C, Morigi M, Buelli S, Batani C, Tomasoni S, Corna D, Rottoli D, Benigni A, Abbate M, Remuzzi G, Zoja C: Protein overload induces fractalkine upregulation in proximal tubular cells through nuclear factor kappaB- and p38 mitogen-activated protein kinase-dependent pathways. *J Am Soc Nephrol* 14: 2436–2446, 2003
25. Pietrzyk MC, Banas B, Wolf K, Rummele P, Woenckhaus M, Hoffman U, Kramer BK, Fischereder M: Quantitative gene expression analysis of fractalkine using laser microdissection in biopsies from kidney allografts with acute rejection. *Transplant Proc* 36: 2659–2661, 2004
26. Reich H, Tritchler D, Herzenberg AM, Kassiri Z, Zhou X, Gao W, Scholey JW: Albumin activates ERK via EGF receptor in human renal epithelial cells. *J Am Soc Nephrol* 16: 1266–1278, 2005
27. Liu GY, Kulasingam V, Alexander RT, Touret N, Fong AM, Patel DD, Robinson LA: Recycling of the membrane-anchored chemokine, CX3CL1. *J Biol Chem* 280: 19858–19866, 2005
28. Robinson LA, Tu L, Steeber DA, Preis O, Platt JL, Tedder TF: The role of adhesion molecules in human leukocyte attachment to porcine vascular endothelium: Implications for xenotransplantation. *J Immunol* 161: 6931–6938, 1998
29. Fong AM, Alam SM, Imai T, Haribabu B, Patel DD: CX3CR1 tyrosine sulfation enhances fractalkine-induced cell adhesion. *J Biol Chem* 277: 19418–19423, 2002
30. D'Souza S, Garcia-Cabado A, Yu F, Teter K, Lukacs G, Skorecki K, Moore HP, Orlowski J, Grinstein S: The epithelial sodium-hydrogen antiporter Na+/H+ exchanger 3 accumulates and is functional in recycling endosomes. *J Biol Chem* 173: 2035–2043, 1998
31. Kurashima K, Szabo EZ, Lukacs G, Orlowski J, Grinstein S: Endosomal recycling of the Na+/H+ exchanger NHE3 isoform is regulated by the phosphatidylinositol 3-kinase pathway. *J Biol Chem* 273: 20828–20836, 1998
32. Chakravorty SJ, Cockwell PP, Girdlestone J, Brooks CJ, Savage CO: Fractalkine expression on human renal tubular epithelial cells: Potential role in mononuclear cell adhesion. *Clin Exp Immunol* 129: 150–159, 2002
33. Hayashi H, Szaszi K, Grinstein S: Multiple modes of regulation of Na+/H+ exchangers. *Ann N Y Acad Sci* 976: 248–258, 2002
34. Alexander RT, Furuya W, Orlowski J, Grinstein S: Rho GTPases dictate the mobility of the Na/H exchanger NHE3 in epithelia: Role in apical retention and targeting. *Proc Natl Acad Sci U S A* 102: 12253–12258, 2005
35. Lippincott-Schwartz J, Presley JF, Zaal KJ, Hirschberg K, Miller CD, Ellenberg J: Monitoring the dynamics and mobility of membrane proteins tagged with green fluorescent protein. *Methods Cell Biol* 58: 261–281, 1999
36. Matter K, Yamamoto EM, Mellman I: Structural requirements and sequence motifs for polarized sorting and endocytosis of LDL and Fc receptors in MDCK cells. *J Cell Biol* 126: 991–1004, 1994
37. Ostedgaard LS, Randak C, Rokhlina T, Karp P, Vermeer D, Ashbourne Excoffon KJ, Welsh MJ: Effects of C-terminal deletions on cystic fibrosis transmembrane conductance regulator function in cystic fibrosis airway epithelia. *Proc Natl Acad Sci U S A* 100: 1937–1942, 2003
38. Naim HY, Joberty G, Alfalah M, Jacob R: Temporal association of the N- and O-linked glycosylation events and their implication in the polarized sorting of intestinal brush border sucrase-isomaltose, aminopeptidase N, and dipeptidyl peptidase IV. *J Biol Chem* 274: 17961–17967, 1999
39. Lisanti MP, Sargiacomo M, Graeve L, Saltiel AR, Rodriguez-Boulan E: Polarized apical distribution of glycosylphosphatidylinositol-anchored proteins in a renal tubular epithelial cell line. *Proc Natl Acad Sci U S A* 85: 9557–9561, 1988
40. Ilangumaran S, Hoessli DC: Effects of cholesterol depletion by cyclodextrin on the sphingolipid microdomains of the plasma membrane. *Biochem J* 335: 433–440, 1998
41. Amundson DM, Zhou M: Fluorometric method for the enzymatic determination of cholesterol. *J Biochem Biophys Methods* 38: 43–52, 1999
42. Oliferenko S, Paiha K, Harder T, Gerke V, Schwarzler C, Schwarz H, Beug H, Gunthert U, Huber LA: Analysis of CD44-containing lipid rafts: Recruitment of annexin II and stabilization by the actin cytoskeleton. *J Cell Biol* 146: 843–854, 1999
43. Goda S, Imai T, Yoshie O, Yoneda O, Inoue H, Nagano Y, Okazaki T, Imai H, Bloom ET, Domae N, Umehara H: CX3C-chemokine, fractalkine-enhanced adhesion of THP-1 cells to endothelial cells through integrin-dependent and -independent mechanisms. *J Immunol* 164: 4313–4320, 2000
44. Isse K, Harada K, Zen Y, Kamihara T, Shimoda S, Harada M, Nakanuma Y: Fractalkine and CX3CR1 are involved in the recruitment of intraepithelial lymphocytes of intrahepatic bile ducts. *Hepatology* 41: 506–516, 2005
45. Muehlhoefer A, Saubermann LJ, Gu X, Luedtke-Heckenkamp K, Xavier R, Blumberg RS, Podolsky DK, MacDermott RP, Reinecker HC: Fractalkine is an epithelial and endothelial cell-derived chemoattractant for intraepithelial lymphocytes in the small intestinal mucosa. *J Immunol* 164: 3368–3376, 2000
46. Niess JH, Brand S, Gu X, Landsman L, Jung S, McCormick BA, Vyas JM, Boes M, Ploegh HL, Fox JG, Littman DR, Reinecker HC: CX3CR1-mediated dendritic cell access to the intestinal lumen and bacterial clearance. *Science* 307: 254–258, 2005
47. Efsen E, Grappone C, DeFranco RM, Milani S, Romanelli RG, Bonacchi A, Caliguri A, Failli P, Annunziato F, Pagliai G, Pinzani M, Laffi G, Gentilini P, Marra F: Up-regulated expression of fractalkine and its receptor CX3CR1 during liver injury in humans. *J Hepatol* 37: 39–47, 2002
48. Powell SK, Lisanti MP, Rodriguez-Boulan EJ: Thy-1 expresses two signals for apical localization in epithelial cells. *Am J Physiol* 260: C715–C720, 1991
49. Potter BA, Ihrke G, Bruns JR, Weixel KM, Weisz OA: Specific N-glycans direct apical delivery of transmembrane, but not soluble or glycosylphosphatidylinositol-anchored forms of endolyn in Madin-Darby canine kidney cells. *Mol Biol Cell* 15: 1407–1416, 2004
50. Martinez-Maza R, Poyatos I, Lopez-Corcuera B, Nu E, Gimenez C, Zafra F, Aragon C: The role of N-glycosylation in transport to the plasma membrane and sorting of the neuronal glycine transporter GLYT2. *J Biol Chem* 276: 2168–2173, 2001
51. Kerfoot SM, Lord SE, Bell RB, Gill V, Robbins SM, Kubes P:

Human fractalkine mediates leukocyte adhesion but not capture under physiological shear conditions; a mechanism for selective monocyte recruitment. *Eur J Immunol* 33: 729–739, 2003
52. Constantin G, Majeed M, Giagulli C, Piccio L, Kim JY, Butcher EC, Laudanna C: Chemokines trigger immediate beta2 integrin affinity and mobility changes: Differential regulation and roles in lymphocyte arrest under flow. *Immunity* 13: 759–769, 2000
53. Suzuki K, Ritchie K, Kajikawa E, Fujiwara T, Kusumi A: Rapid hop diffusion of a G-protein-coupled receptor in the plasma membrane as revealed by single-molecule techniques. *Biophys J* 88: 3659–3680, 2005
54. Neame SJ, Uff CR, Sheikh H, Wheatley SC, Isacke CM: CD44 exhibits a cell type dependent interaction with triton X-100 insoluble, lipid rich, plasma membrane domains. *J Cell Science* 108: 3127–3135, 1995
55. Brand S, Sakaguchi T, Gu X, Colgan SP, Reinecker HC: Fractalkine-mediated signals regulate cell-survival and immune-modulatory responses in intestinal epithelial cells. *Gastroenterology* 122: 166–177, 2002
56. Asselman M, Verhulst A, Van Ballegooijen ES, Bangma CH, Verkoelen CF, De Broe ME: Hyaluronan is apically secreted and expressed by proliferating or regenerating renal tubular cells. *Kidney Int* 68: 71–83, 2005
57. Xie Y, Nishi S, Fukase S, Nakamura H, Chen X, Imai N, Sakatsume M, Saito A, Ueno M, Narita I, Yamamoto T, Gejyo F: Different type and localization of CD44 on surface membrane of regenerative renal tubular epithelial cells in vivo. *Am J Nephrol* 24: 188–197, 2004

Am J Physiol Cell Physiol 298: C1469–C1480, 2010.
First published March 17, 2010; doi:10.1152/ajpcell.00380.2009.

Thromboxane prostanoid receptor stimulation induces shedding of the transmembrane chemokine CX_3CL1 yet enhances CX_3CL1-dependent leukocyte adhesion

Soumitra Tole,* Anne M. Durkan,* Yi-Wei Huang, Guang Ying Liu, Alexander Leung, Laura L. Jones, Jasmine A. Taylor, and Lisa A. Robinson

The Hospital for Sick Children Research Institute, Toronto, Ontario, Canada

Submitted 21 August 2009; accepted in final form 12 March 2010

Tole S, Durkan AM, Huang YW, Liu GY, Leung A, Jones LL, Taylor JA, Robinson LA. Thromboxane prostanoid receptor stimulation induces shedding of the transmembrane chemokine CX_3CL1 yet enhances CX_3CL1-dependent leukocyte adhesion. *Am J Physiol Cell Physiol* 298: C1469–C1480, 2010. First published March 17, 2010; doi:10.1152/ajpcell.00380.2009.—In atherosclerosis, chemokines recruit circulating mononuclear leukocytes to the vascular wall. A key factor is CX_3CL1, a chemokine with soluble and transmembrane species that acts as both a chemoattractant and an adhesion molecule. Thromboxane A_2 and its receptor, TP, are also critical to atherogenesis by promoting vascular inflammation and consequent leukocyte recruitment. We examined the effects of TP stimulation on processing and function of CX_3CL1, using CX_3CL1-expressing human ECV-304 cells and primary human vascular endothelial cells. TP agonists promoted rapid shedding of cell surface CX_3CL1, which was inhibited by pharmacological inhibitors or specific small interfering RNA targeting tumor necrosis factor-α-converting enzyme (TACE). Because it reduced cell surface CX_3CL1, we predicted that TP stimulation would inhibit adhesion of leukocytes expressing the CX_3CL1 cognate receptor but, paradoxically, saw enhanced adhesion. We questioned whether the enhanced ability of the remaining membrane-associated CX_3CL1 to bind targets was caused by changes in its lateral mobility. Using fluorescence recovery after photobleaching, we found that plasmalemmal CX_3CL1 was initially tethered but ultimately mobilized by TP agonists. TP stimulation provoked clustering of transmembrane CX_3CL1 at sites of contact with adherent leukocytes. These data demonstrate that TP stimulation induces two distinct effects: a rapid cleavage of surface CX_3CL1, thereby releasing the soluble chemoattractant, plus mobilization of the remaining transmembrane CX_3CL1 to enhance the avidity of interactions with adherent leukocytes. The dual effect of TP allows CX_3CL1 to recruit leukocytes to sites of vascular inflammation while enhancing their adhesion once recruited.

leukocytes; inflammation; endothelial cells

ATHEROSCLEROSIS is a chronic inflammatory disease involving the vascular wall, leukocytes, and platelets. Thromboxane A_2 (TXA_2), a prostanoid formed from the metabolism of arachidonic acid via the cyclooxygenase (COX) pathway, has long been implicated in the pathogenesis of atherosclerosis and induces platelet aggregation, vasoconstriction, and vascular smooth muscle cell (VSMC) proliferation (42). It is produced mainly by platelets but also by monocytes/macrophages, VSMC, and endothelial cells (37, 41, 42). TXA_2 mediates its effects through the thromboxane prostanoid (TP) receptor, a G protein-coupled receptor expressed in diverse hematopoietic cell types, including platelets and monocytes, as well as in endothelial cells, fibroblasts, and VSMC (15, 41). COX inhibitors, which decrease TXA_2 production, protect against vascular inflammation and acute vascular events in patients at high risk (3). Mice deficient in TP or treated with a TP antagonist show markedly decreased leukocyte accumulation within the vascular wall (5, 22).

In atherogenesis, chemokines recruit circulating leukocytes and other cells to the injured vascular wall. The chemokine CX_3CL1 (fractalkine) plays a key role by recruiting monocytes, T lymphocytes, and other inflammatory cells (6, 24, 28, 29, 32, 40). Most chemokines are small, secreted proteins. CX_3CL1 is one of only two chemokines that have soluble and membrane-anchored species (2, 10, 27). Soluble CX_3CL1 consists of a chemokine domain and mucin stalk and is released from the plasma membrane following cleavage of the full-length protein by ADAM (a disintegrin and metalloprotease)-10 and ADAM17/TACE (tumor necrosis factor-α-converting enzyme) metalloproteases (12, 17, 43). The soluble species thus generated is chemoattractant for monocytes/macrophages, natural killer cells, T lymphocytes, and VSMC, all of which express CX_3CR1, the unique receptor for CX_3CL1 (10, 18, 26).

CX_3CL1-CX_3CR1-mediated cellular traffic is critically implicated in coronary atherosclerosis and stroke. In affected coronary arteries, CX_3CL1 protein expression is increased throughout the vascular wall in endothelium, intima, media, and adventitia (26, 45, 47). CX_3CL1 is also expressed in macrophages, foam cells, and VSMC and acts to recruit monocytes, memory T lymphocytes, and additional VSMC to the injured arterial wall (26, 45, 47). Thus, within the atherosclerotic lesion, CX_3CL1 is expressed by and can recruit cells capable of secreting large amounts of extracellular matrix proteins, thereby favoring formation of stable atherosclerotic plaques (10, 18, 47). By recruiting monocytes to the injured vessels, CX_3CL1 promotes formation of macrophage-rich, unstable plaques. Genetic targeting of *CX_3CL1* or *CX_3CR1* in atherosclerosis-prone mice highly protects them from vascular disease (6, 24, 40). In humans, gene polymorphisms in *CX_3CR1* that impair leukocyte chemotaxis and binding of the receptor to cell surface CX_3CL1 protect against myocardial infarction, unstable angina, cardiac death, and stroke (13, 28, 32).

It is widely recognized that important links exist between the thrombotic events and the vascular inflammation that define atherosclerosis. The precise nature of these links has not yet been well elucidated. TXA_2, acting through TP, potently in-

* S. Tole and A. M. Durkan contributed equally to this work.

Address for reprint requests and other correspondence: L. A. Robinson, 555 Univ. Ave., Rm. 5264, Toronto, Ontario, Canada M5G 1X8 (e-mail: lisa.robinson@sickkids.ca).

duces vascular inflammation, promoting leukocyte recruitment to the injured vascular wall. We studied whether TP mediates these effects by enhancing the exposure and activity of the chemokine CX_3CL1. We found that TP stimulation causes rapid shedding of CX_3CL1 from the cell surface yet, unexpectedly, promotes enhanced CX_3CL1-dependent leukocyte adhesion. TP stimulation mobilizes remaining membrane-associated CX_3CL1, allowing it to cluster at sites of contact with adherent leukocytes. The potential implications of these dual mechanisms of regulation of CX_3CL1 function by TP for the development of vascular inflammation are discussed.

MATERIALS AND METHODS

Cell culture. ECV-304 cells were obtained from the American Type Culture Collection (Manassas, VA), and the generation of cells expressing green fluorescent protein-tagged CX_3CL1 (ECV-CX_3CL1-GFP) or untagged CX_3CL1 (ECV-CX_3CL1) has been described previously (8, 25). A cDNA construct encoding mCherry-tagged CX_3CL1 was generated by PCR amplification of full-length CX_3CL1 with *Eco*R1 and *Bam*H1 sites at the NH_2 and COOH terminus, respectively, and subcloning into the corresponding restriction sites of pmCherry-N1 vector (Clontech Laboratories, Mountain View, CA). The resulting CX_3CL1-mCherry cDNA construct was verified by sequencing and was expressed in ECV-304 cells using FuGene HD transfection reagent according to the manufacturer's specifications (Roche Diagnsotics, Laval, PQ, Canada). Cells were grown in DMEM and Ham's F12 (Wisent, St-Bruno, QC, Canada) supplemented with 5% fetal calf serum. Human K562 erythroleukemia cells that stably express CX_3CR1 (K562-CX_3CR1) were cultured in RPMI supplemented with HEPES and 10% fetal calf serum (8, 10). Primary human umbilical vein endothelial cells (HUVEC) were obtained from Clonetics (La Jolla, CA) and cultured in endothelial cell growth medium (Clonetics) (10). Peripheral blood mononuclear cells (PBMC) were isolated from the blood of healthy volunteers as previously described (8).

Antibodies and reagents. The following primary antibodies were used: goat anti-human CX_3CL1 (R&D Systems, Minneapolis, MN), rabbit anti-Erk (extracellular signal-related kinase) and rabbit anti-phospho-Erk (Cell Signaling Technology, Danvers, MA), mouse anti-actin (Stressgen, Victoria, BC, Canada), mouse anti-GAPDH (Chemicon, Temecula, CA), and mouse anti-Bcr (Santa Cruz Biotechnology, Santa Cruz, CA). Rabbit anti-phospho-c-Raf, rabbit anti-phospho-MEK1/2, and rabbit anti-MEK1/2 were all obtained from Cell Signaling Technology. Rabbit anti-c-Raf was obtained from Santa Cruz Biotechnology. Mouse monoclonal antibody (Ab) directed against human TACE was a kind gift of Dr. Roy Black (Amgen, Sherman Oaks, CA). The following secondary antibodies were used: horseradish peroxidase-conjugated anti-mouse, anti-goat and anti-rabbit IgG, Cy3- and Cy5-conjugated anti-goat IgG, Cy5-conjugated anti-mouse IgG, and phycoerythrin-conjugated anti-goat IgG (Jackson ImmunoResearch Laboratories, Bar Harbor, ME), as well as Alexa488-conjugated anti-mouse IgG (Invitrogen, Burlington, ON, Canada). TP agonists 9,11-dideoxy-11α,9α-epoxymethanoprostaglandin $F_{2\alpha}$ (U46619) and [1*S*-1α,2β(5*Z*),3α(1*E*,3*R**),4α]-7-[3-(3-hydroxy-4-(4′-iodophenoxy)-1-butenyl)-7-oxabicyclo-[2.2.1]heptan-2-yl]-5-heptenoic acid (IBOP), as well as the specific TP antagonist SQ29548 were obtained from Biomol (Plymouth Meeting, PA). The Erk inhibitor U0126 was obtained from LC Laboratories (Woburn, MA). The metalloprotease inhibitors TAPI-2 and GM6001 were obtained from Peptides International (Louisville, KY) and Chemicon International (Temecula, CA), respectively. DNA expression constructs encoding GFP-tagged glycosylphosphatidylinositol (GPI-GFP) and FcγRIIa receptor (FcγRIIa-GFP) were a gift from Dr. Sergio Grinstein (The Hospital for Sick Children Research Institute, Toronto, ON, Canada), and cells were transfected using FuGene (Roche Diagnostics).

Immunoblotting. SDS-PAGE and immunoblotting were performed, as previously described, using anti-CX_3CL1 Ab (0.2 μg/ml) and anti-Erk (0.01 μg/ml) or anti-phospho-Erk Ab (0.2 μg/ml) (8, 25). Anti-actin or anti-GAPDH Ab was used to control for protein loading. Immunoreactive bands were visualized by enhanced chemiluminescence (Amersham Biosciences, Little Chalfont, UK) recorded on X-ray film.

Flow cytometry. ECV-CX_3CL1-GFP cells were grown in 10-cm dishes and treated with the TP agonists IBOP or U46619 for various time periods. Cells were lifted by briefly incubating with 5% EDTA at 4°C, washed, and fixed in 4% paraformaldehyde. Cells were incubated with 5% donkey serum followed by anti-CX_3CL1 Ab for 1 h at room temperature. After further washing, cells were incubated with phycoerythrin-conjugated anti-goat IgG for 1 h at room temperature. Cells were suspended in PBS and analyzed using a fluorescence-activated cell scanner (FACScan; BD Biosciences, San Jose, CA).

Immunofluorescence staining. ECV-CX_3CL1-GFP cells were grown on glass coverslips, fixed using 4% paraformaldehyde, washed, and blocked with 5% donkey serum at room temperature for 1 h. Cells were incubated with anti-CX_3CL1 Ab (2.5 μg/ml) and anti-TACE Ab (2.7 μg/ml) at room temperature for 1 h followed by Cy3-conjugated anti-goat IgG and Cy5-conjugated anti-mouse IgG for 1 h. Cells were mounted onto glass slides and visualized using a spinning disk DMIRE2 confocal microscope (Leica Microsystems, Toronto, ON, Canada) equipped with a Hamamatsu backthinned charge-coupled device (EM-CCD) camera. Images were acquired using ×100 oil immersion and appropriate filters (8, 25).

Fluorescence recovery after photobleaching. Fluorescence recovery after photobleaching (FRAP) was performed as previously described (8, 25). Briefly ECV-CX_3CL1-GFP cells or ECV-CX_3CL1 cells transfected with GPI-GFP or FcγRIIa-GFP cDNA were grown on 25-mm coverslips, mounted into Attafluor chambers, and incubated in RPMI containing 5% fetal calf serum and 25 mM HEPES at 37°C (8, 25). Live cells were analyzed by confocal microscopy. A 30-mW LASOS argon laser was used to irreversibly photobleach the entire juxtanuclear CX_3CL1-containing compartment (8, 25). To prevent potential shedding of cell surface CX_3CL1, cells were treated with the metalloprotease inhibitor GM6001 for 4 h before assays were performed. In other experiments, a 2-μm region of the plasma membrane was irreversibly photobleached. Recovery of fluorescence was measured over time. Control, nonbleached areas of the plasma membrane of the same cell were also serially monitored to quantify the amount of bleaching caused by repeated image acquisition. Results are expressed as the mean (±SE) normalized fluorescence recovery.

Acid-stripping experiments. The rate of delivery of internalized CX_3CL1 back to the plasma membrane was assessed as previously described (25, 44). To prevent potential shedding of cell surface CX_3CL1, cells were pretreated with the metalloprotease inhibitor GM6001 before incubation with anti-CX_3CL1 Ab for 1 h (43). Membrane-associated Ab was removed by acid wash (0.15M NaCl, 50 mM glycine, 0.1% BSA, pH 2.5) on ice for 2 min and then allowed to recover for various time periods in the presence of TP agonist. Cells were washed, fixed, and incubated with Cy3-conjugated secondary Ab. Images were captured using a Leica DMIRE2 microscope and OpenLab software (Improvision, Lexington, MA). Cell surface immunofluorescence intensity was measured using Volocity imaging software (Improvision, Waltham, MA).

Adhesion assays. Stamper-Woodruff assays were performed as described elsewhere with minor modifications (8, 35, 36). Briefly, ECV-304, ECV-CX_3CL1-GFP, or HUVEC cells were grown to confluence on 25-mm coverslips and treated with the TP agonist IBOP for 30 min. In some experiments, HUVEC were incubated with TNF-α (100 U/ml) for 4 h, followed by incubation with function-blocking anti-CX_3CL1 Ab (1 μg/ml) for 30 min before addition of leukocytes. Control human K562 or K562-CX_3CR1 cells were labeled with Alexa555-conjugated cholera toxin to easily visualize them. Cells (5×10^5) were incubated with either ECV-304 or ECV-CX_3CL1-GFP

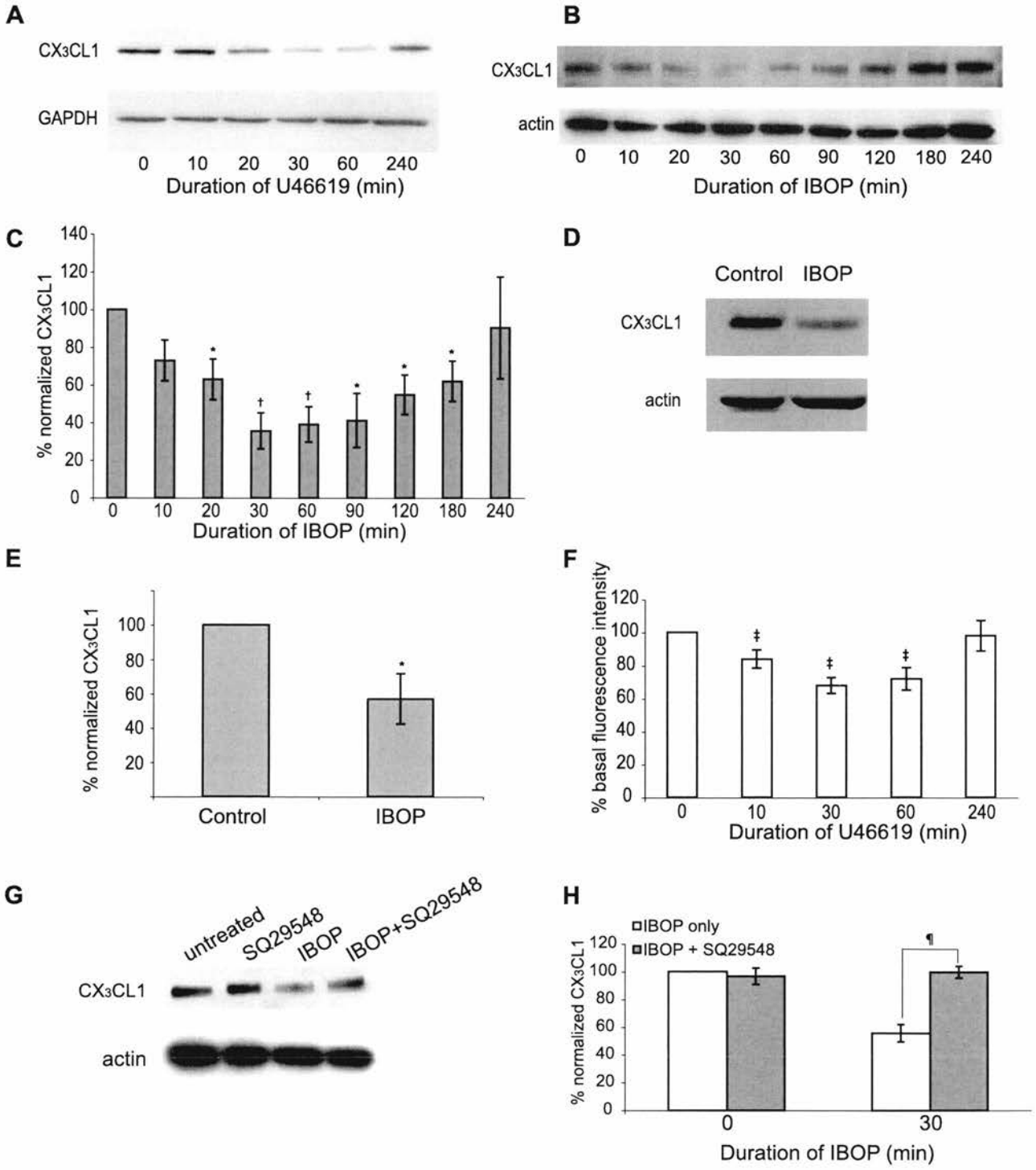

Fig. 1. Thromboxane prostanoid (TP) receptor stimulation decreases surface and total levels of CX_3CL1. *A*: ECV-304 cells expressing green fluorescent protein-tagged CX_3CL1 (ECV-CX_3CL1-GFP) were incubated with U46619 (20 μM) for the indicated time periods. Cell lysates were harvested, and immunoblotting was performed using anti-CX_3CL1 antibody (Ab; 0.2 μg/ml) and horseradish (HRP)-conjugated secondary Ab. To control for protein loading, blots were stripped and reprobed with anti-GAPDH Ab and HRP-conjugated secondary Ab. *B*: cells were incubated with IBOP (0.1 μg/ml), and immunoblotting was performed as described in *A*. To control for protein loading, blots were stripped and reprobed with anti-actin Ab and HRP-conjugated secondary Ab. *C*: experiments were performed as described in *B*. Band intensities for CX_3CL1 were quantified and normalized to actin. Values are means ± SE for 4 separate experiments. $^*P = 0.05$; $^\dagger P < 0.01$ vs. untreated. *D*: ECV-CX_3CL1 cells were incubated with IBOP (0.1 μg/ml) for 30 min, and immunoblotting was performed as described in *B*. *E*: experiments were performed as described in *D*. Band intensities for CX_3CL1 were quantified and normalized to actin. Values are means ± SE for 3 separate experiments. $^*P < 0.01$. *F*: ECV-CX_3CL1-GFP cells were incubated with U46619 (20 μM) for the indicated time periods, fixed, and labeled with anti-CX_3CL1 Ab (2.5 μg/ml) and PE-conjugated secondary Ab, and cell surface CX_3CL1 expression was measured using flow cytometry. Results are means ± SE expressed as a percentage of control fluorescence for 5 separate experiments. $^\ddagger P < 0.05$. *G*: cells were incubated with IBOP (0.1 μg/ml) for 30 min after preincubation with the specific TP antagonist SQ29548 (10 μM for 15 min), and immunoblotting was performed as described in *B*. *H*: experiments were performed as described in *G*. Band intensities for CX_3CL1 were quantified and normalized to actin. Values are means ± SE for 3 separate experiments. $^\P P < 0.05$.

cells using gentle rocking at 10 cycles/min. Nonadherent cells were washed away, and remaining cells were fixed and mounted onto slides. Using a Leica deconvolution microscope, we examined at least 50 high-power fields (×63) to count the number of adherent cells. Results represent the mean values (±SE) and were compared using Student's *t*-test.

To examine localized changes in CX_3CL1 expression at the point of contact with adherent leukocytes, ECV-304 cells were plated in six-well plates and grown to 50% confluence. Cells were transfected with CX_3CL1-mCherry cDNA (1.0 μg) using FuGene HD (Roche Diagnostics). After 36 h, adhesion assays were performed by incu-

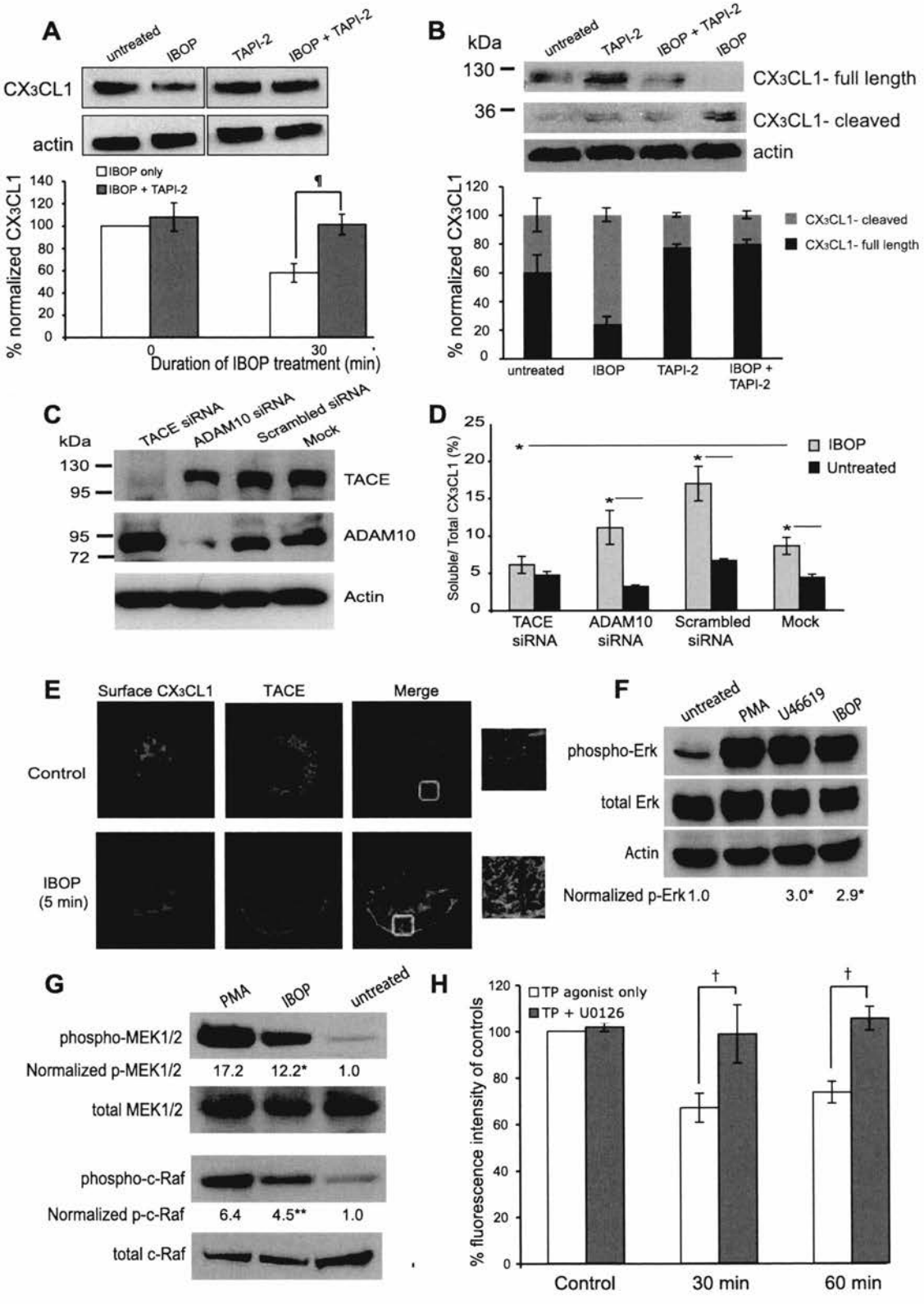

bating ECV-CX_3CL1-mCherry cells with K562-CX_3CR1 cells (5×10^5 cells/well) in the presence or absence of IBOP (2.5 μg/ml). To prevent inadvertent shedding of CX_3CL1 from the plasma membrane, ECV-CX_3CL1-mCherry cells in some wells were incubated with the metalloprotease inhibitor GM6001 for 4 h before experiments were performed. To rule out any inadvertent effects of TP stimulation on cell surface expression and mobility of the CX_3CL1 receptor CX_3CR1, K562-CX_3CR1 cells were fixed using 4% paraformaldehyde and washed with glycine (100 mM) in PBS just before adhesion assays were performed. K562-CX_3CR1 cells were allowed to adhere for 30 min at 37°C under gentle rocking conditions and then gently washed twice with PBS to remove nonadherent cells. Cells were fixed and permeabilized using 0.1% Triton, and K562-CX_3CR1 cells were labeled by incubation with anti-Bcr Ab (2 μg/ml) followed by Alexa-Fluor 488-conjugated anti-mouse IgG secondary Ab (23). Spinning disk confocal microscopy was performed, and *Z*-stack images were captured. *XY* or *YZ* dimensions of the *Z*-stack images were used to compare the localized fluorescence intensity CX_3CL1-mCherry signal on transfected ECV-304 cells at the point of interface with adherent K562-CX_3CR1 cells with the CX_3CL1-mCherry fluorescent signal in an adjacent region of similar size in the plasma membrane, where no leukocyte was attached. Fluorescent signals were quantified using ImageJ software (National Institutes of Health), and the ratio of signal intensities between site of contact and site of no contact was measured for 24 randomly chosen cells for each treatment condition. Experiments were performed three separate times.

CX_3CL1 shedding experiments. Small interfering RNA (siRNA) directed against human ADAM10, human TACE, and control nontargeting siRNA were purchased from Santa Cruz Biotechnology. ECV-CX_3CL1 cells were electroporated with siRNA by nucleofection (Amaxa, Gaithersburg, MD) on *day 0* and *day 2*. After the second electroporation, cells were plated in six-well tissue culture plates at a density of 1×10^5 cells/well and cultured for 48 h. Cells were incubated with IBOP (2.5 μg/ml) for 30 min at 37°C, and conditioned medium was collected. Cells were washed once with PBS and lysed by adding 0.5 ml of RIPA buffer. Protease inhibitor cocktail (Sigma) was added (1:100) to both harvested conditioned medium and cell lysis buffer to prevent protein degradation. Supernatants and cell lysates were cleared by centrifugation at 13,000 rpm at 4°C for 10 min. With the use of fresh samples, CX_3CL1 was detected in conditioned medium and cell lysates using a CX_3CL1 ELISA kit (R&D Systems, Minneapolis, MN) according to the manufacturer's specifications. Three independent experiments were performed, and the data are expressed as the mean (±SE) percentage of soluble CX_3CL1 released into the medium in relation to the total amount of CX_3CL1 (soluble and cell associated).

Statistical analyses. The data were analyzed by comparing the mean values using Student's *t*-test. A value of $P < 0.05$ was considered significant.

RESULTS

Stimulation of the TP receptor decreases surface and total levels of CX_3CL1. When ECV-CX_3CL1-GFP cells were treated with two distinct TP agonists, total levels of CX_3CL1, measured by immunoblotting, fell after just 10 min, with the nadir observed at 30 min (Fig. 1, *A–C*). When experiments were performed using cells that express untagged CX_3CL1, TP stimulation provoked a similar fall in the levels of CX_3CL1 (Fig. 1, *D* and *E*; $P < 0.02$). Cell surface CX_3CL1, measured by flow cytometry, also rapidly fell, reaching minimum levels by 30 min (Fig. 1*F*; $P < 0.05$). Although TP stimulation promoted a significant decrease in both total and cell surface CX_3CL1, the magnitude of the changes was not identical, presumably because the inherent differences in the two methodologies used resulted in a differential ability to detect CX_3CL1. We further found that the specific TP antagonist SQ29548 prevented loss of CX_3CL1, verifying the specificity of the response (Fig. 1, *G* and *H*). Thus TP activation promotes reduction of surface and total levels of CX_3CL1.

TP stimulation induces cleavage of CX_3CL1 by TACE. We questioned whether TP stimulation results in shedding of CX_3CL1 from the plasma membrane, a process mediated by ADAM10 and TACE (12, 17, 43). Consistent with this notion, the metalloprotease inhibitors TAPI-2 and GM6001, which inhibit both ADAM10 and TACE, prevented TP-induced loss of CX_3CL1 (Fig. 2*A*, $P < 0.02$; data not shown for GM6001). To verify these findings, we performed immunoblotting using an antibody directed against GFP, conjugated to the cytoplasmic domain of CX_3CL1 (Fig. 2*B*). TP stimulation resulted in loss of full-length CX_3CL1 ($P < 0.01$) and appearance of a small cell-associated species of CX_3CL1 ($P < 0.01$) after shedding of the extracellular domain of the chemokine (Fig. 2*B*). These events were prevented by TAPI-2 (Fig. 2*B*). To determine whether ADAM10 and/or TACE induced the ob-

Fig. 2. TP stimulation induces cleavage of CX_3CL1 by tumor necrosis factor-α-converting enzyme (TACE). *A*, *top*: ECV-CX_3CL1 cells were incubated with metalloprotease inhibitor TAPI-2 (10 μM for 2 h) and then with IBOP (0.1 μg/ml for 30 min), and immunoblotting was performed using anti-CX_3CL1 Ab. Blots were stripped and reprobed with anti-actin Ab. *Bottom*, CX_3CL1 band intensities normalized to actin. Values are means ± SE for 4 separate experiments. ¶$P < 0.02$. *B*, *top*: experiments were performed as described in *A*, and immunoblotting was performed using anti-GFP Ab. *Bottom*, proportion of full-length and cleaved CX_3CL1 detected for each experimental condition. Values are means ± SE for 3 separate experiments. For full-length and cleaved CX_3CL1: $P < 0.01$, untreated vs. IBOP; $P < 0.0001$, IBOP vs. IBOP + TAPI-2. *C*: cells were electroporated with TACE small interfering RNA (siRNA), ADAM10 siRNA, or control, nontargeting (scrambled) siRNA on *days 0* and *2*. After 48 h, cell lysates were harvested, and immunoblotting was performed using anti-TACE and anti-ADAM10 Ab. *D*: cells were electroporated with the indicated siRNA and incubated with IBOP (30 min), conditioned medium was collected, and cell lysates were harvested. Protease inhibitor cocktail was added to conditioned medium and to cell lysis buffer to prevent protein degradation. Supernatants and cell lysates were cleared by centrifugation. With the use of fresh samples, CX_3CL1 was measured using a CX_3CL1 ELISA kit (R&D Systems). Values are means ± SE, expressed as the percentage of soluble CX_3CL1 released into the conditioned medium relative to the total amount of CX_3CL1 (soluble and cell associated), for 3 separate experiments. *$P < 0.03$. *E*: cells were incubated with IBOP (5 min), and cell surface CX_3CL1 and TACE were immunofluorescently labeled. Images at *right* show a magnified view of the indicated areas. Colocalization between CX_3CL1 and TACE was assessed using Volocity software. Representative photographs show 16 cells from 3 independent experiments. *F*: cells were incubated with PMA (1 μM), U46619, or IBOP for 30 min, cell lysates were harvested, and immunoblotting was performed using anti-phospho-Erk Ab. To control for protein loading, blots were stripped and reprobed with anti-Erk Ab and anti-actin Ab. Phospho-Erk band intensities were normalized to total Erk. Values are means ± SE for 3 separate experiments. *$P < 0.01$ vs. control. *G*: cells were incubated with PMA or IBOP, and immunoblotting was performed using anti-phospho-MEK1/2 and anti-phospho-c-Raf Ab. Blots were stripped and reprobed with anti-MEK1/2 Ab and anti-c-Raf Ab. Phospho-MEK1/2 and phospho-c-Raf band intensities were normalized to total MEK1/2 and total c-Raf, respectively. Values are means ± SE for 4 separate experiments. *$P < 0.01$; **$P < 0.05$ vs. control. *H*: cells were incubated with U46619 after pretreatment with the Erk inhibitor U0126 (5 μM for 30 min). Cell surface CX_3CL1 was detected by flow cytometry. Values are means ± SE, expressed as the percentage of control fluorescence intensity, for 4 separate experiments. ÷$P < 0.05$.

served proteolysis of CX_3CL1, we used siRNA to selectively knock down expression of each protease (Fig. 2*C*) and measured soluble levels of CX_3CL1 generated. In the presence of nontargeting siRNA or ADAM10 siRNA, TP stimulation promoted release of soluble CX_3CL1 (Fig. 2*D*, $P < 0.03$). In the absence of TACE, TP failed to promote shedding of CX_3CL1 (Fig. 2*D*). In keeping with these observations, CX_3CL1 and TACE, which did not colocalize on the cell surface under basal conditions, coassociated after 5 min of TP stimulation, yielding a Pearson's correlation coefficient (r) greater than 0.5 (Fig. 2*E*; basal: $r = 0.429 \pm 0.042$, $P > 0.05$; IBOP: $r = 0.645 \pm 0.031$, $P < 0.01$). After TP stimulation, the increase in soluble CX_3CL1 detected in the medium was not the same as the decrease in the amount of cell-associated chemokine. Although the magnitude of the individual changes is statistically significant, there is likely differential sensitivity of the two assays used to detect soluble and cell-associated CX_3CL1 present. It is further possible that some of the soluble CX_3CL1 released by proteolytic shedding could be bound to the surface of cells or to the underlying extracellular matrix, resulting in a failure to detect it by ELISA.

Since TP can activate a number of signaling pathways, we studied the intracellular mechanisms whereby TP causes shedding of CX_3CL1. TP promoted rapid phosphorylation of Erk (Fig. 2*F*, $P < 0.01$) and its upstream effectors, MEK1/2 (Fig. 2*G*, $P < 0.01$) and c-Raf (Fig. 2*G*, $P < 0.05$) (7). Erk inhibition prevented TP-induced loss of surface CX_3CL1 (Fig. 2*H*, $P < 0.05$). Overall, TP stimulation causes cleavage of plasmalemmal CX_3CL1 by TACE, rather than by ADAM10.

TP stimulation does not affect recycling of CX_3CL1. Because CX_3CL1 recycles between the plasma membrane and an endocytic compartment, we questioned whether TP stimulation might redistribute the chemokine from the superficial to the intracellular pool (25). To prevent inadvertent shedding of CX_3CL1 from the cell surface, cells were preincubated with GM6001 and endocytosis was examined by FRAP, irreversibly photobleaching the entire CX_3CL1-containing intracellular compartment, as previously described (25, 43). Recovery of fluorescence, an index of internalization of CX_3CL1 from the plasma membrane, was recorded over time (25). Fluorescence of the plasma membrane pool remained largely unaffected by the bleaching procedure and was also monitored. Figure 3 depicts a cell before, immediately after, and 5 min after bleaching. Note that the plasmalemmal fluorescence decreased as the juxtanuclear fluorescence recovered, consistent with delivery of unbleached CX_3CL1-GFP from the former to the latter compartment. The juxtanuclear CX_3CL1-GFP compartment recovered to $21.5 \pm 3.1\%$ of its original fluorescence by 170 s and was unchanged by TP stimulation (Fig. 3*D*).

To test whether TP stimulation affects delivery of internalized CX_3CL1 back to the plasma membrane, shedding of the chemokine was inhibited using GM6001, and the endomembrane pool was loaded by incubation with CX_3CL1 Ab at 37°C. Ab bound to the surface was stripped by a short exposure to an acidic solution. Cells were allowed to recover, and reinsertion of CX_3CL1 in the plasma membrane was determined by quantifying the reappearance of Ab (25). Fluorescence at the cell surface increased progressively after acid stripping, confirming that CX_3CL1 within the endomembrane compartment traffics back to the plasma membrane (Fig. 4, *A–E*, $P < 0.02$). TP stimulation did not affect this traffic (compare Fig. 4, *C* and *D*; Fig. 4*E*).

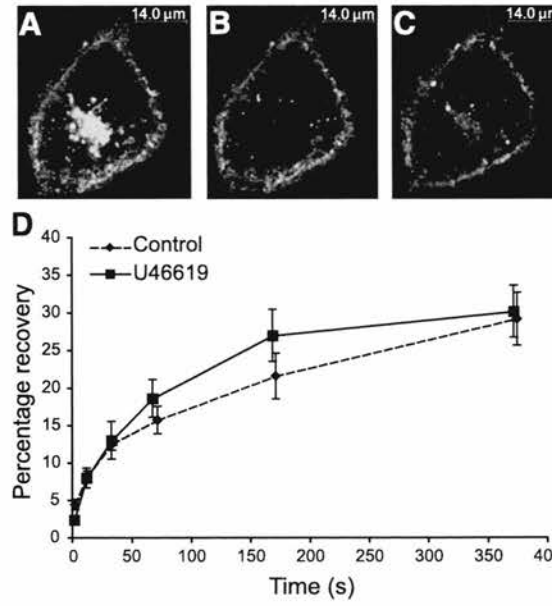

Fig. 3. TP stimulation does not alter endocytosis of CX_3CL1. ECV-CX_3CL1-GFP cells were grown on glass coverslips and incubated for 4 h with the metalloprotease inhibitor GM6001 (20 μM) to prevent inadvertent shedding of CX_3CL1 from the cell surface. Cells were incubated with U46619 (20 μM) for 30 min, and with an argon laser and scanning confocal microscope, the entire juxtanuclear CX_3CL1-containing compartment was irreversibly photobleached, and recovery of fluorescence was determined at 5- to 200-s intervals. To control for inadvertent photobleaching associated with serial image acquisition, nonbleached areas in the plasma membrane were serially observed in parallel. The same cell is shown before bleaching (*A*), immediately after photobleaching (*B*), and 5 min later (*C*). *D*: at each time point, the ratio of the fluorescence intensity of the internal compartment to the mean control membrane fluorescence intensity was calculated. Each point represents the mean ± SE for at least 6 separate experiments. Scale bar, 14 μm.

TP stimulation enhances, not inhibits, CX_3CL1-dependent leukocyte adhesion. We predicted that TP stimulation, which induces rapid loss of CX_3CL1 from the cell surface, would impair adhesion of CX_3CR1-expressing leukocytes. Minimal binding of K562 cells, which do not express CX_3CR1, to either ECV-304 or ECV-CX_3CL1-GFP cells was seen (data not shown). Likewise, there was very little adhesion of K562-CX_3CR1 cells to ECV-304 cells, which do not express CX_3CL1 (Fig. 5*A*) (10). K562-CX_3CR1 leukocytes effectively adhered to ECV-CX_3CL1-GFP cells (Fig. 5*A*). The presence of plasmalemmal CX_3CL1 increased leukocyte adhesion fourfold (Fig. 5*A*, $P < 0.0000001$). Unexpectedly, TP stimulation increased rather than decreased adhesion of K562-CX_3CR1 leukocytes to ECV-CX_3CL1-GFP cells (Fig. 5*A*, $P < 0.05$). TP stimulation did not increase adhesion of K562-CX_3CR1 cells to untransfected ECV-304 cells, ruling out upregulated levels of other adhesion molecules as the cause of the enhanced leukocyte binding observed (Fig. 5*A*) (10).

To verify that the observed responses were not an idiosyncratic feature of the transformed cell lines, we performed experiments performed using primary human vascular endothelial cells. Upon TNF-α stimulation, endogenous expression of CX_3CL1 increased fivefold (Fig. 5*B*, $P < 0.01$). TP stimulation caused a rapid fall in total levels of CX_3CL1 (Fig. 5*B*,

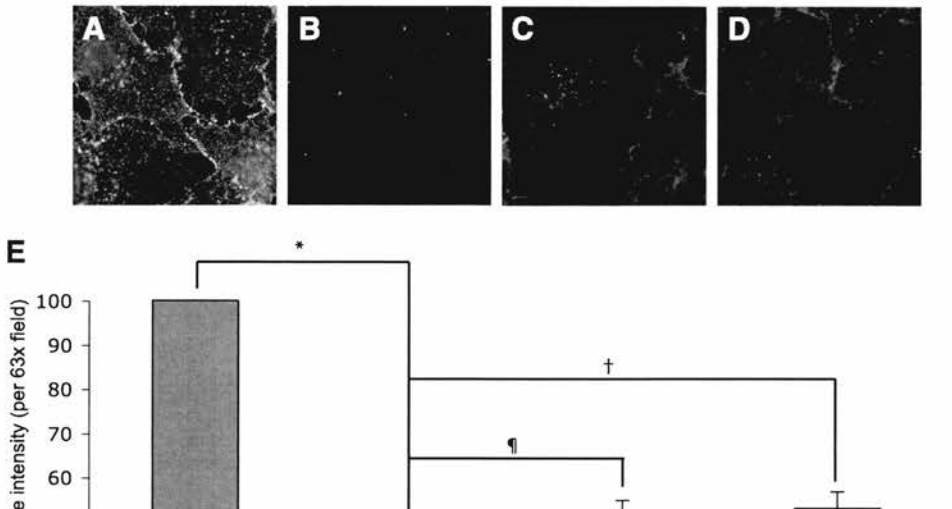

Fig. 4. TP stimulation does not affect traffic of internalized CX_3CL1 to the plasma membrane. ECV-CX_3CL1 cells were incubated with anti-CX_3CL1 Ab (2.5 μg/ml) at 37°C for 1 h, and then membrane-associated Ab was removed by acid wash (pH 2.5) at 4°C for 2 min. Cells were allowed to recover for 30 min in the presence or absence of IBOP (0.1 μg/ml) and were then washed, fixed, and stained with Cy3-conjugated secondary Ab. In all experiments, cells were preincubated with the metalloprotease inhibitor GM6001 (20 μM for 4 h) to prevent cleavage of CX_3CL1 from the cell surface. Immunofluorescent images show cells before acid stripping (*A*), immediately afterward (*B*), and 30 min after recovering from acid shock in the presence (*C*) or absence (*D*). *E*: cell surface immunofluorescence was quantified using Volocity software. Values are means ± SE of at least 30 fields per condition from 3 separate experiments. $^*P < 0.001$. $^\dagger P < 0.03$. $^\P P < 0.02$.

$P < 0.05$). In keeping with these results, TP stimulation significantly enhanced proteolytic release of soluble CX_3CL1 ($P < 0.005$, Fig. 5*C*). The enhanced shedding of CX_3CL1 was prevented when activation of TACE was blocked ($P < 0.005$, Fig. 5*C*). When HUVEC were incubated with TNF-α, adhesion of K562-CX_3CR1 cells increased by 30% (Fig. 5*D*; $P < 0.005$). In this instance, preincubation of endothelial cells with specific function-blocking anti-CX_3CL1 Ab significantly decreased the number of bound leukocytes (Fig. 5*D*, $P < 0.05$). Similarly, TNF-α activation increased binding of primary PBMC 10-fold (Fig. 5*E*, $P < 0.001$). Although TP stimulation resulted in loss of cell-associated CX_3CL1, K562-CX_3CR1 cell adhesion increased by 70% (Fig. 5*D*, $P < 0.005$) and PBMC adhesion increased by 50% (Fig. 5*E*, $P < 0.001$). Preincubation of endothelial cells with anti-CX_3CL1 Ab prevented TP-induced leukocyte adhesion, confirming the observed increase in binding was CX_3CL1 dependent (Fig. 5*D*, $P < 0.01$; Fig. 5*E*, $P < 0.001$). Using a specific antagonist of TP, SQ29548, we verified that the observed increase in leukocyte adhesion was directly related to TP stimulation (Fig. 5*F*, $P < 0.005$). Blocking activation of TACE using the Erk inhibitor U0126 also prevented TP-induced increase in leukocyte adhesion (Fig. 5*F*, $P < 0.001$). Together, these data demonstrate that TP stimulation increases leukocyte adhesion to cell surface CX_3CL1 despite reducing the overall amount of the chemokine present on the plasma membrane.

TP stimulation mobilizes plasmalemmal CX_3CL1 and induces clustering of CX_3CL1 at sites of contact with adherent leukocytes. In principle, increased leukocyte binding to CX_3CL1 could occur despite reduced CX_3CL1 levels if TP stimulation mobilized and redistributed plasmalemmal CX_3CL1, allowing the chemokine to move to sites of contact with CX_3CR1 on leukocytes. TP stimulation could thereby increase the overall avidity of ligand-receptor interactions, strengthening adhesion between CX_3CR1-expressing leukocytes and CX_3CL1-expressing adherent cells.

To test this notion, an area of CX_3CL1-GFP in the plasma membrane was irreversibly photobleached and recovery of fluorescence was serially observed (Fig. 6*A*, prebleaching; Fig. 6*B*, immediately after bleaching; Fig. 6*C*, 5 min after bleaching). As a control, CX_3CL1-expressing cells were transfected with cDNA encoding freely mobile GPI-GFP, and recovery of fluorescence was similarly observed (Fig. 6, *D–F*). CX_3CL1-GFP fluorescence recovered poorly compared with GPI-GFP (Fig. 6, *G* and *H*). For CX_3CL1-GFP, only 25.8 ± 2.6% of fluorescence of the bleached area recovered after 60 s, compared with 85.0 ± 2.9% of GPI-GFP (Fig. 6*H*). As another control, ECV-CX_3CL1 cells were transfected with DNA encoding the single transmembrane-spanning protein, FcγRIIA, conjugated to GFP (FcγRIIA-GFP). FcγRIIA receptors were highly mobile, as indicated by the rapid and near complete recovery of fluorescence after photobleaching (Fig. 6*H*). These data demonstrate that lateral diffusion of transmembrane CX_3CL1 within the membrane is highly impeded, rendering the chemokine largely immobile.

IBOP treatment significantly enhanced mobility of plasmalemmal CX_3CL1, resulting in fluorescence recovery of 48.2 ± 6.2% at 55 s postbleaching, compared with 26.3 ± 2.5% recovery in the absence of IBOP (Fig. 6*G*, $P < 0.05$). After TP-induced ectodomain shedding of CX_3CL1, we reasoned that it might not be possible to distinguish between reappearance of GFP fluorescence due to movement of full-length CX_3CL1 or to

movement of any COOH-terminal cleavage fragments retained within the plasma membrane. To prevent potential shedding of CX_3CL1, cells were pretreated with the metalloprotease inhibitor GM6001. Accordingly, GM6001 did not affect basal mobility of CX_3CL1 (Fig. 6*H*). In the presence of GM6001, TP similarly mobilized CX_3CL1. The bleached area recovered to 55.5 ± 3.5% by 1 min, significantly greater than the 27.7 ± 2.5% recovery observed in the absence of TP stimulation (Fig. 6*H*, $P < 0.001$). At all time points after 20 s, TP facilitated recovery of fluorescence of plasmalemmal CX_3CL1 (Fig. 6*H*,

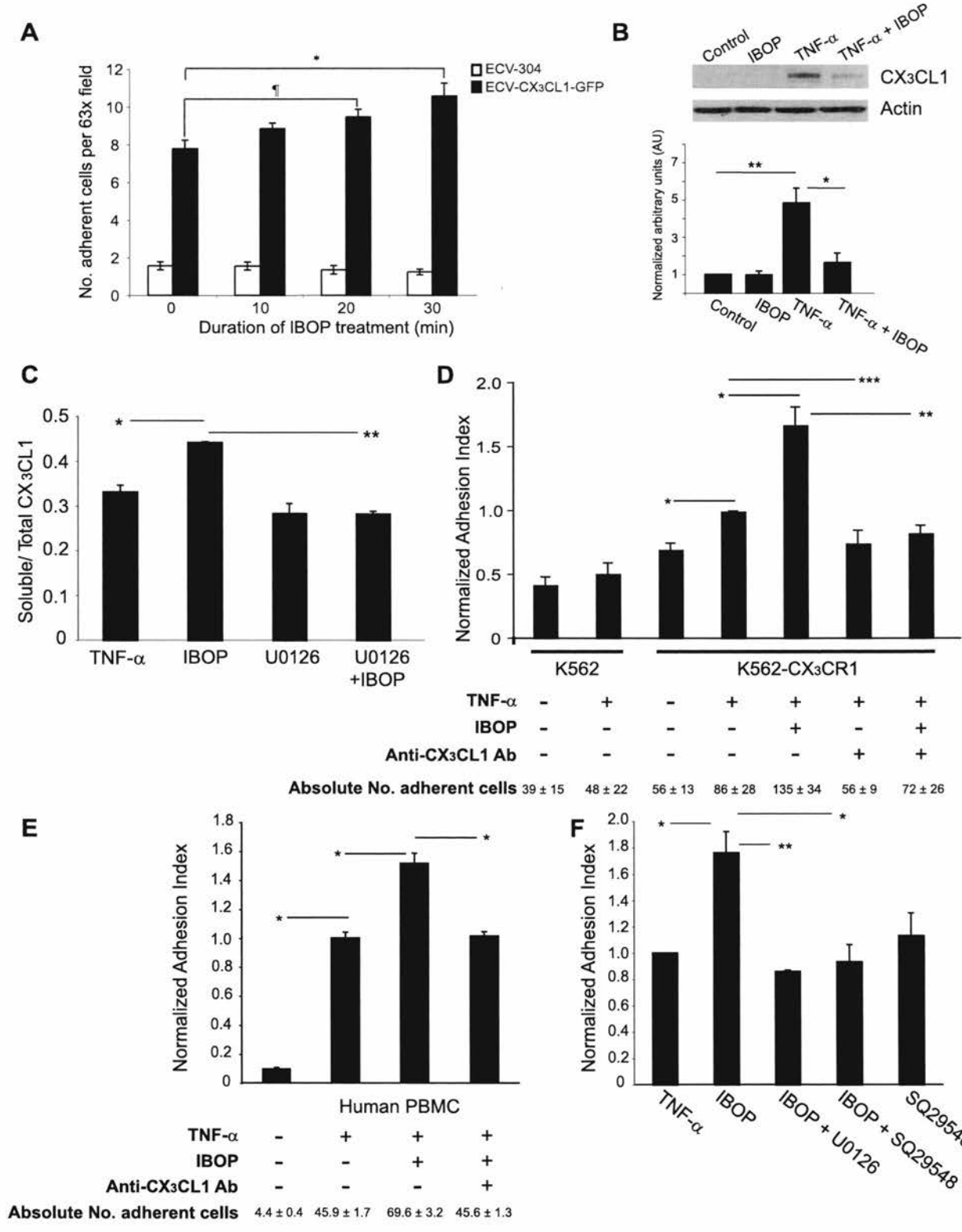

$P < 0.03$ at each point). Thus TP stimulation enhances lateral mobility of CX_3CL1, which is normally tethered within the plasma membrane.

We directly examined whether TP stimulation promotes clustering of CX_3CL1 at sites of contact with CX_3CR1 on adherent leukocytes, by comparing the fluorescent signal of CX_3CL1 at these contact points to that of CX_3CL1 at adjacent sites where no leukocyte was tethered. We reasoned that TP stimulation could conceivably affect mobility of CX_3CR1 receptor present on the surface of leukocytes, resulting in enhanced adhesion between these cells and CX_3CL1-expressing cells. To selectively study the effects of TP stimulation on clustering of plasmalemmal CX_3CL1, leukocytes were prefixed, effectively converting them to "beads" coated with CX_3CR1 (4). After TP stimulation, the ratio of contact site CX_3CL1 to non-contact site CX_3CL1 was greater than in unstimulated cells (Fig. 6, *I* and *J*; control: 1.1 ± 0.1 vs. TP stimulated: 1.7 ± 0.2; Fig. 6*K*, $P < 0.005$). A ratio greater than one was seen in approximately one-half (46%) of unstimulated cells. After TP stimulation, 83% had a ratio greater than one, indicating clustering of CX_3CL1. Collectively, these results demonstrate that TP stimulation promotes rapid shedding of plasmalemmal CX_3CL1 but that despite decreased cell surface levels of the chemokine, CX_3CL1-dependent adhesion of leukocytes is enhanced due to mobilization and clustering of the chemokine at contact sites with adherent leukocytes. In this manner, although net cell surface exposure of CX_3CL1 is decreased, the overall avidity of interactions between leukocytes and CX_3CL1 on the surface of adherent cells is actually strengthened.

DISCUSSION

The principal aim of this study was to examine regulation of CX_3CL1 by TP. For these studies, we used CX_3CL1-expressing ECV-304 cells and primary human vascular endothelial cells. Although derived from bladder epithelial carcinoma cells, ECV-304 cells have many endothelial features, including the propensity to grow in monolayers of flattened cells, formation of moderately tight intercellular junctions, and expression of the endothelial markers Flt-1 and von Willebrand factor (14, 16, 39). Since the identification of CX_3CL1, ECV-304 cells have been used extensively to study distribution, cleavage, and function of the chemokine, because the surface levels of CX_3CL1 mirror those seen in cytokine-activated primary vascular endothelial cells and because expression of other cellular adhesion molecules is minimal (10, 17, 25, 43). We previously showed that addition of a GFP tag alters neither distribution nor subcellular traffic of CX_3CL1 (25). To confirm the key findings of the current study, assays were performed using primary human vascular endothelial cells.

Overall exposure of CX_3CL1 at the cell surface reflects the balance between shedding and recycling. Thus, in principle, the TP-induced decrease in CX_3CL1 could result from *1*) increased endocytosis, *2*) decreased traffic of internalized CX_3CL1 back to the plasma membrane, and/or *3*) increased shedding from the cell surface. TP stimulation did not acutely alter recycling of the chemokine. Sustained TP stimulation (4–24 h) has been shown to augment expression of the vascular adhesion molecules, intercellular adhesion molecule-1 (ICAM-1), vascular adhesion molecule-1 (VCAM-1), and E-selectin (19, 31). The resultant increase reflected enhanced nuclear factor (NF)-κB-dependent transcription and translation (19, 31). ICAM-1 expression is significantly reduced in genetically targeted mice lacking TP, again illustrating the ability of TP to increase adhesion molecule expression over time (22). Likewise, prolonged TP stimulation enhances expression of the chemokine CCL2 (monocyte chemoattractant protein-1, MCP-1), also through protein kinase C and NF-κB (20). To our knowledge, ours is the first study to examine how TP activation posttranslationally regulates cell surface exposure of an endothelial adhesion molecule or chemokine.

Blocking TACE, but not ADAM10, attenuated TP-induced shedding of CX_3CL1 from the cell surface. Erk inhibition similarly blocked CX_3CL1 shedding, consistent with studies demonstrating that TP engagement promotes protein kinase C activation and Erk phosphorylation (11, 30). Erk, in turn, phosphorylates the cytoplasmic domain of TACE at Thr^{735} and Ser^{819}, thereby activating the protease (7, 9). Blocking this phosphorylation prevents activation of TACE and ectodomain shedding of its biological substrates (7, 9). Overall, our results demonstrate that TP stimulation causes rapid loss of CX_3CL1 from the cell surface by promoting TACE-induced, but not

Fig. 5. TP stimulation enhances CX_3CL1-dependent leukocyte adhesion. *A*: K562 cells that express the CX_3CR1 receptor (K562-CX_3CR1) were labeled with Alexa555-conjugated cholera toxin B (0.5 μg/ml) for 30 min to visualize them. ECV-304 and ECV-CX_3CL1-GFP cells were grown to confluence on 25-mm coverslips and treated with IBOP (0.1 μg/ml) for 30 min. K562-CX_3CR1 cells (5×10^5/well) were incubated with ECV-304 or ECV-CX_3CL1-GFP monolayers under gentle rocking conditions (10 cycles/min) at 37°C for the times indicated. Nonadherent cells were removed by washing, and the remaining cells were fixed. Serial fields (×63) were examined using a Leica deconvolution microscope, and the numbers of adherent cells were counted. Values are the mean (±SE) number of adherent K562-CX_3CR1 cells from at least 3 experiments. $*P < 0.01$. $¶P < 0.02$. *B*, *top*: confluent monolayers of human umbilical vein endothelial cells (HUVEC) were incubated with TNF-α (100 U/ml) for 4 h and then with IBOP for 30 min. Cell lysates were harvested, and immunoblotting was performed using anti-CX_3CL1 and anti-actin Ab. *Bottom*, CX_3CL1 band intensities were normalized to actin. Values are means ± SE from 3 separate experiments. $*P < 0.03$. $**P < 0.01$. *C*: HUVEC were grown to confluence and stimulated with TNF-α as describe in *B*, followed by IBOP (0.1 μg/ml for 30 min). In some instances, cells were incubated with U0126 (5 μM) for 30 min before incubation with IBOP. Conditioned medium was collected and cell lysates were harvested. Protease inhibitor cocktail was added to conditioned medium and to cell lysis buffer to prevent protein degradation. Supernatants and cell lysates were cleared by centrifugation. With fresh samples, CX_3CL1 was measured using a CX_3CL1 ELISA kit. Values are means ± SE of the fraction of soluble CX_3CL1 released into the conditioned medium relative to the total amount of CX_3CL1 (soluble and cell associated) from 3 separate experiments. $*P < 0.002$. $**P < 0.0001$. *D*: HUVEC were stimulated with TNF-α, and adhesion assays were performed as described in *A* using K562 or K562-CX_3CR1 cells. In some experiments, HUVEC were preincubated with blocking anti-CX_3CL1 Ab (1 μg/ml) for 30 min. The number of adherent leukocytes was normalized to the number of cells adherent to TNF-α-stimulated HUVEC. Values are means ± SE from 4 independent experiments. $*P < 0.005$. $**P < 0.01$. $***P < 0.05$. *E*: adhesion assays were performed as described in *C* using freshly isolated human peripheral blood mononuclear cells (PBMC). Values are means ± SE from 4 independent experiments. $*P < 0.001$. *F*: adhesion assays were performed as described in *D* using K562-CX_3CR1 cells and TNF-α-stimulated HUVEC. In some experiments, HUVEC were preincubated with U0126 (5 μM for 30 min) or SQ29548 (10 μM for 15 min) before incubation with IBOP. The number of adherent leukocytes was normalized to the number of cells adherent to TNF-α-stimulated HUVEC. values are means ± SE from 3 independent experiments. $*P < 0.005$. $**P < 0.001$.

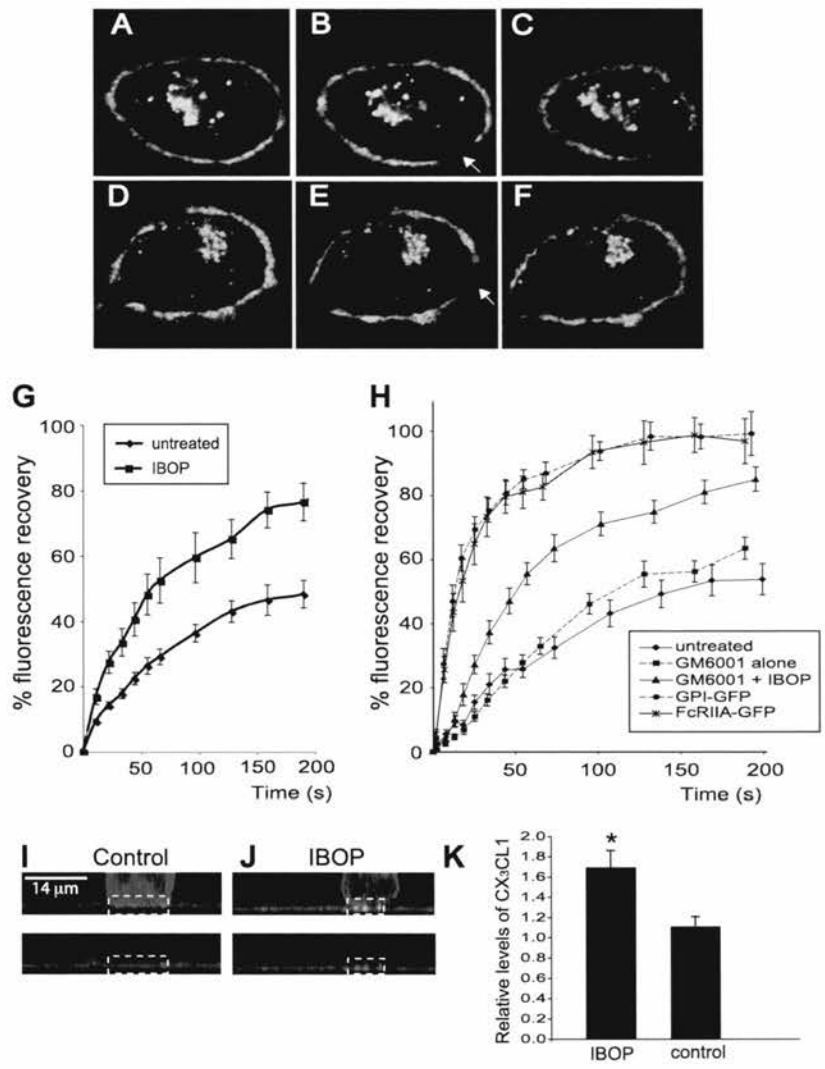

Fig. 6. TP stimulation mobilizes plasmalemmal CX_3CL1 and induces clustering of CX_3CL1 at sites of contact with adherent leukocytes. With the use of ECV-CX_3CL1-GFP cells, fluorescence recovery after photobleaching (FRAP) was performed as described in MATERIALS AND METHODS. *A*: confocal image of single cell (×100). *B*: a region within the plasma membrane was irreversibly photobleached (see arrow). *C*: same cell 5 min after photobleaching. *D–F*: as a control, the membrane mobility of glycosylphosphatidylinositol (GPI)-linked GFP in transfected ECV-CX_3CL1 cells was determined in the same manner. *G*: cells were incubated with IBOP (0.1 μg/ml) for 30 min, and fluorescence recovery of the photobleached area was monitored over time. Values are means ± SE from 9 separate experiments per condition. $P < 0.05$, untreated vs. IBOP at all time points after 11 s. *H*: recovery of fluorescence of the photobleached area was measured over time. In some experiments, ECV-CX_3CL1-GFP cells were preincubated with GM6001 (20 μM for 2 h), to inhibit cleavage of CX_3CL1 from the cell surface, and then incubated with IBOP (0.1 μg/ml) for 30 min. In some experiments, ECV-CX_3CL1 cells were transfected with cDNA encoding GFP-conjugated FcγRIIA. Recovery of fluorescence after photobleaching of untreated ECV-CX_3CL1-GFP, GM6001-treated ECV-CX_3CL1-GFP, and GM6001-treated ECV-CX_3CL1-GFP stimulated with IBOP, GPI-GFP, or FcγRIIA-GFP was measured. At each time point, fluorescence intensity in the bleached region was normalized to the mean control unbleached membrane fluorescence intensity. Values are means ± SE from 5–9 separate experiments per condition. *I* and *J*: ECV-304 cells were transfected with CX_3CL1-mCherry cDNA. Adhesion assays were performed by incubating ECV-CX_3CL1-mCherry cells for 30 min with K562-CX_3CR1 cells (5×10^5/well) in the presence (*J*) or absence (*I*) of IBOP. To prevent unwanted shedding of CX_3CL1, in some wells ECV-CX_3CL1-mCherry cells were preincubated with GM6001. To rule out potential effects of TP stimulation on cell surface clustering of CX_3CR1, K562-CX_3CR1 cells were first fixed using 4% paraformaldehyde and then washed with 100 mM glycine. At the end of the adhesion assay, cells were fixed and permeabilized, and K562-CX_3CR1 cells were visualized by labeling with anti-BCR Ab and Alexa488-conjugated secondary Ab. *Z*-stack images are from spinning disk confocal microscopy (×63). *K*: experiments were performed as described in *I* and *J*. *XY* or *YZ* dimensions of the *Z*-stack images were used to compare the localized fluorescence intensity of CX_3CL1-mCherry at sites of interface with adherent K562-CX_3CR1 cells with the signal in an adjacent, similar-size region in the plasma membrane, where no leukocyte was attached. With the use of ImageJ software, the ratio of fluorescent signal intensities between the site of contact and site of no contact was measured for 24 randomly chosen cells for each treatment condition. Values are means ± SE from 3 separate experiments. *$P < 0.005$ vs. control.

ADAM10-induced, shedding of CX_3CL1, rather than by interfering with recycling of the chemokine.

Despite inducing proteolysis of approximately one-half the CX_3CL1 present, TP augmented CX_3CL1-dependent leukocyte adhesion. Although unexpected, this is not inconceivable, since the overall binding of CX_3CR1 receptor on the leukocyte is determined by two distinct factors, namely, the density of CX_3CL1 ligand present and the mobility of CX_3CL1 within the plasma membrane. We hypothesized that TP stimulation must increase the avidity of remaining CX_3CL1 for its receptor. In

principle, this could occur through mobilization of plasmalemmal CX_3CL1 and subsequent clustering of the chemokine at points of contact with adherent leukocytes. Accordingly, plasmalemmal CX_3CL1 was relatively immobile under basal conditions but became highly mobile following TP stimulation. We previously reported that plasmalemmal CX_3CL1 is also immobile in other cell types under basal conditions (8). TP stimulation promoted clustering of CX_3CL1 at contact interfaces with bound leukocytes. Similarly, Kobayashi et al. (22) reported less leukocyte rolling and adherence in mice lacking TP, perhaps due to the absence of TP-induced clustering of CX_3CL1 on the surface of the vascular wall. Our results are reminiscent of a study demonstrating that isoprostane $iPF_{2\alpha}$-III, a known agonist of TP, enhances neutrophil adhesion to endothelial cells despite no increase in expression of endothelial adhesion molecules (1, 46). Although the authors postulated that release of an unknown endothelial activating factor was responsible, isoprostane activation might also increase mobility of plasmalemmal adhesion molecules, thereby strengthening the avidity of interactions between neutrophils and endothelial cells.

Our results differ somewhat from those of Hundhausen et al. (17), who reported that the synthetic phorbol ester PMA inhibited adhesion of THP-1 monocytic cells to CX_3CL1-expressing adherent cells. Several possible explanations for this apparent discrepancy exist. First, THP-1 cells express other adhesion receptors whose levels and function may be modulated by PMA stimulation. In our study, we purposely used CX_3CR1-expressing K562 cells, which do not express adhesion molecules such as L-selectin (10). Thus any adhesion observed was presumably attributable to interactions between leukocyte CX_3CR1 and CX_3CL1 on the surface of adherent cells. Stimulation by PMA and TP may have differential effects on the cell. TP receptors couple to G_q/G_{11}, with most functioning attributed to signaling via the α- rather than $\beta\gamma$-subunits (21). Thus stimulation by PMA or TP can activate phospholipase C, generating inositol triphosphate (IP_3) and diacylglycerol (DAG), increasing intracellular calcium concentration, and activating protein kinase C (21). In primary human cells, TP also couples to G_i and to $G_{12/13}$ and is linked to cAMP (15, 21). Thus the TP receptor has the potential to utilize at least four distinct intracellular signaling pathways. Mobilization of CX_3CL1 by TP may reflect activation of these pathways. In our study, TP activation consistently increased CX_3CL1-dependent leukocyte adhesion, even to primary human vascular endothelial cells expressing endogenous CX_3CL1, highlighting the physiologic relevance of these observations. This is the first description of regulation of CX_3CL1 exposure and mobility by a G protein-coupled receptor.

An intriguing question is how CX_3CL1 is anchored to the plasma membrane in the first place. Previously, we reported that CX_3CL1 does not directly interact with the actin cytoskeleton (8). Recent work has demonstrated an integral role for dendritic cell (DC) CX_3CL1 in the accumulation of lipid rafts at DC-NK cell synapses (34). However, we found that in adherent cells, plasmalemmal CX_3CL1 does not associate with lipid rafts and, accordingly, that cholesterol depletion does not alter the mobility of the chemokine (8). Future studies are needed to investigate *1*) whether CX_3CL1 indirectly associates with the actin cytoskeleton by one or more Triton-soluble adaptor proteins, *2*) whether CX_3CL1 is "fenced" into discrete regions of the membrane, and *3*) precisely how TP uncouples CX_3CL1 from its membrane anchor (33, 38).

TP plays a complex role in vascular inflammation. Given the timeframe of events that we investigated, it appears that early in the inflammatory cascade, TP stimulation induces shedding of endothelial CX_3CL1 to release the soluble chemoattractant species, thereby recruiting circulating leukocytes. Slightly later, the balance is subtly altered to facilitate adhesion of leukocytes thus recruited to the area of vascular injury. Regulation of CX_3CL1 by TP in this manner may represent a link, heretofore unexplored, between the events accompanying the platelet aggregation and activation and those accompanying the vascular inflammation that, collectively, contribute to atherogenesis. The dynamic interplay among these individual events in vivo remains to be elucidated.

ACKNOWLEDGMENTS

We thank Drs. Mansoor Husain and Sergio Grinstein for helpful discussions.

GRANTS

This work was supported by a Grant-in-Aid from the Heart and Stroke Foundation of Canada (to L. A. Robinson). L. A. Robinson is the recipient of a Canada Research Chair (Tier 2) Award.

DISCLOSURES

A. M. Durkan is the recipient of a Fellowship Award jointly sponsored by North American Pediatric Renal Trials and Collaborative Studies (NAPRTCS) and Roche.

REFERENCES

1. **Audoly LP, Rocca B, Fabre JE, Koller BH, Thomas D, Loeb AL, Coffman TM, FitzGerald GA.** Cardiovascular responses to the isoprostanes $iPF_{2\alpha}$-III and iPE_2-III are mediated via the thromboxane A_2 receptor in vivo. *Circulation* 101: 2833–2840, 2000.
2. **Baan JF, Bacon KB, Hardiman G, Wang W, Soo K, Rossi D, Greaves DR, Zlotnick A, Schall TJ.** A new class of membrane-bound chemokine with a CX_3C motif. *Nature* 385: 640–644, 1997.
3. **Becker RC.** Antithrombotic therapy after myocardial infarction. *N Engl J Med* 347: 1019–1022, 2002.
4. **Chan JR, Hyduk SJ, Cybulsky MI.** Detecting rapid and transient upregulation of leukocyte integrin affinity induced by chemokines and chemoattractants. *J Immunol Methods* 273: 43–52, 2003.
5. **Cheng Y, Austin SC, Rocca B, Koller BH, Coffman TM, Grosser T, Lawson JA, FitzGerald GA.** Role of prostacyclin in the cardiovascular response to thromboxane A_2. *Science* 296: 539–541, 2002.
6. **Combadiere C, Potteaux S, Gao JL, Esposito B, Casanova S, Lee EJ, Debre P, Tedgui A, Murphy PM, Mallat Z.** Decreased atherosclerotic lesion formation in CX_3CR1/apolipoprotein E double knockout mice. *Circulation* 107: 1009–1016, 2003.
7. **Diaz-Rodriguez E, Montero JC, Esparis-Ogando A, Yuste L, Pandiella A.** Extracellular signal-related kinase phosphorylates tumor necrosis factor alpha-converting enzyme at threonine 735: a potential role in regulated shedding. *Mol Biol Cell* 13: 2031–2044, 2002.
8. **Durkan AM, Alexander RT, Liu GY, Rui M, Femia G, Robinson LA.** Expression and targeting of CX_3CL1 (fractalkine) in renal tubular epithelial cells. *J Am Soc Nephrol* 18: 74–83, 2007.
9. **Fan H, Turck CW, Derynk R.** Characterization of growth factor-induced serine phosphorylation of tumor necrosis factor-alpha converting enzyme and of an alternatively translated polypeptide. *J Biol Chem* 278: 18617–18627, 2003.
10. **Fong AM, Robinson LA, Steeber DA, Tedder TF, Yoshie O, Imai T, Patel DD.** Fractalkine and CX_3CR1 mediate a novel mechanism of leukocyte capture, firm adhesion, and activation under physiologic flow. *J Exp Med* 188: 1413–1419, 1998.
11. **Gao Y, Tang S, Zhou S, Ware JA.** The thromboxane A_2 receptor activates mitogen-activated protein kinase via protein kinase C-dependent

G_i coupling and Src-dependent phosphorylation of the epidermal growth factor receptor. *J Pharmacol Exp Ther* 296: 426–433, 2001.

12. **Garton KJ, Gough PJ, Blobel CP, Murphy G, Greaves DR, Dempsey PJ, Raines EW.** Tumor necrosis factor-α-converting enzyme (ADAM17) mediates the cleavage and shedding of fractalkine (CX_3CL1). *J Biol Chem* 276: 37993–38001, 2001.
13. **Ghilardi G, Biondi ML, Turri O, Guagnellini E, Scorza R.** Internal carotid artery occlusive disease and polymorphisms of fractalkine receptor CX3CR1: a genetic risk factor. *Stroke* 35: 1276–1279, 2004.
14. **Haller C, Kiessling F, Kubler W.** Polarized expression of heterologous membrane proteins transfected in a human endothelial-derived cell line. *Eur J Cell Biol* 75: 353–361, 1997.
15. **Hirata T, Ushikubi F, Kakizuka A, Okuma M, Narumiya S.** Two thromboxane A_2 receptor isoforms in human platelets. *J Clin Invest* 97: 949–956, 1996.
16. **Hughes SE.** Functional characterization of the spontaneously transformed human umbilical vein endothelial cell line ECV304: use in an in vitro model of angiogenesis. *Exp Cell Res* 225: 171–185, 1996.
17. **Hundhausen C, Misztela D, Berkhout TA, Broadway N, Saftig P, Reiss K, Hartmann D, Fahrenholz F, Postina R, Matthews V, Kallen KJ, Rose-John S, Ludwig A.** The disintegrin-like metalloproteinase ADAM-10 is involved in constitutive cleavage of CX_3CL1 (fractalkine) and regulates CX_3CL1-mediated cell-cell adhesion. *Blood* 102: 1186–1195, 2003.
18. **Imai T, Hieshima K, Haskell CA, Baba M, Nagira M, Nishimura M, Kakizaki M, Takagi S, Nomiyama H, Schall TJ, Yoshie O.** Identification and molecular characterization of fractalkine receptor, CX_3CR1, which mediates both leukocyte migration and adhesion. *Cell* 91: 521–530, 1997.
19. **Ishizuka T, Kawakami M, Hidaka T, Matsuki Y, Takamizawa M, Suzuki K, Kurita A, Nakamura H.** Stimulation with thromboxane A_2 (TXA_2) receptor agonist enhances ICAM-1, VCAM-1 or ELAM-1 expression by human vascular endothelial cells. *Clin Exp Immunol* 112: 464–470, 1998.
20. **Ishizuka T, Sawada S, Sugama K, Kurita A.** Thromboxane A_2 (TXA_2) receptor blockade suppresses monocyte chemoattractant protein-1 (MCP-1) expression by stimulated vascular endothelial cells. *Clin Exp Immunol* 120: 71–78, 2000.
21. **Kinsella BT.** Thromboxane A_2 signalling in humans: a "tail" of two receptors. *Biochem Soc Trans* 29: 641–654, 2001.
22. **Kobayashi T, Tahara Y, Matsumoto M, Iguchi M, Sano H, Murayama T, Arai H, Oida H, Yurugi-Kobayashi T, Yamashita JK, Katagiri H, Majima M, Yokode M, Kita T, Narumiya S.** Roles of thromboxane A_2 and prostacyclin in the development of atherosclerosis in apoE-deficient mice. *J Clin Invest* 114: 784–794, 2004.
23. **Konopska JB, Watanabe SM, Witte ON.** An alteration of the human c-abl protein in K562 leukemia cells unmasks associated tyrosine kinase activity. *Cell* 37: 1035–1042, 1984.
24. **Lesnik P, Haskell CA, Charo IF.** Decreased atherosclerosis in CX_3CR1 −/− mice reveals a role for fractalkine in atherogenesis. *J Clin Invest* 111: 333–340, 2003.
25. **Liu GY, Kulasingam V, Alexander RT, Touret N, Fong AM, Patel DD, Robinson LA.** Recycling of the membrane-anchored chemokine, CX_3CL1. *J Biol Chem* 280: 19858–19866, 2005.
26. **Lucas AD, Bursill C, Guzik TJ, Sadowski J, Channon KM, Greaves DR.** Smooth muscle cells in human atherosclerotic plaques express the fractalkine receptor CX_3CR1 and undergo chemotaxis to the CX_3C chemokine fractalkine (CX_3CL1). *Circulation* 108: 2498–2504, 2003.
27. **Matloubian M, David A, Engel S, Ryan JE, Cyster JG.** A transmembrane CXC chemokine is a ligand for HIV-coreceptor Bonzo. *Nat Immunol* 1: 298–304, 2000.
28. **McDermott DH, Fong AM, Yang Q, Sechler JM, Cupples LA, Merrell MN, Wilson PW, D'Agostino RB, O'Donnell CJ, Patel DD.** Chemokine receptor mutant CX_3CR1-M280 has impaired adhesive function and correlates with protection from cardiovascular disease in humans. *J Clin Invest* 111: 1241–1250, 2003.
29. **McDermott DH, Halcox JP, Schenke WH, Waclawiw MA, Merrell MN, Epstein N, Quyyumi AA, Murphy PM.** Association between polymorphism in the chemokine receptor CX_3CR1 and coronary vascular endothelial dysfunction and atherosclerosis. *Circ Res* 89: 401–407, 2001.
30. **Miggin SM, Kinsella BT.** Thromboxane A_2 receptor-mediated activation of the mitogen activated protein kinase cascades in human uterine smooth muscle cells. *Biochim Biophys Acta* 1539: 147–162, 2001.
31. **Mitsuhashi M, Tanaka A, Fujisawa C, Kawamoto K, Itakura A, Takaku M, Hironaka T, Sawada S, Matsuda H.** Necessity of thromboxane A_2 for initiation of platelet-mediated contact sensitivity: dual activation of platelets and vascular endothelial cells. *J Immunol* 166: 617–623, 2001.
32. **Moatti D, Faure S, Fumeron F, Amara MW, Seknadji P, McDermott DH, Debre P, Aumont MC, Murphy PM, de Prost D, Combadiere C.** Polymorphism in the fractalkine receptor CX_3CR1 as a genetic risk for coronary artery disease. *Blood* 97: 1925–1928, 2001.
33. **Neame SJ, Uff CR, Sheikh H, Wheatley SC, Isacke CM.** CD44 exhibits a cell type dependent interaction with triton X-100 insoluble, lipid rich, plasma membrane domains. *J Cell Sci* 108: 3127–3135, 1995.
34. **Pallandre JR, Krzewski K, Bedel R, Ryffel B, Caignard A, Rohrlich PS, Pivot P, Tiberghien P, Zitvogel L, Strominger JL, Borg C.** Dendritic cell and natural killer cell cross-talk: a pivotal role of CX_3CL1 in NK cytoskeleton organization and activation. *Blood* 112: 4420–4424, 2008.
35. **Robinson LA, Nataraj C, Thomas DW, Howell DN, Griffiths R, Bautch VL, Patel DD, Feng L, Coffman TM.** A role for fractalkine and its receptor (CX_3CR1) in cardiac allograft rejection. *J Immunol* 165: 6067–6072, 2000.
36. **Robinson LA, Tu L, Steeber DA, Preis O, Platt JL, Tedder TF.** The role of adhesion molecules in human leukocyte attachment to porcine vascular endothelium: implications for xenotransplantation. *J Immunol* 161: 6931–6938, 1998.
37. **Shiokoshi T, Ohsaki Y, Kawabe J, Fujino T, Kikuchi K.** Downregulation of nitric oxide accumulation by cyclooxygenase-2 induction and thromboxane A_2 production in interleukin-1β-stimulated rat aortic smooth muscle cells. *J Hypertens* 20: 455–461, 2002.
38. **Suzuki K, Ritchie K, Kajikawa E, Fujiwara T, Kusumi A.** Rapid hop diffusion of a G-protein-coupled receptor in the plasma membrane as revealed by single-molecule techniques. *Biophys J* 88: 3659–3680, 2005.
39. **Takahashi K, Sawasaki Y.** Rare spontaneously transformed human endothelial cell line provides useful research tool. *In Vitro Cell Dev Biol* 28A: 380–382, 1992.
40. **Teupser D, Pavlides S, Tan M, Gutierrez-Ramos JC, Kolbeck R, Breslow JL.** Major reduction of atherosclerosis in fractalkine (CX3CL1)-deficient mice is at the brachiocephalic artery, not the aortic root. *Proc Natl Acad Sci USA* 101: 17795–17800, 2004.
41. **Thomas DW, Rocha PN, Nataraj C, Robinson LA, Spurney RF, Koller BH, Coffman TM.** Proinflammatory actions of thromboxane receptors to enhance cellular immune responses. *J Immunol* 171: 6389–6395, 2003.
42. **Tilley SL, Coffman TM, Koller BH.** Mixed messages: modulation of inflammation and immune responses by prostaglandins and thromboxanes. *J Clin Invest* 108: 15–23, 2001.
43. **Tsou CL, Haskell CA, Charo IF.** Tumor necrosis factor-α-converting enzyme mediates the inducible cleavage of fractalkine. *J Biol Chem* 276: 44622–44626, 2001.
44. **van Kerkhof P, Sachse M, Klumperman J, Strous GJ.** Growth hormone receptor ubiquitination coincides with recruitment to clathrin-coated membrane domains. *J Biol Chem* 276: 3778–3784, 2001.
45. **Wong BW, Wong D, McManus BM.** Characterization of fractalkine (CX_3CL1) and CX_3CR1 in human coronary arteries with native atherosclerosis, diabetes mellitus, and transplant vascular disease. *Cardiovasc Pathol* 11: 332–338, 2002.
46. **Zahler S, Becker BF.** Indirect enhancement of neutrophil activity and adhesion to cultured human umbilical vein endothelial cells by isoprostanes (iPF2α-III and iPE2-III). *Prostaglandins Other Lipid Mediat* 57: 319–331, 1999.
47. **Zeiffer U, Schober A, Lietz M, Liehn EA, Erl W, Emans N, Tan Z, Weber C.** Neointimal smooth muscle cells display a proinflammatory phenotype resulting in increased leukocyte recruitment mediated by P-selectin and chemokines. *Circ Res* 94: 776–784, 2004.